Characteristics of Ytterbium Ions Stored in Rf Traps

February 1996

Kazuhiko SUGIYAMA

Characteristics of Ytterbium Ions Stored in Rf Traps

February 1997

Kazuhiko SUGIYAMA

abstract

In this thesis, we describe the characteristics of buffer-gas-cooled and laser-cooled Yb^+. Yb^+ is a candidate for providing a frequency reference in future frequency standards. Owing to the suitability of Yb^+ for use in a frequency standard, its potential for it has been extensively investigated. The growing interest in establishing a new frequency standard using the transitions of Yb^+ demands a deeper understanding of the characteristics of Yb^+. The present thesis contributes to this aim.

The characteristics of buffer-gas-cooled Yb^+ has considerably clarified by our investigations. The discovery of the YbH^+ production may present a new problem in using buffer-gas-cooled Yb^+ in a frequency standard. For laser cooling, we succeeded in it from a natural isotope mixture of Yb as a source. This had seemed to be impossible before our investigation. Establishment of methods for deexcitation of the $^2F_{7/2}$ state is necessary toward the realization of an optical frequency standard using the $^2S_{1/2}$ - $^2D_{5/2}$ transition (or sometimes using the $^2S_{1/2}$ - $^2F_{7/2}$ transition). Combining establishment of laser cooling and trapping of single Yb^+ ions with it, we achieved the preparation for high resolution spectroscopy of the optical clock transitions of Yb^+.

For the investigations, we used two rf traps of different sizes. A large trap of $2r_0 = 22.6$ mm was used for investigation of buffer-gas-cooled Yb^+. In this trap, we could confine the ions of which number was up to 10^6 and successfully detected rf signals of trapped ions. A small trap of $2r_0 = 5$ mm was constructed for investigation of laser-cooled Yb^+. For laser cooling, we decreased heat capacities of the oven and the electron source used for production of Yb^+ ions in order to avoid collisonal heating with neutral Yb

atoms and electrons.

In detection of trapped ions by rf resonance absorption method, we focused on the effect of anharmonic oscillation of trapped ions on rf signals. We found that the shapes and sizes of rf signals depended on the pressure of buffer gas while the number of trapped ions was fixed. In addition, we found that the shapes of rf signals changed with the number of trapped ions while the pressure of buffer gas was fixed. We suggested that the buffer-gas-pressure and the ion-number dependence of rf signals could be qualitatively explained if we assume that the space charge potential of trapped ions has an anharmonicity which changes with buffer-gas pressure and ion number.

We pointed out that anharmonicity of rf signals limited accuracy in estimating the number of trapped ions from rf signals.

For detection of the fluorescence and laser cooling of Yb^+, radiation at 369.52 nm is required to drive the $^2S_{1/2}$ - $^2P_{1/2}$ first resonance line. We realized tunable cw radiation at 369.52 nm by a simple and inexpensive method, i.e., sum-frequency mixing of diode-laser radiation at 1310 nm and argon-ion laser at 515 nm. More than $1\mu W$ of UV radiation was generated from a diode-laser power of 21 mW and an argon-ion laser power of 1.3 W with a β-BaB_2O_4 crystal. We successfully observed the fluorescence of trapped Yb^+ ions using this radiation. We found that the phase-mismatching tolerance became larger when we strongly focused input beams than that when the beams were collimated. This is caused by the fact that an aperture length was shorter than the crystal length due to a relatively large double refraction of this material.

We proposed a simple frequency stabilization scheme of sum frequency, i.e., stabilization of sum-frequency by controlling only one of

the fundamental lasers of mixing. We successfully applied this scheme to the sum-frequency mixing of diode-laser and argon-ion-laser radiation. We controlled only the diode laser while the argon-ion laser was free-running. This scheme is effective also for difference-frequency mixing.

We found that more powerful radiation at 369.52 nm was required for laser cooling that that generated by sum-frequency mixing. For this purpose, we generated radiation at 369.52 nm by second-harmonic generation of dye-laser radiation using an external cavity technique. We obtained more than 100 μW of UV radiation by an external cavity We succeeded in laser cooling using this radiation.

For laser cooling, the $^2D_{3/2}$ metastable state must be depleted. For this purpose, we drove the $^2D_{3/2} - {}^3[3/2]_{1/2}$ transition at 935 nm with radiation generated by a Ti:Al$_2$O$_3$ laser. We detected optogalvanic signals of this transition of Yb$^+$ in a lamp and determined the isotope shifts of it, which were not well known. It was necessary to know the isotope shift of this transition for laser cooling, in particular, in the case that a natural isotope mixture of Yb$^+$ is used as is the case with us.

In our investigation of buffer-gas-cooled Yb$^+$, we focused on the characteristics of it continuously irradiated at 369.52 nm. During over five years of our investigations, great progress in the understanding of this phenomenon has been made. It is well known that the fluorescence of trapped Yb$^+$ ions fades with continuous driving the $^2S_{1/2} - {}^2P_{1/2}$ transition with irradiation at 369.52 nm in the presence of buffer gas. For the cause of the fluorescence decay, it was proposed that population trapping in the $^2F_{7/2}$ state of which lifetime is calculated to be over 1000 days.

We found that, in some conditions, the rf signals disappeared as well as the fluorescence faded. Then, we noticed that some gases were

responsible for the rf-signal disappearance, and proved this proposal by the observation that the disappearance was enhanced when we introduced O_2 or H_2O gas into the vacuum chamber. We suggested that chemical reaction of Yb^+ in excited states to produce molecular-ions should occur with the rf-signal disappearance from the change in the resonance point of rf signals.

To investigate these observations more quantitatively, we developed mass selective detection of trapped ions by combining a quadrupole mass analyzer with our rf trap. We found that YbH^+ was produced by chemical reaction of Yb^+ in excited state with residual H_2 gas. The YbH^+ production is one of the causes of the fluorescence decay. The YbH^+ production occurs in the same time scale of the fluorescence decay, and rf signals did not disappear and the resonance point of them just shifted in accordance with the mass change. We found that wavelengths of 369.482 nm, 369.202 nm, and 368.947 nm, formerly assigned as wavelengths for deexcitation of Yb^+ in the $^2F_{7/2}$ state to the $^2S_{1/2}$ ground state, are actually photodissociation lines of YbH^+.

To investigate the disappearance of rf signals, we introduced O_2 gas into the vacuum chamber and detected trapped ions mass-selectively. We found that YbO^+ was produced by chemical reaction of Yb^+ in exited states with O_2 gas, as we predicted. We first considered that the disappearance of rf signals indicated the loss of ions from the trap. However, the results obtained by mass-selective detection in the presence of O_2 gas indicated that the number of trapped ions did not decrease to the minimum detectable level by rf signals. Further investigations should be required to clarify the causes of the rf-signal disappearance.

With a view to establishing a frequency standard using buffer-gas-cooled Yb^+ ions, the production of YbH^+ may limit the performance of the frequency standard owing to the difficulty in removing H_2 gas from the

vacuum system.

We describe a positive application of our results. Knowledge of the wavelengths of photodissociation lines of molecular ions enables the use of laser-cooled ions in the field of molecular physics and chemistry in low temperature. For example, cooled single molecular ion photodissociation spectroscopy is proposed.

In our investigations of laser cooling of Yb^+, we demonstrated that it is possible to laser cool Yb^+ from a natural isotope mixture of Yb as a source by carefully setting the frequencies of the two cooling lasers. It was possible to directly laser cool one of the three major even isotopes without serious laser heating of the other isotopes, owing to relatively large isotope shifts of the $^2D_{3/2}$ - $^3[3/2]_{1/2}$ transition at 935 nm.

It was possible to trap and laser cool single $^{174}Yb^+$ ions also from a natural isotope mixture. We introduced two compensation electrodes to resolve the problem of an unexpected dc field. Applying condensation voltages to the compensation electrodes and one of the endcap electrode, we observed narrow spectra of single $^{174}Yb^+$ ions. We evaluated saturation broadening of the $^2S_{1/2}$ - $^2P_{1/2}$ cooling transition, then, determined the temperature of a laser-cooled single $^{174}Yb^+$ ion to be 150 mK. However, we suppose that residual linewidth of the spectra was still caused by imperfection of the dc field compensation.

We observed quantum jump signals by pumping to the $^2F_{7/2}$ state. This signal was useful to determine the number of ions. To observed quantum jump signals repeatedly, some methods for deexcitation of the $^2F_{7/2}$ state are necessary. We observed the fluorescence recovery by deexcitation of the $^2F_{7/2}$ state with driving the following four transitions: the $^2F_{7/2}$ - $^2D_{5/2}$ transition at 3.43 μm, the $^2F_{7/2}$ - $^1D[5/2]_{5/2}$ transition at 639 nm, the $^2F_{7/2}$ -

$^1D[3/2]_{3/2}$ transition at 760 nm, and the $^2F_{7/2}$ - $^3D[9/2]_{7/2}$ transition at 828 nm. Using radiation for pumping to and deexcitation of the $^2F_{7/2}$ state, we observed quantum jump signals repeatedly.

Contents

Chapter 1

Introduction

This thesis concerns the characteristics of singly ionized ytterbium (Yb⁺) stored in radio-frequency (rf) traps investigated at the National Research Laboratory of Metrology (NRLM). This chapter contains a short review of the ion trap technique for application to frequency standards. The general characteristics of Yb⁺, in particular, its suitability for application to frequency standards, are described. We review the history of investigations of Yb⁺, and mention our contributions to the understanding of characteristics of Yb⁺ in rf traps. An outline of this work is described in the final part of this chapter.

1.1.   Ion Trap Technique

The ion trap technique is one of the candidates for a method of realizing a new frequency standard [1-10]. Its advantages as a frequency standard are as follows.

Ions are stored in a small region for long periods of time. The storage time of trapped ions was recorded over several days. Therefore, a long interrogation time can be obtained. The linewidth of a spectrum $\Delta\omega$ is limited by Einstein's uncertainty law $\Delta\omega\Delta t \approx 1$, where Δt is the interrogation time. Therefore, a long interrogation time results in a high

resolution or high Q of the spectra, where Q is defined by $Q = \Delta\omega/\omega_0$ and ω_0 is the transition angular frequency.

When ions are confined within the region of $\lambda/2\pi$, where λ is the wavelength of the interrogated electromagnetic field, the observed spectra are free from the first-order Doppler shift [11]. This is, the non-Doppler shifted carrier at ω_0 is observed as the strongest peaks with sidebands of weaker strength [11]. The region $\lambda/2\pi$ is called the Lamb-Dicke region. Confinement within the Lamb-Dicke region is easily realized in the microwave region. For example, $\lambda/2\pi$ is 5 mm at $\omega_0/2\pi = 10$ GHz and confinement in this range is realized by using a trap of a conventional size, and a ring electrode with an inner diameter of (see below) a few cm.

The ion trap technique is free from frequency shifts due to collisions with the wall. When ions are trapped in an ultrahigh vacuum (UHV), frequency shifts due to collision with background gas, i.e., pressure shift, can be negligible.

For ions which have a strong transition, with which the cycle of absorption of a laser photon and subsequent spontaneous emission is repeated continuously for over several tens of thousand times, laser cooling can be combined with the ion trap technique. Laser cooling was proposed for neutral atoms [12] and trapped ions [13]. Laser cooling of trapped ions was first demonstrated in 1978 for Mg^+ stored in a Penning trap at the National Institute of Standards and Technology (NIST) [14] and for Ba^+ in a rf trap at Universitat Hamburg [15]. Laser cooling with a strong transition decreases the kinetic energy of trapped ions to the order of 1 mK. This results in a very small second-order Doppler shift. The second-order Doppler shift is due to the special relativistic law, and is a major factor in the uncertainty of present frequency standards. By cooling to a temperature of 1 mK, its fractional shift should be reduced to

10^{-18} or less. This value may be smaller than that of the other factors of frequency shift.

The decrease of kinetic energy of trapped ions, upon laser cooling, means that the amplitude of the ion oscillation is also very small. Therefore, only a single ion can be observed in traps by observing its fluorescence, in combination with the effect that the absorption rate of laser photons increases due to the decrease in the first-order Doppler shift. Laser cooling and observation of a single ion was first realized by Neuhauser et al. at Universitat Hamburg [16]. Moreover, the amplitude of the ion motion can be reduced within the Lamb-Dicke region even for an optical wavelength [17]. For example, if $^{171}Yb^+$ is confined in a trap with a harmonic potential well of an oscillation frequency of 1 MHz, the amplitude of $^{171}Yb^+$ is 35 nm at 1 mK, while $\lambda/2\pi$ is 59 nm at 370 nm.

The disadvantage of the ion trap technique is that density, and consequently, the number of trapped ions, cannot increase due to Coulomb force repulsion because of the charges of trapped ions. This results in a poor signal-to-noise ratio.

We introduce ion traps briefly. On the basis of Laplace's equation, it is impossible to confine a charged particle in space using only a static electric field. Here, we use cylindrical coordinates with their origin at the center of the trap. When a charged particle is to be confined in a harmonic potential well in the radial r or the axial z direction using a static electric field, the electric potential $\phi(r, z)$ is represented in the form of,

$$\phi(r,z) = A(r^2 - 2z^2) \tag{1.1}$$

3

where A is a constant. To realize this potential, three electrodes are prepared with their inner surfaces shaped into a truncated hyperboloid, as shown in Fig. 1.1, because the inner surfaces of the electrodes should correspond to an equal electric potential surface. The electrode shaped as a ring is usually called the ring electrode, and the other two electrodes which have the same inner surface and potential are the endcap electrodes. When an electric voltage V_0 is applied between the ring electrode and the two endcap electrodes, the constant A is given by
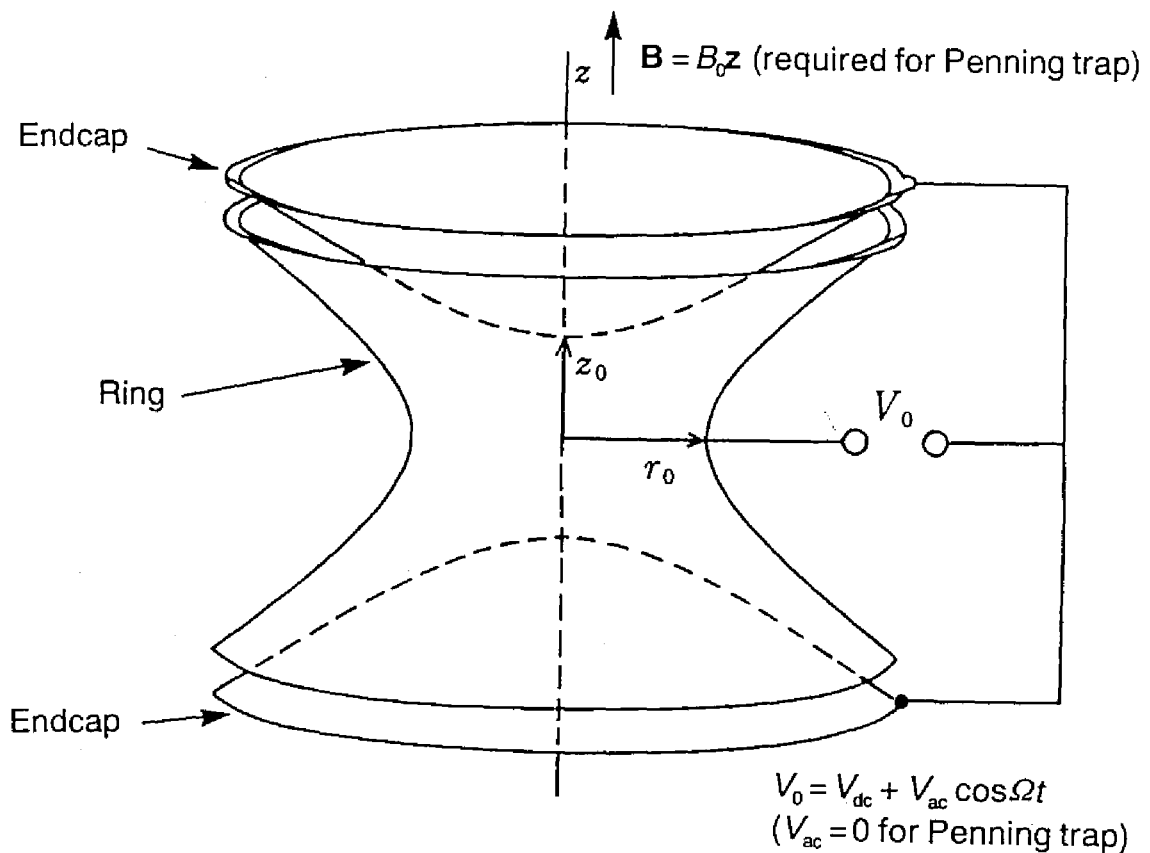

Fig. 1.1   Schematic representation of the electrode configuration for the rf (Paul) or Penning trap. The inner surface of the electrodes are assumed to be equipotentials of $\phi(r, z) = A(r^2 - 2z^2)$, where $A = V_0/(r_0^2 + 2z_0^2)$. r_0 is the minimum inner radius of the ring electrode, and z_0 is the minimum half-distance between the two endcap electrodes.

$$A = \frac{V_0}{r_0^2 + 2z_0^2} = \frac{V_0}{2r_0^2},$$ (1.2)

where $r_0 = \sqrt{2}z_0$, r_0 is the minimum inner radius of the ring electrode, and z_0 is the minimum half-distance between the two endcap electrodes.

From Eqs. (1.1) and (1.2), it is also clear that one cannot trap a charged particle cannot be trapped in three dimensions by applying only a static voltage as V_0. To overcome this problem, two methods were devised. One is the Penning trap and the other is the Paul or rf trap. In the case of the Penning trap, a static electric voltage is applied as V_0 to trap a charged particle in the z direction. Simultaneously, a static magnetic field is applied in the z direction. This results in confinement in the r direction due to the motions of the cyclotron and magnetron about the trap axis.

In the case of the rf trap, a time-varying rf electric field is applied as V_0. Although a charged particle has an oscillation motion at the frequency of the applied rf driving field, it drifts toward the region of the weaker field due to inhomogeneity of the rf electric field. This results in confinement around the trap center where the rf field is weakest. The oscillation at the frequency of the rf driving field is called micromotion, and the oscillation in the psuedopotential well caused by the inhomogeneous rf field is called secular motion. Principles of the rf trap are described in detail in Sec. 2.2, since we use rf traps.

The advantages and disadvantages of both types of traps are briefly described. In the case of the Penning trap, there is no strong heating mechanism from the trapping fields. It is suitable for laser cooling a large number of ions. On the other hand, no restoring force acts

in the r direction. Therefore, it is important not to interrupt the magnetron motion for trapping a charged particle, otherwise it is lost in the r direction. Therefore, an UHV condition is needed to avoid collision with background gases. When laser cooling is applied, the direction of the laser beam must be the same as that of magnetron motion [18]. The magnetic field applied for confinement in the r-direction causes the Zeeman shift in transitions of trapped particles. This complicates the level structure, and demands that the magnetic field strength be set to the point where the Zeeman shift does not depend on magnetic field to the first order, but to the second order to avoid broadening of spectra due to fluctuation of the magnetic field strength.

In the case of the rf trap, a heating mechanism exists. The energy of the micromotion, caused by the rf driving field, of a trapped charged particle is converted to a secular motion via ion-background gas or ion-ion collisions. This is called rf heating [1]. As the number of trapped charged particles increases, a cloud of trapped charged particles spreads outwards from the trap center due to the Coulomb repulsion force caused by their charges. The rf driving field becomes stronger as the distance from the trap center increases. Therefore, an increase of the number of trapped charged particles results in increase in the energy of micromotion, and consequently, of secular motion due to the rf heating. Therefore, to reduce the kinetic energy of the trapped charged particles, their number must be decreased [19]. To cool the particles as low as possible, it is necessary to trap only a single ion and to locate it at the trap center where no trapping rf driving field exists. On the other hand, the restoring force acts in all directions. Therefore, trapped charged particles can be cooled by collision with light buffer gases, to a kinetic energy at which rf heating balances collisional cooling with light buffer gases [20,21]. To reduce rf

heating, the linear trap was devised, where four parallel rods produce a inhomogeneous quadrupole rf field in the space surrounded by the rods to confine charged particles in the direction perpendicular to the trap axis, while a static voltage is applied to confine them in the direction of the trap axis (i.e., rf heating acts on the particles only in the direction perpendicular to the trap axis.) [22].

We describe the expected performance of the frequency standard based upon the ion trap technique. To evaluate the performance of the frequency standard, three parameters are used: accuracy, stability and reproducibility.

Laser-cooled single ions have a very high accuracy potential [5-7,23,24]. As mentioned, the fractional second-order Doppler shift can be reduced to the order of 10^{-18} or less at a temperature on the order of 1 mK. The second-order Doppler shift is a large factor of uncertainty in the current frequency standard. Therefore, other factors of uncertainty may also be observable.

The second-order Stark shift is caused by the electric field of the trap and blackbody radiation. For the former case, the value of the shift was measured by Yu et al., at the University of Washington, to be ~10 mHz/(V/cm)^2 for the $^2S_{1/2}$ - $^2D_{5/2}$ transition of Ba$^+$ [25]. The average fractional shift of the transition is predicted to be 10^{-17} at 1 mK [25]. (This range of temperature is realized by laser cooling to the Doppler cooling limit. See Chapter 5.) For the latter case, the value of the fractional shift would be 10^{-15} at room temperature, where the blackbody radiation field has a value of ~70 (V/cm)^2 [23].

In the case that the lower or upper states have an electronic electric quadrupole moment, e.g., S - D transitions of ions of group IIa

7

and IIb elements, a shift is caused by quadrupole interaction with the static electric field of quadrupole symmetry. If the trap has perfect axial symmetry along $r = 0$, and the magnetic field is aligned with the z axis of the quadrupole field, the shift is estimated to be ~ -2 Hz when 1 V is applied to the ring electrode for the trap of $2r_0 = 0.93$ mm [24]. It is pointed out that, in practice, the shift would be a few tenths of a hertz due to imperfection of the magnetic field alignment and of the axial symmetry of the trap [25]. However, it has been proposed that this shift can be calibrated [24]. The $^1S_0$ - $^3P_0$ transition of ions of group IIIa elements is free from the quadrupole electric field shift [6].

Even isotopes of ions of group IIa and IIb elements have angular momentum $J = 1/2$, and their Zeeman shift around the zero magnetic field depends on the magnetic field to the first order. The value of the shifts in those ion species is estimated to be on the order of 10 MHz/mT. The fluctuation of ambient magnetic field broadens the observed spectral linewidth, e.g., if a 1 μT fluctuation of the magnetic field exists, the spectra would have a linewidth of 10 kHz. To avoid this problem, $m_F = 0$ $\rightarrow$ $m_F = 0$ transitions of odd isotopes of ions of group IIa and IIb elements are useful. The transitions depend on the magnetic shift to the second order, e.g., for the ^{199}Hg$^+$ $^2S_{1/2}$(F=0, m$_F$ = 0) $\rightarrow$ $^2D_{5/2}$(F=2, m$_F$ =0) transition, the fractional shift is estimated to be ~ -2 $\times$ 10^{-5} B^2 [/T^2] [24]. If we again assume the fluctuation in the magnetic field to be 1 μT, the spectral width would be 20 mHz. In the case of the ion species of group IIIa elements, the magnetic field dependence on the $^1S_0$ - $^3P_0$ clock transition is of the first order, but much smaller than that of the even isotopes of the ion species of group IIa and IIb elements. For example, it is estimated to be 20 kHz/mT for Tl$^+$ [6]. The spectral width would be broadened to 20 Hz by a 1 μT fluctuation of the magnetic field. This may

require careful shielding of the magnetic field.

Frequency stability, or measurement imperfection, is proportional to the inverse of the product of Q and S/N, where S/N is the signal-to-noise ratio for detecting the number of ions that have made the transition. If we assume that the time-domain Ramsey method is used to interrogate the clock transition, the frequency stability, expressed in terms of Allan variance, is given by [11,24]

$$\sigma_y(\tau) = \frac{1}{\sqrt{N\omega_0^2 T_R}\sqrt{\tau}}, \qquad (1.3)$$

where τ is the averaging time and T_R is the interrogation time between pulses in the Ramsey method.

Although laser-cooled single ions have a potential of high accuracy, they have a disadvantage in S/N. A long averaging time may be required to obtain a measurement precision comparable to the accuracy. One solution to this problem is to increase Q using a transition at a high ω_0. In this sense, single ion spectroscopy is performed in the optical region. Single ion spectroscopy was first demonstrated by Bergquist et al. at NIST in 1988, where they observed the $^2S_{1/2}$ - $^2D_{5/2}$ transition at 282 nm of $^{198}Hg^+$ [17]. Since then, researchers in several laboratories have applied single ion spectroscopy to optical regions of various ion species, i.e., Ca^+, Sr^+, Ba^+, Yb^+, Hg^+, and In^+ [26]. The observed linewidths are limited in the range from 1 kHz to 10 MHz. The narrowest spectra obtained so far had the full width at half-maximum (FWHM) of 80 Hz, where the $^2S_{1/2}$ - $^2D_{5/2}$ transition at 282 nm of $^{199}Hg^+$ was again detected by Bergquist et al. at NIST [27]. However, frequency stabilization of lasers to the clock transition of trapped ions has not yet been realized. This is mainly because

the spectral purity of lasers is not sufficient. By using a fast servo and FM sideband technique [28], the frequency of the laser can be locked to the resonance of a high-finesse cavity with a relative linewidth of less than 1 Hz [29,30]. However, the absolute linewidth is limited by fluctuation of the cavity resonance caused by vibration and/or interference by acoustic noise [31].

On the other hand, in the microwave region, an increase of the number may be desirable to obtain high-frequency stability. To this end, a large number of ions are trapped in rf traps by means of buffer-gas cooling. So far, two groups have demonstrated prototype microwave frequency standards with very high stability. Tjoelker et al. at JPL reported $\sigma_y(\tau) = 6.5 \times 10^{-14} \ \tau^{1/2}$ ($\tau < 10000$ s) and a sensitivity floor better than 7×10^{-16} was recorded at 10000 s, where they used the ground-state hyperfine transition of $^{199}Hg^+$ ions as a reference and number of trapped $^{199}Hg^+$ ions was 10^6 in the related paper [32]. Fisk et al. at CSIRO reported $\sigma_y(\tau) = 6 \times 10^{-14} \ \tau^{1/2}$ ($\tau < 10000$ s) and a sensitivity floor better than 1.9 $\times$ 10^{-15} was recorded at 1000 s, where they used the ground-state hyperfine transition of $^{171}Yb^+$ ions as a reference and number of trapped $^{171}Yb^+$ ions was 10^5 [33]. In these works, linear traps were used.

The accuracy of these frequency standards was limited of the order of 10^{-13}. A major source of the uncertainty was that in estimating the second-order Doppler shift. To reduce the second-order Doppler shift, laser cooling is a solution. A Penning trap is used for this purpose because a large number of ions can be laser cooled. Bollinger et al. at NIST first demonstrated a prototype microwave frequency standards based on laser-cooled ions, where they used a 303-MHz hyperfine transition in the ground state of $^9Be^+$ ions as a reference [34]. Later, they improved its performance using sympathetic cooling, where the fractional second-

order Doppler shift was obtained to be $(-1.2 \pm 0.5) \times 10^{-14}$ [35]. For rf trap, if a linear trap is used, the number of cold ions can be increased by arranging the ions in a string along the trap axis, as demonstrated by Raizen et al. [36].

For a frequency standard based on laser-cooled ions, pressure shift was found to be an unexpected problem. Bollinger et al. measured the pressure shift of a laser-cooled Be^+ microwave standard to be three orders magnitude larger than the expected value, and suggested that this would limit the inaccuracy to about 1 part in 10^{13} [35]. To avoid the pressure shift, using a cryogenic system is suggested. [35,37].

Apart from application to a frequency standard, trapped ions has have been used for precise experiments in basic physics, because they offer a pure and isolated sample: for example, experiments on observation of quantum jumps [38,39,40], ion crystallization [41], photon antibunching [42], laser cooling to the zero-point energy of motion [43], quantum Zeno effect [44], and quantum logic gate [45].

1.2. Singly Ionized Ytterbium (Yb^+)

Yb^+ is a candidates for providing a frequency reference in future frequency standards [8,46,47]. Yb is involved a lanthanide rare earth, and its singly ionized ion Yb^+ has a term scheme similar to that of singly ionized group IIa and IIb atoms. The partial term scheme of Yb^+ is shown in Fig. 1.2. Some of basic characteristics of Yb^+ are listed in Table 1.1.

Yb^+ has characteristics which are suitable for use in a frequency standard. Yb^+ has several clock transitions from the microwave to optical region, as listed in Table 1.1. The wavelengths of three clock transitions
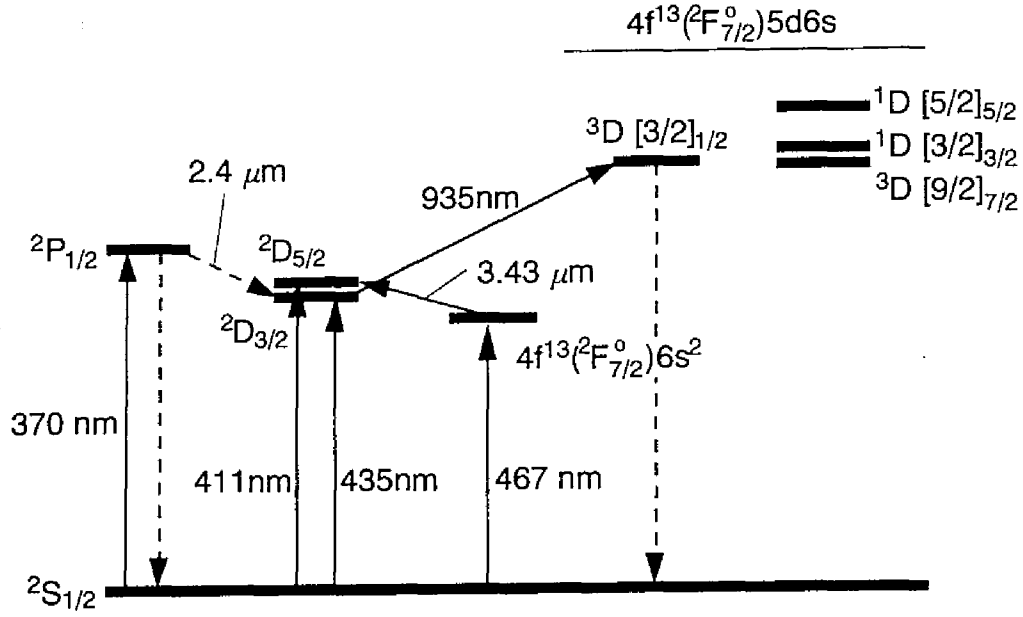
11

$4f^{13}(^2F^o_{7/2})5d6s$

$^1D\,[5/2]_{5/2}$

$^3D\,[3/2]_{1/2}$ $^1D\,[3/2]_{3/2}$

$^3D\,[9/2]_{7/2}$

2.4 μm   935nm

$^2P_{1/2}$ $^2D_{5/2}$ 3.43 μm

$^2D_{3/2}$ $4f^{13}(^2F^o_{7/2})6s^2$

370 nm   411nm   435nm   467 nm

$^2S_{1/2}$

Fig. 1.2.   Partial energy term scheme of Yb^+ related to this thesis. The three states in the $4f^{13}(^2F_{7/2}{}^o)5d6s$ configuration, shown in the right side of the figure, were used for pumping to and deexcitation of the $^2F_{7/2}$ state (see Sec. 5.4).

in the violet region, i.e., the 411 nm $^2S_{1/2}$ - $^2D_{5/2}$, the 435 nm $^2S_{1/2}$ - $^2D_{3/2}$, and the 467 nm $^2S_{1/2}$ - $^2F_{7/2}$ transitions, are accessible by frequency-doubled all-solid-state lasers including diode lasers. The $^2S_{1/2}$ - $^2D_{5/2}$ transition at 411 nm can be easily detected, because electron shelving in the $^2F_{7/2}$ state with a lifetime of 1533 days [48] occurs due to a decay from the $^2D_{5/2}$ state. For this transition, the 6S-8S two-photon transition of Cs atoms, which is 0.5 THz away from the $^2S_{1/2}$ - $^2D_{5/2}$ transition of Yb^+, has the potential for use as a reference or transfer standard [49]. However, pumping to the $^2F_{7/2}$ state requires some methods for deexciting the $^2F_{7/2}$

state quickly. For the $^2S_{1/2}$ - $^2D_{3/2}$ transition at 435 nm, it is difficult to detect electron shelving in the $^2D_{3/2}$ state in the case of even isotopes of Yb$^+$, because this state is already used in laser cooling. However, Tamm and Engelke proposed that the $^2S_{1/2}$(F=0) - $^2D_{3/2}$(F=2) transition of ^{171}Yb$^+$ can be used to observe electron shelving in the $^2D_{3/2}$(F=2) state, because the $^2D_{3/2}$(F=2) state is not included in the cycling transitions in the proposed laser-cooling scheme [47]. An advantage of this transition is that Yb$^+$ does not decay to the $^2F_{7/2}$ state and no methods for deexciting the $^2F_{7/2}$ state are required. Use of ^{171}Yb$^+$ is necessary to observe narrow spectra to avoid broadening due to fluctuation of the magnetic field. The $^2S_{1/2}$ - $^2F_{7/2}$ transition at 467 nm has the potential of very narrow spectra due to a long lifetime of the $^2F_{7/2}$ state [48]. Driving this transition requires a narrow and/or high-intensity coherent light sources.

Yb$^+$ can be laser cooled using coherent light sources, which is available with a current technique. An all-solid-state cooling laser system was realized by Tamm et al. [50,51]. Yb$^+$ has a large mass-to-charge ratio. This means that it is slow and the second-order Doppler shift is small at a given kinetic energy. The relation between temperature and the second-order Doppler shift is shown in Fig. 1.3 for the case of ^{171}Yb$^+$. When Yb$^+$ is laser cooled using the $^2S_{1/2}$ - $^2P_{1/2}$ transition at 369.52 nm, one can expect the kinetic energy of Yb$^+$ to be decreased to the Doppler cooling limit of this transition, i.e., 430 μK, where the second-order Doppler shift is as much as 3×10^{-19}.

Yb$^+$ has odd isotopes, i.e., ^{171}Yb$^+$ with a nuclear spin $I = 1/2$ and ^{173}Yb$^+$ with $I = 5/2$, which have hyperfine structures. Therefore, the transition between the hyperfine splitting in the $^2S_{1/2}$ ground state provides the reference in a microwave frequency standard. The frequencies of the transitions are 12.6 GHz and 10.5 GHz for ^{171}Yb$^+$ and ^{173}Yb$^+$, respectively.

Table 1.1.   Summary of characteristics of Yb⁺

Clock Transitions			
Optical	**Transitions**	**Wavelength**	**Natural linewidth**
	$^2S_{1/2} - \,^2D_{5/2}$	411 nm	30 Hz [48]
	$^2S_{1/2} - \,^2D_{3/2}$	435 nm	3 Hz [54]
	$^2S_{1/2} - \,^2F_{7/2}$	467 nm	$<2 \times 10^{-9}$ Hz [48]
	$^2F_{7/2} - \,^2D_{5/2}$	3.43 μm	30 Hz [48]
	$^2D_{3/2} - \,^2D_{5/2}$	7.3 μm	30 Hz [48]
microwave	**Isotope**	**Frequency**	
	171	12.6 GHz	
	173	10.5 GHz	

Natural abundance	
Isotope	**abundance**
168	0.1 %
170	3.1 %
171	14.4 %
172	16.2 %
174	3 1.6 %
176	12.6 %

Isotope shifts for the $^2S_{1/2} - \,^2P_{1/2}$ transition

Ref. [81]		Ref. [82]	
172 - 170	-1.640(3)	172 - 170	-1.6233(8)
174 - 172	-1.265(3)	172 - 171$_T$	-1.0343(8)
174 - 170	-2.896(3)	172 - 173$_T$	0.5699(7)
176 - 174	-1.205(3)	172 - 174	1.2753(7)
176 - 172	-2.470(3)	172 - 176	2.4928(10)
174 - 173$_T$	-0.75(30)		
174 - 171$_T$	-2.41(30)		

Lifetime (experiment)[*]

State	Lifetime			
$^2P_{1/2}$	6.9(6) ns	[83]	8.9(5) ns	[84]
	7.1(4) ns	[85]	8.10(13) ns	[86]
	8.0(2) ns	[87]		
$^2P_{3/2}$	7.2(8) ns	[83]	7.3(6) ns	[84]
	5.5(3) ns	[85]	5.8(6) ns	[88]
	6.3(3) ns	[87]		
$^3[3/2]^o_{1/2}$	42(3) ns	[85]	37.7(5) ns [86]	
$^3[5/2]^o_{3/2}$	16(1) ns	[85]		
$^1[3/2]^o_{3/2}$	31(3) ns	[85]	28.6(4) ns [86]	
$^2D_{3/2}$	52.15(100) ms [54]			

*) Lifetimes of some other states were calculated by Fawcett and M. Wilson [48]

Like ions of group IIa and IIb elements, even isotopes of Yb^+ have angular momentum $J = 1/2$, and their energy levels around zero magnetic field depend on the magnetic field to the first order. This causes broadening of the spectra due to fluctuation of ambient magnetic fields. Odd isotopes have $m_F = 0 \rightarrow m_F = 0$ transitions which are dependent on magnetic field only to the second order. The level structure of odd isotopes of Yb^+ is complicated, like ions of group IIa and IIb elements, due to the hyperfine structure and Zeeman splitting. However, the level structure of $^{171}Yb^+$ is the simplest in such alkali-metal-like ion species because $I = 1/2$. In ions of group IIa and IIb elements, $^{199}Hg^+$ is the only other ion with $I = 1/2$.

These following are the disadvantages of Yb^+. The level scheme of Yb^+ is complicated. The low-lying term scheme of Yb^+ is primarily a
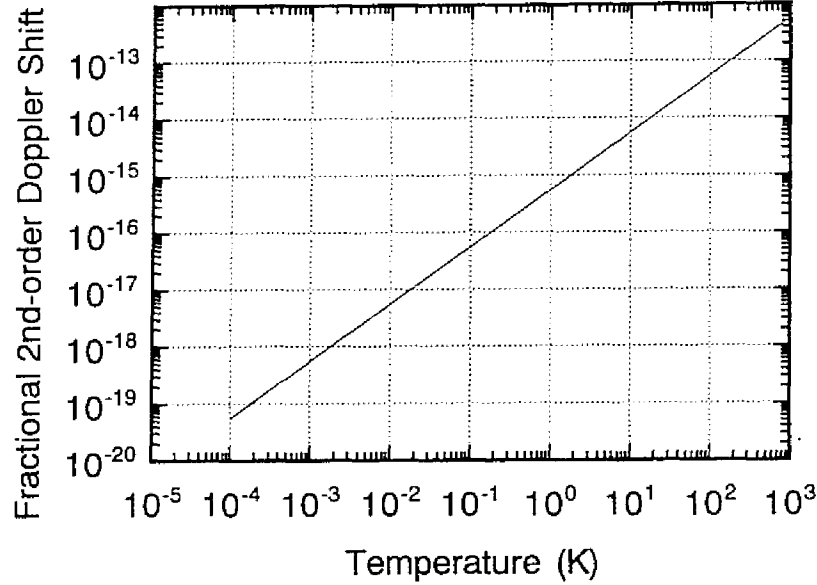
Fig. 1.3.   Second-order Doppler shift of $^{171}Yb^+$ as a function of temperature.

three-level system. The branching ratio of the $^2P_{1/2}$ state to the $^2D_{3/2}$ metastable state has been calculated to be 1/152 [48]. Therefore, to continue the cycle of absorption of laser photons and subsequent spontaneous emission in the $^2S_{1/2}$ - $^2P_{1/2}$ transition over several thousand times for laser cooling, the $^2D_{3/2}$ metastable state must be depleted. This means that two collars of lasers are needed for laser cooling. In addition, in some experiments, we must consider the $^2F_{7/2}$ state which lies below the $^2D_{3/2}$ state. The lifetime of the $^2F_{7/2}$ state was calculated to be 1533 days [48] .The existence of the $^2F_{7/2}$ state is a unique characteristic which is due to the fact that Yb is a lanthanide and is different from other ion species in the IIa and IIb family.

Natural Yb is composed of several isotopes the abundances of which are similar. In usual trapping parameters, all isotopes of Yb^+ are trapped simultaneously. However, owing to isotope shifts, only one of the isotopes of Yb^+ interacts with coherent radiation. This results in weak signal strength in spectroscopy and low cooling power in laser cooling. Therefore, enriched isotopes of Yb^+ are often used to avoid this disadvantage.

We introduce the history of the investigation of Yb^+ ions stored in ion traps. In 1982, to our knowledge, the use of Yb^+ in the ion trap technique appeared in literature for the first time, when Blatt et al. at the Universitat Maintz performed high-resolution microwave spectroscopy of the transition between the hyperfine structure of the $^2S_{1/2}$ ground state of $^{171}Yb^+$ ions stored in a rf trap in the presence of buffer gas [52]. Subsequently, at the Universitat Maintz, Munch et al. performed high-resolution microwave spectroscopy of the same transition of $^{173}Yb^+$ [53], and Gerz et al. measured the lifetime of the $^2D_{3/2}$ metastable state to be 52 ms [54].

In the work of the group at the Universitat Maintz, researchers drove the $^2S_{1/2}$ - $^2P_{1/2}$ transition at 369.52 nm using radiation from a pulsed laser. However, it is now well-known that when the $^2S_{1/2}$ - $^2P_{1/2}$ transition is continuously driven by radiation from a cw laser in the presence of buffer gases, fluorescence of trapped Yb^+ ions fades with a decay time much faster than their storage time [46,55-58]. Lehmitz et al. in Hamburg first reported this phenomenon in 1988 [46]. The $^2P_{1/2}$ state of Yb^+ spontaneously decay to the $^2D_{3/2}$ metastable state. However, the lifetime of the $^2D_{3/2}$ state, measured to be 52 ms [54], is much faster than the fluorescence decay time. Other explanations of the fluorescence decay

17

were required. Lehmitz et al. explained that it was caused by population trapping in the $^2F_{7/2}$ state, the lifetime of which exceeds 8 days [46]. The use of a cw laser was essential for observing the fluorescence decay, since Lehmitz et al. had found that the fluorescence was recovered upon irradiation with radiation close to 369.52 nm [46], and this fluorescence recovery line may be simultaneously driven by radiation from a pulsed laser with a broad linewidth.

After the first observation in Hamburg, the fluorescence decay was observed at every laboratory when the $^2S_{1/2}$ - $^2P_{1/2}$ transition of trapped Yb$^+$ ions was driven by radiation from a cw laser in the presence of buffer gases [46,55-58]. The pressure dependence of the fluorescence decay time was observed by Klein et al. at the National Physical Laboratory (NPL) [55]. Bauch et al. at the Physikalisch-Technische Bundesanstalt (PTB), on the basis of their detailed investigation, concluded that population trapping in the $^2F_{7/2}$ state was induced by collision with buffer gas [56].

At our laboratory, in 1992, we reported that rf resonance absorption signals (rf signals) also disappeared as fluorescence faded when we continuously drove the $^2S_{1/2}$ - $^2P_{1/2}$ transition in the presence of buffer gases. RF signals originate from the trapped ions that absorb rf electric power of which the frequency is the same as that of the secular motion of the trapped ions. Therefore, we proposed the existence of effects due to which trapped Yb$^+$ ions disappeared in the trap [57,58].

One of the main subjects of this thesis is the clarification of the cause of fluorescence decay and rf signal disappearance. Chapter 4 describes our observations of these phenomena and our present conclusions.

Laser cooling of Yb$^+$ was first realized by Klein et al. at NPL in

1990 [55]. In their experiment, depletion of the $^2D_{3/2}$ state was realized by driving the $^2D_{3/2}$ - $^2P_{1/2}$ transition at 2.4 μm. After that, Bell et al. at NPL and PTB demonstrated laser cooling of Yb^+ by a four level term scheme, where they depleted the $^2D_{3/2}$ state by driving the $^2D_{3/2}$ - $^3[3/2]_{1/2}$ transition at 935 nm [59]. So far, laser cooling of Yb^+ has been achieved by Enders et al. at Universitat Hamburg [60], Fisk et al. at CSIRO [61], and Tamm and Engelke at PTB [47]. In their experiments, enriched isotopes of Yb were used as a source of Yb^+. We have demonstrated that it is possible to laser cool a natural isotope mixture of Yb^+ [62]. This is the other main subject of this thesis.

Owing to the suitability of Yb^+ for use in a frequency standard, as described, its potential for a frequency standard has been extensively investigated. Using buffer-gas-cooled $^{171}Yb^+$, the performance of a prototype microwave frequency standard has been investigated by Tamm et al. at PTB [63] and by Fisk et al. at CSIRO [33,64]. In the optical region, spectroscopy and wavelength measurements of the $^2F_{7/2}$ - $^2D_{5/2}$ transition at 3.43 μm were performed by Bell et al. at NPL for $^{172}Yb^+$ in the presence of buffer gas [65]. Using laser-cooled Yb^+, a wavelength measurement of the $^2S_{1/2}$ - $^2D_{5/2}$ transition at 411 nm was carried out by Gill et al. at NPL [66]. Recently, this value was improved by Taylor et al. using a single ion and the quantum jumps [67]. The $^2S_{1/2}(F=0)$ - $^2D_{3/2}(F=2)$ clock transition at 435 nm of $^{171}Yb^+$ was observed by Engelke and Tamm at PTB [68]. The very weak octupole transition of $^2S_{1/2}$ - $^2F_{7/2}$ at 467 nm was recently successfully driven by Roberts et al. at NPL [69].

The growing interest in establishing a new frequency standard using the transitions of Yb^+ demands a deeper understanding of the characteristics of Yb^+. We believe that the present work contributes to this aim. For example, our discovery of YbH^+ production [70] may

present a problem in using buffer-gas-cooled Yb^+ in a frequency standard because it is difficult to remove H_2 gas in the presence of buffer gases. The establishment of optical methods for deexcitation of the $^2F_{7/2}$ state [71] is an important step toward the realization of an optical frequency standard using the $^2S_{1/2}$ - $^2D_{3/2}$ transition or $^2S_{1/2}$ - $^2F_{7/2}$ transition as a reference [66,67,69].

1.3. Outline of Present Work

As described in the previous section, the main themes of this thesis are the elucidation of the characteristics of Yb^+ in the presence of buffer gases and laser cooling of Yb^+ from a natural isotope mixture.

For the former, in Chapter 4, we describe our observations concerning fluorescence decay and rf signal disappearance, and how we have been approaching to a complete understanding of these phenomena. After our first observation of rf signal disappearance [57,58], we found that the disappearance of rf signals was caused by some background gases [72]. This proposal was supported by our observation that the disappearance of rf signals was enhanced with the introduction of O_2 or H_2O gas into the vacuum chamber [73]. We observed that the resonance point of the rf signals shifted toward that of heavier mass before they finally disappeared. Therefore, we suggested the possibility of the production of molecular ions via a chemical reaction of Yb^+ in excited states with background gases. As a related observation, Seidel and Maleki recently conjectured the possibility of the formation of molecular ions, based on their observations with continuous driving of the $^2S_{1/2}$ - $^2P_{3/2}$ transition [74].

In order to conduct a quantitative study of the disappearance of rf signals, we developed a mass-selective ionic detection system by combining a quadrupole mass analyzer with our rf trap. First, we found that YbH^+ was produced by chemical reaction of Yb^+ in excited states with H_2 gas [70]. The production of YbH^+, which should be considered to be different from our former proposal of molecular-ion formation, is one of the causes of fluorescence decay. We found that some observations formerly interpreted to be associated with Yb^+ in the $^2F_{7/2}$ state are actually caused by YbH^+. We overlooked the YbH^+ production by confusing it with population trapping in the $^2F_{7/2}$ state, as did other researchers [70].

Second, in the presence of O_2 gas, we found that YbO^+ and some other molecular ions were produced from Yb^+ in excited states, which proved our proposal of molecular-ion production [49]. The number of YbO^+ ions did not show a significant decrease from that of initially trapped Yb^+ ions, even after the rf signals disappeared. Therefore, we need explanations of the rf signal disappearance other than the decrease of the total number of trapped ions [49].

For the latter subject, i.e., laser cooling of Yb^+, Chapter 5 describes that it has been performed using a natural isotope mixture of Yb as a source of Yb^+ ions [62], unlike in other laboratories. Under ordinary trapping parameters, all isotopes of Yb^+ are trapped simultaneously. Owing to the isotope shift of the cooling transition, however, only one of the isotopes can be laser cooled. On the other hand, heating power due to rf heating is a function of the total number of trapped ions. In addition, owing to Doppler broadening of the spectra before the start of laser cooling, the spectra of isotopes overlap and there is the possibility of laser heating of some isotopes. To avoid this difficulty, we carefully set the

21

frequencies of the two cooling lasers.

Here, we outline the content of each chapter. In Chapter 2, we describe the experimental setup used for investigation of Yb^+. We introduce the theory of rf traps in more detail than that described in this chapter. Then, we describe our rf traps. We use two sizes of rf trap. The larger one of $2r_0 = 22.6$ mm [75] is used for investigations of buffer-gas-cooled Yb^+, and the smaller one of $2r_0 = 5$ mm, for laser-cooled Yb^+ [62]. In the case of the larger trap, we were able to detect rf signals of trapped ions. We paid particular attention to anharmonic oscillation of trapped ions [76]. A harmonic oscillation of trapped ions is well known in the case of Penning traps [77]. In the case of rf traps, however, there were no detailed observations in literature when we investigated this phenomenon. Investigation had been conducted using Ba^+ before we started our Yb^+ work. The trap used was the same as the larger trap for Yb^+. We found that the shapes and sizes of rf signals changed as a function of the pressure of buffer gases, even when the same number of ions were trapped [76]. Also, we later found that the change of rf signals occurred as a function of the number of trapped ions at a fixed buffer gas pressure [73]. RF signals are conventionally used to determine the absolute or relative number of trapped ions [75,78]. However, our observation indicates that care must be taken when estimating the number by using rf signals [76].

In Chapter 3, we describe our light sources for Yb^+. We first produced radiation at 369.52 nm to drive the $^2S_{1/2}$ - $^2P_{1/2}$ transition using simple and inexpensive methods, i.e., sum-frequency mixing of diode-laser and argon-ion-laser radiation [79]. We demonstrated a simple method of stabilizing sum frequency, i.e., stabilization of sum or difference frequency by controlling only one of the fundamental lasers of

mixing [80]. We found that we needed more power for laser cooling. Therefore, we generated another UV beam by SHG of dye-laser radiation by an external cavity technique [62]. We describe its performance. To laser cool Yb^+, the $^2D_{3/2}$ metastable state must be depleted. For this purpose, we generated radiation at 935 nm using a ring $Ti:Al_2O_3$ laser. We found that setting the frequency of cooling lasers was important due to the isotope shifts because we used a natural isotope mixture of Yb^+. The isotope shifts of the $^2D_{3/2}$ - $^3[1/2]^o_{1/2}$ transition were not measured for even isotopes of Yb^+. Therefore, we measured them by installing a rough frequency scanning system made by us into the $Ti:Al_2O_3$ laser [62].

In Chapter 4, we present the characteristics of Yb^+ stored in a rf trap in the presence of buffer gases. We first describe the observed spectra of the $^2S_{1/2}$ - $^2P_{1/2}$ transition [57]. Then, we proceed to one of the main themes of this thesis, i.e., investigation of the characteristics of Yb^+ in the presence of buffer gases with continuous irradiation at 369.52 nm to drive the $^2S_{1/2}$ - $^2P_{1/2}$ transition. First, we present our original observation of the disappearance of rf signals [57]. Then, we describe our observation that the disappearance of rf signals should be caused by some background gases, and that it should be possible to produce molecular ions by chemical reaction of Yb^+ in the excited states with some background gases while rf signals disappear [72]. These proposals were supported by the observation that the disappearance of rf signals was enhanced with the introduction of O_2 or H_2O gas [73].

We developed a mass-selective ionic detection system of trapped ions to clarify the reason for rf signal disappearance, including confirmation of molecular ion production. Section 4.4 describes the results obtained by mass-selective detection and includes a discussion of them [49,70]. In Sec. 4.5, we present our current interpretation of the

cause of fluorescence decay and the disappearance of rf signals. We also present prospects for these phenomena, in particular, we mention that the production of molecular ions as an obstacle to establishing of a new frequency standard using buffer-gas-cooled Yb^+ [70].

Chapter 5 is devoted to the other main theme of this thesis, i.e., laser cooling of Yb^+. Unlike in other laboratories where laser cooling of Yb^+ is performed, we have succeeded in laser cooling Yb^+ using a natural mixture of Yb as a source [62]. We found that it is possible to laser cool and observe single $^{174}Yb^+$ ions even from a natural isotope mixture [49]. We must compensate unexpected DC field, as is often the case with other laboratories. We describe our compensation characteristics and our estimation of the temperature obtained after compensation. Saturation of fluorescence intensity is also observed. To measure the number of trapped Yb^+ ions, we observed the sudden drop of the fluorescence intensity, or quantum jump signals, by electron shelving of individual ions to the $^2F_{7/2}$ state [62]. To observe the quantum jump signals repeatedly, we must deexcite the $^2F_{7/2}$ state to the $^2S_{1/2}$ ground state because the lifetime of the $^2F_{7/2}$ state is extremely long. We found that several transitions can be used for this purpose [71].

Chapter 6 gives conclusions of our work.

Chapter 2

RF Traps,

and

Detection of Trapped Ions by

RF Resonance Absorption Method

2.1. Introduction

In this chapter, we describe the experimental setup of rf traps used for investigation of Yb^+ stored in them, and the results obtained by detection of trapped ions by rf resonance absorption methods.

After we introduce an theory of the rf trap in Sec. 2.1, we describe our setup of two rf traps with different sizes in Sec. 2.2. The bigger one has a dimension of $2r_0 = 22.6$ mm [1-7] and is used for investigation of the characteristics of Yb^+ in the presence of buffer gas, the smaller one of $2r_0 = 5$ mm for laser cooling of Yb^+ in an UHV condition [8].

As a first step, it must be checked that ions are certainly confined in the trap. We performed rf resonance absorption methods for this purpose. RF resonance absorption signals (rf signals) are caused by the fact that trapped ions absorb rf electric power, of which frequency is coincident with that of ion motion, i.e., secular motion in rf traps. This is a simple method for detecting trapped ions because no lasers are required. This method allows us to detect only a single charged particle in the case of
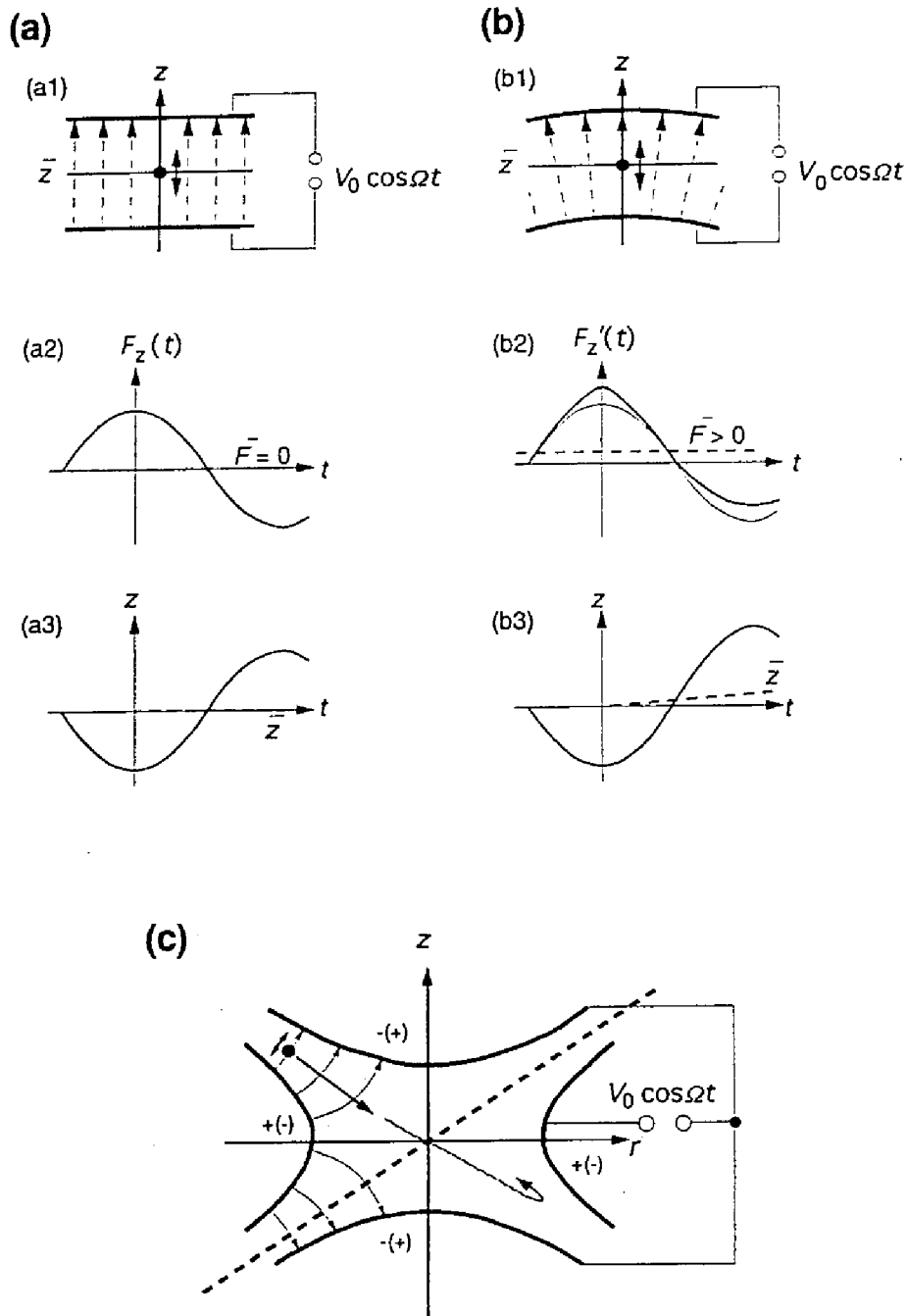
Fig. 2.1.   Principle of rf trap. (a) RF electric field is applied between two parallel conductive plain. The averaged position, or guiding center of the charged particle, $\bar{z}$, does not changed due to the homogeneity of the rf field. (b) In the case of an inhomogeneous rf field, a nonvanishing average force, $\bar{F}$, arises, which points towards the region of weaker fields. (c) The cross section of rf trap with the plain along the z-axis. If we divide this figure into two parts by the dashed line, we can undarstand that the inhomogeneous rf field exists in each part, and that an average force always points the weakest field, i.e., the center of the trap.

Penning traps and is applied to precise mass measurements [9]. In the case of rf traps, however, a large number of ions are required for detection. This is caused by background noise from rf driving field. We applied rf resonance absorption method only for the large trap of $2r_0 = 22.6$ mm, where the number of trapped ions was $10^5 \sim 10^6$.

Not only for detecting trapped ions, one can use rf signals but also for estimation of the number of them [1,10]. When the number of trapped ions is estimated from rf signals, it is assumed that the center of mass of trapped ions oscillates in a manner of a perfect harmonic motion. Actual ion motion, however, has a small deviation from harmonic and shows characteristics of anharmonic oscillation [3,9]. Anharmonic oscillation causes shift and hysteresis of the resonance frequency. We investigated the effect of anharmonic oscillation on rf signals in detail as described in 2.3.2. The investigation of the anharmonic oscillation was made using Ba^+ ions before we started studying Yb^+ ions. We used the same trap for investigation of buffer-gas-cooled Yb^+ ions as used for Ba^+ ions. Therefore, the anharmonicity of the trap itself was the same in the experiments of the two ions.

2.2. RF Traps

2.2.1.   Theory of RF Traps

In this subsection, we present a principal of trapping of a charged particle in rf traps. We first make a qualitative explanation of it according to the discussion made by Dehmelt [11], referring to Fig. 2.1. We assume that a charged particle is placed between two parallel conductive plain plate. If we apply a rf voltage between the two plate, the charged particle oscillates with the frequency of the rf voltage in the homogeneous rf

electric field. The position averaged over 1 cycle of the rf voltage does not change in this case (Fig. 2.1(a)). However, in the case that the two plates are not parallel plain, the averaged position of the charged particle drifts toward the region of a weaker field (Fig. 2.1(b)). Figure 2.1(c) shows the cross section of the rf trap with the plain along the z-axis. If we divide the figure into two parts by the dashed line shown in Fig. 2.1(c), we can understand a non-uniform rf electric field explained with Fig. 2.1(b) exists between the ring electrode and one of the endcap electrodes in each parts. Therefore, if we put a charged particle at the place where the distance between the ring electrode and one of the endcap electrodes is narrow, the charged particle drifts toward the trap center where the field is the weakest. The situation is the same in the other divided part in Fig. 2.1(c) because the center of the trap is a point of symmetry for the two parts. Therefore, the charged particle always receives a force toward the center of the trap. The trap is figures of revolution about z-axis. Therefore, restoring force to the center of the trap acts on the charged particle in all directions, and thus the charged particle is confined in the rf trap.

We next show a principle of the rf trap more quantitatively [11,12]. Between the endcap and ring electrodes, rf driving field of an amplitude V_{ac} and of a frequency $\Omega/2\pi$ superimposed dc voltage V_{dc} is applied, i.e.,

$$V_0 = V_{dc} + V_{ac} \cos \Omega t . \tag{2.1}$$

The equations of motion of a single charged particle of a rf trap are given by

$$m \frac{d^2}{dt^2} \begin{bmatrix} r \\ z \end{bmatrix} = e \frac{V_{dc} + V_{ac} \cos(\Omega t)}{2r_0^2} \begin{bmatrix} r \\ -2z \end{bmatrix}, \tag{2.2}$$

where m the mass of a ion, and e the charge of an ion. Introducing dimensionless constants

$$a_z = -2a_r = \frac{8eV_{dc}}{mr_0^2\Omega^2}$$ (2.3)

and

$$q_z = -2q_r = -\frac{4eV_{ac}}{mr_0^2\Omega^2},$$ (2.4)

and transforming the time scale

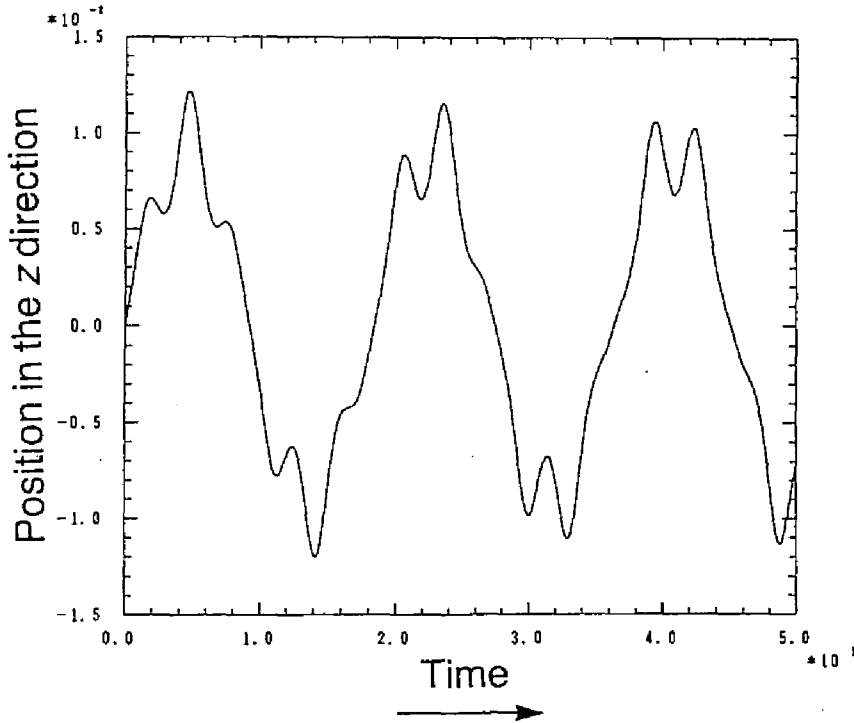$$\tau = \frac{1}{2}\Omega t,$$ (2.5)

Fig. 2.2. Motion of a charged particle stored in the rf trap. The parameters of a_z and q_z were 0.524 and -0.0294, respectively.

29

we obtain Mathieu-type equations given by

$$\frac{d^2}{d\tau^2}\begin{bmatrix} r \\ z \end{bmatrix} + \begin{bmatrix} a_r - q_r\cos(2\tau) \\ a_z - q_z\cos(2\tau) \end{bmatrix}\begin{bmatrix} r \\ z \end{bmatrix} = 0.$$ (2.6)

An example of the ion trajectory, numerically calculated from Eq. (2.6), is shown in Fig. 2.2. The solutions of Eq. 2.6 $u(\tau)$ ($u(\tau) = r(\tau)$, $z(\tau)$) are represented as Fourier series of frequencies $\omega_{ni} = n \pm \omega_{0i}$ ($i = r, z$):

$$u(\tau) = A_M \sum_{n=-\infty}^{\infty} C_{2n}\cos(2n + \beta_i)\tau + B_M \sum_{n=-\infty}^{\infty} C_{2n}\sin(2n + \beta_i)\tau.$$ (2.7)

where β_i and ω_{0i} are given by

$$\beta_i^2 = a_i + \frac{1}{2}q_i^2$$ (2.8)

and

$$\omega_{0i} = \frac{1}{2}\beta_i\Omega,$$ (2.9)

respectively, n is an integer, the parameters A and B are functions of the initial condition, and C_{2n} depends on a_i and q_i. Only for certain ranges of the parameters of a_i and q_i, the eigensolutions are stable. The stability diagram of Mathieu's equation is shown in Fig. 2.3, This is the first region of stability and is usually used. A simplified approximate solution is obtained when β_i and q_i are small, $a_i << q_i$, and the secular motion is much slower than the micromotion:

$$u(t) = A_M'\left[1 - \frac{1}{2}q_i\cos(\Omega t)\right]\cos(\omega_{0i}t),$$ (2.10)
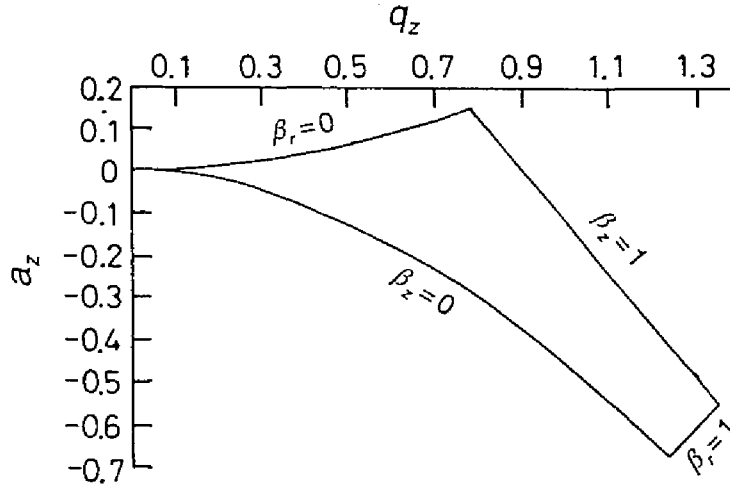
30

Fig. 2.3.   Stability diagram of Mathieu's equation. The region bounded by the solid curve shows the value of a_z and q_z with which the eigensolution is stable.

where A'_M is a functions of the initial condition. The depth of the effective psuedopotential well $eD_{\text{eff},i}$ ($i = r, z$) is given by

$$eD_{\text{eff},r} = \frac{1}{8}m\Omega^2\beta_r^2 r_0^2,$$

(2.11)

and

$$eD_{\text{eff},z} = \frac{1}{8}m\Omega^2\beta_z^2 z_0^2.$$

(2.12)

Ifflander and Werth calculated and experimentally confirmed the optimum parameters in the stability diagram for increase of the number of trapped ions as many as possible, and their experimental results were a_z = -0.03 ± 10 %, and q_z = 0.55 ± 15 % [13]. We usually set our trap parameters close to these values when we used a large trap of $2r_0$ = 22.6 mm.

2.2.2. Details of our RF Traps

We used two setups of rf traps. A larger trap of $2r_0 = 22.6$ mm [1-3] was used for investigation of buffer-gas-cooled Yb^+ [4-7], and a smaller one of $2r_0 = 5$ mm for laser cooling of it [8].

(1) A trap of $2r_0 = 22.6$ mm for buffer-gas experiment

The trap which we used for investigation of buffer-gas-cooled Yb^+ had been fabricated to confine N_2^+ ions [1], and was later modified to store Ba^+ ions and to allow us to observe the fluorescence of trapped ions [2]. The dimensions and the typical operating parameters of the trap are listed in Table 2.1. The ring electrode and one of the endcap electrodes were made of aluminum. The other endcap electrode was made of mash coated with gold to observe the fluorescence of trapped ions through it. The surfaces of the electrodes were shaped in hyperboloid. The ring electrode had four holes at the plane $z = 0$. One of the hole was used for introduction of an atomic beam, and two of them were for passing a laser beam through the center of the trap.

The ions were produced inside the trap by electron impact ionization of neutral atoms introduced from an oven. The oven was made of boron nitride, respectively. A tungsten wire wound directly on the oven, and the oven had a ditch on the surface to fix the wire. With applying a current to the wire, we heated the oven. The temperature of the oven was measured by a thermocouple attached to the bottom of the oven. The electron source was a hot tungsten filament located outside the solid endcap electrode. The electrons were introduced into the trap through a small hole made at the center of the endcap electrode. The filament was biased to -150 V to produce Yb^+ ions.

The trap, the oven, and the electron source were placed in a

Table 2.1.   Dimensions and typical parameters of rf Trap of $2r_0 = 22.6$ mm

Axial dimension	$z_0 = 8.0$ mm
Radial dimension	$r_0 = 11.3$ mm
Probing voltage	$v_0 = 1$ mV
Series resister of probing voltage	$R_f = 2$ MΩ
Admittance of LC circuit at resonance	$G_0 = 1.5 \times 10\text{-}6\ \Omega^{-1}$
Background pressure	$<1 \times 10^{-7}$ Pa

For Ba⁺

AC voltage	$V_{ac} = 285$ V
DC voltage	$V_{dc} = 4 - 6$ V
Driving AC frequency	$\Omega/2\pi = 550$ kHz
Probing frequency	$\omega_p/2\pi = 86$ kHz
Oven temperature	470 °C

For Yb⁺

AC voltage	$V_{ac} = 310$ V
DC voltage	$V_{dc} = 4 - 6$ V
Driving AC frequency	$\Omega/2\pi = 550$ kHz
Probing frequency	$\omega_p/2\pi = 83.5$ kHz
Oven temperature	340 °C
Acceleration voltage of an electron gun	150 V

UV beam at 370 nm[*]
  power
  beam size
	
	16 μW
	2 mm × 2 mm

[*) in the case of second-harmonics of dye-laser radiation using an external cavity technique (see. Sec. 3.4).

vacuum chamber evacuated by an ion pump of a evacuation speed of 32 ℓ/s (Ulvac PST-2AT). The pressure was determined from the discharge current of the ion pump. We later introduced a nude Bayard-Alpert gauge when we started mass-selective ionic detection described in Sec. 4. 4 [14]. The background pressure was below 1×10^{-7} Pa and 5×10^{-7} Pa with the oven and electron gun off and on, respectively. The vacuum chamber had two inlets of gas introduced through variable leak valves. One of the inlets was used for He and N_2 gas, and the other for H_2, O_2, and H_2O gas. (The variable leak valves used were Ulvac VAV-3 for the former inlet, and Anelva 951-7172 for the latter one.)

The fluorescence was detected by a photomultiplier (Hamamatsu R464). The output signal of the photomultiplier was measured by a system of photon counting (Hamamatsu C1230) with a gate time of 1 s and a dead time of 2 ms. The overall detection efficiency was 2.7×10^{-4}.

When we investigated trapping of Ba^+ ions, we observed that Ba^+ ions were produced just by heating the oven without turning on the electron source. Sankey and Madej reported this phenomenon and found that this was caused by the fact that the electrons generated in the oven by thermal ionization were introduced into the trap [15]. We confirmed that the electron emission was certainly generated from the oven also in our case. However, we did not observe this phenomenon in the case of Yb^+ ions. We must turn on the electron source to produce Yb^+ ions.

(2) A trap of $2r_0= 5$ mm for laser cooling experiment

For laser cooling experiment, we constructed a smaller rf trap than that used for buffer gas experiment. The inner surfaces of this trap was machined with conical cuts. Beaty investigated the electric potential produced by the electrodes with conical cut and determined several

dimensions for a small anharmonicity [16]. We adopted Case 6 in Table I in Ref. [16]. The dimensions and the typical operating parameters of the trap are listed in Table 2.2. A picture of this trap is shown in Fig. 2.4. The electrodes and the insulators between the electrodes were made of phosphor bronze and pure boron-nitride, respectively. No holes were made in the electrodes. Therefore, a laser beam, an electron emission, and an atomic beam were introduced from the gap between the electrode. The fluorescence of trapped ions was observed also through the gap.

Yb^+ ions was produced again by electron impact ionization. For laser cooling, to avoid heating by collision with neutral Yb atoms or accelerated electrons, it is desirable to reduce heat capacities of the oven and the electron source as small as possible. Therefore, we adopted simple configurations of them. The electron source was a tungsten filament of a diameter of 0.15 mm at the ground potential. Neutral Yb vapor was

Table 2.2   Dimensions and typical parameters of rf Trap of $2r_0 = 5$ mm

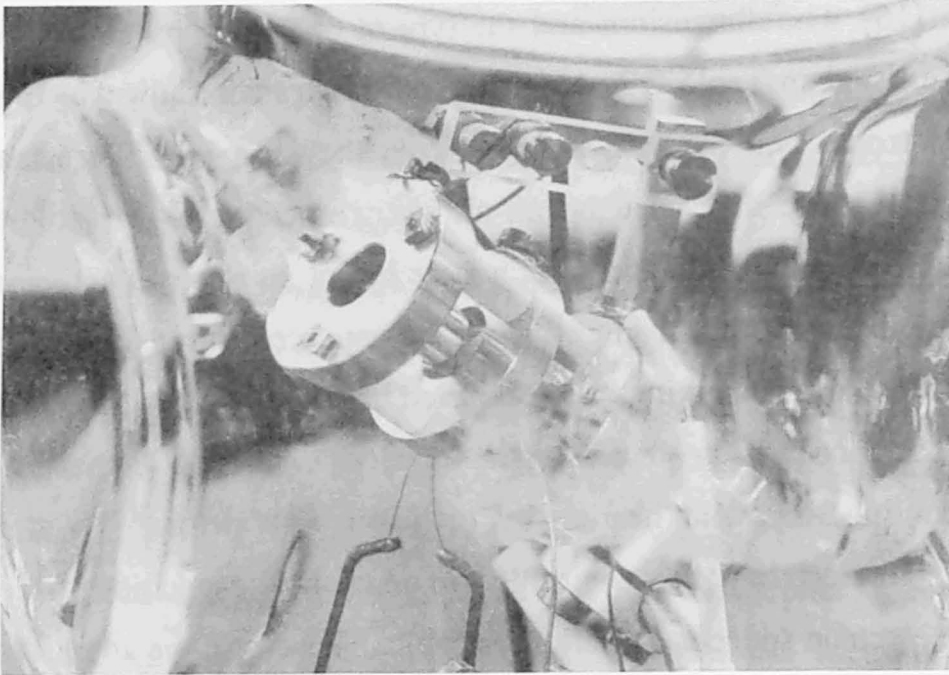|	
Axial dimension	$z_0 = 1.77$ mm
Radial dimension	$r_0 = 2.5$ mm
Driving AC frequency	$\Omega/2\pi = 2.2$ MHz
Background pressure	$<3 \times 10^{-8}$ Pa
Storage time of	< 1 min
uncooled Yb^+	
UV beam at 370 nm	
power	$70 \sim 350$ μW
beam size	20 μm $\times$ 70 μm
IR beam at 935 nm	
power	$30 \sim 40$ mW
beam diameter	>1 mm

35

Fig. 2.4.   A picture of a rf trap of $2r_0 = 5$ mm used for laser cooling of Yb$^+$.

generated from a piece of Yb metal attached to a hot tantalum wire of a diameter of 0.4 mm. The distances from the gap of the electrodes to the tungsten filament or the Yb piece were about 5 mm.

The trap, the oven, and the electron source were placed in a vacuum chamber evacuated by an ion pump of a evacuation speed of 60 ℓ/s (Anelva 912-7160). The pressure was determined from the discharge current of the ion pump. The vacuum chamber had a inlets of gas introduced through a variable leak valve (Anelva 951-7172). The He gas was used as a buffer gas for confirming that Yb$^+$ ions were certainly trapped. After we succeeded in laser cooling, no buffer gas was used. The background pressure was below 3×10^{-7} Pa when we first succeeded in laser cooling, and was improved to be below 3×10^{-8} Pa after we started

laser cooling of a small number of Yb$^+$ ions. The improvement was caused by removing a valve between the ion pump and the vacuum chamber. However, we observed a slow increase in the vacuum pressure after we baked out the whole vacuum system. (We continued baking for two days or more at a temperature of 250 °C at the ion pump.) Therefore, we baked it again (once in a few month) when the vacuum pressure reached 6×10^{-8} Pa. The storage time of uncooled Yb$^+$ was only 1 minute at $q_z = 0.53$ and $a_z = -0.03$ with no buffer gas.

The fluorescence of trapped ions was collected and focused on a pinhole with a diameter of 400 μm to minimize a stray light, and then detected by a photomultiplier of which the output was measured by the same system of photon counting as used for the large trap. Overall detection efficiency of the fluorescence was 1×10^{-4}. The numerical aperture of the gap between the electrodes, through which we observed the fluorescence, limited the detection efficiency.

2.3. RF Resonance Absorption Methods

In this section, we describe our results of rf resonance absorption methods. We first present a general principal of rf resonance absorption methods in 2.3.1. Then, we proceed to showing our results. We concentrated on investigating anharmonic oscillation of trapped ions. We describe the observations and discussion of it in detail in 2.3.2.

2.3.1 Principals of RF Resonance Absorption Methods

In this subsection, we describe a general principle of rf resonance absorption methods. Figure 2.5 shows schematic diagram of detection

PROBING VOLTAGE
$V_o \cos \omega_p t$

FREQUENCY SYNTHESIZER

R_f

v_1

$V_{dc} + V_{ac} \cos \Omega t$

DRIVING OSC.

G_0
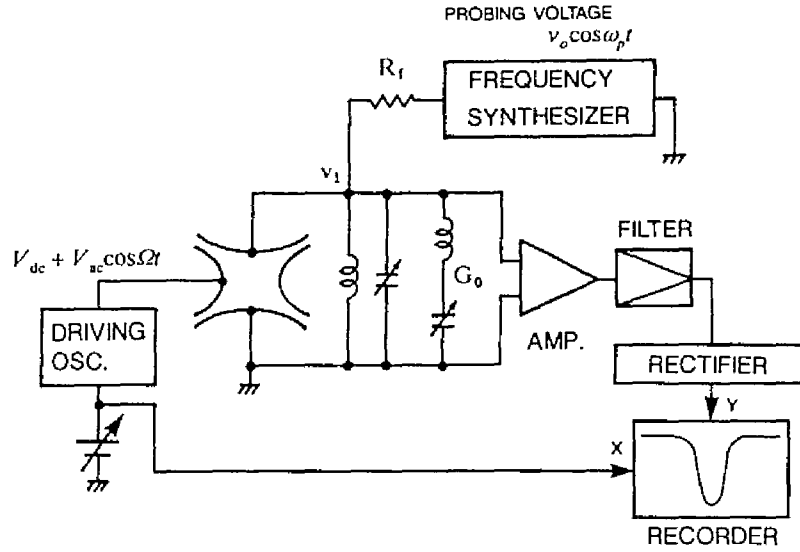
AMP.

FILTER

RECTIFIER

Y

X

RECORDER

Fig. 2.5.   Block diagram of the detection of rf signals

system of rf signals. Trapped ions absorb rf electric power of which frequency is in accordance with that of the secular motion. Therefore, if the proving rf electric power is provided through a high-resistance resister, the decrease in the amplitude at the parallel resonance circuit, v_1, is observed, when trapped ions absorb the proving rf electric power.

RF signals can be obtained by three methods, i.e., the sweep of the trapping dc voltage, of the trapping ac voltage (in other word in this thesis, rf driving voltage) and of the probing rf frequency. The total number of trapped ions N_0 are proportional to the product of the relative signal height Y_{max} and the FWHM of the signals $\Delta \omega$ taken by the frequency sweep of the probing rf electric field [1,10], i.e.,

$$N_0 = Y_{max} \cdot \Delta \omega \left(\frac{4mz_0^2}{\alpha_{ed}^2 e^2} \right) \left(G_0 + \frac{1}{R_f} \right) \left(\frac{1}{b} \right),$$ (2.13)

38

where Y_{max} and b are defined by

$$Y_{max} = \frac{v_{10} - v_{1min}}{v_{10}}$$ (2.14)

and

$$b = \sqrt{\frac{2 - 1,5Y_{max}}{2 - 0.5Y_{maz}}},$$ (2.15)

where v_1 is the amplitude of the probing voltage applied on the endcap electrodes, v_{10} the value of v_1 when no ions are trapped, v_{1min} the minimum value of v_1 at resonance when the ions are trapped, α_{ed} a compensation factor due to the fact that the electrode surfaces are not parallel, and G_0 the admittance of the LC circuit at resonance. It is known that the product of the relative signal height and the FWHM of a signal is proportional to the total number of trapped ions for the trapping dc voltage sweep as well as the probing frequency sweep [17]. In rf resonance absorption methods, it is assumed that the trapped ions oscillate in a perfect harmonic potential well. However, the potential produced by a laboratory trap usually has a small deviation from the harmonic, and the trapped ions show the characteristics of the anharmonic oscillation [9].

2.3.2. Anharmonic Oscillation of Trapped Ions

(1) Theory

The anharmonicity is caused by a small deviation from the quadrupole potential. The deviation is originated from the fact that the

electrodes are not infinitely-extended perfect hyperbolas of revolution [9]. We assume axial symmetry about the line $r = 0$ and reflection symmetry about the plane $z = 0$. Near the center of the trap, the anharmonicity results mainly from an octopole potential of the forth-order term in the expansion of the solution to Laplace's equation at the center of the trap. This potential is given by

$$\Delta V = \frac{1}{2} V_0 C_4 \left(\frac{\rho}{z_0} \right)^4 P_4 (\cos \theta)$$

$$= \frac{1}{2} V_0 C_4 \left(\frac{1}{z_0} \right)^4 \left[z^4 + 3z^2 r^2 + \left(\frac{3}{8} \right) r^4 \right],$$

(2.16)

where position (ρ, θ, φ) is expressed in spherical coordinates; P_k are the Legendre polynomials, V_0 the potential applied between the ring electrode and the endcap electrodes, and C_k is a constant. The anharmonic oscillation of a single electron in a Penning trap was discussed by Brown and Gabrielse [9], and of many electrons in a Penning trap by Wineland and Dehmelt [18].

For simplicity, only the z-axial secular motion in the pseudopotential well of a rf trap is considered here. Because the ion density was large and ions coupled with each other in this experiment, the ions can be described by the motion of their center of mass which oscillates at the z-axial frequency ω_z which is the spatial average over the ion cloud of the z-axial oscillation frequency shifted by the $z^2 r^2$ term in Eq.(2.16) [18]. The equation of the z-axial motion of the trapped ions is given by

$$m \left[\frac{d^2}{dt^2} + \gamma_z \frac{d}{dt} + \omega_z^2 \left(1 + C_4' \frac{2z^2}{z_0^2} \right) \right] z = \frac{\alpha_{ed} e v_1}{2 z_0} \cos \omega_p t,$$

(2.17)

40

where γ_z is the damping constant, and ω_p the frequency of the probing field. This equation describes the observable anharmonicity for the secular motion. The relation between ΔV and the observable anharmonicity should be checked. Therefore, C_4 was adjusted to C_4'.

Anharmonic oscillation expressed like Eq. (2.17) shows hysteresis with direction of frequency sweep of the external force, i.e., sweep of ω_0 here.

The resonance frequency (for the sweep direction f in this work) of the anharmonic oscillation shifts from that of the harmonic oscillation. The resonance frequency shift $\Delta\omega_z$ between the resonance frequency of the anharmonic oscillation and that of the harmonic oscillation is given by [9,18,19]

$$\frac{\Delta\omega_z}{\omega_z} \approx \frac{3}{2} C_4' \frac{E_z}{m\omega_z^2 z_0^2} \qquad (2.18)$$

where E_z is the time-averaged energy in the axial oscillation of the center of mass. In the case of large anharmonicity, the difference of the frequency at the peak of the signals between the two sweep directions can be used as an approximation of $\Delta\omega_z$, because the frequency difference between ω_z and the frequency at the peak of the signals for the sweep direction of the lower signal height (the sweep direction r in this work) is small and negligible as compared with the large frequency difference between ω_z and the shifted resonance frequency for the other sweep direction (the sweep direction f in this work).

(2) Pressure dependence of anharmonic oscillation of trapped ions [3]

(2.1) Results

We investigated anharmonic oscillation by using Ba^+ ions trapped in the large rf trap of $2r_0 = 22.6$ mm. The operating parameters are listed in Table 2.1. The dc voltage sweep was mainly used for detection of rf signals in this experiment.
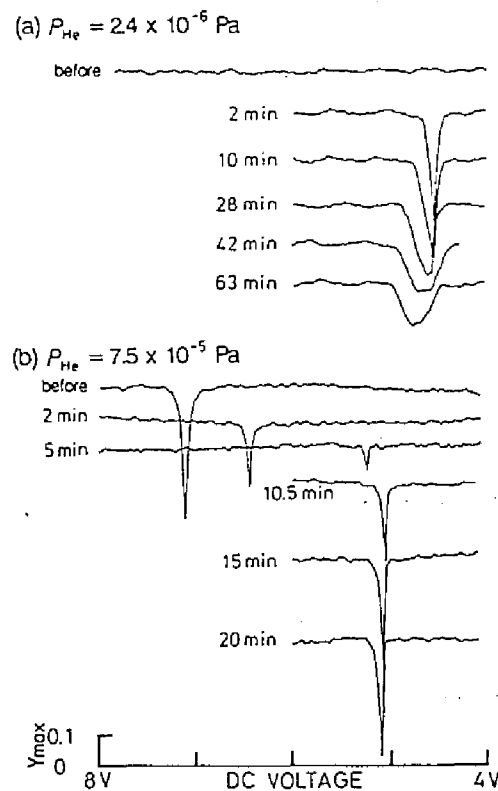

Fig. 2.6. Change of the signals after the oven and the electron gun were turned off. (a) $p_{He} = 2.6 \times 10^{-6}$ Pa, sweep direction f. (b) $p_{He} = 7.5 \times 10^{-5}$ Pa, sweep direction r. The time was measured after the oven and the electron gun were turned off. The signal shapes in (b) did not change up to the point at which they could no longer be detected (for several hours, see Fig. 2. 10(a)). The signals which were detected before the oven and the electron gun were turned off are also shown as "before". It is noted that no signals were detected at $p_{He} < 4 \times 10^{-6}$ Pa when the oven and the electron gun were operating [2].

42

Figure 2.6 shows the time variance of rf signals after the oven and the electron gun were turned off. The time measurement began after the oven and the electron gun were turned off. At a low He pressure, the signal shapes gradually changed over the period from 1 to 2 h as shown in Fig. 2.6(a). Therefore, we waited for over 2 h when we made experiments at a low He pressure. At the higher He pressure, the time until equilibrium was reached was shorter. For example, it took about 15 min at 7.5×10^{-5} Pa. This is shown in Fig. 2.6(b). This shorter time to the equilibrium can be explained by the collision rate of Ba^+ and He [2]. In both cases, large differences in rf signals (e.g., difference in the resonance dc voltage, the fact that no signals were detected at a He pressure below 4×10^{-6} Pa) were observed whether the oven and the electron gun were operating or not. In the case of Yb^+ ions, we could detected rf signals only at a He or N_2 pressure over 1×10^{-4} Pa after the oven and the electron gun were turned off. The period required for the equilibrium was about 5 min. The change in the resonance dc voltage just after the oven and the electron gun were turned off, was much smaller in the case of Yb^+ ions than that observed in Ba^+ ions.

To compare the effect of the pressure of buffer gases on rf signals, the total number of trapped ions should be the same in each measurement. Therefore, all measurements were accomplished after just one ion loading. The procedure of the experiment is described as follows: (i) The oven and the electron gun were turned on to prepare the trapped ions. (ii) The oven and the electron gun were turned off. (iii) The detections started 2 h 30 min after the oven and electron gun had been turned off. This waiting time was needed until size and shapes of rf signals became stable in each detection. (iv) The signals were taken for both sweep directions at one pressure of the He gas. (v) The pressure of the He gas was increased. (vi) Steps (iv) and (v) were repeated from the lowest He pressure until the He pressure reached 2.1×10^{-4} Pa.

Typical rf signals are shown in Fig. 2.7. The upper trace shows the signal which was taken when the dc voltage was swept from a high voltage to a low voltage (sweep direction f) and the lower trace from a low voltage to a high voltage (sweep direction r). The sweep rate is 0.064 V/s in both sweep directions.

The relative signal height Y_{max} and the FWHM of the rf signal as a function of the pressure of the He gas are plotted in Fig. 2.8(a) and (b), respectively. The resonance dc voltage vs. the pressure is shown in Fig. 2.8(c).

All detections in Figs 2.7 and 2.8 (steps (iv) - (vi)) were completed for 8×10^3 s after the ions were produced. Because this time was much shorter than the storage time of 1.3×10^5 s (see (3) in this subsection), almost the same number of the trapped ions were detected in the experiment shown in Fig. 2.7 and in Fig. 2.8. Therefore, Y_{max} and the FWHM changed not by change of the total number of trapped ions, but by the pressure of the He gas.

First, the signal change for the sweep direction f is described. At a low pressure, the signals were much larger than those for the sweep direction r. Y_{max} grew larger and the FWHM became narrower as the pressure of the He gas was increased until the pressure reached the "critical" pressure of 4×10^{-5} Pa. When the pressure was increased beyond the critical pressure, the signal suddenly became smaller, and after a further increase, no signal could be detected.

Second, for the sweep direction r, the signal became large near the critical pressure. Y_{max} still grew larger even beyond the critical pressure, had a maximum value at a certain pressure and then gradually grew smaller as the pressure of He gas was increased.

After the pressure reached 2.1×10^{-4} Pa, the signals continued to be detected as the pressure of He gas was decreased. The signal change shown in Fig. 2.8 was reproduced, although a small decrease of Y_{max} was

44

(a) $P_{He} = 1.3 \times 10^{-5}$ Pa

(b) $P_{He} = 3.3 \times 10^{-5}$ Pa

(c) $P_{He} = 4.2 \times 10^{-5}$ Pa

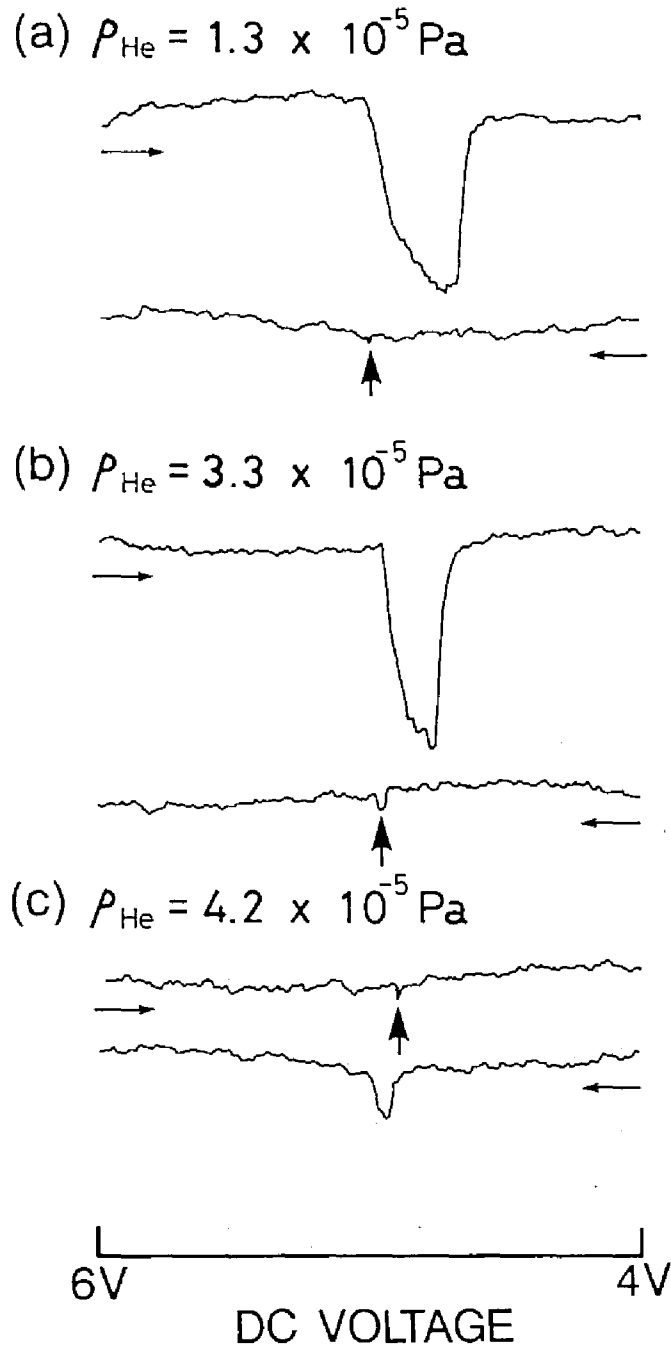6V ──────────────────── 4V
DC VOLTAGE

Fig. 2.7.   Typical rf resonance absorption signals at various pressure of the He gas for approximately equal numbers of trapped ions. The electron gun and the Ba^+ oven were turned off. The upper trace is the signal taken as the dc voltage was swept from 6 V to 4 V (sweep direction f), the lower trace is the signal taken as the dc voltage was swept from 4 V to 6 V (sweep direction r). (a) $p_{He} = 1.3 \times 10^{-5}$ Pa (b) $p_{He} = 3.3 \times 10^{-5}$ Pa, and (c) $p_{He} = 4.2 \times 10^{-5}$ Pa. The sweep rate of dc voltage was 0.064 v/s for both sweep directions.

(a)

RELATIVE SIGNAL HEIGHT Y_{max}

0.2

0.1

0

10^{-6} 10^{-5} 10^{-4} 10^{-3}

HELIUM PRESSURE (Pa)

(b)

FWHM (V)

0.3

0.2

0.1

0

10^{-6} 10^{-5} 10^{-4} 10^{-3}

HELIUM PRESSURE (Pa)

(c)

RESONANCE DC VOLTAGE (V)

5.1
5.0
4.9
4.8
4.7
4.6
4.5

10^{-6} 10^{-5} 10^{-4} 10^{-3}

HELIUM PRESSURE (Pa)
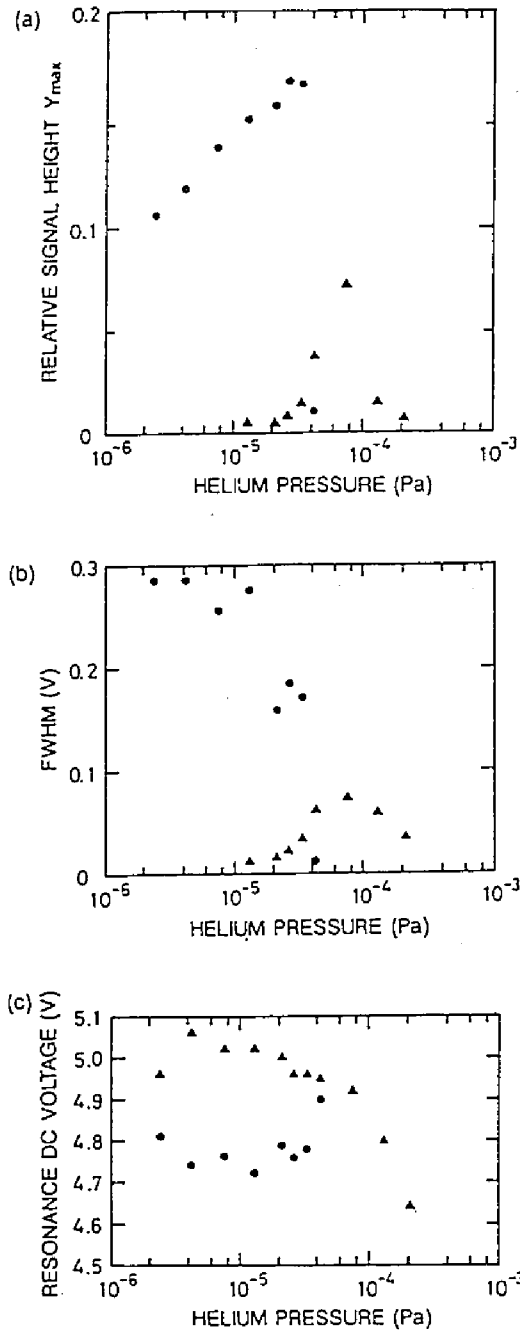
Fig. 2.8.   He gas pressure and sweep direction dependence of (a) the relative signal height of Y_{max}, (b) the FWHM of the signals, and (c) the resonance dc voltage when the same number of trapped ions were detected. ● : sweep direction f ; ▲ : sweep direction r . No ion signals could be detected by the sweep direction f above p_{He} = 4 × 10^{-5} Pa. Signals could be detected by the sweep direction r below p_{He} = 8 x 10^{-6} Pa, but Y_{max} and the FWHM of the signals could not be determined because the signals were too small. The dc voltage sweep of 0.1 V causes the frequency shift of the secular motion of 140 Hz.

46

observed due to the loss of ions from the trap. Therefore, we conclude that the rf signals changed with the pressure of buffer gas and the sweep direction although the total number of trapped ions was almost constant.

To confirm the effect of buffer gas as shown in Fig. 2.8, the same experiment as Fig. 2.8 was repeated many times. The tendency as shown in Fig. 2.8 was always reproduced except that the value of the critical pressure changed from 1×10^{-5} Pa to 1×10^{-4} Pa in each experiment. The observed effect of the He gas on rf signals can be summarized as follows: (1) The signals disappeared for the sweep direction f when the pressure of the He gas was higher than the critical pressure. (2) The change of Y_{max} and of the FWHM of the signals in relation to the pressure of the He gas were different for each of the sweep directions. (3) For the sweep direction f, Y_{max} grew larger and the FWHM of the signals grew smaller as the pressure of the He gas was increased to the critical pressure.

The same phenomena were observed when N_2 gas was used as a buffer gas. It was confirmed that the detection by the probing frequency sweep brought the same result as detection by the dc voltage sweep.

A comparison with the results obtained at slower sweep rate of 0.013 V/s for the sweep direction f is shown in Fig. 2.9. The experimental procedure was the same as that of Fig. 2.8. The detections were made at two sweep rates in turn, at one He pressure [in place of procedure (iv)]. Y_{max} and the FWHM were smaller at a sweep rate of 0.013 V/s than at 0.067 V/s. The sharp transition from resonance to non-resonance was not observed at 0.013 V/s at the He pressure below 1×10^{-5} Pa. (The signal shapes were the same as Fig. 2.6(a) 63 min.) The critical pressure at 0.013 V/s was a little higher than that at 0.067 V/s. For the sweep direction r, Y_{max} at 0.013 V/s was larger than that at 0.067 V/s (still smaller than that for the sweep direction f) and the FWHM at 0.013 V/s was not different from that at 0.067 V/s at every He pressure. The
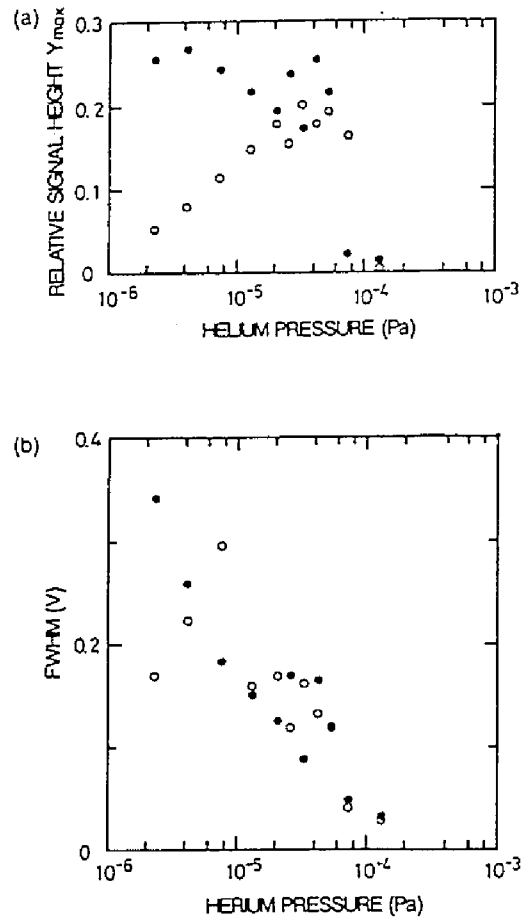
Fig. 2.9. Sweep rate dependence on (a)Y_{max} and (b) the FWHM of signals. ○: at sweep rate of 0.013 V/s. ●: at sweep rate of 0.067 V/s which was the same as that of Figs. 2.7 and 2.8. The sweep direction was f. The sharp transition from resonance to non-resonance was not observed at the He pressure below 1×10^{-5} Pa for a sweep rate of 0.013 V/s.

pressure at the maximum of Y_{max} for the sweep direction r at 0.013 V/s was the same as that at 0.067 V/s.

(2.2) Discussion

The difference of Y_{max} and the resonance dc voltage between the two sweep directions of the dc voltage below the critical pressure can be explained by the anharmonic oscillation. Overlaying the signals for the

48

two sweep directions shown in Fig. 2.7(a) or (b), one sees that the two signals coincide except for the difference of the dc voltage at the sharp transition between resonance and non-resonance. This resonance with hysteresis shows the characteristics of an anharmonic oscillation.

One of the endcap electrodes constructing this trap was made of mesh. This may be the major cause of the anharmonicity. There was the possibility of a small violation of reflection symmetry about the plane $z =$ 0 in this trap construction. In this case, the coefficient C_4 would be modified by including the higher-order even and the odd terms.

The relation between the hysteresis loop and the sweep direction decides the sign of the coefficient C_4' below the critical pressure. Fig. 2.7(a) and (b) show that this trap had $C_4' < 0$. The value of the coefficient C_4' of this trap can be estimated from Eq. (2.18). The frequency difference between the two peaks, obtained from the difference between the resonant dc voltages shown in Fig. 2.8(c), was about 400 Hz at a He pressure lower than 1.3×10^{-5} Pa. We used the empirical expression of $E_z \approx 0.1 \, D_{eff}$ with no buffer gas [20,21]. Because the effective potential of the radial direction is smaller than that of the axial direction [20], E_z was about 1.2 eV for this trap. The C_4' of this trap was estimated from Eq.(2.18) to be about -0.07. This value agrees with that listed in [9] for laboratory Penning traps without anharmonicity compensation. The empirical expression was proved not to be valid in every trapping condition by Siemers et. al. [22]. The calculation shown in [22] or the measurement of the Doppler width of the fluorescence is necessary to determine E_z, i.e., C_4' more precisely.

The difference between the two dc voltages at the signal peak, i.e., $\Delta\omega_z$, decreased as the pressure of the He gas was increased (Fig. 2.8(c)). This result indicates that the trapped ions were cooled by the He gas as expected from Eq.(2.18). Cooling of the trapped ions results in a higher density and a smaller cloud size for the same number of ions. This makes

ω_z or the resonance dc voltage shift due to the change of the space charge effect [11,23] and of the $z^2 r^2$ term effect [18]. By using the resonant frequency (dc voltage) difference between the two peaks, however, these shifts were canceled out and $\Delta \omega_z$ (the resonance dc voltage difference between the peaks) can be compared at various pressures. Compared the resonance dc voltage difference between the two peaks at 3.3×10^{-5} Pa with that at a pressure lower than 1.3×10^{-5} Pa, it was found from Eq.(2.18) that the energy of the trapped ions was reduced to half its value at the pressure lower than 1.3×10^{-5} Pa. (This analysis may be required for a correction. See (4).)

The product of Y_{max} and the FWHM of the signals not constant in Fig. 2.8(a) and (b), although almost the same number of the trapped ions were detected, in contrast to the signals in the harmonic oscillation. Below the critical pressure, however, Y_{max} still gives information concerning the number of the trapped ions even in the anharmonic oscillation, because the maximum amplitude of the anharmonic oscillation is equal to that of the harmonic oscillation [9]. The relation between Y_{max} and the total number of the trapped ions N_0 at slow sweep rate is given by [10,24],

$$N_0 = \gamma_z m \left(\frac{2z_0}{\alpha e} \right)^2 \frac{\frac{1}{R_f} + G_0}{\frac{1}{Y_{max}} - 1}, \qquad (2.19)$$

where R_f is the series resistor of the probing voltage.

Y_{max} grew larger as the pressure of the He gas was increased to the critical pressure as shown in Fig. 2.8(a). From Eq.(2.19), this increase of Y_{max} indicates that γ_z grew smaller because the total number of the trapped ions was almost constant throughout this experiment. This effect

was not clearly observed due to the saturation of Y_{max} at large value, i.e., the large number of ions were trapped [10,24].

We discuss the differences in the results shown in Fig. 2.9 obtained by the two sweep rates. At 0.013 V/s, the sharp transition from resonance to non-resonance was not observed at the He pressure below 1×10^{-5} Pa. This type of signal shape indicates that the ion cloud was spread and the coupling of each ion became weak. This is caused by the larger interaction between the trapped ions and the rf probing field. In Fig. 2.9(a), Y_{max} at 0.067 V/s did not increased as the He pressure was increased, in contrast to Fig. 2.8(a). This fact may be explained by the saturation of Y_{max} or the loss of ions due to the larger interaction with the probing rf field at the slower sweep rate of 0.013 V/s because the detections were made at two sweep rate in turn. The faster sweep rate may be have significant influence on the signals due to the anharmonicity. The detection system should be improved to detect the signals at a higher sweep rate.

The sharp transition from resonance to non-resonance was not observed even at sweep rate of 0.064 V/s when Y_{max} was small (i.e., the number of the trapped ions was small) and the He pressure was low (e.g., Fig. 2.6(a) 63 min). This also indicates the coupling of the ions was weak.

The existence of the critical pressure and the behavior of the signals above the critical pressure are not well understood. We made the following suggestion when this experiment was performed [3]: When the signals were detected above the critical pressure with the oven and the electron gun operating, the signals for sweep direction f did not disappear and showed no difference to the signals for the sweep direction r. This fact suggests that the critical pressure is dependent on the ion distribution, because the ion distribution is considered to be affected by the electrons from the electron gun and from the oven [15] and the neutral Ba from the oven when the oven and the electron gun are operating. One possible

influence on the ion distribution is the high collision rate of Ba^+ and He. Actually, the collision rate of about 4 s at 7.5×10^{-5} Pa is derived from the decay rate of $5^2D_{3/2}$ state measured by Schneider and Werth [25]. A strange distribution of the trapped ions at the high buffer gas pressure of 10^{-3} Pa was also reported [26]. As we will show in (4) in this section, we later found that the total number of trapped ions also influenced in rf signals. Combining the results described here, i.e., the pressure dependence on rf signals, we can suggest that the ion distribution certainly has an effect on rf signals. We will later propose that the dependence of rf signals of the pressure of the buffer gas and the total number of trapped ions may be expressed in the anharmonicity in the space charge potential of trapped ions. We will discuss this in (4) in this section.

(3) Storage-time measurement: an effect of pressure-dependent anharmonic oscillation [3]

As mentioned above, the signal height of the trapped ions changed with the pressure of buffer gas and the sweep direction, although almost the same number of ions were trapped. This means that the highest sensitivity can be obtained by the appropriate choice of the pressure of buffer gas and the sweep direction. The optimum sweep direction can be decided from the sign of C'_4 when the He pressure is below the critical pressure. The dc voltage should be swept from a high voltage to a low voltage when $C'_4 < 0$, and from a low voltage to a high voltage when $C'_4 > 0$. The He pressure should be just below the critical pressure when the trap has anharmonicity with $C'_4 < 0$. The optimum He pressure for the traps with $C'_4 > 0$ should be examined by using another trap with $C'_4 > 0$.

We have applied this idea to the measurement of the storage time of the trapped ions. The result is shown in Fig. 2.10. The time measurement
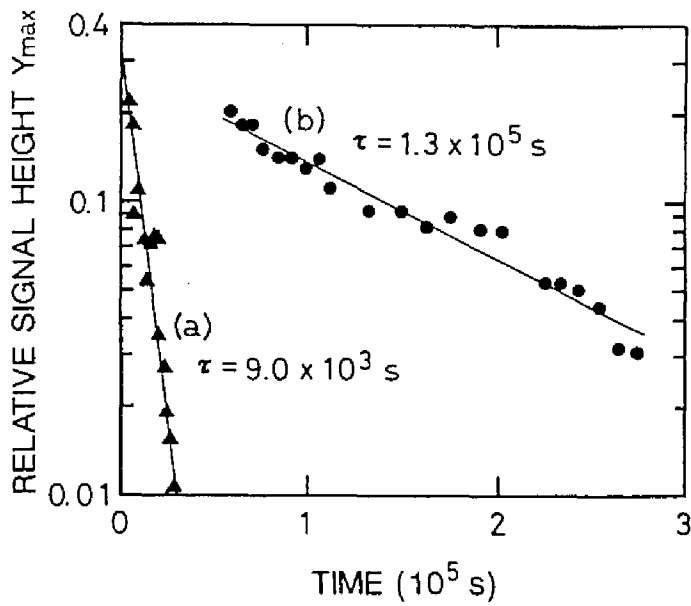
Fig. 2.10. The Decrease of Y_{max} for both sweep directions after ion production was stopped. (a) sweep direction r , p_{He} = 7.5 × 10^{-5} Pa; (b) sweep direction f , p_{He} = 8.4 × 10^{-6} Pa. The He gas pressure was chosen in order to obtain the largest signal-to-noise ratio for each sweep direction. The results in (b) were obtained after the signals in (a) could no longer be detected.

began after the Ba oven and the electron gun were turned off. First, the dc voltage was swept in the sweep direction r (4 V → 6 V), corresponding to the sweep direction of smaller Y_{max} as shown in Fig. 2.7. The highest signal was obtained at a pressure of the He gas of 7.5 × 10^{-5} Pa for this sweep direction. The signal could be detected for 8 h 30 min. This is shown in Fig. 2.10(a).

When the signal could no longer be detected with the sweep direction r, the sweep direction was reversed to direction f (6 V → 4 V) and the He pressure decreased to 8.4 × 10^{-6} Pa to obtain the highest sensitivity for this sweep direction. The signal could again be detected and was observed for 76 h 20 min after the ion production had been stopped.

This is shown in Fig. 2.10(b). In this case, the He gas was introduced to the vacuum chamber only when the signals were taken in order to prevent damage to the ion pump by the He gas due to the expected length of the measurement.

Y_{max} of Fig. 2.10(b) is related to the total number of the trapped ions by Eq.(2.19) because the signals of Fig. 2.10(b) were taken with the sweep direction f below the critical pressure. The saturation of Y_{max} was negligible because the measured Y_{max} was smaller than 0.3 [24]. Therefore, Y_{max} was considered to be proportional to the total number of trapped ions and could be used for the determination of the storage time τ_s defined by exp($-t$ / τ_s). A τ_s value of 1.3 × 10^5 s was determined by least square fitting from Fig. 2.10(b). The change in γ_z was small as the total number of the trapped ions decreased because the pressure of the He gas was the same at every detections. This effect should be considered in a more quantitative discussion

The value of τ_s for Fig. 2.10(a) was also determined to 9.0 × 10^3 s ; it was much smaller than that for Fig. 2.10(b). We had no way of establishing the relation between Y_{max} and the number of the trapped ions in Fig. 2.10(a) because the He pressure was above the critical pressure. The difference in the He pressure and of dc voltage between interrogations (the voltage was kept at the final voltage of the sweep) should be also investigated to explain the difference in τ_s between Fig. 2.10(a) and (b).

(4) Number dependence on anharmonic oscillation of trapped ions [7]

We trapped Yb$^+$ ions in the same trap used for Ba$^+$ ions, and we detected rf signals of trapped Yb$^+$ ions at a He pressure up to 4 × 10^{-4} Pa.

The parameters are listed in Table 2.1. Below 1×10^{-4} Pa, rf signals disappeared after the oven and electron gun were turned off. This was caused by the fact that the number of trapped Yb^+ ions, estimated to be 10^5, was smaller than that in the case of Ba^+ ions. We observed the change in shape and size of rf signals as a function of the pressure of buffer gas. The results were similar to that around the critical pressure in the case of Ba^+: At low pressure, we could detect rf signals only by the sweep direction f. As we increased the pressure of He gas, rf signals for the sweep direction f grew larger and steeper. As we further increased the pressure of He gas, rf signals for the sweep direction f grew smaller and those for the sweep direction r became detectable sizes and then grew larger. The decrease in the height of rf signals for the sweep direction f, observed with increase of the pressure of He gas, was not drastic compared with the observation at the critical pressure in the case of Ba^+.

In Sec. 4.3, we observed that the change of rf signals when we continuously irradiated trapped Yb^+ ions with radiation at 369.52 nm in the presence of buffer gases. RF signals finally disappeared in that observation. Therefore, we considered that the number of trapped Yb^+ ions decreased in that observation, and that the observed change in rf signals was caused by the change in the anharmonicity due to the decrease of the number of trapped ions. Therefore, we investigated the effect of the number of trapped ions on the anharmonic oscillation at a fixed pressure of buffer gas [7]. (It should be noted that we recently found that the disappearance of rf signals with irradiation at 369.52 nm was *not* caused by decrease of the number of trapped ions [27]. The detailed observations and analyses will be presented in Sec. 4.3.)

The results are shown in Fig. 2.11. We prepared a variety of number of trapped Yb^+ ions by changing the time during which the electron gun was turned on. According to Fig. 2.11(c), the linewidth of the spectra was independent from the fluorescence intensity in this
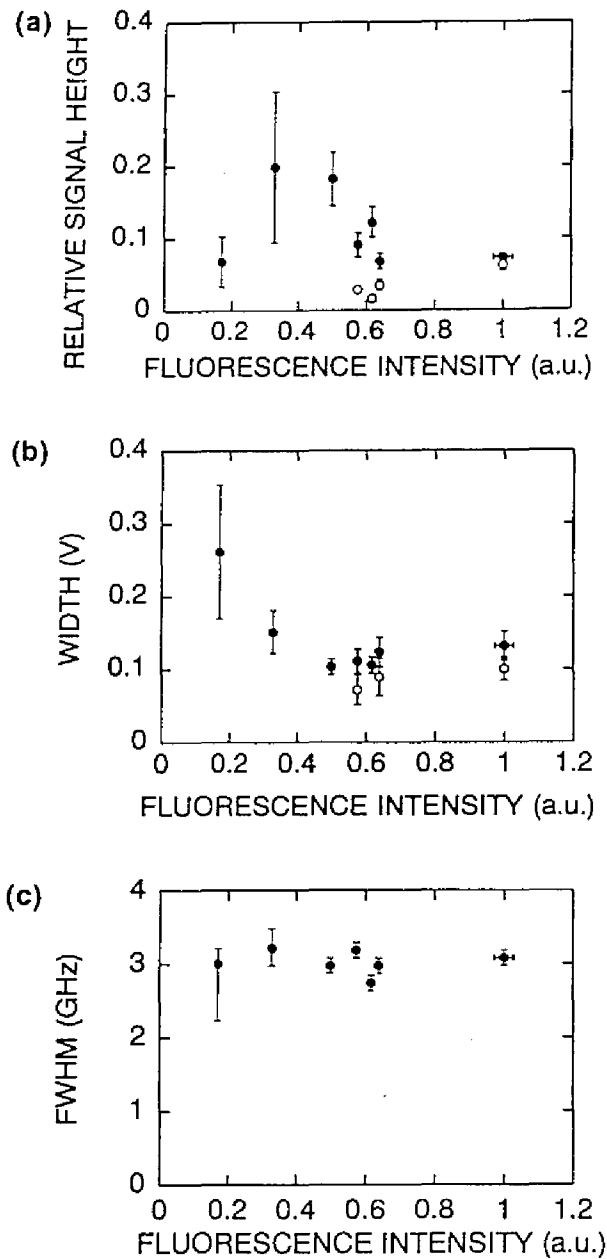
Fig. 2.11. Number dependence of anharmonic rf signals. (a) Relative signal height of rf signals, Y_{max}. (b) the FWHM of rf signals. ● : sweep direction f, ○: sweep direction r. The error bars show the fluctuations of the signals obtained by about 15-times detections. The number of trapped ions was changed by shortening the period when the electron gun was turned on at ion production. The fluorescence intensity at the resonance center, used as the abscissas of the figures, corresponds to the number of trapped ions. This is supported by the fact that the observed linewidths of the spectra were the same in this measurement region, as shown in (c). The He gas pressure was fixed to be 4×10^{-4} Pa. (For detection of the fluorescence, see Sec. 4.2). We used UV radiation generated by sum-frequency (see Sec. 3.2). IR radiation from a Ti:Al$_2$O$_3$ laser was also used to prevent the fluorescence decay and the rf signals disappearance (Chapter 4).

measurement range. (Detection of the fluorescence of trapped Yb^+ ions will be described in Sec. 4.2.) Therefore, the fluorescence intensity, used as the abscissas in Fig. 2.11, was proportional to the number of trapped Yb^+ ions. We observed that, as the number of trapped Yb^+ ions was decreased, the height of rf signals for the sweep direction f once grew larger, and then it did smaller, while rf signals for the sweep direction r became under the detectable level. This observation shows that the anharmonicity is a function of the number of trapped ions.

The pseudopotential of trapped ions is modified by the potential caused by their charges, i.e., the space charge potential ϕ_{ion} [11,23],

$$\phi_{eff} = \phi_{trap} + \phi_{ion},\qquad(2.20)$$

where ϕ_{trap} is the effective psuedopotential of the rf trap.

We observed the change in the anharmonicity with the pressure of buffer gas and the number of trapped ions. Increase of the buffer gas pressure results in a high density of the ion cloud due to the buffer gas cooling. Therefore, both increases of the pressure of buffer gas and of the number of trapped ions enlarge ϕ_{ion}. From the increase in the height of rf signals for the sweep direction r with increase of the buffer gas pressure or the ion number, it may be possible to consider that the space charge potential should have an anharmonicity of $C_4'{}_{(ion)} > 0$, and the anharmonicity in the space charge potential should be comparable to that of the trap itself. When the pressure of buffer gas is low, or the number of trapped ions is small, we suppose that ϕ_{ion} is small because of low ion density and the observed anharmonicity should be close to that of the trap itself. Here, the trap used had an anharmonicity of $C_4'{}_{(trap)} < 0$.

We guess that the anharmonicity in the space charge potential may be related to the origin of the critical pressure observed in the case of Ba^+ ions. Also, we guess that the shorter storage time determined above the

critical pressure, shown in Fig. 2.10(a), may be caused by the change in anharmonicity by the number of trapped ions.

We proposed, in 2.3.2(2), that the Y_{max} should be used for the estimation of the total number of trapped ions below the critical pressure, in place of the product of Y_{max} and the FWHM of signals for a harmonic oscillation. This proposal should be experimentally proved because we found that the shapes of rf signals depended on the number of trapped ions. The region below the critical pressure corresponds to the region below the fluorescence intensity of ~0.3 in Fig. 2.11.

In 2.2.3(2), we discussed the narrowing the width of rf signals as the decrease of energy of trapped ions. We should check the effect of the change in anharmonicity of the space charge potential on this observation.

2.3.3.   Conclusions of Anharmonic Oscillation

We found that rf signals changed in the shapes and sizes with the pressure of buffer gas when we trapped Ba^+ ions (before we started investigation of Yb^+ ions). In particular, we observed that rf signals drastically changed at a certain "critical" pressure of buffer gas. A similar pressure dependence was observed in the case that Yb^+ ions were trapped. In addition, we found that the shapes of rf signals changed as a function of the number of trapped ions. We suggested that these phenomena may be understood by assuming that a significant anharmonicity exists in the space charge potential of trapped ions as well as in the psuedopotential of the rf trap itself. Our observations suggest that the anharmonic rf signals may be used to analyze the dynamics of trapped ions. Introducing a certain pressure of buffer gas is effective for improving the relative detection sensitivity of trapped ions. Further investigations should be made for complete understanding of the change

in anharmonicity of rf signals with the pressure of buffer gas and the number of trapped ions, including to reveal the causes of the critical pressure. The experiment using a trap which has $C'_{4(trap)} > 0$ may be helpful.

This experiment shows that two precautions should be taken for the rf resonance absorption detection: (1) The detection should be done by using both sweep directions. It is possible that one may fail to detect the trapped ions at a certain pressure of buffer gas or at a certain number of trapped ions even when the number of ions is much greater than the smallest detectable number of the detection system. (2) The anharmonic rf signals causes an error in estimating the number of trapped ions if one determines the number from the product of Y_{max} and the FWHM of the signals. Practically, it is reasonable compromise to give the upper and the lower limit of the number determined from the product of Y_{max} and the FWHM of the signals obtained using the two sweep directions [6].

To eliminate the anharmonicity of traps, compensation electrodes have been introduced to Penning traps [9,19,28] and the detailed calculation for the design of the traps has been made [16,29]. The perfect quadruple potential trap is necessary when the frequency of the motion of the trapped particles must be measured precisely in experiments such as the measurement of the g-2 factor of the electron [9]. In the case that a large number of ions are trapped, however, it is required to compensate the observed anharmonicity, which may be composed of the anharmonicity of the trap itself and of the space charge potential of trapped ions. Our observations indicate the observed anharmonicity changes due to the change in the anharmonicity of the space charge potential. Therefore, compensation may be complicated because it should be adjusted for each trapping condition.

2.4. Conclusions

In this chapter, we described our apparatus of rf traps and the results obtained by detection of trapped ions by rf resonance absorption methods.

After a short review of a principle of the rf trap, we described two rf traps used for our investigations of Yb^+. A large trap of $2r_0 = 22.6$ mm was used for investigation of buffer-gas-cooled Yb^+. In this trap, we could confine the ions of which number was up to 10^6, and successfully detected rf signals of trapped ions. A small trap of $2r_0 = 5$ mm was constructed for investigation of laser-cooled Yb^+. For laser cooling, we reduced heat capacities of the oven and the electron source used for production of Yb^+ ions in order to avoid collisonal heating with neutral Yb atoms and electrons.

In detection of trapped ions by rf resonance absorption method, we focused on the effect of anharmonic oscillation on rf signals. We found that the shapes and sizes of rf signals depended on the pressure of buffer gas while the number of trapped ions was fixed. This phenomenon was found when we confined Ba^+ ions before we started investigation of Yb^+ ions. A similar pressure dependence on rf signals was observed also in the case of Yb^+ ions. In addition, we found that the anharmonicity of rf signals changed with the number of trapped ions while the pressure of buffer gas was fixed. We suggested that the observed dependence of the buffer-gas pressure and of the ion number on anharmonic rf signals could be qualitatively explained by assuming that the space charge potential of trapped ions has an anharmonicity, which changes as a function of those parameters.

We pointed out that, due to anharmonic oscillation, a care must be taken in detection of the trapped ions by rf resonance absorption methods and in estimation of the number of trapped ions from rf signals.

Chapter 3

Light Sources for Yb$^+$

3.1. Introduction

In this chapter, we describe light sources for the investigation of Yb$^+$. To observe the fluorescence of trapped ions and to laser cool them, it is usually necessary to drive the first resonance lines of the ions, because these transitions have large rates of spontaneous emission. The first resonance lines of atomic ions are usually in the ultraviolet (UV) region. Therefore, it is necessary to produce radiation in UV regions by frequency conversion of laser radiation at longer wavelengths, because no tunable cw lasers are available in the UV region. In addition, it is essential to use tunable continuous-wave (cw) radiation because, for laser cooling, over ten thousand cycles of absorption of photons and subsequent spontaneous emission are required. The minimum cw power required for laser cooling of trapped ions in a rf trap is estimated to be of the order of microwatts on the basis of experiments on single Hg$^+$ at the National Institute of Standards and Technology (NIST) [1].

In the case of Yb$^+$, the $^2S_{1/2}$ - $^2P_{1/2}$ first resonance line is a wavelength of 369.52 nm. To produce radiation at 369.52 nm over one microwatt, we first performed sum-frequency mixing (SFM) of diode-laser and argon-ion-laser radiation [2]. The wavelengths of a diode laser and an argon-ion laser are 1310 nm and 515 nm, respectively. This UV generation method is inexpensive and simple compared with conventional second-harmonic generation (SHG) using a dye laser, and a relatively

large output UV power can be obtained because high-power radiation is available from an argon-ion laser. SHG using a diode laser is less expensive and simpler than our SFM scheme. However, it seems to be impossible to generate over 1 μW of radiation by SHG of a single-mode diode laser owing to its low power, except in the fundamental wavelength region longer than 840 nm where a noncritical phase-matching condition can be obtained with a $KNbO_3$ crystal which has a large nonlinear coefficient [3]. To generate a sufficiently large second-harmonic power from diode-laser radiation, some special devices or techniques, such as a waveguide [4], quasi-phase matching of periodical-poled material [5], external cavity techniques [6,7], injection locking of high-power diode lasers [8], and a optical power amplifier [9] are usually required. We obtained more than one μW of radiation at 370 nm radiation using our SFM method with a single-pass configuration and successfully observed fluorescence of trapped Yb^+ ions.

When it is necessary to observe the fluorescence of trapped ions for a long time, the frequency of the radiation, by which one drives some transitions to detect fluorescence, should have a stability well within the spectral width. When two laser beams are frequency mixed to extend the available wavelength of coherent radiation, as in our SFM, the frequency stability of the output radiation generated by mixing reflects the frequency stabilities of the two fundamental lasers. The two fundamental lasers, therefore, should be frequency stabilized when the output radiation with high frequency stability is required. However, we proposed and demonstrated that the frequency-stabilized output radiation can be obtained by controlling only one of the fundamental lasers [10]. This stabilization method is generally applied for other combinations of lasers.

To laser cool Yb^+, however, we found that we needed more power than that obtained by SFM. For this purpose, we produced radiation at 369.52 nm by SHG of radiation from a dye laser using an external cavity

technique [6,7,11]. When an external cavity technique is used, SHG is more suitable than SFM because output power increases as the square of a fundamental enhancement factor with one cavity. In the case of SFM, a cavity is needed for each of two fundamental lasers to obtain the same improvement as in the case of SHG.

The $^2P_{1/2}$ state of Yb^+ has a branch to the $^2D_{3/2}$ metastable state with a branching ratio of 1 : 152 [12], Therefore, to laser cool Yb^+ with the $^2S_{1/2}$ - $^2P_{1/2}$ transition, it is necessary to deplete the $^2D_{3/2}$ state. For this purpose, two methods are known, i.e., driving the $^2D_{3/2}$ - $^2P_{1/2}$ transition at 2.4 μm [13], or the $^2D_{3/2}$ - $^3[3/2]_{1/2}$ transition at 935 nm [14]. We adopted the latter and produced radiation at 935 nm using a ring-Ti:Al$_2$O$_3$ laser (Swartz Electro-optic). This Ti:Al$_2$O$_3$ laser could not be frequency scanned. We modified it for frequency scanning. Although the frequency scanning was not perfect, we determined the isotope shifts of the $^2D_{3/2}$ - $^3[3/2]_{1/2}$ transition which had not previously been established [11]. Knowledge of the isotope shift of this transition was indispensable for laser cooling, as described in Chap. 5.

3.2. Sum Frequency Mixing of Diode-Laser and Argon-Ion-Laser Radiation [2]

(1) Sum frequency mixing in β-BaB$_2$O$_4$ crystal

We chose β-BaB$_2$O$_4$ (BBO) as a material of a mixing crystal. BBO crystals were found to be highly efficient frequency-conversion crystals in the UV region at the time when this experiment was performed [15, 16]. The BBO crystal was cut to the polar angle $\theta = 29$ deg to satisfy the type-I phase matching at normal incidence to the x-axis (the x-, y-, and z-axis are shown in Fig. 3.1), and the azimuthal angle was $\phi = 0$ deg to

63

obtain the largest effective nonlinear coefficient. The calculated walk-off angle was 3.9 deg. The parameters for SFM were derived from the dispersion equation given by Kato [17]

The experimental result described here shows the characteristics of the frequency conversion in BBO for strong focusing of input beams under the condition that the double refraction of this material should not be neglected. Owing to a relatively large double refraction of this material, the conversion efficiency should be estimated using a theory including the effect of walk-off. We adopted the theory established by Boyd and Kleinmann (BK) [18] for this propose. From the BK theory, the sum-frequency power P_3 is given by

$$P_3 = \frac{4\omega_1\omega_2\omega_3 d_{\text{eff}}^2}{\pi\varepsilon_0 c^4 n_3^2} \exp(-\alpha'l)P_1 P_2 lh,$$ (3.1)

where P_i are the powers, ω_i are the angular frequencies, n_i the indices of the crystal, d_{eff} is the effective nonlinear coefficient, l is the crystal length, $\alpha' = (\alpha_1 + \alpha_2 + \alpha_3) / 2$, α_i are the absorption coefficients, ε_0 is the permittivity of vacuum, c is the speed of light in vacuum, and h is a dimensionless focusing function introduced by BK [18]. The subscripts 1, 2, and 3 refer to the 515, 1310, and 370 nm beam, respectively.

The value of h is a function of the double-refraction parameter B, given by

$$B = \frac{1}{2}\rho\sqrt{\frac{l(k_1 + k_2)}{2}}$$ (3.2)

in the case of SFM [19], where ρ is the walk-off angle, and k_i the propagation constant in the crystal. The value of h is also a function of the parameter $\alpha = (\alpha_1 + \alpha_2 - \alpha_3)/2$, but we neglected the effect of α on h

judging from Eq.(2.16) in BK because $\exp(\pm\alpha l/2) = 1 \pm 0.01$. We estimate that h has the maximum of apploximately 0.06 from Fig. 2 of BK [18], taking $B = 11$. Using the reported nonlinear coefficients [20] and the equation of d_{eff} [21], we calculated $d_{eff} = (1.56 \pm 0.24) \times 10^{-12}$ m/V. The values of α_i were determined from the transmissivities of the crystal. Substituting of $\alpha_1 = 15$ m^{-1}, $\alpha_2 = 2.9$ m^{-1}, $\alpha_3 = 15$ m^{-1}, $n_3 = 1.67$, $l = 7$ mm, $P_1 = 1.34$ W and $P_2 = 2.1 \times 10^{-2}$ W into Eq.(3.1), we obtain $P_3 = 4.4 \times 10^{-6}$ W.

We discuss the optimum focusing condition for SFM in detail. The optimum focusing condition for SFM was investigated by Guha and Falk(GF) [19]. Taking $k_1/k_2 = 2.6$ and $B = 11$, we roughly estimated the optimum focusing parameters in crystal to be $\xi_{1m} \approx 1.0$ and $\xi_{2m} \approx 2.0$ (from Fig. 10 in GF), where

$$\xi_i = \frac{l}{b_i} = \frac{l}{w_i^2 k_i},$$

(3.3)

b_i are the confocal parameter of the circular Gaussian beams and w_i are

Table 3.1.   Phase-Mismatching Tolerance for SFM of 515- and 1310-nm Radiation in BBO

	Angle (deg)	Diode Laser Wavelength (nm)
Measured		
With focusing	0.18	>2.8 nm (HWHM)
Without focusing	0.02-0.03	Not measured
Calculated	0.022	2.0

All tolerances are given in FWHM except the diode-laser wavelength tolerance. The spot size or beam radius measured in air was as follows (in micrometers): With focusing,$(w_{x1}, w_{y1}) = (30,32)$, $(w_{x2}, w_{y2}) = (30, 34)$; without focusing, $(w_{x1}, w_{y1}) = (880, 860)$, $(w_{x2}, w_{y2}) = (1080, 970)$.

the spot sizes. These values of ξ_{im} imply that the maximum conversion efficiency does not occur with the same confocal parameters for the two input beams. The BK theory assumes that two input laser beams have the same confocal parameter [$\xi_{1m} = \xi_{2m} = 1.39$. (ref. [18])] Therefore, the maximum sum-frequency power should be estimated to be larger than that from Eq.(3.1).

The calculated tolerances are derived from $\mathrm{sinc}^2(\Delta k l/2)$, where $\mathrm{sinc}(x) = \sin(x)/x$, and $\Delta k = k_1 + k_2 - k_3$ and are shown in Table. 3.1. The values of tolerances are given for the FWHM.

(2) Experimental setup

The experimental setup is shown in Fig. 3.1. The single frequency output of an Ar^+ laser (LEXEL 95-5) at 515 nm and that of λ /4 shifted distributed-feedback-type InGaAsP diode laser at 1310 nm (NEC NDL5600) were mixed. The crystal length was 7 mm. The crystal faces
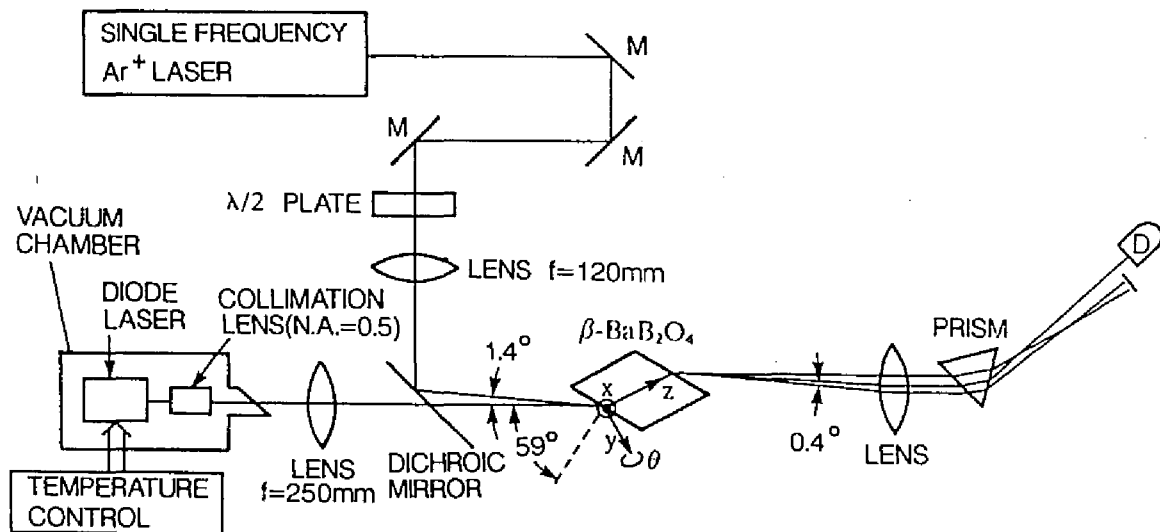
Fig. 3.1.   Experimental setup for SFM of diode laser and Ar^+ laser radiation. M's, mirror; D, detector.

were cut at Brewster's angle to the radiation at 1310 nm in the ordinary wave to minimize Fresnel losses and to compensate for beam astigmatism when the crystal is put into an external ring cavity to enhance the sum-frequency power [22]. The temperature of the crystal was held at (50 ± 1) °C to prevent surface degradation due to atmospheric water vapor [23].

The diode laser was mounted on a temperature-stabilized heat sink, of which temperature was adjusted by a Peltier cooler, with a temperature stability of better than 1 mK at room temperature. The wavelength tuning of the sum-frequency output to the $^2S_{1/2}$ - $^2P_{1/2}$ line of Yb^+ was made by cooling the diode laser and was confirmed by the detection of the absorption signal of Yb^+ in a hollow-cathode lamp at the diode laser temperature of -7 °C. The advantage of cooling the diode laser is to increase its output power. The diode laser and a collimation lens were placed in a small evacuated chamber to prevent the condensation of atmospheric water vapor for the operation at lower than room-temperature. The collimated beam was almost circular due to the property of distributed-feedback-type diode lasers.

The two input beams were independently focused to satisfy the optimum focusing condition. The Ar^+ laser beam has to be incident on the BBO crystal at 1.4 deg with the diode laser beam, as indicated in Fig. 3.1, owing to the dispersion of BBO, to make the two laser beams collinear in the crystal. Alignment of the two input beams and the measurement of the spot size were made by scanning pinholes.

(3) Result

Figure 3.2(a) and (b) show the measured sum-frequency power as a function of the Ar^+ laser power and the diode-laser power, respectively. The maximum UV radiation of 1.3 μW was generated from
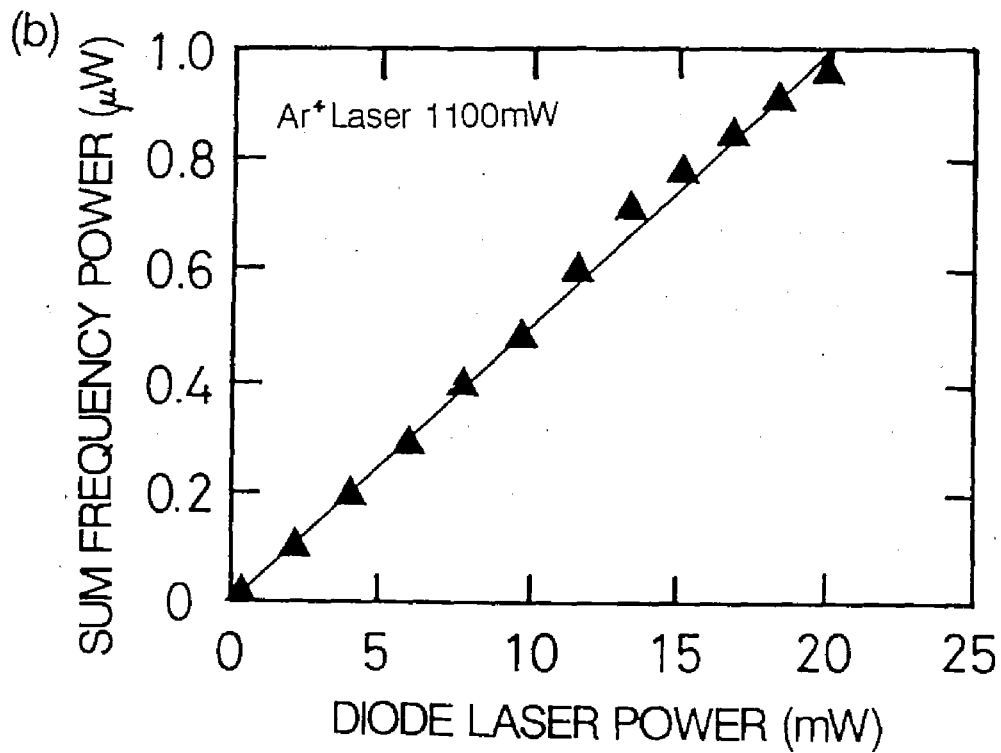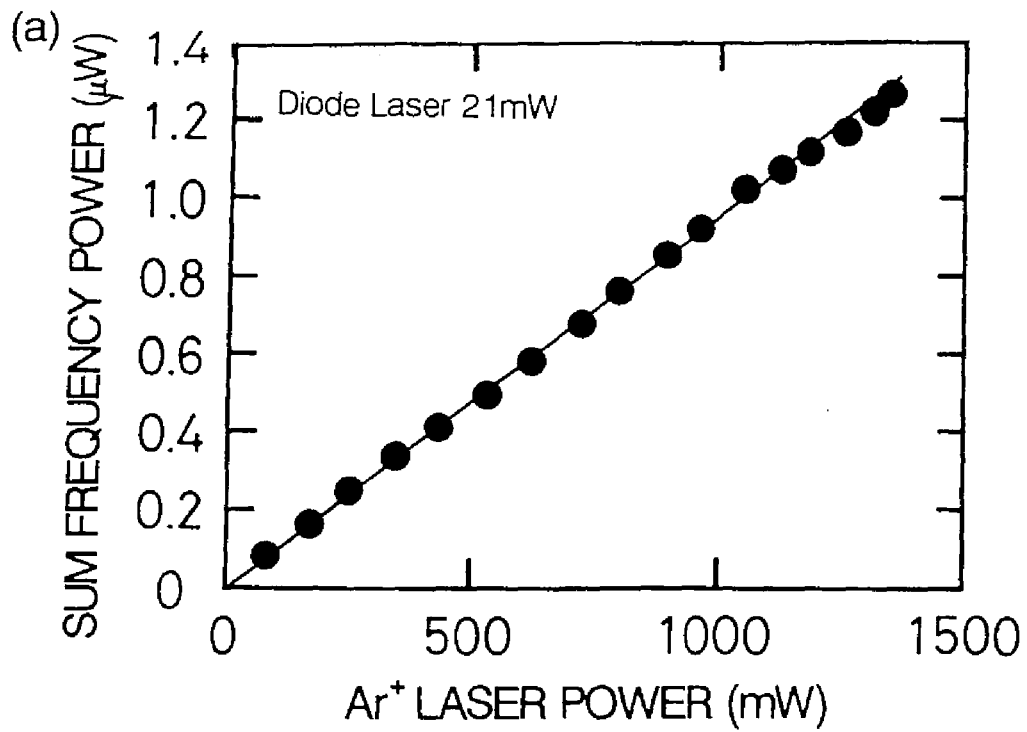
Fig. 3.2.   Measured sum-frequency power versus input power from (a) an Ar+ laser, and (b) a diode laser. The measured spot sizes were 24 μm in air for the two laser beams.

the diode-laser radiation of 21-mW power and the Ar^+ laser radiation of 1.34-W power. The sum-frequency power was stable and was proportional to the input power of each laser within the intensity range of the input beams in this research.

We measured the d_{eff} of our crystal to be $(1.56 \pm 0.6) \times 10^{-12}$ m/V from the conversion efficiency with no focusing (collimated) beams.

Figure. 3.3(a) and (b) show the dependence of the sum-frequency power on the polar angle and the diode-laser wavelength, respectively. We show the tolerances of the polar angle and the diode-laser wavelength, determined from Fig. 3.3, in Table 3.1. The values of the measured angle tolerances were compensated for refraction at the incident face of the crystal. The tolerance of the diode-laser wavelength was measured as the temperature of the diode laser was scanned between 20 °C and 70 °C. The measured tolerance was influenced by the misalignment due to thermal expansion or contraction of the diode laser mount with a change of the temperature. The measurement of the tolerances of the diode laser wavelength without focusing could not be made because the sum-frequency power was too small to detect owing to the small output power of the diode laser at high temperature. The frequency drift of the Ar^+ laser was less than 150 MHz, the free spectral range of this laser cavity. The contribution of this value to the tolerances is negligible.

(4) Discussion

We compare the experimental results with the theoretical estimations. If we considered the calculated reflectivity of 23 % for the sum-frequency beam at the Brewster-angled face and the loss of 20 % in the optics for UV separation, a sum-frequency power of 2.7×10^{-6} W would be extracted. In the experiment of Fig. 3.2, the measured spot sizes in air were $w_{1air} = w_{1air} = 24$ μm. This means that $\xi_1 = 0.6$ and $\xi_2 = 1.5$,
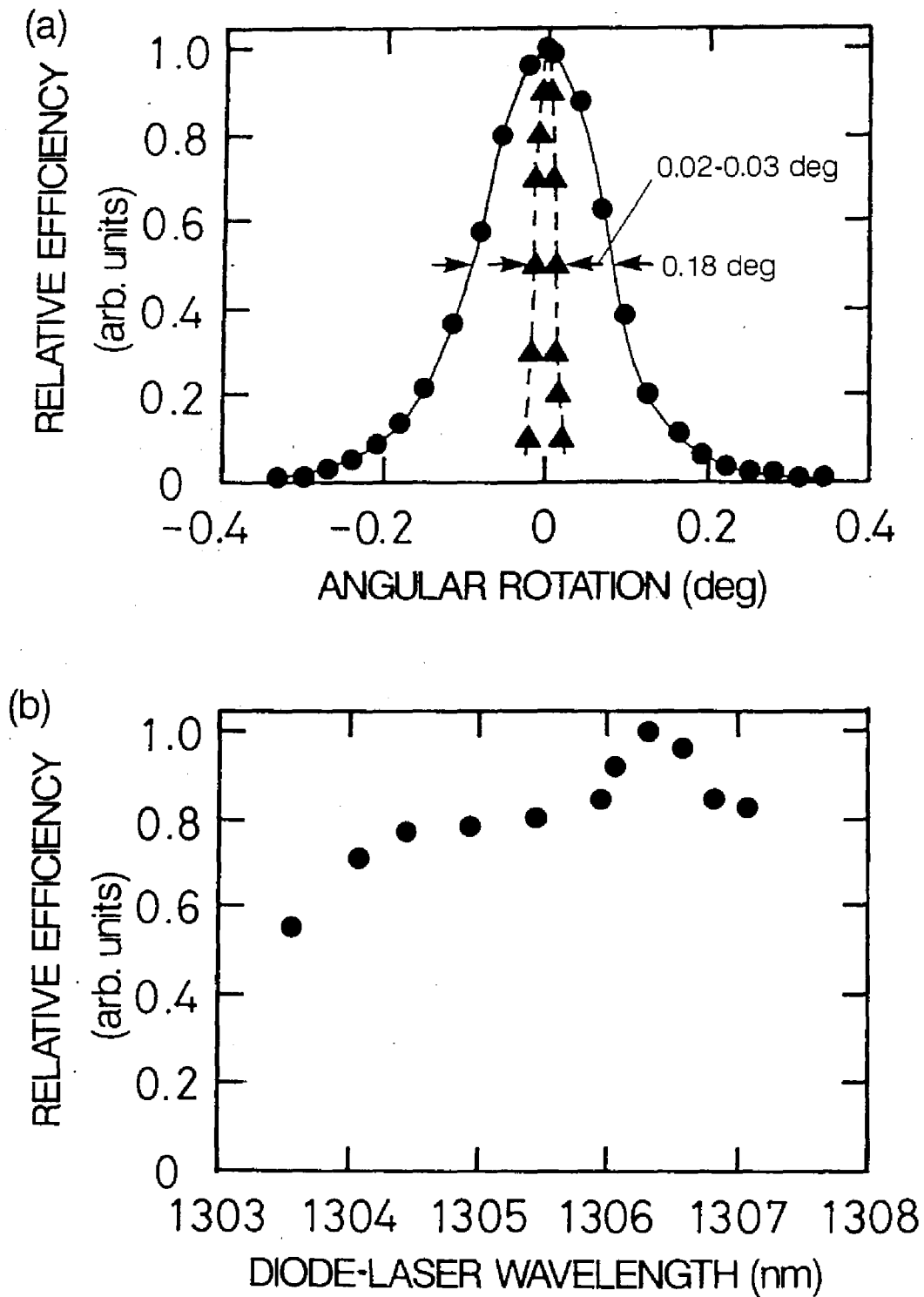
Fig. 3.3. (a) Angular sensitivity for SFM with the two input beams strongly focused (circles) or not focused (triangles) (collimated). The measured spot size and beam waists are listed in Table. I. (b) Diode-laser wavelength sensitivity for SFM obtained by changing the temperature of a diode laser between 20 °C and 70 °C. Efficiency means P_3/P_1P_2. (The diode laser used here could not tune to the Yb[+] line.)

which are close to the optimum derived from GF if the two input beams are at normal incidence to the crystal face. We measured sum-frequency power of 1.3×10^{-6} W is nearly half as large as the calculated value from Eq.(3.1).

The discrepancy may be caused mainly by astigmatism introduced at the Brewster-angled face. For weak focusing of $\xi_i < 1$ and $l_a > l$, where l_a is the aperture length given by [19]

$$l_a = \frac{3.89}{\rho \sqrt{\dfrac{1}{w_{x1}^2} + \dfrac{1}{w_{x2}^2}}}, \tag{3.4}$$

P_3 is reduced by a factor of $n_1 \approx n_2 \approx 1.65$ owing to the expansion of w_{yi} to $n_i w_{yi}$ [24]. For the experiment of Fig. 3.2, we cannot estimate the reduction factor simply, because the focusing was close to optimum [18, 19] and because the beam areas at the locations in z axis of w_{xi} are important since $l_a = 0.97$ mm $< l$, where the beam areas at the locations in z axis of w_{xi} are a function of the location in the z-axis of w_{xi} [24].

Comparing between the measured and the calculated tolerances, we found that the measured angle tolerance without focusing was in agreement with the calculated value. When we strongly focused the input beams, the measured angle tolerance was 7 times as large as the calculated tolerance. GF showed that the tolerance for phase mismatch of Δkl is much greater for strong focusing and/or in the presence of walk-off than that in the absence of walk-off for weak focusing [19]. They insist that the substantial Δkl tolerance is caused by the fact that only the aperture length, l_a, which contributes in a coherent way to the build up of the generated electric filed, is limited. The angle tolerance of 0.14 deg was derived from $\text{sinc}^2(\Delta kl_a /2)$ and $l_a = 1.2$ mm in this focusing condition. This is close to the measured value.

(5) Prospect of this technique

By replacing an InGaAsP diode laser with a AlGaInP or GaAlAs diode laser and choosing an appropriate Ar^+ laser line, we are able to generate tunable single-frequency cw radiation in the region between 265 and 320 nm.

The large tolerance of diode-laser wavelength allows us to generate simultaneously two (or more) UV beams which have different frequencies, when the beams of two (or more) diode lasers are combined by a half mirror and are simultaneously inputted into the β-BaB_2O_4 crystal. We successfully used the two UV beams generated by this method for detecting the spectra of the odd isotopes of Yb^+ ions and photodissociation of YbH^+ at 369.48 nm. The wavelengths of the diode lasers were 1309.7 nm and 1310. 2 nm for 369.48 nm and 369.52 nm, respectively. (When we observed the fluorescence recovery by irradiation at 369.48 nm with this radiation, we believed that the wavelength of 369.48 nm was that for deexcitation of Yb^+ in the $^2F_{7/2}$ state. See Chap. 4.)

3. 3. Stabilization of Sum Frequency [10]

(1) Basic idea of sum or difference frequency stabilization and its limitations

When sum or difference frequency mixing of two laser beams are performed, it is possible to frequency stabilize output radiation by controlling only one of the fundamental lasers. The basic idea of this method is shown in Fig. 3.4. The error signal to a frequency reference is detected with the generated radiation and is fed-back to one of the

(a) Sum-Frequency Mixing
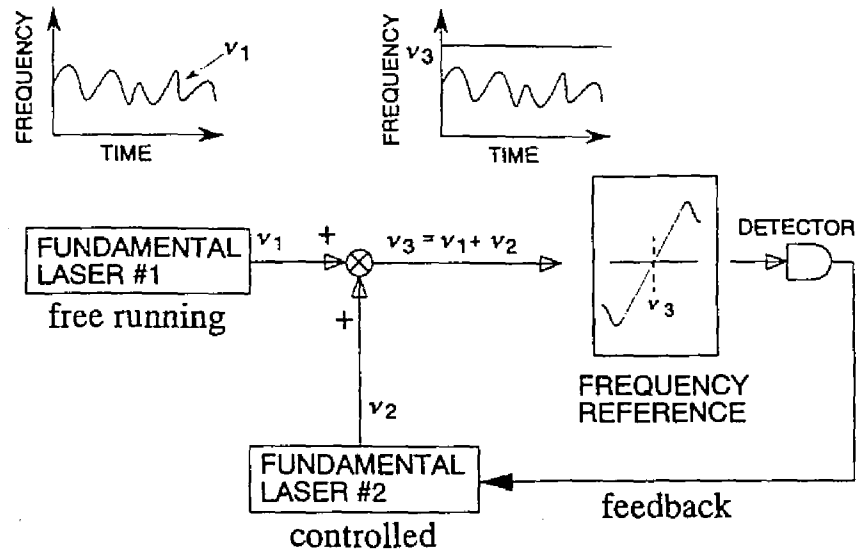
(b) Difference-Frequency Mixing
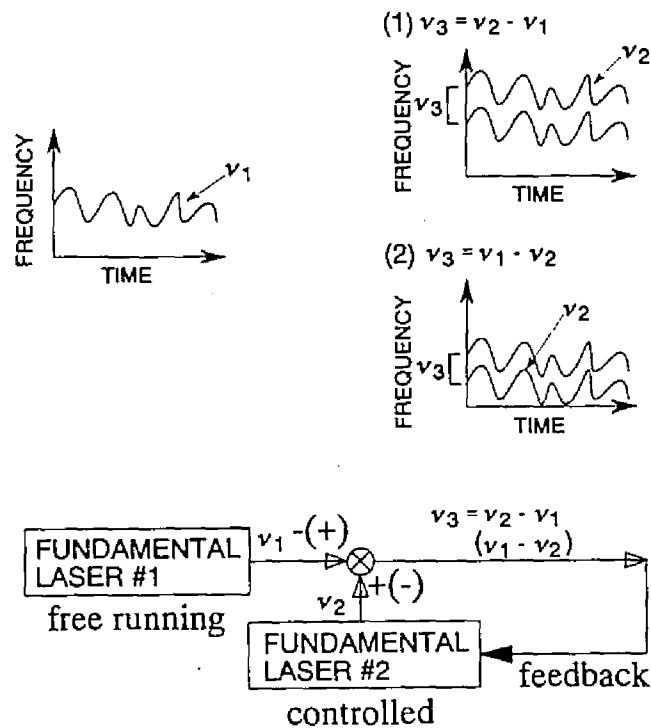
Fig. 3.4. Block diagram of sum or difference frequency stabilization of the radiation generated by frequency mixing. (a) in case of sum-frequency mixing (b) in case of difference-frequency mixing.

73

fundamental lasers in order to lock the output frequency to the frequency reference. The servo loop shown in Fig. 3.4 anti-correlates the frequency fluctuation of the controlled fundamental laser (#2 in Fig. 3.4) with that of the free-running fundamental laser (#1 in Fig. 3.4) in case of sum-frequency mixing, or correlates in case of difference frequency mixing.

To perform this frequency stabilization method, the following conditions should be satisfied: (i) One of the fundamental lasers, which is to be controlled, should have a continuous frequency-tuning range over the frequency drift of the free-running fundamental laser. (ii) The frequencies of the two lasers should be well within the phase mismatching tolerance of frequency mixing when the output frequency is locked to the frequency reference. Otherwise the power of the radiation generated by mixing would fluctuate.

We applied this method to our SFM. We controlled the injection current of the diode laser to lock the sum-frequency to a frequency reference, while the Ar^+ laser was free running. The two conditions mentioned above are well satisfied as follows:

(1) Diode lasers have a large frequency-tuning range to compensate the frequency drift of Ar^+ lasers. For our diode laser, e.g., the frequency shift by the dc injection current was measured to be -1.7 GHz/mA at an operating current of 100 mA, a temperature of -7 °C, and an output power of 20 mW. We assume the maximum frequency drift of the Ar^+ laser to be 2 GHz, which is the oscillating range of Ar^+ lasers. From these values, we find that the frequency drift of the Ar^+ laser can be compensated by controlling the injection current of the diode laser only within 1.2 mA (1.2 % at the operating condition mentioned above) to lock the sum-frequency to the reference.

(2) The power fluctuation due to the phase mismatching was estimated from the equation that $(\sin(\Delta k l /2) / (\Delta k l /2))^2$, where l is a crystal length of 7 mm and $\Delta k = k_3 - k_2 - k_1$, k_i are the propagation

constants in crystal. The subscripts 1, 2, and 3 refer to the 515-, 1310-, and 370-nm beams, respectively. The power reduction of the sum-frequency power is expected to be below 0.01 % when the sum frequency is locked to reference and the frequency drift Δv_1 of Ar^+ laser is 2 GHz (Δv_2 = -2 GHz, Δv_3 = 0).

There is an undesirable possibility that output power of the diode laser fluctuates by controlling the injection current of the diode laser to cancel the frequency drift of the Ar^+ Laser. For our diode laser, the power fluctuation by the dc injunction current was measured to be 0.23 mW/mA. Therefore, the power fluctuation additionally caused by the frequency stabilization is expected to be only within 1.4 %.

(2) Experimental setup

Figure 3.5 shows the schematic diagram of the whole system. We used the absorption signal of the Yb^+ $^2S_{1/2}$ - $^2P_{1/2}$ transition at 369.52 nm as a frequency reference. We detected Yb^+ in a commercial hollow-cathode
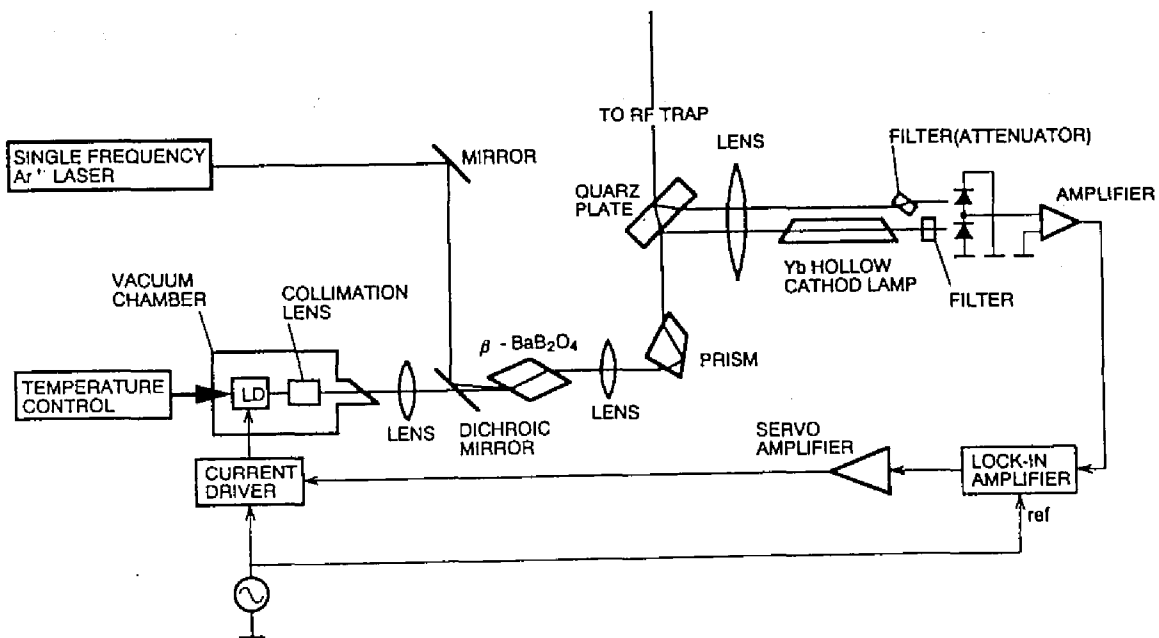
Fig. 3.5.   Whole experimental setup.

lamp (Hamamatsu L2783). The injection current of the diode laser was modulated to modulate the sum frequency. The absorption signal was detected at the modulation frequency to obtain the zero-crossing signal which provided a frequency discriminator slope. The differential detection was used to remove the amplitude modulation which was simultaneously caused by modulating the injection current of the diode laser. The differential detection was also effective to reduce the amplitude noise of the sum-frequency radiation. Color glass filters were necessary to avoid the saturation of photodiodes' amplifier with the radiation from the lamp. The balance between the signal beam and the reference beam of the differential detection was achieved by rotating one of the color glass filters. Rotating the filter changes the loss by Fressnel reflection as well as by the absorption owing to changing the optical path length.

(3) Result

Figure 3.6 shows the typical absorption spectra of Yb^+ in the hollow-cathode lamp. The frequency intervals between each isotope line [25] and the strength of the lines are also indicated. The absorption of Yb^+ was 2% at a discharge current of 10 mA which was the maximum rating of the lamp. A few nW of the uv radiation was sufficient to detect the signals. The modulation frequency and the modulation depth of the sum-frequency are 158 Hz and ±170 MHz, respectively. We tried to detect opto-galvanic signals of Yb^+ in the lamp. However, no signals were detected although we increased the sum-frequency power to 1 μW.

Figure 3.7 shows the error signal at the lock-in amplifier output when the sum-frequency was locked to the $^{174}Yb^+$ line. The frequency deviation in locking was measured to be ±3 MHz from the error signal. We confirmed that we were able to lock the sum-frequency to all of the zero crossing points of the absorption signal.
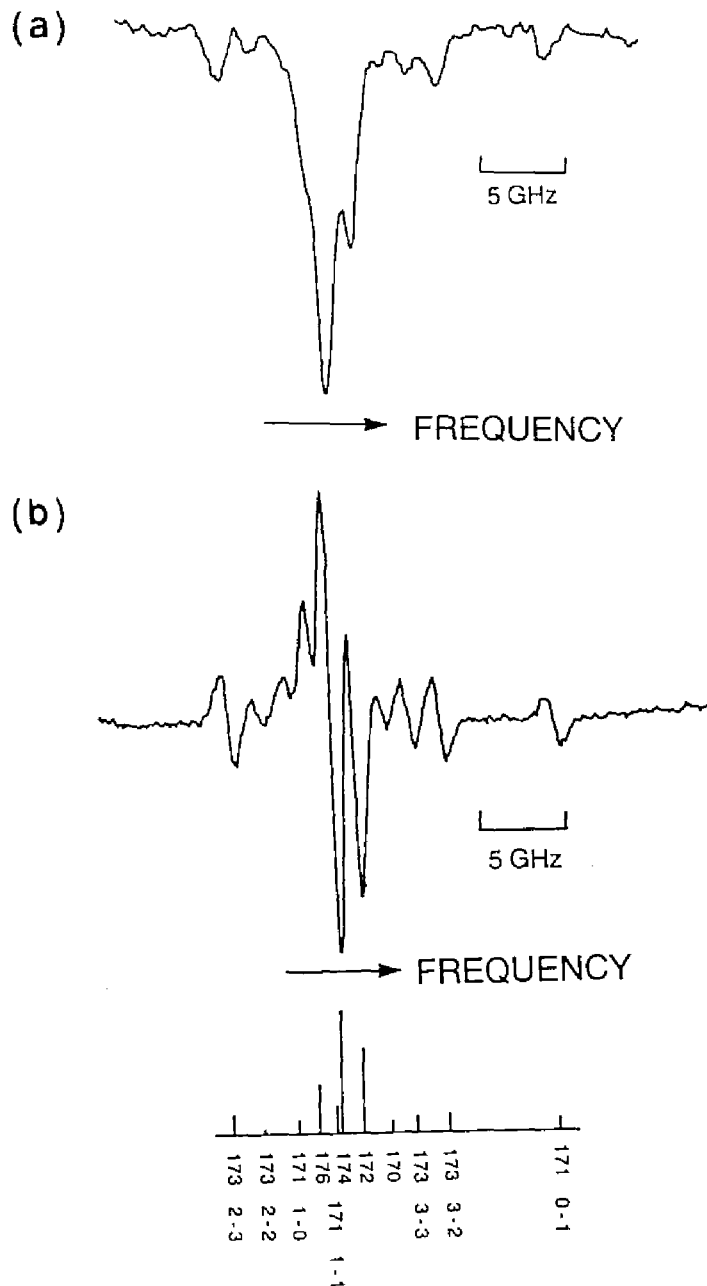
Fig. 3.6.   Typical absorption signals of Yb^+ in a hollow-cathode lamp. (a) Sum-frequency beams were chopped to avoid a stray light from the hollow cathode lamp. The signal was detected at the chopping frequency using a lock-in amplifier. The signal beam power of the differential detection was 140 nW. The chopping frequency was 41 Hz. (b) The injection current of diode-laser was modulated to frequency modulate sum-frequency. The signal was detected at the modulation frequency using a lock-in amplifier. The signal beam power of the differential detection was 27 nW. The modulation frequency and the modulation depth of the sum-frequency are 158 Hz and ±170 MHz, respectively. The time constant of the lock-in amplifier was 1 s.
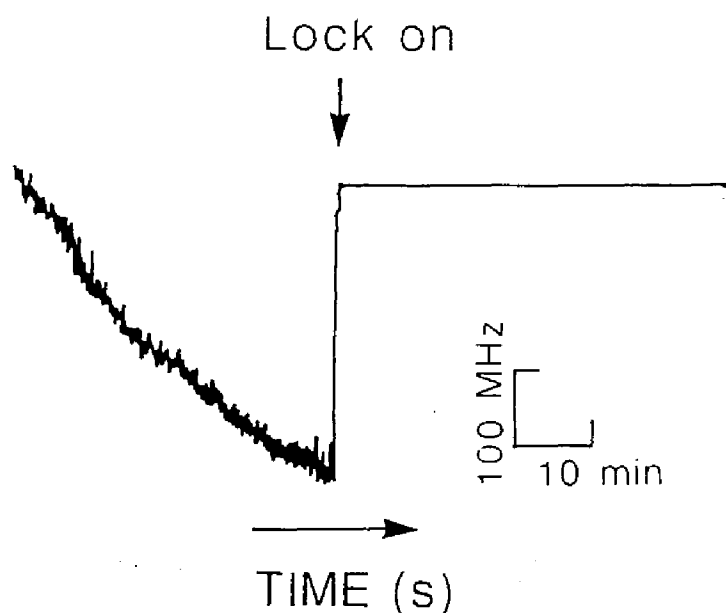
Fig. 3.7. Time recording of the error signal of the sum-frequency stabilization at the lock-in amplifier output. The sum-frequency was locked to the ^{174}Yb$^+$ line. The experimental conditions were the same as those of Fig. 3.6(b) except that the signal beam power was 23 nW.

The power fluctuation of the sum-frequency radiation, measured to be below ±5 % with a detection bandwidth from dc to 2 Hz, did not increase even when the servo loop of the frequency stabilization was closed. The locking range, which was ±360 MHz because the Doppler broaden linear absorption signal was used as a frequency reference, was more than two times as large as the free spectral range of the Ar$^+$ laser of 150 MHz. Therefore, even when the longitudinal mode of the Ar$^+$-laser cavity hopped to neighbor one, the frequency locking of the sum-frequency was automatically recovered in almost every case.

(4) Prospect of this stabilization method

In this experiment, we stabilized the sum-frequency with a slow servo loop. However, diode lasers are frequency modulated at a modulation frequency over 1 GHz and are frequency stabilized to a line width below 1 kHz with fast servo loop controlling the injection current of diode lasers [26]. The Fourier frequency of the frequency fluctuation of Ar^+ lasers is spread in at most a few MHz. Therefore, it would be possible to narrow the spectral line of the sum-frequency radiation to be below the linewidth of the Ar^+ laser with fast electric feedback. To realize the reduction of the frequency fluctuation to the shot-noise limit [27], however, one would need much higher sum-frequency power. (it depends on the value of photodiode's load resister, in order to keep the needed servo bandwidth, e.g., at least 100 μW was necessary for 510 Ω in Ref. [28]).

This frequency-stabilization method could be applied to other combinations of fundamental lasers. Especially, when diode lasers are used for (at least) one of the fundamental lasers and are controlled to stabilize the output frequency, this method would be effective owing to the wide tunability of diode lasers.

3.3. Second-Harmonic Generation of Dye-Laser Radiation Using an External Cavity Technique [11]

To laser cool trapped Yb^+ ions, we found that we needed more powerful radiation than that generated by the SFM of diode-laser and Ar^+-laser radiation. For this purpose, we produced another source of UV radiation generated by SHG of dye-laser radiation using an external cavity technique [29]. In an external cavity technique, in the case of SHG, the

output power is enhanced in proportion to the square of an enhancement factor of the cavity. In contrast, in the case of SFM, the output power increases in proportion only to the enhancement factor of the input beam resonant to the cavity. To obtain the same improvement using SFM as that using SHG, two fundamental beams should be simultaneously enhanced and this is more complicated than the case of SHG. Therefore, we adopted SHG as an external cavity technique.

When the frequency of a single-frequency laser beam is resonant to an eigenfrequency of an external cavity, the fundamental enhancement factor A_{cav} is given by [30]

$$A_{cav} = \eta_m \frac{1 - r_i}{\left(1 - \sqrt{r_i r_c}\right)^2},$$

(3.5)

where r_i is the reflectivity of the input mirror, r_c is the fraction of the intracavity beam after one round trip inside the cavity, η_m is the matching ratio of the input beam to the cavity at resonance. The losses at other mirrors and in the nonlinear crystal determine the value of r_c. At a given value of r_c, the enhancement factor A has a maximum value of $\eta_m/(1 - r_c)$. This condition is realized when the input mirror reflectivity r_i is equal to r_c.

(a) Design and setup

We constructed a ring cavity as an external cavity. We designed the ring cavity using the following procedure. First, we calculated the optimum spot size as in the case of the SFM. The double refraction parameter for SHG, B_{SH}, is calculated from

$$B_{SH} = \frac{1}{2} \rho \sqrt{lk_{1c}} , \tag{3.6}$$

where k_{1c} is the propagation constant of the fundamental radiation in the crystal, ρ is the walkoff angle, and l is the crystal length. From the value of B_{SH}, we estimate the optimum focusing parameter ξ_m referring to Fig. 4 in BK [18]. Then, the spot size in the crystal is determined from Eq.(3.3).

Second, we determine the cavity length for a given radius of curvature of the spherical concave mirrors, R, to satisfy the optimum spot size in the crystal. We assume here that the two spherical concave mirrors have the same radius of curvature. With reference to Ref. [31], referring to Fig. 3.8, we calculate the spot size in the crystal located between the two concave mirrors, w_{0c}, the spot size at the back focal point, w_{0r}, and the beam radius at the surface of the concave mirror, w_m, from the equations given by

$$w_{0c}^2 = \left(\frac{\lambda}{2\pi}\right) \sqrt{\frac{(d - R)(dR + xR - dx)}{x - R}} \tag{3.7}$$

$$w_{0r}^2 = \left(\frac{\lambda}{2\pi}\right) \sqrt{\frac{(R - x)(dR + xR - dx)}{R - d}} \tag{3.8}$$

$$w_m^2 = \left(\frac{\lambda}{2\pi}\right) \frac{R(2dx - dR - xR)}{\sqrt{(R - x)(R - d)(dR + xR - dx)}} , \tag{3.9}$$

where d is the distance between the two concave mirrors, and x is the pass length from one of the two concave mirrors to the other via the two plane mirrors. (The cavity length corresponds to $(d + x)$.) The stability region of the cavity is given by
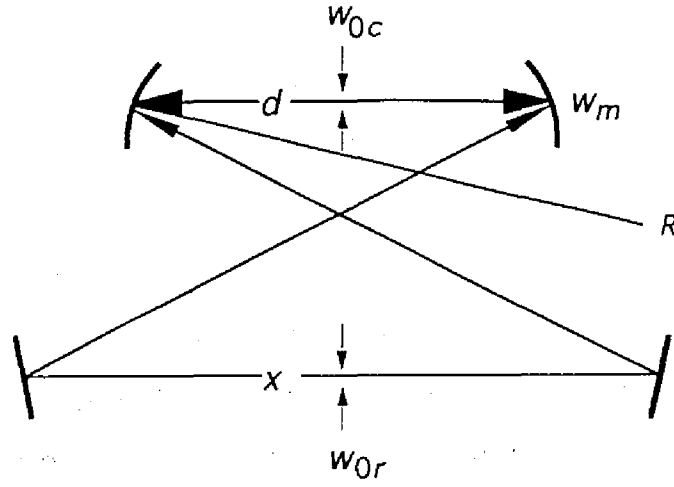
Fig. 3.8. Design of four-mirror ring cavity arranged in loop (or bow-tie) shape.

$$0 < \delta < \frac{R^2}{x - R} \qquad (3.10)$$

where δ is defined as $\delta \equiv d - R$. At the center of the stability region where

$$\delta_c = \frac{R^2}{2(x - R)}, \qquad (3.11)$$

Eq. (3.7) has a pole. This means that the change of w_0 with d is small around $\delta = \delta_c$. Therefore, we set δ to this point due to this practical advantage. At $\delta = \delta_c$, the spot size in the crystal located between the two concave mirrors, w_{0cc}, is given by

$$w_{0cc}^2 = \left(\frac{\lambda}{2\pi}\right) \frac{R^2}{2(x - R)}. \qquad (3.12)$$

To realize the determined spot size in the crystal, we determined x, i.e., the cavity length from Eq. (3.12), with the given curvature of the mirror, R.

The cavity length is limited by the condition that the resonance width of the cavity is well within the linewidth of radiation from the laser. The FWHM linewidth of cavity resonance, Δv, is given by

$$\Delta v = \frac{v_{FSR}}{F}, \tag{3.13}$$

where v_{FSR} is the free spectral range of the cavity, and F, the finesse of the cavity, is given by

$$F = \pi \frac{\sqrt{r_{rms}}}{1 - r_{rms}}, \tag{3.14}$$

where

$$r_{rms} = \sqrt{r_i r_c}. \tag{3.15}$$

According to Ref. [32], in the case of a four-mirror cavity with two off-axis spherical mirrors, it is possible to compensate the astigmatism and the coma introduced at the reflection on the concave mirror by inserting a Brewster-angle-cut crystal. For the astigmatism, whether the cavity is arranged in a Z shape or a loop (or bow-tie) shape, it can be compensated within the crystal as well as the overall cavity. To accomplish astigmatism compensation, the reflection angle at the curvature mirror must be set to the value θ_{ast} calculated from

$$R \sin \theta_{ast} \tan \theta_{ast} = \frac{t(n^2 - 1)\sqrt{n^2 + 1}}{n^4},$$ (3.16)

where R is the radius of curvature of an off-axis spherical mirror, n is the refractive index of a medium, and t is the length of the medium.

In the case of a Z-shaped four-mirror cavity with two off-axis spherical concave mirrors, an coma introduced at the reflection on the concave mirror can be compensated by inserting a Brewster-angle-cut crystal within the crystal as well as the overall cavity. For coma compensation, the reflection angle at the concave mirror must satisfy

$$R \sin \theta_{coma} = \frac{2t(n^4 - 1)\sqrt{n^2 + 1}}{n^7}.$$ (3.17)

Also, although there are two orientations of the Brewster-angled face in the cavity, the coma is compensated with only one of the two orientations, that shown as orientation A in Ref. [32]. In the case of arrangement in a loop (or bow-tie) shape, the come introduced at the reflection on the concave mirror is compensated through the overall cavity by the two concave mirrors without insertion of a Brewster-angle-cut crystal. When a Brewster-angle-cut crystal is inserted, the coma cannot be compensated either within the crystal or the overall cavity.

In the case of a Z-shaped four-mirror cavity, it is possible to satisfy the two compensation conditions simultaneously by setting the angle of incidence to the off-axis spherical mirror, θ_{corr}, to be

$$\theta_{corr} = \tan^{-1}\left(\frac{n^3}{2(n^2 + 1)}\right).$$ (3.18)

We chose a BBO crystal with a length of 7 mm as the nonlinear crystal for SHG. When the cavity was arranged in a Z shape and the crystal was cut to the Brewster-angled face, it was possible to compensate astigmatism and coma simultaneously. We calculated θ_{corr} and R at θ_{corr} from Eq. (3.18) and Eq. (3.17) to be 31.1 deg and 0.01 m, respectively. This is, in practice, difficult because the mirror curvature is close to the crystal length. Also, in the case of a Z-shaped cavity, the crystal is placed close to the intersection point of the intracavity beam. To simplify the construction of the cavity, we adopted a four-mirror ring cavity in the loop-type arrangement. The crystal faces were cut to right angles and coated with antireflection for both fundamental and second-harmonic wavelengths. To obtain the second-harmonic radiation from the cavity, we inserted a dichroic mirror. The dichroic mirror was designed to be used at the Brewster's angle. This allowed us to minimize the insertion loss and to compensate astigmatism. We set the curvature of the spherical mirrors to 0.1 m for easy alignment of the angle-phase-matched crystal and the dichroic mirror. To realize the optimum focusing of $w_0 = 19$ μm in w_{0cc} given by Eq. (3.12), $x = 1.73$ m was needed. We compromised with $w_0 = w_{0cc} = 30$ μm with $x = 0.733$ m. This compromise decreased the conversion efficiency to 70% of that in the case of optimum focusing. The configuration of the designed external cavity is schematically shown in Fig. 3.9.

To lock the resonance of the cavity to the frequency of the dye-laser radiation, we used the polarization technique demonstrated by Hänsch and Couliaud [33]. In this case, the polarization of the resonant radiation in the cavity was defined by the double reflection of the BBO crystal and/or the Brewster-angled dichroic mirror. The error signal was fed back to the PZT to control the cavity length. We found that the external cavity could not follow the frequency of the dye laser when it was frequency scanned beyond 1 FSR of the external cavity. Therefore, we inserted a set of dual
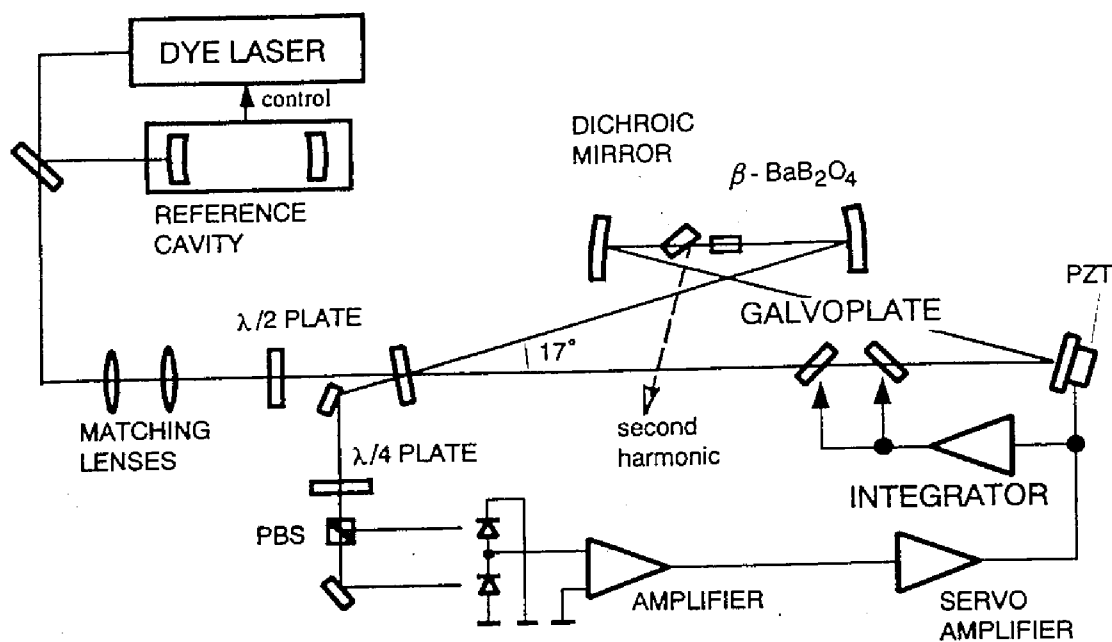
Fig. 3.9. Schematic diagram of an external cavity for SHG of a dye-laser radiation.

galvoplates controlled by an integrated error signal to follow the cavity resonance of the frequency of the dye laser during frequency scanning.

We used a commercial ring dye laser (Spectra Physics 380D). This laser contains a unidirectional device, a thick etalon locked to the resonance of the laser cavity, and a set of dual galvoplates in the laser cavity. The frequency of this laser was locked to the resonance frequency of a temperature-stabilized reference cavity. In the specification of the dye laser, this laser can be continuously frequency scanned in the range over 30 GHz while its frequency is locked to the resonance of the reference cavity, and has a linewidth narrower than 500 kHz. We first used pyridin-1 as a dye for oscillation at 740 nm and then changed to pyridin-2. This change increased the output power to 30 % at 740 nm. In both cases, the laser oscillated stably in a single frequency. In the summer and when an air conditioner is not used, however, there were many bubbles in the dye

stream. This resulted in mode hopping every minute. We found that the output power of the dye laser decreased on depositing dust in air. We cleaned the optics once every few days of operation.

(b) Result and analysis

Figure 3.10(a) shows the output power obtained from the external cavity. For comparison, we also show the output power obtained by a single pass in the crystal in Fig. 3.10(b). In Fig. 3.10(b), we measured the output power after removing the coupling mirror of the external cavity. From the fitting of the results in Fig. 3.10, we obtained conversion efficiencies as follows:

cavity enhanced   (meas.) $P_2 = 6.5 \times 10^{-3} \, P_1^2$

single pass   (meas.) $P_2 = 3.1 \times 10^{-5} \, P_1^2$.

For a single pass, the theoretical second-harmonic power calculated by the BK theory [18] is given by

$$P_2 = \frac{\omega_2^3 d_{\text{eff}}^2}{4\pi\varepsilon_0 c^4 n_1^2} \exp(-\alpha' l) P_1^2 \, lh \,. \tag{3.19}$$

In this case, the expected second-harmonic power is

single pass   (theory) $P_2 = 4.5 \times 10^{-5} \, P_1^2$.

The measured conversion efficiency was 84 % of the theoretical value in the case of a single pass. The fundamental enhancement factor was 14. From Eq. (3.5) and the input mirror reflectivity r_i of 88 %, we estimated the fraction of intracavity beam after one round trip, r_p, to be 0.94, if the
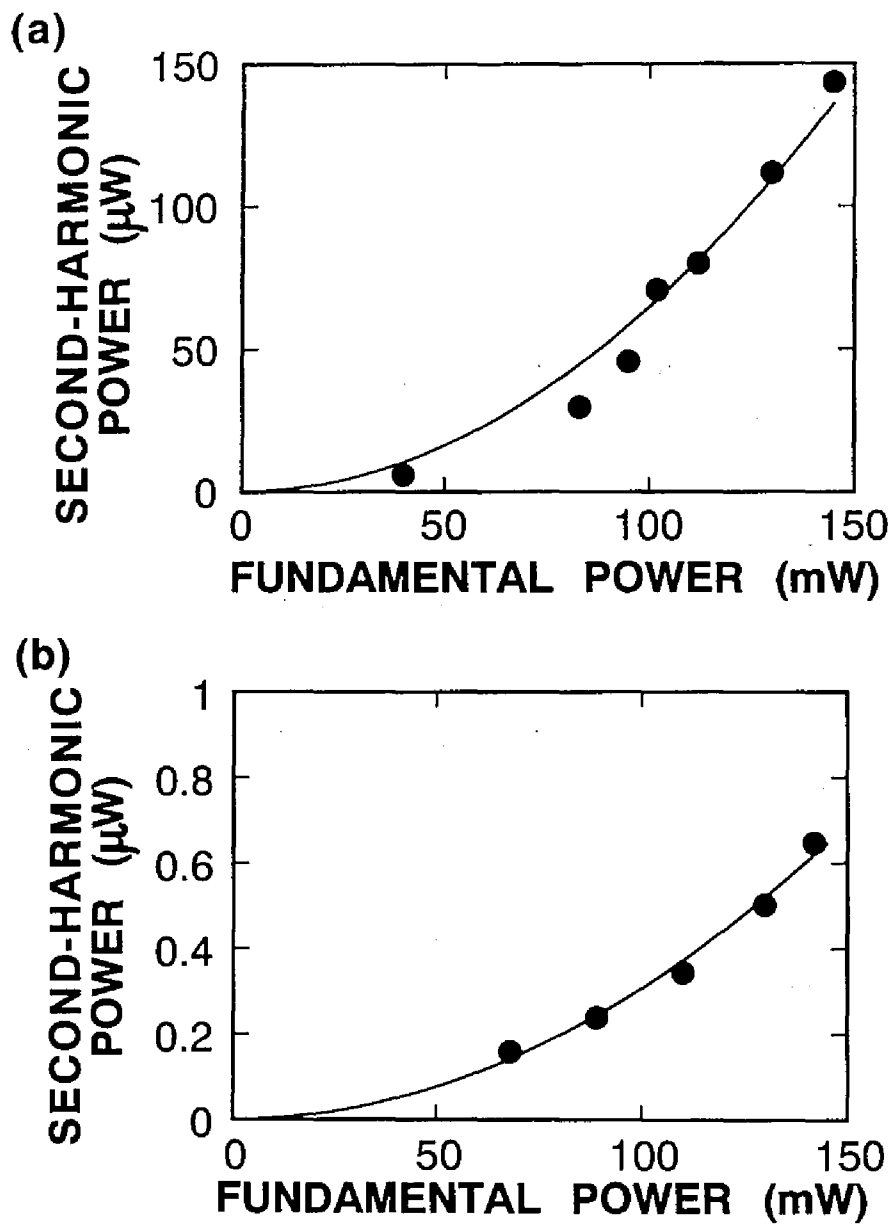
Fig. 3.10. Second-harmonic power at 369.52 nm vs. fundamental power from a dye laser. (a) External cavity technique. (b) Single pass.

matching ratio η_m is assumed to be 1. Therefore, if we change r_i to 0.94, we could increase the fundamental enhancement factor to 16. The second harmonic power would increase by 24 %. The cavity finesse was 32 and the FWHM cavity resonance width was 5 MHz. This value seemed to be close to the actual laser linewidth, because we observed output power fluctuation. Actually, when we did not lock the dye laser frequency to the reference cavity, we could not lock the resonance of the external cavity to the frequency of the dye laser.

Theis analysis was performed before insertion of a set of dual galvoplates to enable a wide range of frequency scanning. Insertion of the dual galvoplates degraded the enhancement factor to 13.

3.4. Ti:Al$_2$O$_3$ Laser for Radiation at 935 nm [11]

To laser cool Yb$^+$, it is necessary to deplete the $^2D_{3/2}$ state. We adopted the method, demonstrated by researchers at NPL and PTB, of driving the $^2D_{3/2}$ - $^3[3/2]°_{1/2}$ transition at 935 nm [14], because tunable radiation at this wavelength is directly generated by a Ti:Al$_2$O$_3$ laser, a Nd^{3+} fiber laser [34], or a diode laser [35]. Another method of depleting the $^2D_{3/2}$ state is to drive the $^2D_{3/2}$ - $^2P_{1/2}$ transition at 2.4 μm [36]. However, generation of radiation at 2.4 μm needs frequency conversion, because no reliable lasers are available at that wavelength.

We produced radiation at 935 nm using a commercial single-frequency ring Ti:Al$_2$O$_3$ laser (Swartz Elecro-Optic). The cavity of this laser incorporates an unidirectional device, and a thin etalon for single-frequency operation. One of the cavity mirrors is mounted on PZT. This laser was operated stably at a single frequency after a few hours of warming up. We modified the laser for frequency scanning over 1 FSR of the laser cavity by installing a set of dual galvoplates, and mounted the

thin etalon on a galvanometer. We rotated the dual galvoplates and the galvano-driven thin etalon synchronously during frequency scanning. When we continuously frequency scanned beyond 3 GHz, however, a mode hop occurred because there was no feedback loop to make the resonance of the thin etalon in accordance with that of the laser cavity. Part of the beam from the $Ti:Al_2O_3$ laser went to the wavemeter for rough frequency setting of the IR frequency, and to a confocal cavity with a FSR of 2 GHz to monitor the longitudinal mode of the $Ti:Al_2O_3$ laser.
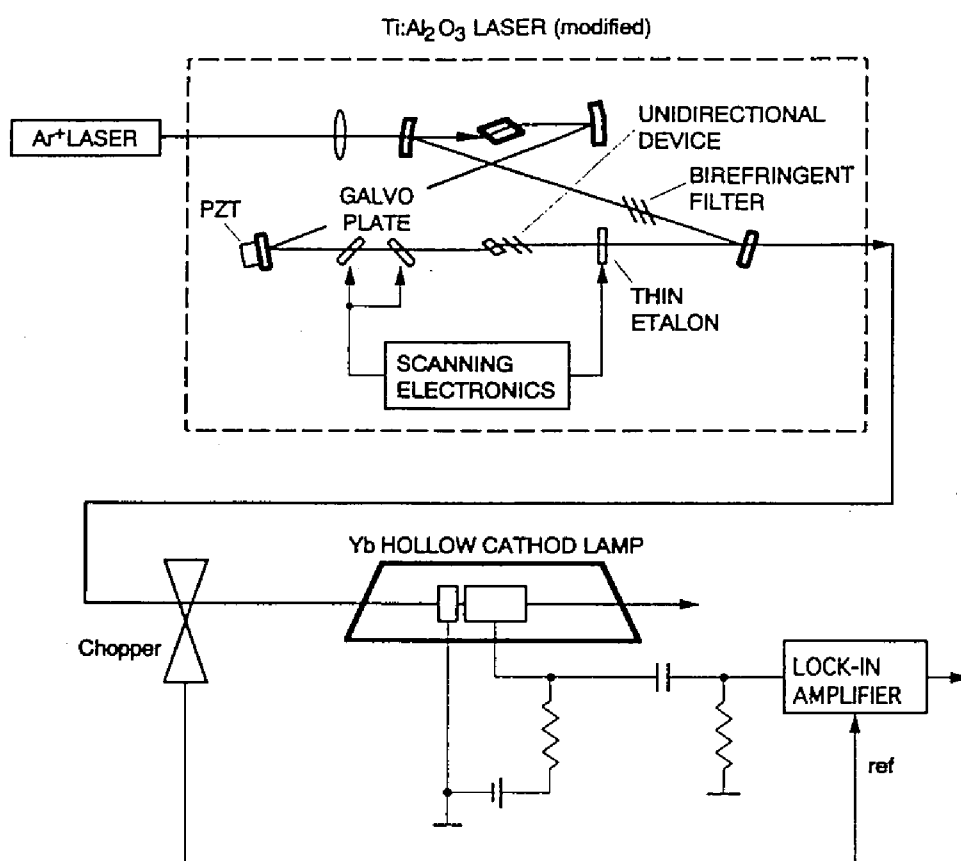
Fig. 3.11. Experimental setup for detection of optogalvanic signals of the $^2D_{3/2}$ - $^3[3/2]°_{1/2}$ transition of Yb^+ at 935 nm.
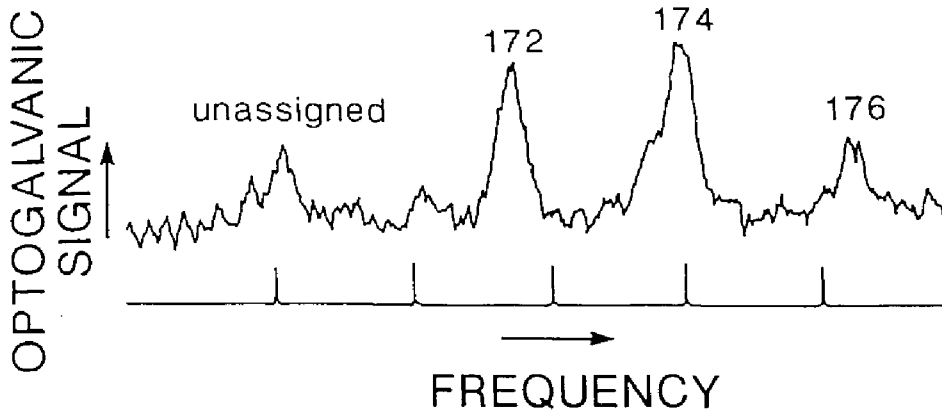
Fig. 3.12. Optogalvanic signals of the $^2D_{3/2}$ - $^3[3/2]^{\circ}_{1/2}$ transition of Yb$^+$ in a hollow cathode lamp. The lower trace is a 2 GHz maker signal by the transmission signal of a confocal cavity.

To measure the isotope shifts of the $^2D_{3/2}$ - $^3[3/2]^{\circ}_{1/2}$ transition, we detected optogalvanic signals of Yb$^+$ in the hollow cathode lamp. The experimental set up is shown in Fig. 3.11. The observed signals are shown in Fig. 3.12. In Fig. 3.12, we show the transmission signal from the confocal cavity as a 2 GHz frequency marker. Assignment of the isotopes was performed by detecting the spectra of the laser-cooled Yb$^+$ ions described in Chap. 5, because fluorescence of the isotope is observed only when radiation at 369.52 nm and 935 nm is resonant simultaneously. The measured isotope shifts are listed in Table 3.2. The uncertainties are caused by imperfection of frequency scanning of the Ti:Al$_2$O$_3$ laser. In the table, we include the values measured at PTB for ^{172}Yb$^+$ and two lines of ^{171}Yb$^+$ [37,38]. According to Refs. [37,38], one of the ^{171}Yb$^+$ lines overlaps with the ^{172}Yb$^+$ line. This is in agreement with our result because the ratio of the signal assigned to ^{172}Yb$^+$ to those of ^{174}Yb$^+$ and ^{176}Yb$^+$ was

larger than that of natural abundance. The other ^{171}Yb$^+$ line reported in ref. [37,38] may coincide with our unassigned peak.

Table 3.2. Isotope shifts of the $^2D_{3/2}$ - $^3[3/2]^o_{1/2}$ transition of Yb$^+$ at 935 nm

Present Work

Isotopes	Frequency Intervals
176 - 174	2.6 (0.2) GHz
174 - 172	2.7 (0.2) GHz

Isotopes	Wavelength
176	935.172 (1) nm
174	935.179 (1) nm
172	935.187 (1) nm
unassigned	935.196 (1) nm

PTB [36,37]

Isotope	Wavelength
171(F=1 – F=0) and 172	935.1880(30) nm
171(F=1 – F=1) and 171(F=2 – F=1)	935.1953(30) nm

3.5. Conclusions

In this chapter, we described our light sources for investigation of Yb$^+$. For detection of the fluorescence and laser cooling of Yb$^+$, radiation at 369.52 nm is required to drive the $^2S_{1/2}$ - $^2P_{1/2}$ first resonance line. We produced tunable cw radiation at 369.52 nm by a simple and inexpensive method, i.e., sum-frequency mixing of diode-laser radiation at 1310 nm and argon-ion laser at 515 nm. More than 1μW of UV radiation was generated from a diode-laser power of 21 mW and an argon-ion laser power of 1.3 W with a β-BaB$_2$O$_4$ crystal. We successfully observed the fluorescence of trapped Yb$^+$ ions, as described in Chapter 4. We found that the phase-mismatching tolerance became large when we strongly focused input beams. This is caused by the fact that an aperture length was shorter than the crystal length due to a relatively large double refraction of this material.

We proposed a simple frequency stabilization scheme of sum frequency, i.e., stabilization of sum-frequency by controlling only one of the fundamental lasers of mixing. We successfully applied this scheme to the sum-frequency mixing of diode-laser and argon-ion-laser radiation. We controlled only the diode laser while the argon-ion laser was free-running. This scheme is effective also for difference-frequency mixing.

We found that more powerful radiation at 369.52 nm was required for laser cooling. For this purpose, we generated radiation at 369.52 nm by second-harmonic generation of dye-laser radiation using an external cavity technique. We obtained more than 100 μW of UV radiation by an external cavity of which fundamental enhancement factor was 14. We succeeded in laser cooling of trapped Yb$^+$ ions using this radiation, as described in Chapter 5.

For laser cooling, the $^2D_{3/2}$ metastable state must be depleted. For this purpose, we generated radiation at 935 nm by a Ti:Al$_2$O$_3$ laser to

drive the $^2D_{3/2}$ - $^3[3/2]^o_{1/2}$ transition. We detected optogalvanic signals of Yb^+ in a lamp to determine the isotope shifts of this transition, which were not well known. Knowledge of the isotope shifts of this transition is important for laser cooling, in particular, in the case that a natural isotope mixture of Yb^+ is used as is the case with us.

Chapter 4

Yb^+ Stored in a RF Trap with Buffer Gases

4.1. Introduction

In this chapter, we describe the characteristics of buffer-gas-cooled Yb^+. In our study, we concentrated mostly on investigating the characteristics when the trapped Yb^+ ions were continuously irradiated with radiation at 369.52 nm which is in resonance with the $^2S_{1/2}$ - $^2P_{1/2}$ transition. The basic experimental setup is shown in Fig. 4.1. All components of the setup have been explained in Chapter 2 and Chapter 3.

When the $^2S_{1/2}$ - $^2P_{1/2}$ transition at 369.52 nm of trapped Yb^+ ions is continuously driven in the presence of buffer gases, the fluorescence of the trapped Yb^+ ions fades with a decay time much shorter than their storage time (see Fig. 4.4). The $^2P_{1/2}$ state of Yb^+ has a spontaneous decay pass to the $^2D_{3/2}$ metastable state. However, the lifetime of the $^2D_{3/2}$ state, measured to be 52 ms by Gerz et al. [1], is much faster than the fluorescence decay time. Therefore, the fluorescence decay requires further explanation. In this chapter, we mainly describe our observations related to fluorescence decay and how we have been getting closer to fully understanding the observations.

First, we introduce the history of investigations on this phenomenon, although a brief summary has already been given in Sec. 1.2. In 1988, researchers in Hamburg first recognizing fluorescence decay and explained that it was caused by population trapping in the $^2F_{7/2}$
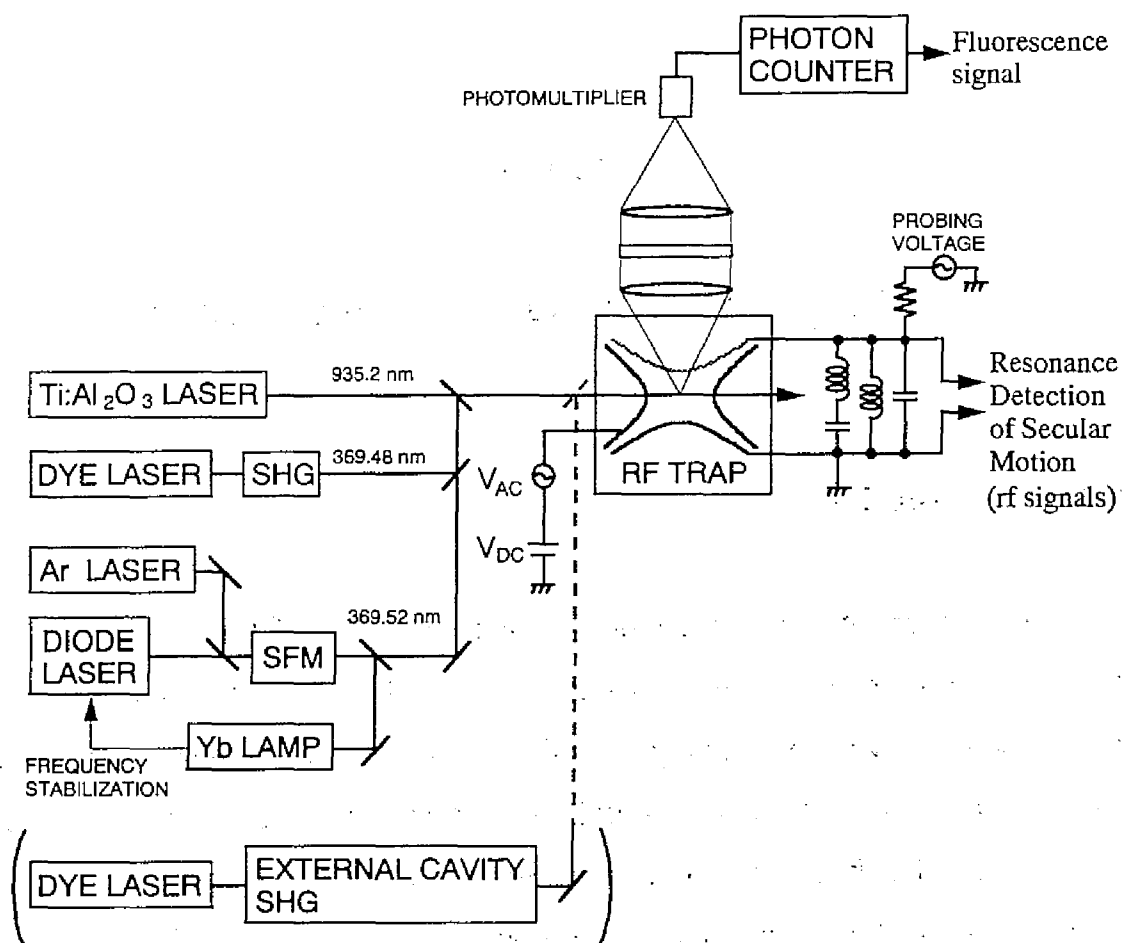
Fig. 4.1. Experimental setup for buffer-gas-cooled Yb^+.
(The later experiments, i.e., in the experiments of the O_2 and H_2O introduction and of mass selective detection, we used the UV radiation generated by SHG of dye-laser radiation using an external cavity technique (in parentheses), in place of that realized by a frequency-stabilized sum-frequency.)

state, the lifetime of which exceeds 8 days [2]. Since then, fluorescence decay has been observed in every laboratory when the $^2S_{1/2}$ - $^2P_{1/2}$ transition of trapped Yb^+ ions is driven in the presence of buffer gases [3-6]. After the first observation in Hamburg, the pressure dependence of the fluorescence decay time was observed at NPL [3]. Researchers at PTB, based on detailed investigation, concluded that population trapping in the

$^2F_{7/2}$ state was induced by collision with buffer gas [4].

At our laboratory, in 1991, we observed that rf signals also disappeared as fluorescence faded when we continuously drove the $^2S_{1/2}$ - $^2P_{1/2}$ transition in the presence of buffer gases. RF signals, in the case of rf traps, are based on the fact that trapped ions absorb rf electric power of which the frequency is the same as that of the secular motion of the trapped ions. Therefore, we proposed the existence of effects due to which trapped Yb^+ ions disappeared in the trap [5,6].

In subsequent work, almost one year later, we found that rf signals did not disappear even when we drove the $^2S_{1/2}$ - $^2P_{1/2}$ transition at 369.52 nm in the presence of buffer gases unlike the results of our previous work [7]. The difference in the experimental conditions from our former experiments was the vacuum condition and/or the buffer gases used. Therefore, we suggested that the disappearance of Yb^+ ions must depend on the type of gas [7]. In support of this proposal, we observed that the disappearance of rf signals was enhanced by the introduction of O_2 and H_2O gases into the vacuum chamber [8]. When rf signals disappeared, their resonance points were shifted those of heavier mass and then finally disappeared. Therefore, we suggested the possibility of the production of molecular ions by chemical reaction of Yb^+ in excited states with background gases. Shifting of rf signals has been observed since we found the disappearance of rf signals, and has already been described in Ref. [5]. However, we recognized the possibility of molecular ion formation during the investigations described in Ref.[7].

At that time [7,8], we concluded that both population trapping in the $^2F_{7/2}$ state and disappearance of Yb^+ due to background gases occurred. When the partial pressure of the gases which cause the disappearance was sufficiently low, fluorescence decay was caused by population trapping in the $^2F_{7/2}$ state, followed by the disappearance of Yb^+ was followed on a slower time scale. As a related observation, Seidel and Maleki recently

conjectured the possibility of the formation of molecular ions based on their observation with continuous driving of the $^2S_{1/2}$ - $^2P_{3/2}$ transition [9].

In order to conduct a more quantitative study of the disappearance of rf signals, including obtaining direct evidence of the production of molecular ions, we have been developing a mass-selective ionic detection system by combining a quadrupole mass analyzer with our rf trap. Until now, we have obtained the following two results. (i) We found that YbH^+ was produced by the chemical reaction of Yb^+ in excited states with H_2 gas [10]. (ii) In the presence of O_2 gas, we found that YbO^+ and some other molecular ions were produced from Yb^+ in excited states [11].

For the production of YbH^+ [10], we actually found the YbH^+ production when no buffer gas were introduced into the vacuum chamber and YbH^+ was produced by chemical reaction with H_2 gas in residual background gases. The production of YbH^+ is distinguished from our former proposal of molecular-ion formation. In refs. [7,8], as described above, the disappearance and shifting of rf signals had a slower time constant than did fluorescence decay. However, the production of YbH^+ occurred on the same time scale as the fluorescence decay, and rf signals did not disappear but were merely just shifted with the production of YbH^+. In addition, we found that some observations formerly interpreted to be associated with Yb^+ in the $^2F_{7/2}$ state were actually caused by YbH^+. Therefore, the production of YbH^+ should be considered as another reason for fluorescence decay. We overlooked the YbH^+ production by confusing it with population trapping in the $^2F_{7/2}$ state, as did other researchers.

From experiments performed in the presence of O_2 gas [11], we proved that the production of YbO^+ and some other molecular ions is the reason for the shifting of rf signals. However, the number of YbO^+ ions did not show a significant decrease from that of the initially trapped Yb^+ ions, even after the rf signals disappeared. We now consider that the

decrease in the total number of trapped ions does not seem to be an appropriate reason for the disappearance of rf signals.

We organize this chapter in the following manners: We start the next section with a description of the spectra of the $^2S_{1/2}$ - $^2P_{1/2}$ transition in the presence of buffer gas. Then, we move on to results of the fluorescence decay when the $^2S_{1/2}$ - $^2P_{1/2}$ transition at 369.52 nm was continuously driven in the presence of buffer gases. We also show the fluorescence signals by simultaneously irradiating the trapped Yb^+ ions at other wavelengths. We reproduced early observations made at other laboratories, in particular, those of the detailed investigations at PTB [4]. In Sec. 4.3, we describe the disappearance of rf signals and how we noticed that some background gases should be responsible for the disappearance of rf signals in 4.3.2. In 4.3.2, we clarify the effect of some gases on the disappearance of rf signals by introducing O_2 and H_2O gases into the vacuum chamber. In Sec. 4.4, We describe the results obtained using mass-selective ionic detection. The experimental setup is presented in 4.4.1. The production of YbH^+ and reaction with introducing O_2 gas are described in 4.4.2 and 4.4.3, respectively. In Sec. 4.5, we summarize our present conclusion, obtained from five years of investigation, concerning the characteristics of Yb^+ with continuous driving of the $^2S_{1/2}$ - $^2P_{1/2}$ transition in the presence of buffer gases. We point out the remaining problems to be clarified. The production of molecular ions may be a problem in establishing a frequency standard with buffer-gas-cooled Yb^+. In particular, the production of YbH^+ may be serious because of the difficulty in removing H_2 gas from the vacuum system. We make some discuss this problem from this point of view, including the case of other ion species. Also, in the final part of this section, we demonstrate an positive application of molecular-ion production to chemical investigation.

4.2. Fluorescence signals with resonant light

4.2.1. Spectra of the $^2S_{1/2}$ - $^2P_{1/2}$ Transition at 369.52 nm [5]

We detected the fluorescence of trapped Yb^+ ions by driving the $^2S_{1/2}$ - $^2P_{1/2}$ transition at 369.52 nm. The fluorescence, emitted by spontaneous emission from the $^2P_{1/2}$ state to the $^2S_{1/2}$ state was detected. We used tunable cw radiation at 369.52 nm generated by the sum-frequency mixing of diode-laser radiation at 1310 nm and argon-ion-laser radiation at 515 nm described in Secs. 3.2 and 3.3.

The fluorescence signals are shown in Fig 4.2(a). The temperature of the diode laser was constantly changed to sweep the frequency of the UV radiation. Although we used natural Yb, no hyperfine components of odd isotopes were observed. Figure 4.2(b) shows the fluorescence signal obtained using the two uv beams. One of the UV beams was frequency stabilized to the $^{173}Yb^+$ 3-2 line while the frequency of the other was swept. The signal of the $^{173}Yb^+$ 2-3 line was observed because the frequency-stabilized UV beam prevented optical pumping.

The temperature of the trapped Yb^+ ions was determined from the width of the fluorescence signal to be 3600 ± 800 K at a He pressure of 4×10^{-6} Pa. The contribution of isotopes was considered and the saturation was ignored to determine the temperature. Light buffer gas was effective in reducing the kinetic energy of the trapped ions [12,13]. The pressure dependence of the temperature of trapped Yb^+ ions is shown in Fig. 4.3. The ions were cooled to 1200 (+700, −500) K at a He pressure between 4×10^{-5} Pa and 4×10^{-4} Pa.
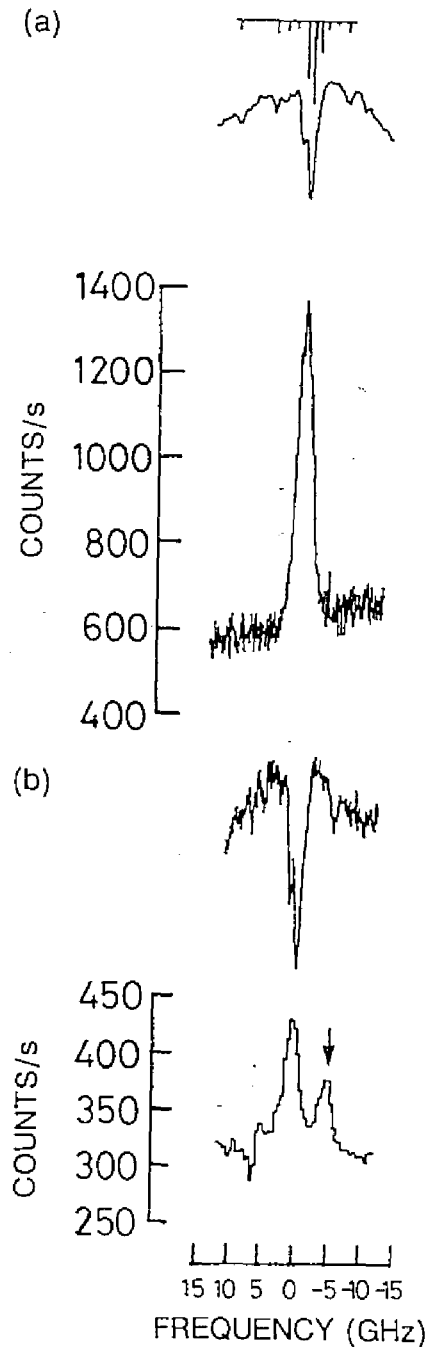
Fig. 4.2. Fluorescence signal of the trapped Yb^+ ions. In both (a) and (b), the upper trace is the absorption signal of Yb^+ in a hollow cathode lamp and the lower the photon counting signal of the Yb^+ ions trapped in a rf trap. The strength and the frequency of each absorption of isotopes is shown at the top of the figure. (a) The frequency of one UV radiation was swept around the $^2S_{1/2}$ - $^2P_{1/2}$ transition. The UV power (All UV power mentioned in this paper was measured at the window of the vacuum chamber) was 170 nW, the He pressure 4×10^{-4} Pa, the sweep rate of the UV radiation 110 MHz/s, and the gate time of the photon counting 1 s. (b) The signal obtained by two UV beams; One was frequency stabilized to the $^{173}Yb^+$ 3-2 line, the frequency of the other was swept. The arrow indicates the $^{173}Yb^+$ 2-3 line. The frequency-stabilized UV power was 300 nW, the frequency-swept UV power 65 nW, the He pressure 4×10^{-4}, the sweep rate 42 MHz/s, and the gate time 10 s.
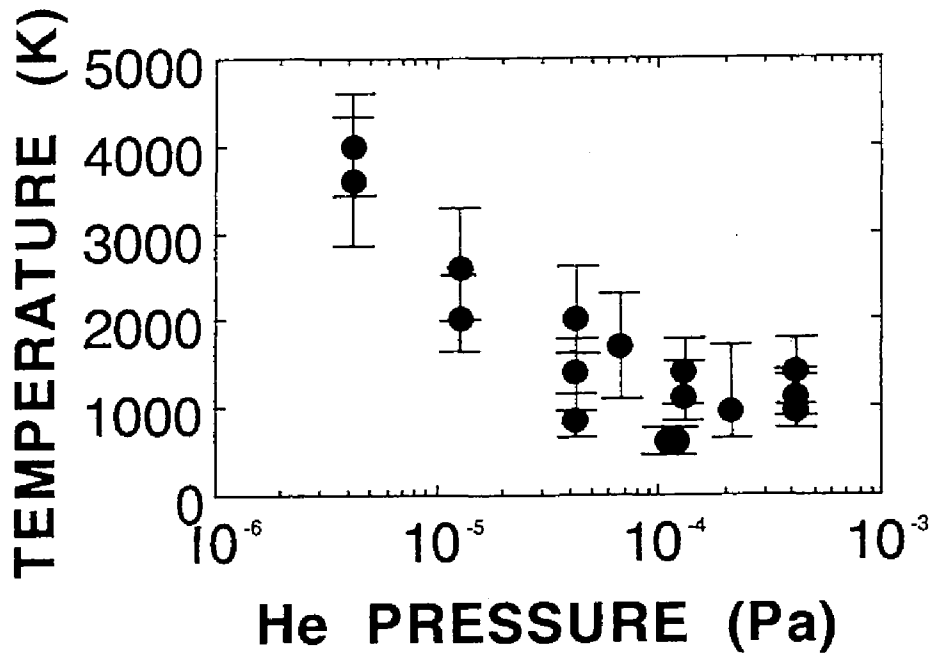
Fig. 4.3. He pressure vs. temperature of trapped Yb^+ ions. The temperature was determined from the Doppler width of the spectra of the $^2S_{1/2}$ - $^2P_{1/2}$ transition at 369.52 nm. The error bars are due to the noise in the spectra.

4.2.2. Fluorescence Signals with Continuous Irradiation with Resonant Light [7]

In this subsection, we describe the fluorescence signals obtained when we continuously irradiated Yb^+ ions trapped in the presence of buffer gases with resonant light beams, i.e., radiation at 369.52 nm to drive the $^2S_{1/2}$ - $^2P_{1/2}$ transition, radiation at 935 nm to drive the $^2D_{3/2}$ - $^3[3/2]_{1/2}$ transition to deplete the $^2D_{3/2}$ state [14,15], and radiation at around 369.48 nm which was assigned to be the wavelength to deexcite the $^2F_{7/2}$ state when the experiments described in this subsection were performed.

102

(As we will show in 4.4.2, these wavelengths are those for photodissociation lines of YbH^+ [10].) The results shown in this subsection were obtained under the condition that rf signals did not disappear.

Tunable cw radiation at 369.52 nm was the sum-frequency radiation frequency locked to the absorption signal of Yb^+ in the lamp as described in Sec. 3.3. Sources of radiation at 935.2 nm and 369.48 nm were the ring-Ti:Al_2O_3 laser and the frequency-doubled dye-laser, respectively. The frequency doubling of dye laser radiation was made in the crystal with single pass. The wavemeter for monitoring the wavelengths of the two lasers in the experiments here had a resolution of 1×10^{-3} nm and an uncertainty of $\pm 5 \times 10^{-6}$. The frequency drifts of the two lasers were below the resolution. Power levels of radiation at 369.52 nm, 369.48 nm, and 935.2 nm were a few hundreds nW, about 100 nW, and a few mW, respectively.

We also obtained radiation at 369.52 nm and 369.48 nm simultaneously by sum-frequency mixing. In this case, we input the two diode laser beams at different wavelengths to the β-BaB_2O4 crystal. The large phase-mismatching tolerance of this sum-frequency mixing resulted in the same conversion efficiency for the two UV generations as we previously proposed in Sec. 3.2.. However, second-harmonics is more convenient for detailed investigations, such as wavelength measurement.

The frequency and amplitude of ac voltage of the rf trap were 550 kHz and 310 V, respectively. DC voltage (V_{dc}) was continuously scanned between 6 and 9 V to detect rf signals, while the frequency of the probing rf field was fixed at 83.5 kHz. He or N_2 gases were used as buffer gas. Pressure of buffer gas was measured by the discharge current of the ion pump which evacuated a vacuum chamber. Fluorescence was collected and transported by lenses, and was detected by a photomultiplier of which output was measured by a system of photon counting with a gate time of 1 s and a dead time of 2 ms.

The total number N_0 of trapped Yb^+ ions was determined from rf signals [16,17] . Owing to anharmonicity of the potential, shapes of rf signals depend on the sweep direction of V_{dc} or frequency of the probing field as described in Sec. 2.3. The two signals, obtained by the two sweep directions, give the upper and lower limits of N_0. The storage time was beyond 10^4 s without irradiation at 369.52 nm. We determined the temperature of trapped Yb^+ ions to be 1400 K at a He pressure of 4×10^{-4} Pa from the linewidth of the $^2S_{1/2}$ - $^2P_{1/2}$ transition, as described in Sec. 4.2.1.
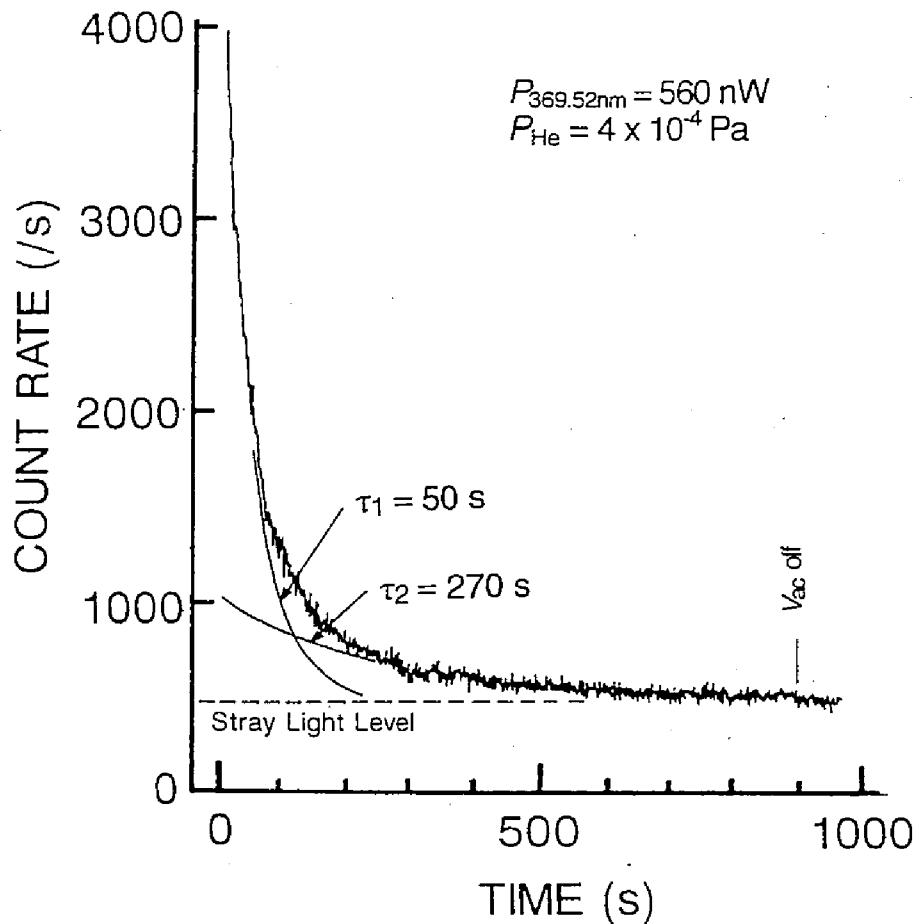
Fig. 4.4. Decay curve of the fluorescence signal by irradiation only at 369.52 nm. The decay curve was fitted with two decay times. Faster decay time is indicated by τ_1 and the slower one, τ_2. The spot size of the UV beam was 0.05 mm $\times$ 0.05 mm at the center of the trap.
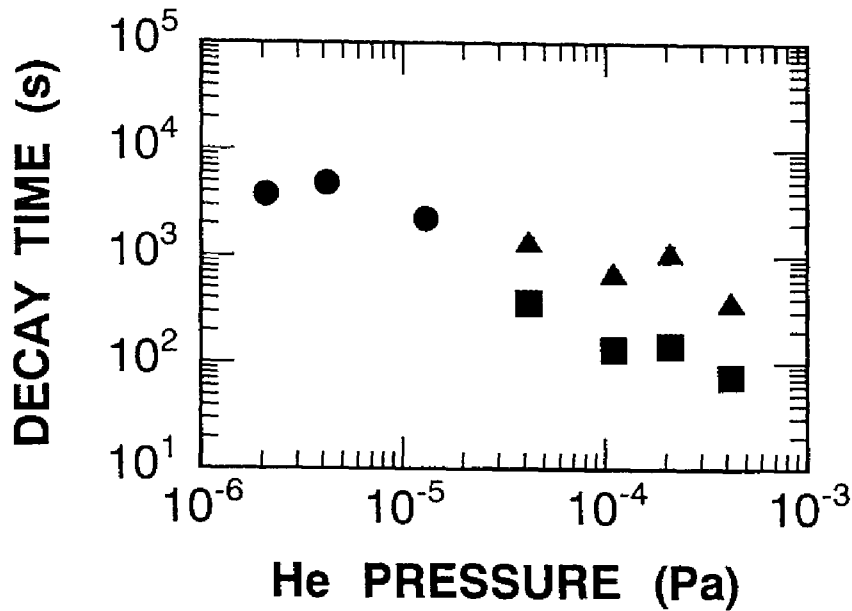
Fig. 4.5. Dependence of the decay time on He pressure. ■:faster decay time τ_1, ▲:slower one τ_2. We could not distinguish the two decay curves below a He pressure of 4×10^{-5} Pa. Longer observation time is necessary to distinguish them. The power of radiation at 369.52 nm was 440 nW and the beam size was 0.5 mm × 0.5 mm.

(1) Irradiation with radiation at 369.52 nm driving the $^2S_{1/2}$ - $^2P_{1/2}$ transition

When we continuously irradiated trapped Yb^+ ions with radiation at 369.52 nm in the presence of buffer gases, fluorescence faded in a decay time shorter than the storage time. Typical decay curve of fluorescence intensity is shown in Fig. 4.4. The decay times grew shorter as the power of radiation at 369.52 nm, or the He pressure, was increased. The tail with a slower decay time became apparent in the fluorescence decay curve as the power of radiation at 369.52 nm and He pressure were increased. Figure 4.5 shows the dependence of the decay times on He pressure. Whether rf signals disappeared or not, we observed that the fluorescence

faded in similar time constants, although we described in this subsection the fluorescence signals when rf signals did not disappear.

(2) Irradiation at 369.48 nm

When the experiment described in this subsection was performed, researchers, including us, believed that trapped Yb^+ ions were pumped to the $^2F_{7/2}$ state in the presence of buffer gases by driving the $^2S_{1/2}$ and $^2P_{1/2}$ transition at 369.52 nm, and Yb^+ in the $^2F_{7/2}$ state was deexcited with irradiation at 369.48 nm. As we will describe in 4.4.2, we recently found
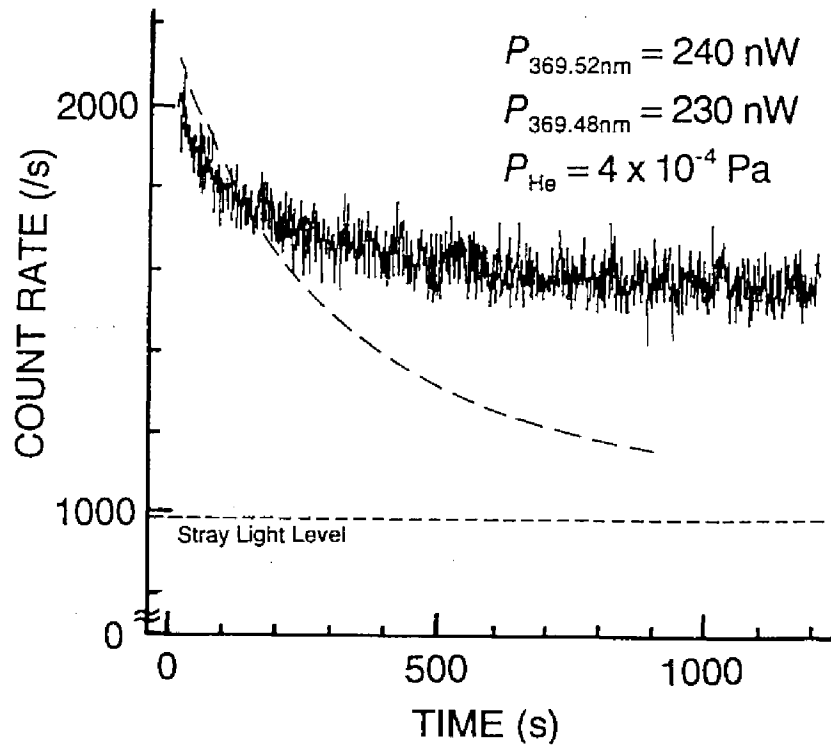
Fig. 4.6. The fluorescence signal by irradiation at 369.52 nm and 369.48 nm simultaneously; Beam sizes were 1.5 mm × 0.5 mm and 0.5 mm × 2 mm, respectively. Dashed curve shows the fluorescence signal with radiation only at 369.52 nm. $N_0 = (4 \sim 7) \times 10^5$ and $r_1 S_1 = 1 \sim 2$ s^{-1}.
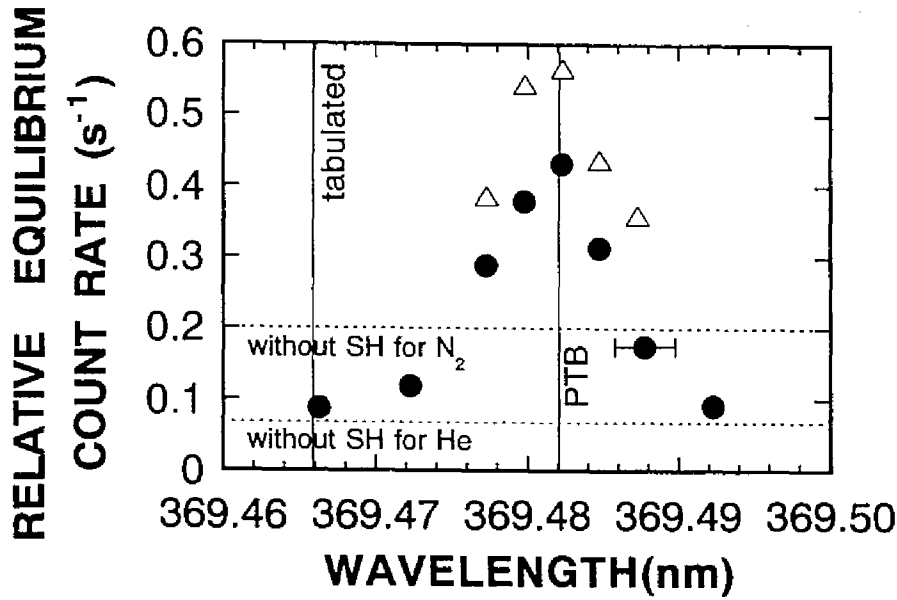
Fig. 4.7. Equilibrium count rate relative to the count rate just after the start of irradiation as a function of the wavelength of radiation at 369.48 nm. He gas was used as a buffer gas for ● , and N_2 gas for △ . Dashed lines indicate the count rate which remained after 20 minutes of irradiation only at 369.52 nm. The error bar shows our wavelength-measurement accuracy of ±0.002 nm. To calibrate the wavemeter, the second harmonics of dye-laser radiation was tuned around the $^2S_{1/2}$ - $^2P_{1/2}$ transition and the wavelength at the maximum fluorescence signal was determined to be the tabulated wavelength of 369.524 nm. Power levels of radiation at 369.52 nm and 369.48 nm were 250 nW and 130 nW, respectively, in the case of He, and at 369.48 nm was 100 nW in the case of N_2. The center wavelength of our results confirmed the results obtained at PTB [4], which are not in agreement with tabulated energy level separation, within our wavelength-measurement accuracy.

that 369.48 nm is a wavelength of photodissociation of YbH^+ [10]. In Ref. [7], we described the following results as deexcitation of the $^2F_{7/2}$ state. However, these actually show that the fluorescence signals when we irradiate trapped Yb^+ ions simultaneously with radiation to photodissociate YbH^+.

We show the results when we irradiated trapped Yb ions at a He pressure of 4×10^{-4} Pa with radiation at 369.52 nm and 369.48 nm

simultaneously. The fluorescence was observed for a longer time than that in the case of radiation only at 369.52 nm as shown in Fig. 4.6. After more than 15 minutes of irradiation with the two UV beams, the count rate became almost constant. We could not decide whether the photodissociation of YbH$^+$ by radiation at 369.48 nm was perfect or not, because it was difficult to keep the power of the dye laser radiation constant over several tens of minutes and there is a possibility that some other molecular ions not photodissociated by the two wavelengths of UV radiation would be produced in a slow rate.

The equilibrium count rate is plotted in Fig. 4.7. as a function of the wavelength of radiation at 369.48 nm. The fluorescence recovery by irradiation at the wavelength in vicinity of 369.52 nm has already been found at the first observation of the fluorescence decay in Hamburg [2]. The researchers at PTB, from their detailed investigation, determined the center wavelengths of the four lines for the fluorescence recovery [4]. Our result at 369.48 nm confirmed the center wavelength determined at PTB within our wavelength-measurement accuracy. Since the fluorescence recovery was first found in Hamburg, it had been believed that the fluorescence-recovery lines were those for deexcitation of the $^2F_{7/2}$ state. As we described in 4.4.2, we found that at least three of the four lined, including 369.48 nm, are photodissociation lines of YbH$^+$. Researchers at PTB pointed out that the wavelengths of the fluorescence-recovery lines were not in agreement with tabulated energy level separation from the $^2F_{7/2}$ state of Yb$^+$ [4].

We also alternated radiation at 369.52 nm and 369.48 nm. After fluorescence disappeared due to radiation only at 369.52 nm, we blocked radiation at 369.52 nm and used radiation at 369.48 nm. After about four minutes of irradiation at 369.48 nm, the fluorescence signal by radiation at 369.52 nm recovered to be within 40 % and 80% of the disappearance count rate.

108

(3) Depletion of the $^2D_{3/2}$ state

Figure 4.8. shows typical fluorescence signals and the decay times when we deplete the $^2D_{3/2}$ state by irradiating at 935.2 nm simultaneously at 369.52 nm. Even at a He pressure of 4×10^{-4} Pa, fluorescence was observed for a long time when the power of radiation at 935.2 nm was sufficiently strong. The count rate just after the start of irradiation did not increase from that with radiation only at 369.52 nm owing to the small excitation rate of the $^2S_{1/2}$ - $^2P_{1/2}$ transition.

After the fluorescence signal decreased and stabilized to a constant value in the case of sufficiently strong power of radiation at 935.2 nm, we blocked the two beams and irradiated at 368.48 nm for over 5 minutes. We observed that more than half of the decreased signals recovered by this means. This means that the observed initial decay was attributed to production of YbH$^+$ or population trapping in the $^2F_{7/2}$ state followed the YbH$^+$ formation in the state.

(4) Discussion and rate analyses

Fluorescence faded with the two decay times when we irradiated at 369.52 nm as shown in Fig. 4.4. A possible explanation of the two decay times is effect of isotope shifts of the $^2S_{1/2}$ - $^2P_{1/2}$ transition. We calculated the excitation rates of the $^2S_{1/2}$ - $^2P_{1/2}$ transition for Yb$^+$ isotopes relative to that for ^{174}Yb$^+$ from the isotope shifts reported in [18] and the overlap between the modulation depth of sum frequency and Doppler-broadening each isotope line at a temperature of 1400 K: These are 0.20 and 0.24 for ^{172}Yb$^+$ and ^{176}Yb$^+$, respectively. ^{168}Yb$^+$ and ^{170}Yb$^+$ are negligible. Therefore, decay times for ^{172}Yb$^+$ and ^{176}Yb$^+$ would be five and four times,
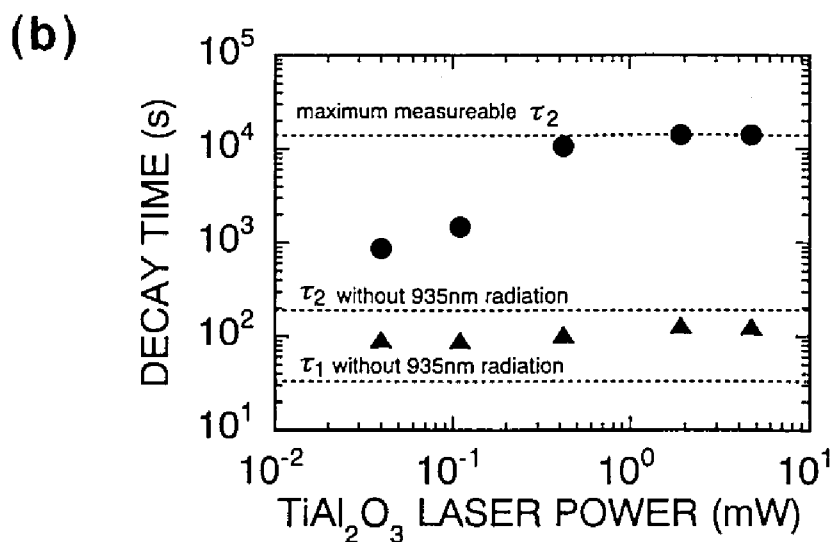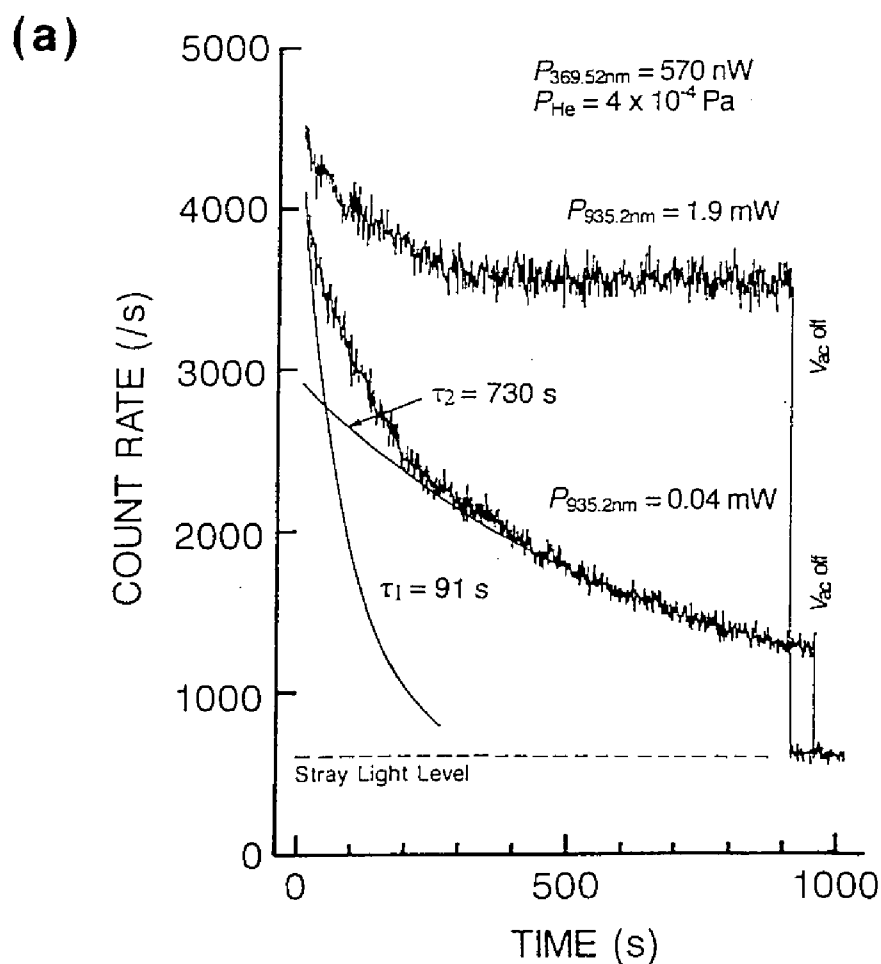
(a)

$P_{369.52nm} = 570$ nW
$P_{He} = 4 \times 10^{-4}$ Pa

$P_{935.2nm} = 1.9$ mW

$\tau_2 = 730$ s

$P_{935.2nm} = 0.04$ mW

$\tau_1 = 91$ s

Vac off

Vac off

Stray Light Level

COUNT RATE (/s)

TIME (s)

(b)

maximum measureable τ_2

τ_2 without 935nm radiation

τ_1 without 935nm radiation

DECAY TIME (s)

$TiAl_2O_3$ LASER POWER (mW)

Fig. 4.8. (a) The fluorescence signals by irradiation at 369.52 nm and 935.2 nm simultaneously. The beam diameter of radiation at 935.2 nm was 2 mm or larger. The beam size of radiation at 369.52 nm was the same as that for Fig. 4.1. $N_0 = (3 \sim 5) \times 10^5$ and $r_1 S_1 = 7 \sim 12$ s^{-1}. (b) The two decay times are shown as a function of IR power. Faster decay time is indicated by τ_1 (▲), and the slower one τ_2 (●).

110

respectively, as long as that for ^{174}Yb$^+$. Taking into account the natural abundance, we estimated that relative count rates just after the start of irradiation would be 0.12, 0.81, and 0.08 for ^{172}Yb$^+$, ^{174}Yb$^+$, and ^{176}Yb$^+$, respectively. If we assume that the faster decay comes from ^{174}Yb$^+$ and the slower one from ^{172}Yb$^+$ and ^{176}Yb$^+$, the observed fluorescence decay curve can be fitted.

From Fig. 4.5, we estimated a pumping rate R_6 to the "dark" state, assuming the faster decay time τ_1 was related to only ^{174}Yb$^+$ as explained above. As we will clarify in Sec. 4.4., the possible explanations of the fluorescence decay at present are population trapping in the $^2F_{7/2}$ state and the production of YbH$^+$. It has not yet been clarified the superiority between the two explanations and the detailed paths to the two states. Therefore, we introduce the "dark" state including the two states. Other notations are given in the Appendix. In our experiment, the excitation rate $r_1 S_1$ of the $^2S_{1/2}$ - $^2P_{1/2}$ transition was small and florescence was not saturated, i.e. $r_1(S_1/A_1)(A_2/R_3)$ <<1. In this case, the relation between the inverse of the observed decay time τ and R_6 is given by [2]

$$\frac{1}{\tau} = r_1 S_1 \frac{A_2}{A_1 + A_2} \frac{R_6}{R_3 + R_6} \ . \tag{4.1}$$

For the result in Fig. 4.2 at a He pressure of 4×10^{-4} Pa, we estimated that $r_1 S_1 = (4 \sim 7)$ s^{-1} from Eq.(A.2'), with $N_0 = (4 \sim 7) \times 10^5$ determined from the rf signal. We obtained $R_6 = (8 \sim 20)$ s^{-1}, substituting $A_1 = 1.14 \times 10^8$ s^{-1} [19], $A_2 = 7.09 \times 10^5$ s^{-1} [19], and $R_3 = 19$ s^{-1} [1] into Eq. (4.1). Our result is close to that at PTB, i.e., $R_6 = 4$ s^{-1} at a He pressure of 4×10^{-4} Pa [4]. The fact that the observed decay times were several tens of times as long as those in Ref. [4], therefore, was attributed to our smaller excitation rate $r_1 S_1$. Power of radiation at 369.52 nm was close to that in Ref. [4]. Therefore, the smaller excitation rate would be caused by a

larger ion cloud and lower ion density than those in Ref. [4]. Ion density at the space charge limit is lower than that in Ref. [4] owing to our lower secular frequency [20].

As we described in Sec. 4.4, we now know that the wavelength of 369.48 nm is that of photodissociation line of YbH$^+$. We estimated a photodissociation rate R_7' to be $(3 \times 10^{-3} \sim 1 \times 10^{-2})$ s^{-1} for Fig. 4.6 from the equilibrium count rate and using Eqs.(A.2$'$) and (A.4), where we treat a overall deexcitation rate R_7 from the 'dark' state as a photodissociation rate R_7'. In the estimation, we used the value of $r_1 S_1$ determined by use of Eq.(A.2$'$) from the count rate just after the start of irradiation. We also estimated an excitation rate S_4 of the transition at 935.2 nm to be $(4 \times 10^5 \sim 1 \times 10^7)$ s^{-1} for Fig. 4.8 at 1.9 mW from the equilibrium count rate and using Eqs.(A.2$'$) and (A.4). The value of $r_1 S_1$ needed in the estimation was also determined by use of Eq.(A.2$'$) from the count rate just after the start of irradiation. For the estimation of S_4, the following assumptions are made: The photodissociation line at 369.48 nm has the same line shape and width as Ref. [4]. Then, we assumed a deexcitation rate R_7'' from the 'dark' state by radiation at 369.52 nm to be $(2 \sim 9) \times 10^{-5}$ s^{-1} from our estimated photodissociation rate R_7' by radiation at 369.48 nm, ignoring the difference of the overlap between the ion cloud and the uv beams between Fig. 4.6 and Fig. 4.8. A collisional deexcitation rate from the 'dark' state, measured to be of the order of 10^{-5} s^{-1} at a He pressure of 4 $\times$ 10^{-4} Pa, was ignored. The diameter of the 935.2 nm beam was as large as that of the ion cloud, i.e., $r_4 = 1$, because the cloud diameter would be estimated to be 2.5 mm if ion distribution was uniform. We substituted $A_4 \approx A_2$ as in [5] and $A_5 = 4.2 \times 10^7$ s^{-1} [21].

The initial decay, observed by irradiating at 369.52 nm and 935.2 nm simultaneously, cannot be explained by rate analysis. The decay time for pumping to the dark state increases by a factor of $(1 + r_4 S_4/(R_3 + R_6))$ from Eq. (4.1) in the case of simultaneous irradiation at 935.2 nm, and is

expected to be $(1 \times 10^4 \sim 4 \times 10^5)$ times as long as that with radiation only at 369.52 nm in the case of Fig. 4.5 at 1.9 mW. One possible explanation for the initial decay is the isotope shift of the transition at 935.2 nm because we drove this transition with a narrow-band laser beam. No initial decay was observed by excitation with a wide-band laser beam [15]. Our result, however, cannot compare with that in Ref. [15] owing to the difference in He pressure.

4.3. Disappearance of RF Signals

In this section, we describe the time variance of rf signals when we continuously irradiated trapped Yb^+ ions with radiation at 369.52 nm in the presence of buffer gases. In 4.3.1, we describe the experiment when we first clearly recognized the disappearance of rf signals. And then, we devote to explain how we notice that some background gases should be responsible for the disappearance. To confirm this hypothesis, we introduced O_2, and H_2O gases into the vacuum chamber, and observed the enhancement of the disappearance by those gases. The details of this experiment is presented in 4.3.2.

4.3.1. Disappearance of RF Signals in the Presence of Buffer Gases [7]

(1) Results

First, we describe the first clear observation of the disappearance of rf signals. Figure 4.9 shows the relative signal height of the rf
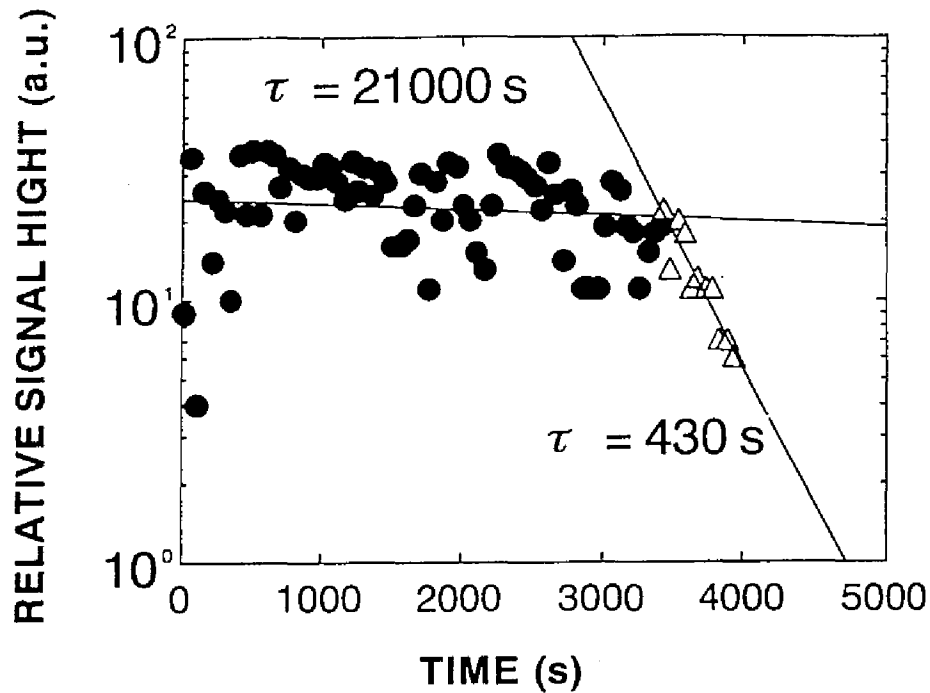
Fig. 4.9.   Decreasing the relative signal height of the rf signals with (triangles) and without (circles) the irradiation of the UV radiation. The time was measured after the stop of the ion production. From 3.4×10^3 s, we started to irradiate the trapped Yb^+ ions with the UV radiation. The decay time of the fluorescence was 100 s.

resonance absorption signal with and without radiation at 369.52 nm. The time was measured after the electron gun and the oven were turned off. From 3.4×10^3 s, we started to irradiate trapped Yb^+ ions with radiation at 369.52 nm. And then, the relative signal height of the rf signal rapidly decreased with a time constant of 4×10^2 s. Simultaneously, the fluorescence signal faded out with a decay time of 1×10^2 s. At the initial observation of the disappearance of rf signals, thus the decay time of the rf signals was close to that of the fluorescence signal at the same pressure and UV power. The dependence of the decay time of the fluorescence and rf signals on the pressure of the buffer gas at the initial observation was reported in Ref.[6]. As the signal height of the rf signals decreased, the

114
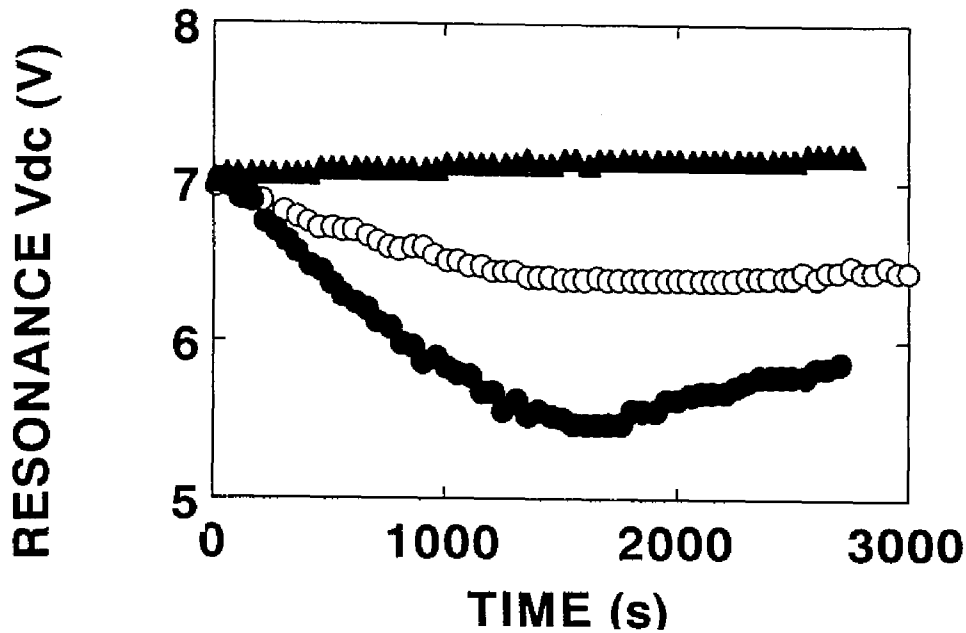
Fig. 4.10. The shift of the resonance V_{dc} of rf signals with and without the irradiation of the uv radiation. The UV beam was introduced immediately after the stop of the ion production. The N_2 at the pressure of 4×10^{-4} Pa was used as the buffer gas. ● ; the UV power was 600 nW. ○ ; 200 nW. ▲ : without irradiation of the UV radiation.

resonant V_{dc} was shifting toward that of a heavier mass as shown in Fig. 4.10. The final dc voltage and the rate of the shift were dependent on the UV power.

Almost one year after the initial observation, we measured the time variance of rf signals again with irradiation at 369.52 nm in the presence of buffer gas, and found that rf signals did not disappear. Figure 4.11 compares the time variance of the rf signals between our former and present experiment. In the case where rf signals did not disappear, as in the present experiment, resonance V_{dc} gradually shifted toward the resonance point for the heavier mass. In the case where rf signals disappeared, as in our former experiment, resonance V_{dc} was first gradually changed, and then, stabilized to a constant value and returned toward the initial resonance. The V_{dc} shift at the stabilized point was observed to be at most -2.6 V in many runs.

In addition, after the experiments described in Sec. 4.2 and Fig. 4.11(2) and we reprepared the buffer gas (The repreparation included evacuation of gas inlet.) , we observed that rf signals faded out after the fluorescence disappeared (Intermediate decay times of rf signals between Fig. 4.11 (a) and (b).) When we blocked radiation at 369.52 nm just after fluorescence disappeared, we observed that rf signals shifted and disappeared, the same as in the observation without blocking radiation. At the moment when this observation was made, we supposed that this fact
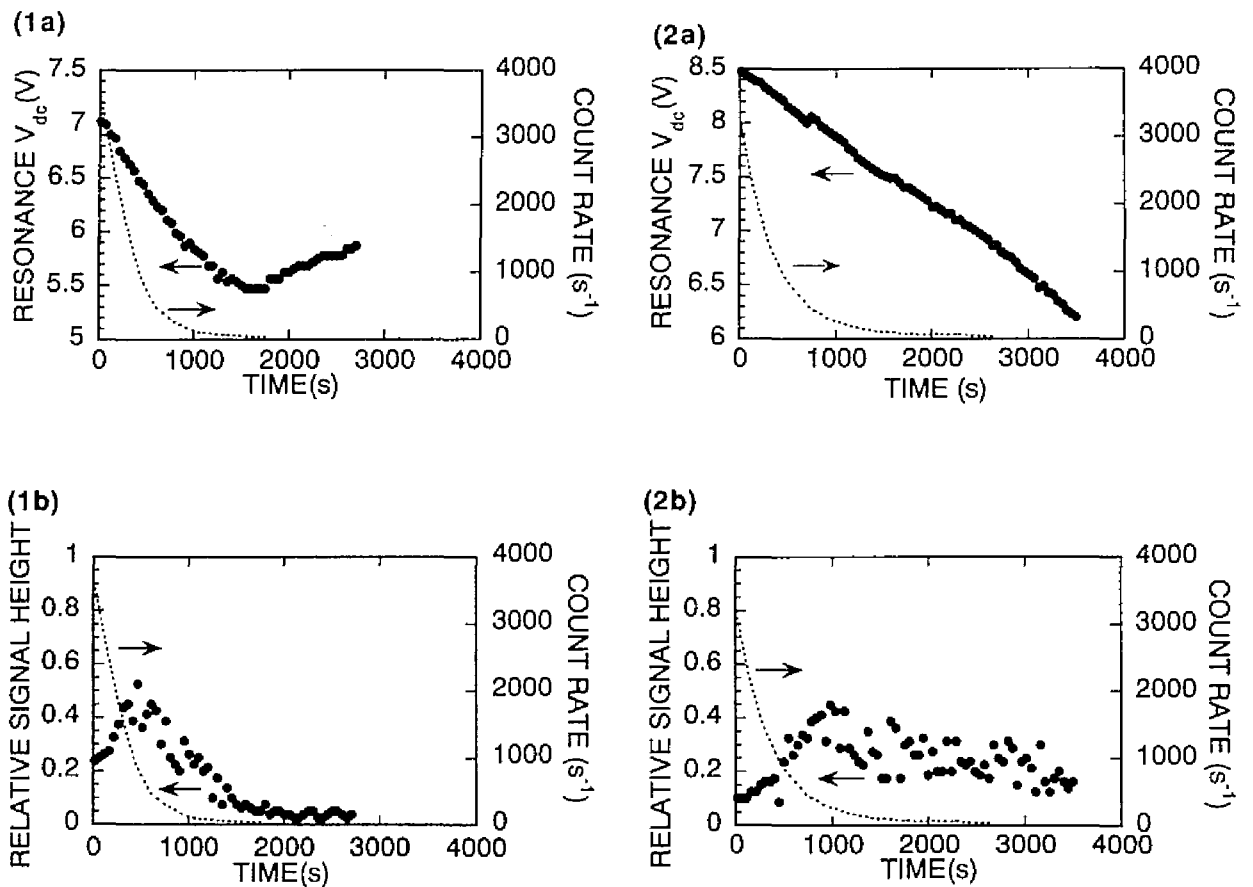
Fig. 4.11   Comparison of the time variances in (a) resonance V_{dc} and (b) relative signal height of rf signals by irradiation at 369.52 nm between (1) our former and (2) the later (one-year after) experiment. N_2 gas at a pressure of 4×10^{-4} Pa was used as a buffer gas. For the former experiment, the power level and beam size of radiation at 369.52 nm were 600 nW and 4 mm × 0.5 mm, respectively. For the present one, 300 nW and 0.5 mm × 0.5 mm.

indicated that Yb^+ ions in the $^2F_{7/2}$ state would disappear. However, at present, we have a different explanation of this. We will present a clearer observation of this fact in Sec. 4.3, and describe the present explanation in Sec. 4.4.

The disappearance occurred only when we irradiated at 369.52 nm. This shows that the disappearance occurred only when Yb^+ ions are in the excited states. Therefore, it is interesting to check whether or not the odd isotopes of Yb^+ were still in the trap when rf signals disappeared, because the odd isotopes of Yb^+ are in the $^2S_{1/2}$ ground state even when we irradiate it with radiation at 369.52 nm owing to the isotope shifts and optical pumping in the hyperfine structure as described in 4.2.1. We observed that $^{171}Yb^+$ and $^{173}Yb^+$ were still in the trap even after the
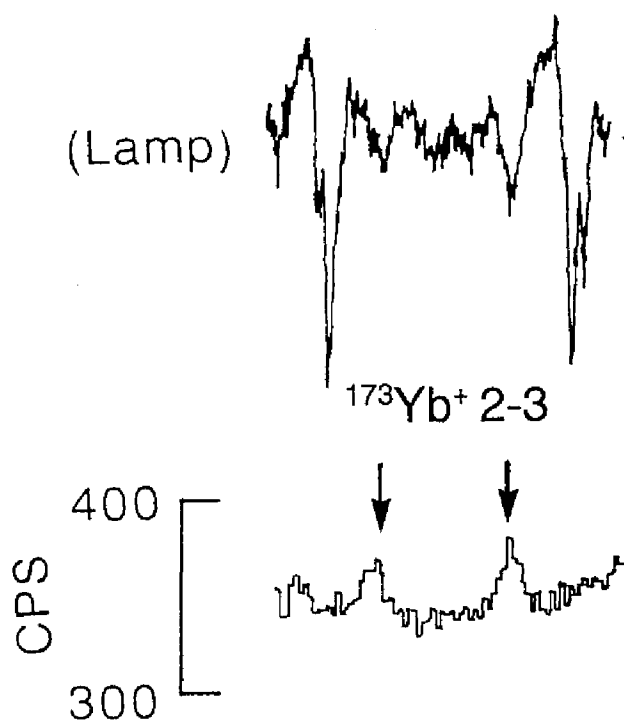
Fig. 4.12. Fluorescence signals of $^{173}Yb^+$ after rf signals disappeared by continuous irradiation with radiation at 369.52 nm locked to the $^{174}Yb^+$ line. Detection was accomplished by a double sum-frequency mixing scheme as used in the case of Fig. 4.2(b). The upper trace is absorption signal of Yb^+ in lamp simultaneously detected. (The spectrum shown in Fig. 4.2(b) was actually taken just before continuous irradiation with radiation at 369.52 nm locked to the $^{174}Yb^+$ line (same loading of ions). We can compare with each other.)

117

fluorescence and the rf signals disappeared. Figure 4.12 shows the fluorescence signals of ^{173}Yb$^+$ after rf signals disappeared. (Detection was accomplished by a double sum-frequency mixing scheme to prevent optical pumping to the hyperfine structures of the $^2S_{1/2}$ state as described in 4.2.1. This experiment was performed before we changed the He gas.)

When we irradiated at 369.52 nm and 369.48 nm simultaneously, V_{dc} shifted with a slower rate than that with radiation only at 369.52 nm. And, when we irradiated at 935.2 nm simultaneously, resonance V_{dc} shifted with a slower rate than that with radiation only at 369.52 nm, and then, it was stabilized to a constant value. The final shift was smaller than that with radiation only at 369.52 nm.

(2) Discussion

RF signals are obtained by detecting the absorption of rf electric power of which frequency is in accordance with that of the secular motion of trapped ions. In a conclusion from the initial observation, we suggested that some other effects different to population trapping in the $^2F_{7/2}$ state caused the trapped Yb$^+$ ions to disappear.

Almost one year after the initial observation, we found that rf signals did not disappear as described above. Therefore, the difference in the experimental conditions between where rf signals disappeared and not disappeared suggested the cause of the disappearance of rf signals. The major differences from our initial observation are the change of buffer gas bottle, evacuation of the system of gas inlet again, and/or improvement of background vacuum pressure owing to long-time evacuation. These indicate that the disappearance was caused by the effects of some gases in our vacuum system including the gas inlet or in contamination of buffer gas. Resonance V_{dc} shifted toward the resonance of heavier mass. This facts suggested a possibility that production of

molecular ions would occur by chemical reactions while rf signals disappear.

We estimate the mass of the produced molecular ions from the shift of resonance V_{dc}. As described above, we assume that only even isotopes of Yb^+ ions would react to molecular ions and the resonance V_{dc} shift would be caused by the collective oscillation in strong coupling [22] among odd isotopes of Yb^+ and molecular ions of even isotopes. From the maximum shift, the increased mass for even isotopes was estimated to be up to 9 in atomic mass units. For calculation, we used the average quantity $<1/m> \equiv \sum(1/m_i)(N_i/N_0)$ and $<1/m^2> \equiv \sum(1/m_i^2)(N_i/N_0)$, where m_i is mass and N_i the number. However, we could not find reactive atoms of an atomic unit below 10. We supposed possible partners of reaction would be some light atoms and molecules, such as O and OH, and H_2O. It is also possible that partners would have much heavier mass which makes the coupling weak. Kalber et al. also found that resonant light irradiation enhanced the loss of trapped Th^+ ions in the presence of buffer gas and suggested the possibility of chemical reaction [23]. Chemical reactions of single trapped Ba^+ ions with background gases were reported by Sankey and Madej [24].

If molecular ions are produced, the disappearance of rf signals requires for its explanation a loss process of molecular ions. Further investigation is necessary for understanding the reason for the disappearance of rf signals. Finally, judging from the fact that odd isotopes of Yb^+ were still in the trap even after rf signals disappeared, this phenomenon has the potential for application to isotope separation.

For shifting the resonance point of rf signals, researchers at PTB also found it and considered that the shift was related to the $^2F_{7/2}$ state [4]. However, the final shift at our laboratory was several times as large as that observed at PTB. Researchers at PTB found that the shifted resonance V_{dc} gradually returned to the initial V_{dc} when we switched the UV

119

wavelength to 369.48 nm after fluorescence faded out and resonance V_{dc} shifted with irradiation at 369.52 nm [4]. We reproduced the similar effect in our laboratory. However, it seemed that resonance V_{dc} did not completely return to the initial V_{dc}. The causes of this small shift and meaning of the returning the resonance point will be clarified in 4.4.2.

4.3.2. Enhancement of the Disappearance by O_2 and H_2O Gas [8]

As described in 4.3.1, we suggested that some gases are responsible for the disappearance of the rf signals. To confirm this proposal, we introduced other gases, i.e., O_2, H_2O, and H_2 gas into the vacuum chamber in addition to He gas, and investigated the effect of those gases on rf signals.

(a) Experimental setup

We used the same experimental setup as that used for the experiments described in 4.3.1 with some small modification. The difference in experimental parameters from those in 4.3.1 are as follows. When we detected rf signals, we modulated V_{dc} into a triangular wave from 5.2 ± 1 V to 11.2 ±1 V with a period of 60 ~ 62 s, while the frequency of the probing rf field was fixed at 83.5 kHz.

Radiation at 369.52 nm used here was produced by SHG of radiation from a dye laser with an external cavity technique described in Sec. 3.4 The power of radiation at 369.52 nm was set at 16 μW at a window of the vacuum chamber. The beam size was 2 mm × 2 mm at the center of the trap. In the measurement of the storage time of Yb^+ in the

$^2S_{1/2}$ ground state, we used other radiation at 369.52 nm, i.e., frequency-stabilized sum-frequency radiation described in Sec. 3.2 owing to the better power stability than that of the second harmonic of the dye laser radiation. The sum-frequency radiation had a power level below 200 nW at the window of the vacuum chamber. When we needed to avoid population trapping to the $^2F_{7/2}$ state (also, to avoid the production of YbH^+. We did not recognized the YbH^+ production at the moment when this investigation was performed.) and the disappearance of Yb^+, we drove the $^2D_{3/2}$ - $^3[3/2]_{1/2}$ transition at 935 nm, using radiation generated by a ring $Ti:Al_2O_3$ laser which had a power level of about 200 mW at the window of the trap with a beam diameter of about 3 mm.

(b) Experimental procedure

We measured the time variance of the rf signals for trapped Yb^+ ions continuously irradiated with radiation at 369.52 nm in the presence of O_2, H_2O or H_2 gas in addition to He gas. The measurements were performed by the following procedure: (1) the temperature of the oven was increased, (2) gases were introduced into the vacuum chamber, (3) the electron gun was turned on to begin production of Yb^+ ions, (4) after the rf signals reached a constant height, the oven and electron gun were turned off, (5) after the oven cooled down sufficiently, we started irradiation at 369.52 nm and rf signals were recorded.

Setting the pressure of the gases was performed as follows. The test gas, i.e., O_2, H_2O or H_2 gas, was first introduced into the vacuum chamber. About 20 minutes after the start of the introduction of the test gas, the pressure, i.e., the current of the ion pump, reached an equilibrium and was kept constant while the variable leak valve was open at a fixed degree. We set the pressure of the test gases at 1.3×10^{-5} Pa.

We then added He gas to a total pressure of 4.2×10^{-4} Pa through the other variable leak valve. The ion pump continued to evacuate the vacuum chamber and the two variable valves remained open during the measurement. The pressure of the test gases was set to 3 % of that of He gas, so that the damping efficiency could be determined from the He pressure in all cases and we could compare the results of the test gases.

(c)   **Result**

We show, in Fig. 4.13, the time variance as the relative signal height and the resonance V_{dc} after the start of irradiation in the presence of (a) O_2, (b) H_2O and (c) H_2 gas. The time was counted after the start of irradiation. The resonance V_{dc} is shown as the shift from the resonance point detected just before the start of irradiation. The decay times of the fluorescence are given in the figure caption. In all experiments shown in the case of Fig. 4.13, the fluorescence faded completely within 60 s. Shorter decay times of the fluorescence than those in the former experiments described in Sec. 4.2 and 4.3.1, are caused by stronger UV power. The time scale of the disappearance of rf signals was clearly separated from and much slower than that of the fluorescence decay.

When we first observed the disappearance of the rf signals, it occurred when we introduced only He gas into the vacuum chamber [5-8]. Before we investigated the effect of these test gases, therefore, we had checked that the rf signals had not disappeared with introduction of only He gas. To clarify that this precaution was indeed effective, in Fig. 4.13, we simultaneously show the time variance of the rf signals with introduction of only He gas, obtained within one week of when the experiments of the mixture gas shown in the same figure were made.

The resonance V_{dc} shifted to -0.2 ~ -0.25 V within 30 s after the
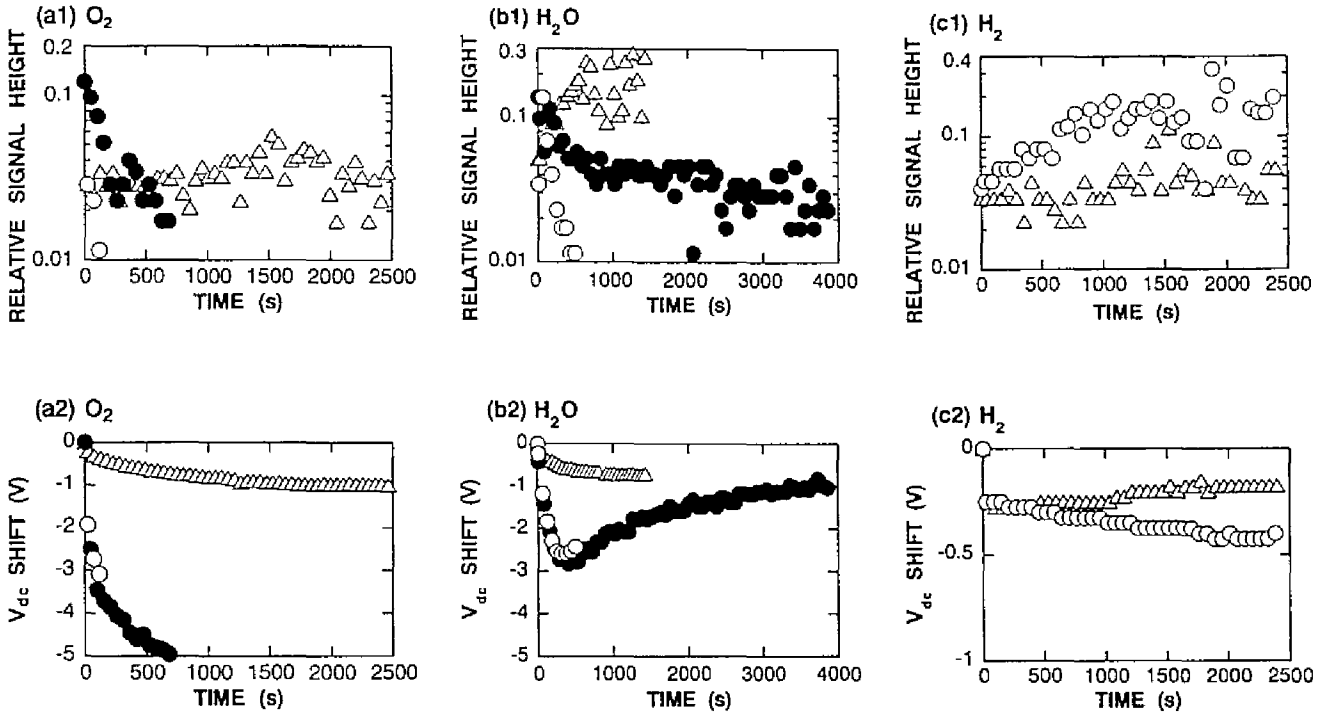
Fig. 4.13. Time variances in (1) relative signal height and (2) shift of resonance V_{dc} of the rf signals with continuous irradiation of radiation at 369.52 nm: (a) in presence of O_2 gas, (b) H_2O gas, and (c) H_2 gas. Pressure of these test gases was 1.3×10^{-5} Pa, and He gas was added to reach a total pressure of 4.2×10^{-4} Pa . ● : sweep direction f, ○ : sweep direction r. For comparison, results in the presence of only He gas at 4.2×10^{-4} Pa of sweep direction r are shown by ▲ . In all cases, the fluorescence faded within 60 s. The decay times of the fluorescence were as follows: (a) O_2 added: $\tau = 0.75(0.03)$ s, He only: $\tau_1 = 2.3(0.2)$ s, $\tau_2 = 9.7(2.1)$ s: (b) $\tau_1 = 2.9(0.2)$ s, $\tau_2 = 11(3)$ s, (c) $\tau = 0.98(0.03)$ s. The two decay times indicated by the subscript may be caused by the isotope shift as discussed in Sec. 4.2. We could not obtain a well-fitted curve from the two decay times when the decay was faster than 1 s.

start of irradiation, as clearly indicated in Fig. 4.13(c2). We revealed the reason of this fast and small shift and described in Sec. 4.4. We will discuss later the observed larger and slower shifts in the presence of O_2 or H_2O gas.

We found that O_2 gas largely enhanced the disappearance of the rf signals. H_2O gas also enhanced the disappearance but the rate of disappearance was slower than that of O_2 gas. The rf signals of the sweep direction r disappeared faster than those of the sweep direction f. We will discuss this observation later. In the case of H_2 gas, we show the time variance of the rf signals of the sweep direction r in Fig. 4.13(c). H_2 gas has little effect on Yb^+, at least at 1.3×10^{-5} Pa. However, as we clarify in 4.4.2, YbH^+ were performed whether H_2 gas additionally introduced or not.

To verify that the disappearance of Yb^+ ions occurs only when the Yb^+ ions are in excited states even in the presence of O_2 or H_2O gas, we determined the storage time of the Yb^+ ions in the $^2S_{1/2}$ ground state, from the time variance of the fluorescence intensity. We must avoid fluorescence decay due to the 'dark' state during this measurement. We irradiated the ions with 369.52 nm radiation with a weak power of 150 nW for 10 seconds at intervals of 10 minutes, and simultaneously with radiation at 935 nm. The storage time τ was determined by fitting the time variance of the fluorescence intensity to the function of $\exp(-t/\tau)$. The determined storage times of the Yb^+ ions in the $^2S_{1/2}$ ground state were over 6×10^4 s, $(2 \pm 1) \times 10^4$ s, and $(2.3 \pm 0.6) \times 10^4$ s for He gas only, O_2 gas with He, and H_2O gas with He, respectively. The pressure of each gas was the same as that in the case of Fig. 4.13. These results show that, even in the presence of O_2 or H_2O gas, the Yb^+ ions in the $^2S_{1/2}$ ground state were trapped and alive for a long time. We monitored the time variance of the rf signals during these measurements. The rf signals, even in the presence of O_2 or H_2O, showed very small change only at 10 seconds of irradiation.

In addition, we performed the two additional experiments. First, we checked that the $^{173}Yb^+$ ions remained in the trap even after the rf signals disappeared in the presence of O_2 gases, as described in 4.3.1. This

is caused by the much slower excitation rates of the $^2S_{1/2}$ - $^2P_{1/2}$ transition for odd isotopes owing to isotope shift and hyperfine splitting [18], because the disappearance occurs only when the Yb^+ ions are in the excited states

Second, as described above, the fluorescence faded much faster than the rf signals. This indicates that at least some of Yb^+ ions are first pumped to the 'dark' state and then disappear. We therefore checked the disappearance of Yb^+ in the 'dark' state by the following procedure: First, we irradiated the Yb^+ ions with radiation at 369.52 nm in the presence of only He gas at 4.2×10^{-4} Pa. This procedure caused Yb^+ ions to transfer the 'dark' state. After the fluorescence disappeared, we blocked radiation at 369.52 nm, and then introduced O_2 gas. In this case, we opened the variable leak valve to the same degree as in the case of 1.3×10^{-5} Pa, because we could not measure the pressure from the discharge current of the ion pump. The observed time variance of the rf signals is shown in Fig. 4.14 after the introduction of the O_2 gas. As we observed in the experiment of Fig. 4.13, the signals in sweep direction r disappeared, and resonance V_{dc} shifted. The small signals in sweep direction f were observed for a long time. However, this remaining signal disappeared when we irradiated with radiation at 369.52 nm again. (Owing to the deviation of the rf signals, it is difficult to see that the rf signals disappeared in Fig. 4.14. We confirmed the disappearance by failures to detect the rf signals five times after the final detection shown in Fig. 4. 14.) We should note that, when this experiment was performed, we believed that Yb^+ ions were first pumped to the $^2F_{7/2}$ state with irradiation at 369.52 nm and a large part of the trapped Yb^+ ions in the $^2F_{7/2}$ state disappeared by O_2 gases. However, we found that fluorescence disappearance was also caused by the production of YbH^+ as described in 4.4.2. We describe our present and more reliable interpretation of this observation in 4.4.2.
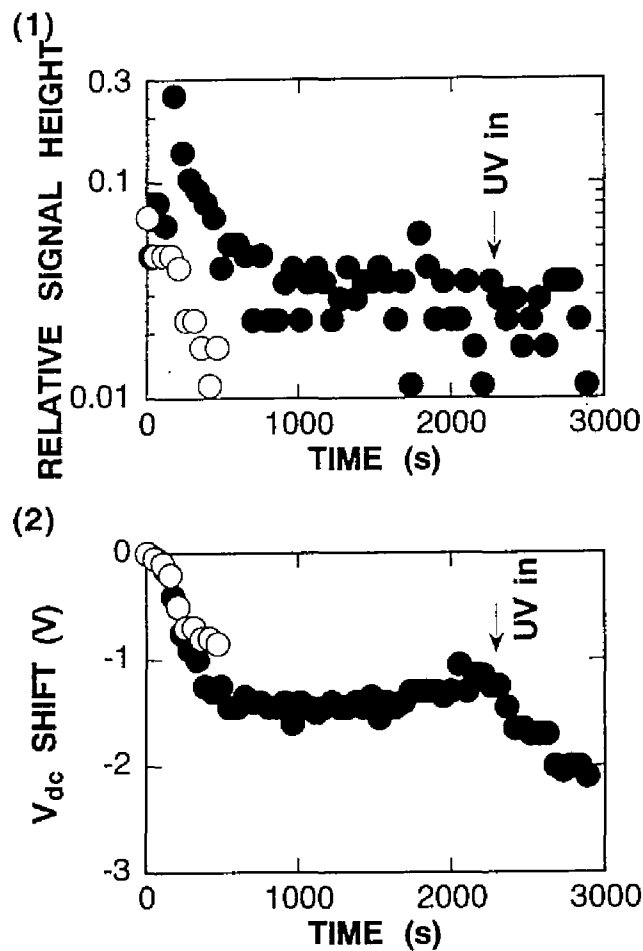
Fig. 4.14. Time variance of rf signals with introduction of O_2 gas into the vacuum chamber after Yb^+ ions were pumped to the "dark" state. (1) Relative signal height and (2) shift of resonance V_{dc}. ● : sweep direction f, ◯ : sweep direction r. First, we irradiated Yb^+ ions with radiation at 369.52 nm with introduction of only He gas at 4.2×10^{-4} Pa to pump Yb^+ ions to the "dark" state. After the fluorescence disappeared, we blocked radiation at 369.52 nm, and then introduced O_2 gas at about 1.3×10^{-5} Pa. Time was measured from the instant O_2 gas was introduced. The shift of resonance V_{dc} is shown as the shift from the resonance point just before the introduction of O_2 gas. At the time indicated by arrow, we re-irradiated the ions with radiation at 369.52 nm, after which rf signals disappeared.

(d) Discussion

The experimental results in the cases of O_2 and H_2O were similar to our former observation of the disappearance of Yb^+ ions. Therefore, we

126

conclude that the disappearance of Yb^+ ions was due to some background gases as proposed in 4.3.1.

We now discuss more carefully the fact that the resonance V_{dc} shifted as the rf signals became smaller. We will discuss the possibility of the following two effects: (1) change of the space charge potential upon decreasing the number of Yb^+ ions, and (2) production of molecular ions as pointed out in 4.3.1, since the direction of the shift correspond to the resonance of a heavier mass.

To investigate (1), we examined the resonance V_{dc} as we decreased the number of trapped Yb^+ ions. Decrease of the number was achieved by the same procedure as described in 2.3.2(4). and we introduced only He gas at 4.2×10^{-4} Pa in this measurement. We found that the shift of the resonance V_{dc} was within ± 0.3V even when we decreased the number to 17 %. This value was much smaller than the shift observed with the disappearance of ions. Therefore, we cannot explain the resonance V_{dc} shift by (1). If it was caused by the change of the space charge potential, we must assume that a large change in ion distribution occurred .

For (2), we assume that the following reaction occurs:

$$Yb^+ + O_2 \rightarrow YbO^+ + O. \tag{4.2}$$

The dissociation energies D_0 of YbO^+ and O_2 are 3.87 eV [25] and 5.116 eV [26], respectively. Therefore, Yb^+ requires energy greater than 1.25 eV to undergo this reaction. With H_2O, the reaction

$$Yb^+ + H_2O \rightarrow YbO^+ + OH \tag{4.3}$$

requires the energy greater than 1.1 eV because of the dissociation energy of 5.0 eV for the O-OH bond [26]. All of the known excited states of Yb^+ satisfy these conditions. This agrees with the observation that trapped Yb^+

127

ions disappear only with irradiation of radiation at 369.52 nm, which transfers Yb^+ to excited states. Next, we will estimate the shift of the resonance V_{dc}. According to the estimation described in 4.3.1, we assume that all odd isotopes of Yb^+ ions do not react and all even isotopes of Yb^+ ions change to YbO^+. If all of these ions are still trapped and make a collective oscillation [22], the shift of resonance V_{dc} should be -4.6 V. The value of -4.6 eV is close to the observed maximum shift. We therefore suggest that the chemical reaction plays a role in the disappearance of the trapped Yb^+ ions. With O_2 gases, reactions of the 5d transition series of metal ions trapped in a rf trap were reported by Matsuo et al. [27].

As shown in Fig. 4.13, the rf signals of the sweep direction r disappeared faster than those of the sweep direction f. When these measurements were performed, we supposed that this was caused by the change of anharmonicity with the change of the space charge potential by decreasing the number of trapped Yb^+ ions as described in Sec. 2.3.2(4). We found that the rf signals of the sweep direction r were not detected when the number of trapped Yb^+ ions was below 50 % of the usual initially-loaded number, while the rf signals of the sweep direction f were still observed. Therefore, when the major three even isotopes, which amount to about 70 % of the number of trapped Yb^+ ions, disappear, the rf signals of the sweep direction r cannot be detected. In the case of the experiments the O_2 gas introduction after the fluorescence fade (Fig. 4. 11.), by the same reason, we thought that a large part of the trapped even isotopes of Yb^+ ions in the 'dark' state disappeared.

However, as discussed in 4.4.3, the number of the produced YbO^+ ions seems not decrease to the minimum detectable number by rf signals. If this is true, the observed anharmonicity is not caused by the decrease of the number of trapped ions. We must search other causes of changing the anharmonicity of the space charge potential. Actually, the observed change of rf signals, shown in Fig. 4.13, indicates a possibility of other

cause of anharmonicity. For example, rf signals disappeared completely in the case of O_2 gas; however, signals remained in the case of H_2O gas and of the O_2 gas introduction after the fluorescence decay. The odd isotopes still remained in the trap after signals disappeared.

More quantitative investigations are required to clarify the disappearance of rf signals by use of other ionic detection systems. We made a mass-selective ionic detection system using a mass analyzer as in Ref. [27]. This methods is also useful to catch direct evidence of molecular ion formation. We described the results by our mass-selective detection in Sec. 4.4. It is also desirable to use enriched isotopes of Yb and a precise partial-pressure measurement system.

4.4. Chemical Reaction of Yb^+ in Excited States with Gases [10,11]

In order to make more quantitative study of the disappearance, including catch direct evidence of the production of molecular ions, we detected trapped ions mass selectively by combining a quadrupole mass analyzer with our rf trap. We describe the setup for mass-selective detection in 4.4.1. Using this setup, we found that YbH^+ was produced by chemical reaction of Yb^+ in excited states with H_2 gas in residual background gases [10,11]. The production of YbH^+ occurs in the same time scale of the fluorescence decay. Therefore, the production of YbH^+ is one of the reason of the fluorescence decay. We found that some observations formally interpreted to be associated with Yb^+ in the $^2F_{7/2}$ state are actually caused by YbH^+. We describe the results in 4.4.2. To investigate the disappearance of rf signals, we performed mass-selective detection in the presence of O_2 gas. We found that YbO^+ and some other molecular ions were produced by chemical reaction of Yb^+ in excited

states [11]. The results are shown in 4.4.3.

4.4.1.   A Mass-Selective Detection of Trapped Ions

The schematic diagram of our mass-selective detection system is shown in Fig. 4.15. The mass selective detection system was added to the trap of $2r_0 = 22.6$ mm used in the disappearance experiment. The mesh endcap electrode, formally aimed to observe fluorescence of trapped ions, was used to extract ions from the trap to transfer them to a quadrupole mass analyzer.   Parameters of the trap, the detection method of rf signals and UV beam were the same as those used in the disappearance
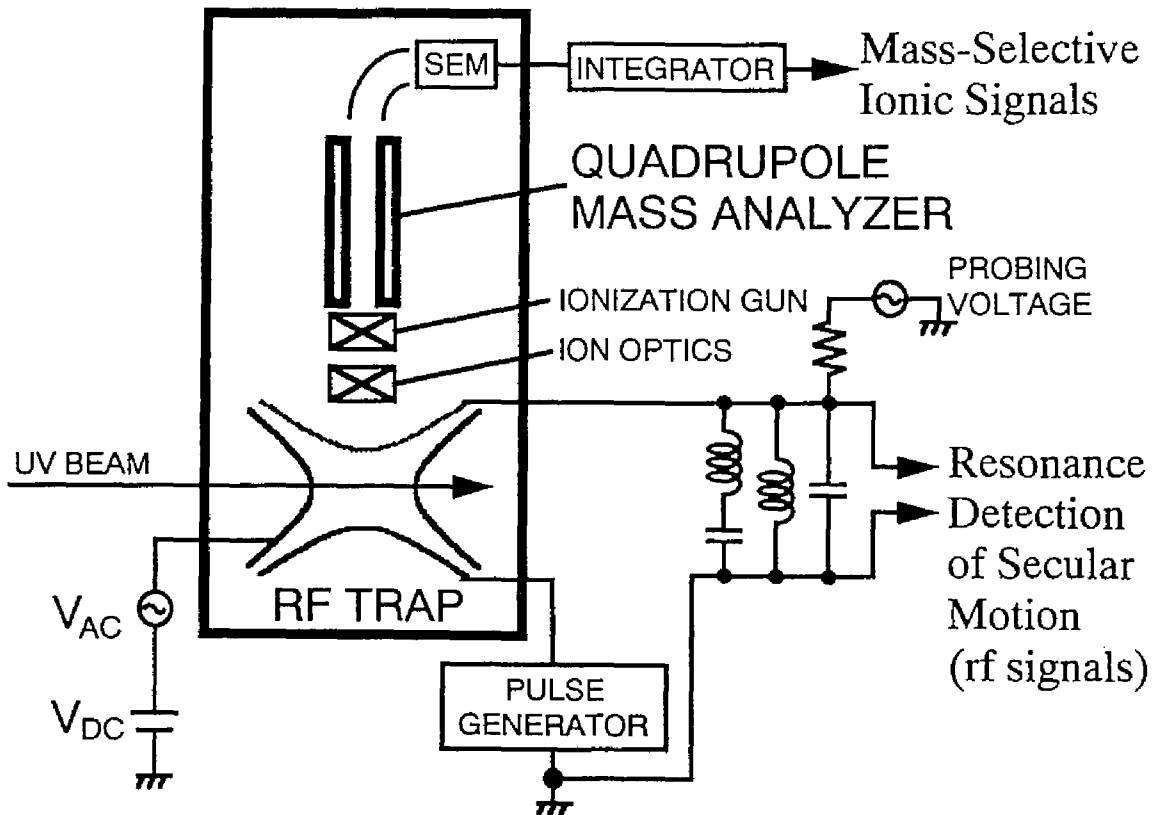
Fig. 4.15.   Experimental setup for mass-selective ionic detection

experiment with O_2 and H_2O gases descried in 4.3.2, to refer in the case of need, because we lost information of fluorescence of trapped Yb^+ ions. We here describe the parameters different from those in 4.3.2. When we didn't detect rf signals, the V_{dc} was fixed to 8.0 V. When we detected them, V_{dc} was modulated into a triangular wave from 5.2 ± 1 V to 11.2 ± 1 V with a period of $60 \sim 62$ s, while the frequency of the probing rf fields was fixed at 83.5 kHz. From this experiment, we installed a nude Bayard-Alpert gauge to the vacuum chamber to measure the total vacuum pressure. The background pressure was below 1×10^{-7} Pa and 5×10^{-7} Pa with oven and electron gun off and on, respectively. Other parameters should be referred to 4.3.2.

We placed a quadrupole mass analyzer (Blazers QMG421C-3) above the mash endcap electrode. The ions stored in the trap were expelled by a pulsed voltage of 50 V applied between the two endcap electrodes. This voltage was higher that the axial psuedopotential depth of 19 eV and sufficient to expelling the trapped ions. Then, ions of a specific atomic mass passed through the mass analyzer and were detected by a secondary electron multiplier (SEM) followed by an integrator and a peak holder. Similar mass-selective ionic detection system was developed by Matsuo et. al. [27]. Our mass analyzer had a resolution below 1 atomic mass unit (amu) between 1 and 400 amu, and an ionization gun set in front of the quadrupole rods. This allowed us to measure the relative partial pressure of background gases. We calibrated the mass spectrometer for absolute amu and resolution below 1 amu around 174 amu by detecting neutral Yb from the oven.

Trapped Yb^+ ions were prepared by the following procedure. After the oven and electron gun were turned on and the temperature of the oven reached equilibrium, we introduced gases into the vacuum chamber. About 15 minute was required for stabilization of the total and partial pressure of gases. In order to load the same number of trapped Yb^+ ions

in a series of measurement, we fixed the time during which Yb^+ ions were being loaded, i.e., we switched off the trapping ac voltage for a short time, switched it on again, and after 5 min, turned off the oven and electron gun. After the oven was sufficiently cooled, we started to irradiating the Yb^+ ions with UV radiation. The number of Yb^+ ions loaded was of the order of 10^5 and 10^4 at a He pressure of 8.5×10^{-5} Pa and a H_2 pressure of 4×10^{-6} Pa, respectively. The equivalence of the load-to-load number was checked by the fact that rf signals were in the same size and shape. At a H_2 pressure of 4×10^{-6} Pa, until the oven cooled, the number of trapped Yb^+ ions decreased to the minimum detectable number by rf signals. After the oven cooled, however, the decay time of the number was negligibly slow. We checked this by detecting the fluorescence of trapped Yb^+ ions, before we introduced the mass analyzer. We assumed that this initial decrease of the number was the same in the load-to-load.

4.4.2.   Reaction with H_2 to form YbH^+ [10,11]

(1)   Result

We detected mass selective signals at 177 amu at a total pressure of 4×10^{-6} Pa composed 99 % of H_2 gas after we irradiated Yb^+ ions with radiation at 369.52 nm for 1 minute. We checked, without irradiation at 369.52 nm, that no signals were detected at 177 amu. We used a natural isotope mixture of 168, 170, 171, 172, 173, 174, and 176 amu isotopes of Yb. Therefore, it is possible that the signals at 177 amu represent ions between (176 + 1) amu and (168 + 9) amu. We searched the signals between 177 and 185 amu, which corresponded to ions between (176 + 1) amu and (176 +9) amu, to resolve the ambiguity, and found that signals were detected only at 177 amu. Therefore, signals at 177 amu represent

the ions at (176 + 1) amu, i.e., $^{176}YbH^+$.

We found that YbH^+ was photodissociated by radiation at the wavelengths formally assigned to deexcitation lines of Yb^+ in the $^2F_{7/2}$ state to the $^2S_{1/2}$ ground state. Bauch et. al. determined the four wavelengths for the center of the deexcitation lines and found that these wavelengths were not in agreement with those expected from tabulated energy levels of Yb^+ [4]. We confirmed the photodissociation of $^{174}YbH^+$ ions with irradiation at three of the four wavelengths, i.e., 369.482 nm, 369.202 nm and 368.947 nm. In Fig. 4.16(a)-(c), we show the wavelength dependence of the photodissociation of $^{174}YbH^+$ ions. At present, a large scattering of signal height in each measurement of our mass-selective detection only allow us to judge whether the signals can be detected or not. However, we observed that signals of $^{174}YbH^+$ ions were below the detectable level around the center wavelengths determined in Ref. [4].

At another wavelength determined in ref. [4], i.e., 369.443 nm, no significant decrease in signal height of $^{174}YbH^+$ was observed. However, we cannot determine, only from this result, that 369.443 nm is a true wavelength of the deexcitation line of the $^2F_{7/2}$ state, because, in Ref. [4] the fluorescence recovery rate at 369.443 nm was reported to be one order of magnitude slower than those at other three wavelengths.

We also observed that $^{174}Yb^+$ ions were recovered by photodissociation of $^{174}YbH^+$ ions by detecting the signals at 174 amu after irradiation at around 369.482 nm as shown in Fig. 4.17. (We checked that the signals at 174 amu could not be detected after irradiation at 369.52 nm. This means that the number of $^{173}YbH^+$ was below the detectable level as a result of the slow excitation rate of the $^2S_{1/2}$ - $^2P_{1/2}$ transition for $^{173}Yb^+$ ions due to hyperfine structure and isotope shift.) We could not obtain a strong wavelength dependence, unlike the measurements shown in Fig. 4.16. Even if the wavelength is away from the center wavelength of photodissociation line, photodissociation may occur in a slower rate and
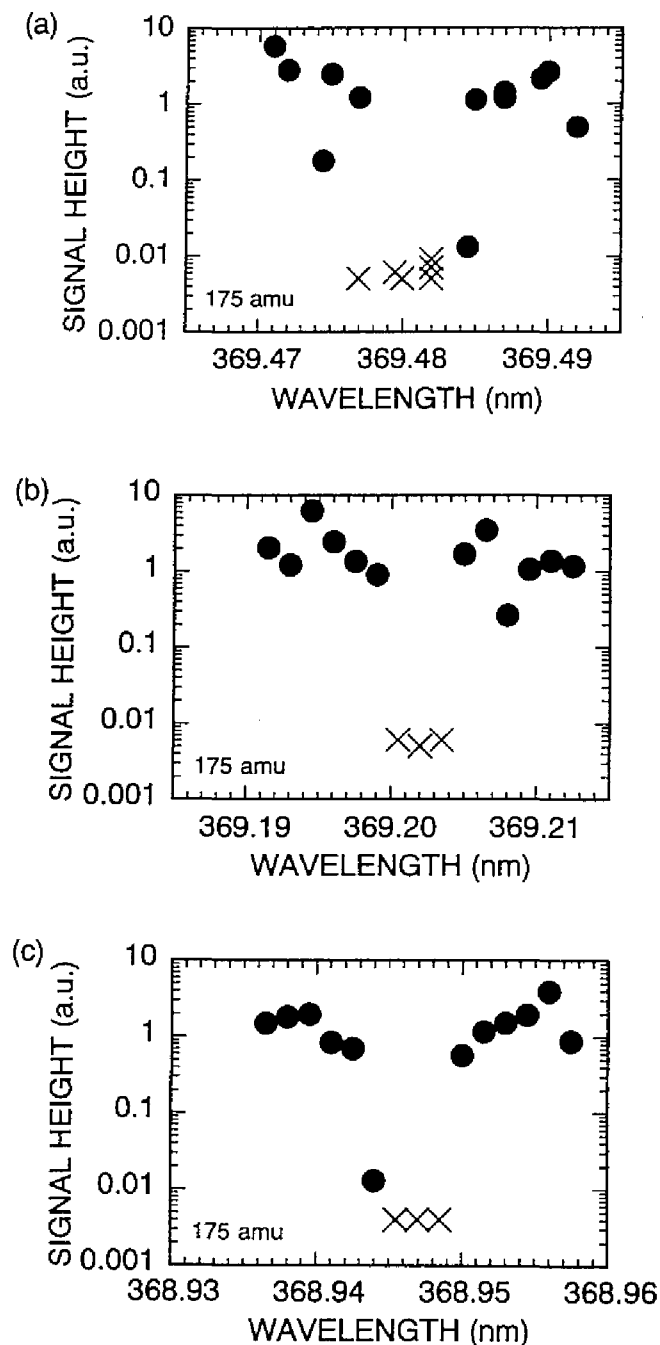
Fig. 4.16. Mass-selective signals of trapped ions at 175 amu after irradiation at around (a) 369.482 nm, (b) 369.202 nm, and (c) 368.947 nm. We irradiated ^{174}Yb$^+$ ions first with radiation at 369.52 nm for 2 minutes to produce ^{174}YbH$^+$ (without irradiation at 369.52 nm, no signals were detected at 175 amu.), and then we switched the UV wavelength to that indicated in the abscissas. After 10 s of irradiation, we applied a pulsed voltage to transfer the trapped ions to the mass analyzer set to detect the ions at 175 amu. At the wavelength where we could not detect the signals, we indicated the noise level at the time of detection by ×.
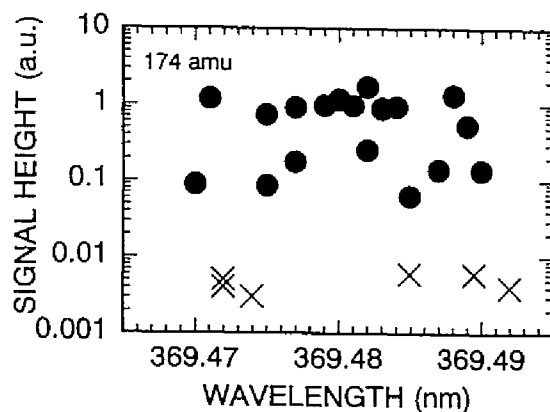
Fig. 4.17. Recovery of ^{174}Yb$^+$ by photodissociation of ^{174}YbH$^+$ with irradiation around 369.48 nm. Detection procedure was the same as that for ^{174}YbH$^+$ shown in Fig. 4.16, except that the mass analyzer was set to 174 amu and the time from the start of irradiation at around 369.482 nm to the eject pulse was 0.5 s. At the wavelength where we could not detect the signals, we indicated the noise level at the time of detection by ×.

the number of the dissociated ^{174}Yb$^+$ ions reach the detectable. However, a large scattering of signal height in each measurement prevented us to obtain the profile of the line. We shortened the irradiation time of radiation around 369.482 nm to 0.5 s. However, we can only say, from Fig. 4.17, the number of points which indicate that no signals were detected increased, as the UV wavelength was far from the center of the photodissociation line. We need to improve the detection system for further discussion.

Even when we introduced only He gas into the chamber to a total pressure of 8.5 x 10^{-5} Pa, we obtained mass selective signals of YbH$^+$ with irradiation at 369.52 nm and a photodissociation spectrum at around 369.482 nm similar to these in Fig. 4.16, as shown in Fig. 4.18. The signal height of mass-selective signals, before irradiation at 369.52 nm, was one order magnitude of higher than that at the pressure of 4 × 10^{-6} Pa,

SIGNAL HEIGHT (a.u.)

100
10
1
0.1
0.01

175 amu

369.47   369.48   369.49
WAVELENGTH (nm)
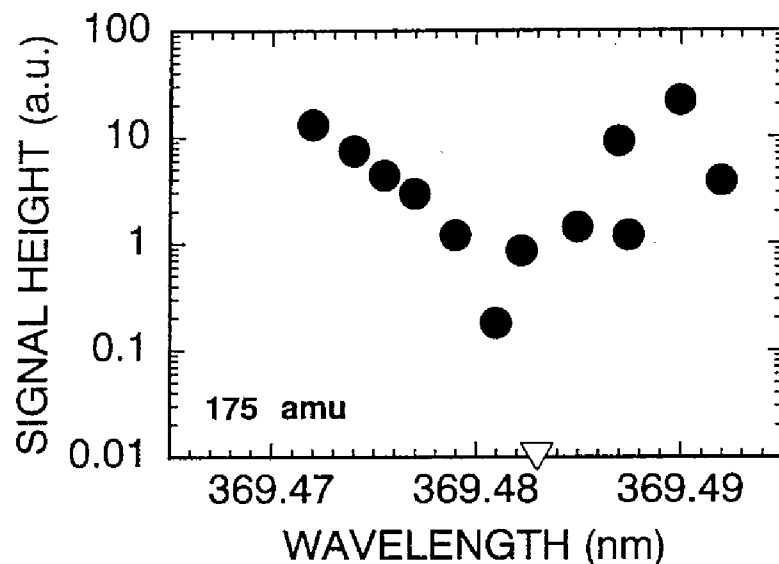
Fig. 4.18. Mass-selective signals of trapped ions at 175 amu after irradiation at around 369.482 nm, even when we introduced only He gas into the chamber to a total pressure of 8.5 × 10^{-5} Pa. Experimental procedure is the same as that in the case of Fig. 4.16. At the wavelength where we could not detect the signals, we indicated the noise level at the time of detection by ∇.

due to increase in the number of ions as a result of buffer-gas cooling. Fluctuation in the signal height reduced within one order magnitude of the ordinate in Fig. 4.18. We analyzed the composition of gases in the chamber and found, as shown in Fig. 4.19, that the pressure of H_2 gas increased as the pressure of He gas increased. At a total pressure of 8.5 × 10^{-5} Pa, composition of gases were 86 % He, 13% H_2, and 1 % others. This may be one reason why YbH$^+$ formation was overlooked in previous work, including ours. The purity of the He gas used was 99.995 %. Therefore, H_2 gas was produced or mixed somewhere in the whole vacuum system.
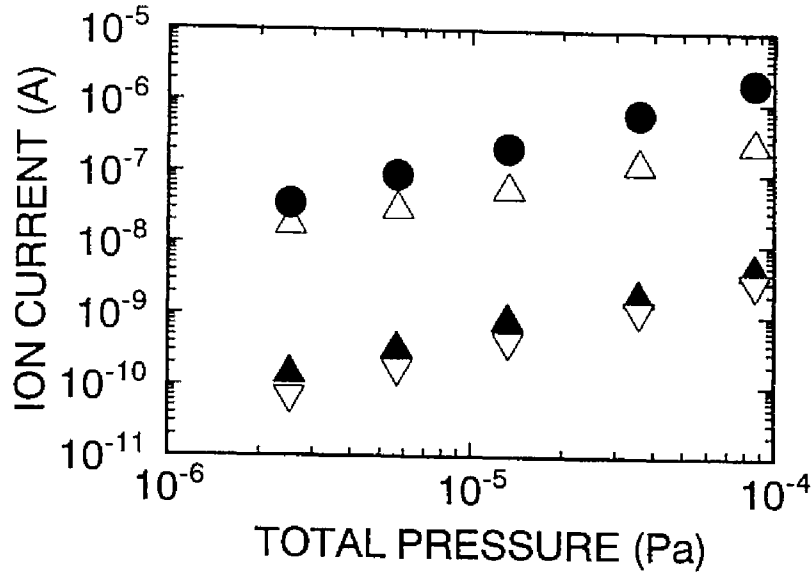
Fig. 4.19. Composition of gases in the chamber when we introduced only He gas into the vacuum chamber. $\triangle$: 2 amu (H_2), $\bullet$: 4 amu (He), $\blacktriangle$: 16 amu (CH_4), $\triangledown$: 28 amu (N_2 + CO). The ordinate is proportional to the pressure.

(2) Discussion

YbH^+ is produced from Yb^+ in excited states by

$$Yb^{+*} + H_2 \rightarrow YbH^+ + H \tag{4.4}$$

When the $^2D_{3/2}$ state is optically depleted, even in the presence of buffer gases, it is not observed that fluorescence of Yb^+ ions fades as described Sec. 4.2 [7,15]. Therefore, reaction (4.4) occurs when Yb^+ is in the $^2D_{3/2}$ state (2.85 eV). Or, if population trapping in the $^2F_{7/2}$ state occurs (see below) and the proposed path, i.e., fine structure mixing collision between the $^2D_{3/2}$ and $^2D_{5/2}$ states and subsequent spontaneous decay from the $^2D_{5/2}$ to $^2F_{7/2}$ states [4,28], is true, there is a possibility that the reaction

(4.4) occurs in the $^2F_{7/2}$ (2.66 eV) and/or $^2D_{5/2}$ (3.02 eV) state.

To our knowledge, the dissociation energy D_0 of YbH$^+$ have not been measured. Because the reacted Yb$^+$ should have an internal energy below 3.02 eV and $D_0(H_2)$ is 4.478 eV [26], we estimate D_0(YbH$^+$) to be greater than 1.5 eV. As a reference, the known dissociation energies of metal-hydride ions range from 0.7 to 3.2 eV [29]. Even if the produced YbH$^+$ keeps all of the excess energy after reaction (4.4) as its internal energy, its photodissociation requires an energy greater than that obtained from ($D_0(H_2)$) - [energy of Yb$^+$ at reaction (4.4)]. We estimate this value to be 1.6 eV, assuming that reaction (4.4) occurs in the $^2D_{3/2}$ state and ignoring kinetic energy. Radiation at 369.48 nm (3.36 eV) satisfies this criterion.

Determination of rate of reaction (4.4) and the profile of the photodissociation lines are left for future study, because we must first improve our detection system to decrease scattering of the signal height of each detection, or to average a large number of data. The three wavelengths of the photodissociation may be assigned to some structure such as vibration or rotation [30]. Search for photodissociation lines of YbH$^+$ in a wider wavelength region will determine the entire structure and molecular constants.

When rf signals was detected, the resonance point of rf signals slightly shifts toward that of heavier mass in the same time scale of the fluorescence disappearance. This is shown in Fig. 4.20 and is clearly noticeable in Fig. 4.13(c). (This shift is distinguished from a subsequent larger and slower shift due to the reaction with other gases such as O_2 and H_2O gas [7,8].) and moved back to the initial resonance point with irradiation at photodissociation wavelengths. These phenomenon were first reported by Bauch et. al. [4], who thought that it might be related to Yb$^+$ ions in the $^2F_{7/2}$ state. According to our present result, however, it is reasonable to interpret this phenomenon as being due to the production
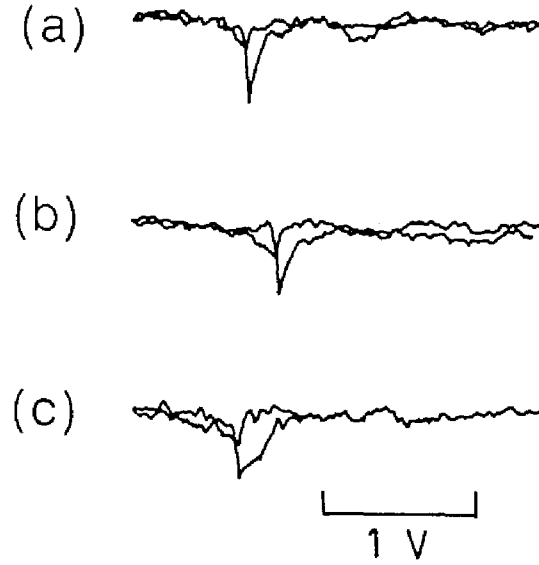
Fig. 4. 20. Shift of the resonance point of rf signals with irradiation at 369.52 nm (a → b), and recovery of the shift with irradiation at 369.48 nm (b → c) when we introduced only He gas to a pressure of 8.5×10^{-5} Pa. DC voltage was swept to detect rf signals. We show the signals for both sweep directions.

and dissociation of YbH^+. In our present setup, we observed the shift of -0.25 V. We estimate the shift of resonance V_{dc} by producing YbH^+ ions. In Sec. 4.3., we proved that all odd isotopes of Yb^+ are unreactive because their excitation rate is too small owing to optical pumping in the hyperfine structure of the $^2S_{1/2}$ ground state and isotope shifts [7,8]. The shift is calculated in the manner described Sec. 4.3 to be -0.31 V from the collective oscillation in strong coupling [22] among odd isotopes of Yb^+ and even isotopes of YbH^+. This value is close to the observed shift.

It should be noted that our present results do not deny the possibility of population trapping in the $^2F_{7/2}$ state when one drives the $^2S_{1/2}$ - $^2P_{1/2}$ transition in the presence of buffer gases. To support the existence of the population trapping, Bell et al. at NPL observed that fluorescence was recovered by irradiation at 3.43 μm, which drove the $^2F_{7/2}$ - $^2D_{5/2}$

transition [28]. The energy of radiation at 3.43 μm (0.36 eV) is much smaller than the energy required for dissociation of YbH$^+$, as discussed above. Therefore, if the result obtained at NPL was due to photodissociation, it should be a multi-photon process with radiation at 3.43 μm or 3.43 μm + 369.52 nm (They irradiated with radiation at 369.52 nm simultaneously.). A possible way of generating Yb$^+$ in the $^2F_{7/2}$ state may be slow photodissociation of produced YbH$^+$ by radiation at 369.52 nm. However, this process seems to be impossible because the excess energy after photodissociation is estimated to be 1.7 eV (with assuming that reaction (4.4) occurs in the $^2D_{3/2}$ state and ignoring kinetic energy) which is smaller than the energy of the $^2F_{7/2}$ state. Therefore, it is still possible that at least some of Yb$^+$ are trapped in the $^2F_{7/2}$ state with driving the $^2S_{1/2}$ - $^2P_{1/2}$ transition.

We here correct our interpretation of the following two observations descried in 4.3.2:

(a) In 4.3.2, we had observed that little difference in the time variance of rf signals between with and without addition of H$_2$ gas. This result was due to the fact that the partial pressure of H$_2$ gas was sufficiently high for the reaction (4.4) to proceed even if we intended to introduce only He gas. As shown in Fig. 4.13(c2), regardless of whether or not we additionally introduced H$_2$ gas, we observed a shift of ~ -0.25 V in resonance V_{dc} within 30 s after the start of irradiation at 369.52 nm. This fast, small shift actually indicated the production of YbH$^+$.

(b) In 4.3.2, we described that we had confirmed that the disappearance of Yb$^+$ in the $^2F_{7/2}$ state in the presence of O$_2$ gas. We intended to prepare Yb$^+$ in the $^2F_{7/2}$ state by irradiation at 369.52 nm with introduction of He gas at that time. In this procedure, however, YbH$^+$ ions were produced. Therefore, the observed change in rf signals with subsequent introduction of O$_2$ gas without UV irradiation indicates the possibility of chemical reaction of YbH$^+$ with O$_2$ gas.

4.4.3. Reaction with O_2 Gas

(a) Result

Apart from the YbH^+ formation, to investigate more our founding of the rf-signals disappearance, we performed mass selective detection under the condition similar to that in the experiment of Fig. 4.13, i.e., at the total pressure of 4.2×10^{-4} Pa with a composition of 98 % He, 1 % O_2, 1 % H_2, 0.1 % at 16, 17, and 28 amu. After irradiation at 369.52 nm, we could detect mass selective signals at 15, 16, 17, 29, and 32 amu of heavier that the mass of Yb^+, which may correspond to $+CH_3$, $+O$, $+OH$, $+C_2O_5(?)$, and $+O_2$), respectively.

We measured the time variance of mass selective signals for some ions with continuous irradiation at 369.52 nm with introduction of O_2 gas. The experimental procedure was the same as that described in 4.3.2. The result is shown in Fig. 4.21(a). We also show that a typical time variance of rf signals in this measurement Fig. 4.21(b). Although rf signals disappeared within 600 s in all detections, the number of $^{174}YbO^+$ did not show a significant decrease from that of initially trapped $^{174}Yb^+$, even after rf signals disappeared.

In addition, UV radiation was terminated after rf signals disappeared, and then rf signals recovered very slowly as shown in Fig. 4.22. We once measured mass selective signals 40 min after the termination of the UV radiation. The signal heights were measured to be 7.89 and 0.67 in the same units as used in the ordinate of Fig. 4,20(a) for $^{174}Yb^+$ and $^{174}YbO^+$, respectively. Therefore, a large part of YbO^+ changed back to Yb^+ and this results in the recovery of rf signals. We suggest, as a possible explanation of the recovery of Yb^+, reduction of YbO^+ with the residual H_2 gas in the vacuum chamber, i.e., $YbO^+ + H_2 \rightarrow Yb^+ + H_2O$.

(a)

(b)
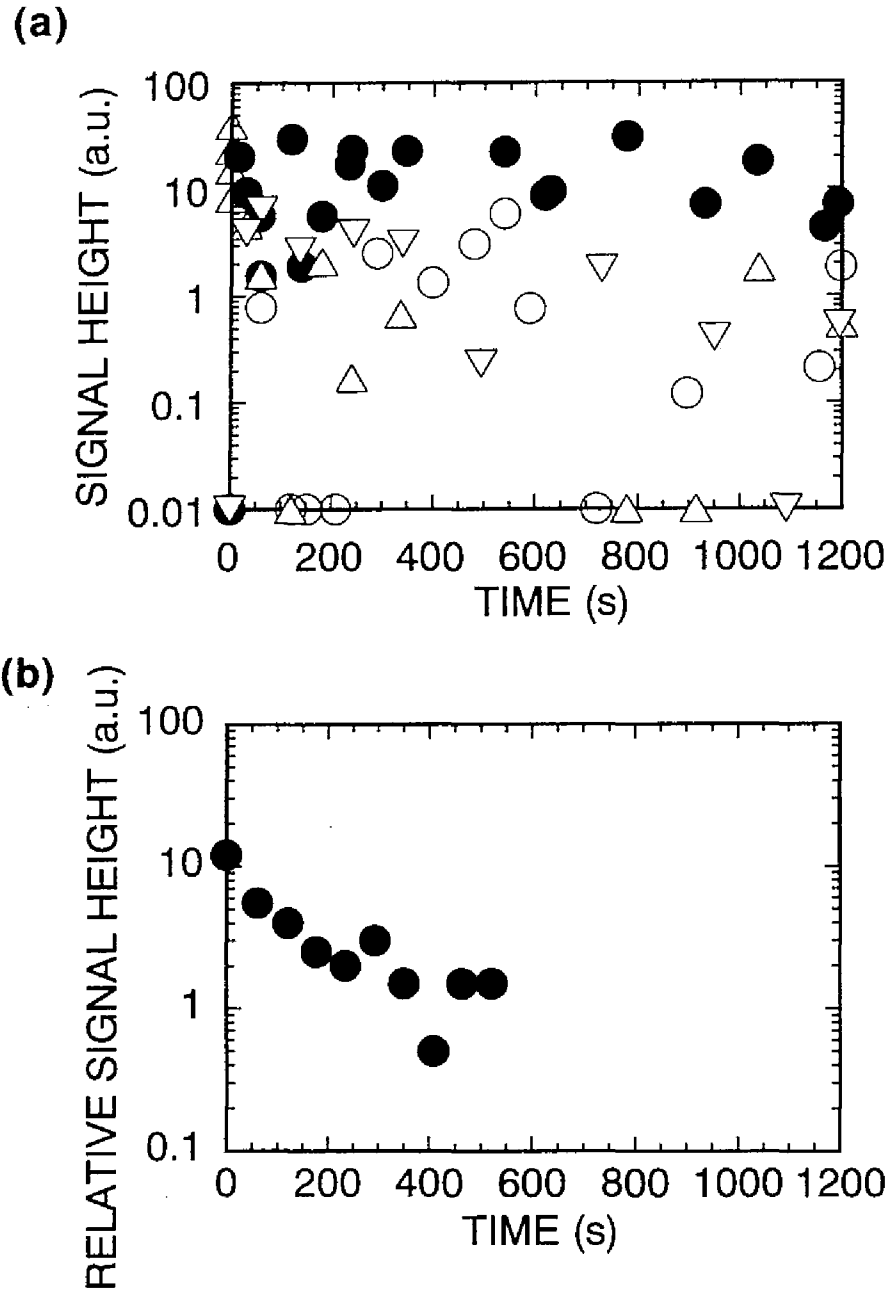
Fig. 4.21. (a) Time variance of mass-selective signals with introduction of O_2 gas with continuous irradiation at 369.52 nm.

$\triangle$:$^{174}Yb^+$; $\bullet$:$^{174}YbO^+$; $\bigcirc$:$^{174}YbO^{2+}$; $\triangledown$:$^{174}YbH^+$. RF signals disappeared within 600 s in all detections. A typical time variance of rf signals during this measurement is shown in (b) (sweep direction f). The total pressure was 4.2×10^{-4} Pa, and the gas composition are 98% He, 1% O_2, and 1% H_2
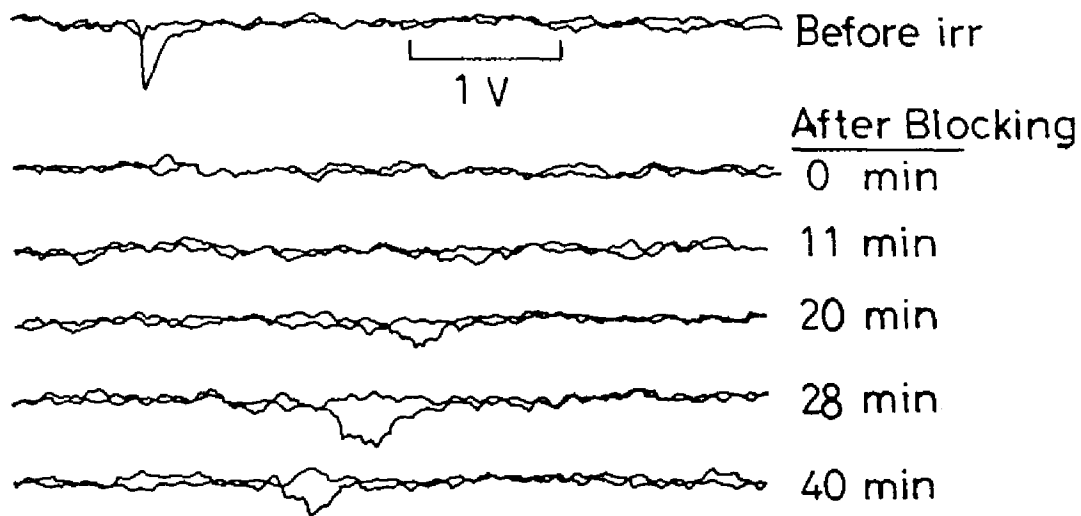
Fig. 4.22. Recovery of rf signals after UV radiation was terminated. The trace at the top of the figure shows the rf signal before continuous irradiation at 369.52 nm. When the UV radiation was terminated, rf signals had already disappeared (see the signal at 0 min). The time was measured after UV radiation was terminated. The composition of background gases were the same that in the measurement of Fig. 4.21, i.e., the total pressure was 4.2×10^{-4} Pa, and the gas composition are 98% He, 1% O_2, and 1% H_2.

(b) Discussions

The results described above indicate that the disappearance of the rf signals is not caused by the decrease in the total number of trapped ions. If the trapped ions does not oscillate in a collective oscillation of strong coupling due to the mass difference between Yb^+ and YbO^+, rf signals should be detected at close to the resonance point of YbO^+ [22]. However, no rf signals could be detected around this point. Therefore, other explanation of the rf-signal disappearance should be investigated.

We mentioned, in Sec. 4.3, that some behavior of rf signals was not explained with the change of anharmonicity by decease in the total number of trapped ions. This fact indicates the change in anharmonicity

of the space charge potential of trapped ions, which may be caused by change in spatial distribution of trapped ions.

To find the explanations of the disappearance of rf signals, we will next investigate the possibility of the following ideas; effect of simultaneous trapping of ions with different masses on ion distribution (because odd isotopes of Yb^+ are not reactive and still in the trap after rf signals disappear as described in Sec. 4.3), or of a smaller damping efficiency of molecular ions by buffer gases to cause the change in spatial distribution. A more quantitative detection of mass-selective signals are required for further investigations of the rf-signal disappearance. Use of enriched isotopes, and simultaneous observation of fluorescence of trapped Yb^+ may be helpful for investigation.

4.5. Conclusions and Prospect

In this chapter, we described the characteristics of buffer-gas-cooled Yb^+. First, we showed the results obtained by frequency scanning of radiation at 369.52 nm with which we drove the $^2S_{1/2}$ - $^2P_{1/2}$ transition. We proved that the spectra of odd isotopes of Yb^+ cannot be observed by irradiation with only one beam at 369.52 nm, owing to the optical pumping between hyperfine structures in the $^2S_{1/2}$ ground state. We confirmed the cooling effect by collision with the light buffer gas.

In our investigation, we focused on the characteristics of buffer-gas-cooed Yb^+ ions continuously irradiated at 369.52 nm. During over five years of investigations, great progress in the understanding of the characteristics of Yb^+ with continuous irradiation at 369.52 nm has been made. Below, we describe our present conclusions.

(1)   When we irradiate trapped Yb^+ ions at 369.52 nm to drive the $^2S_{1/2}$ -

$^2P_{1/2}$ transition in the presence of buffer gases, their fluorescence fades. There are two possible explanations for this phenomenon.

(i) The production of YbH$^+$ by chemical reaction of Yb$^+$ in excited states with H$_2$ gas.

(ii) Population trapping in the $^2F_{7/2}$ state of Yb$^+$.

As described in 4.4.2, we proved the production of YbH$^+$ by chemical reaction of Yb$^+$ in excited states with H$_2$ gas. We found that wavelengths of 369.482 nm, 369.202 nm, and 368.947 nm, formerly assigned as wavelengths for deexcitation of Yb$^+$ in the $^2F_{7/2}$ state to the $^2S_{1/2}$ ground state, are actually photodissociation lines of YbH$^+$. On the other hand, population trapping in the $^2F_{7/2}$ state of Yb$^+$ due to collision with buffer gases has not yet been proven. However, observation of spectra of the $^2F_{7/2}$ - $^2D_{5/2}$ transition in the presence of buffer gas, by Bell et al. at NPL [28], seems to support the proposal of population trapping in the $^2F_{7/2}$ state in the presence of buffer gases.

The remaining problems concerning fluorescence decay can be summarized as follows.

(i) To verify whether or not population trapping in the $^2F_{7/2}$ state of Yb$^+$ is due to collision with buffer gases.

(ii) If the population trapping is true,

(a) What is the mechanism of the population trapping? Is the proposed path, i.e., the fine structure mixing collision between the $^2D_{3/2}$ and $^2D_{5/2}$ states and subsequent spontaneous decay from the $^2D_{5/2}$ to $^2F_{7/2}$ states [4,28], true or not?

(b) In what state does the production of Yb$^+$ occur? Is Yb$^+$ first trapped in the $^2F_{7/2}$ state, and then changed to YbH$^+$?

(c) In connection to (b), which is the faster process, YbH$^+$ production or population trapping in the $^2F_{7/2}$ state?

In ultrahigh vacuum (UHV), the existence of the $^2F_{7/2}$ state of Yb$^+$ itself has been proved at NPL, where pumping to the $^2F_{7/2}$ state was

achieved by optically driving to the $^2D_{5/2}$ state with subsequent spontaneous decay to the $^2F_{7/2}$ state, and recovery from the $^2F_{7/2}$ state was accomplished by driving the $^2F_{7/2}$ - $^1[5/2]_{5/2}$ transition at 638 nm [31]. We recently followed up on this result in UHV, as described in Sec. 5.4, and we checked, by the same experiment as in the case of Fig. 4.16, that YbH$^+$ was not photodissociated by irradiation at 638 nm. Therefore, the $^2F_{7/2}$ - $^1[5/2]_{5/2}$ transition at 638 nm is confirmed to be a deexcitation line for the $^2F_{7/2}$ state. This transition will be useful in further investigations for fully understanding buffer-gas-cooled Yb$^+$.

(2)   The disappearance of rf signals with irradiation at 369.52 nm is caused by the reactivity of various gases, except for H_2 gas, with Yb$^+$ in the excited state. This phenomenon includes the production of molecular ions by chemical reaction of Yb$^+$ in the excited state with the gases. One can monitor the production and dissociation of molecular ions, including YbH$^+$, by the change of the resonance point of rf signals. When we first observed this phenomenon, the decay time of the disappearance of rf signals was close to that of fluorescence decay. However, this was because the vacuum condition was not well controlled. The disappearance of rf signals is not observable when the vacuum condition is high. We first considered that the disappearance of rf signals indicated the loss of ions from the trap. However, the results of mass-selective detection in the presence of O_2 gas indicate that the number of trapped ions does not decrease to the minimum detectable level by rf signals even after the disappearance of rf signals. We observed the recovery of rf signals simply by waiting for several tens of minutes while blocking the radiation at 369.52 nm. The reason for the disappearance of rf signals must be clarified.

With a view to establishing a frequency standard using buffer-gas-

146

cooled Yb^+ ions, the production of YbH^+ may limit the performance of the frequency standard owing to the difficulty in removing H_2 gas from the vacuum system. A effective solution to this problem may be to irradiate Yb^+ ions simultaneously with radiation to deplete the $^2D_{3/2}$ metastable state [3,7,10] or to photodissociate YbH^+. However, if the excitation rate of the $^2S_{1/2}$ - $^2P_{1/2}$ transition is high enough to populate a number of stationary Yb^+ ions in the $^2P_{1/2}$ state, YbH^+ production may occur even in the $^2P_{1/2}$ state.

The production of hydride ions may be observed for other ion species when the energy of the ions, including their kinetic energy, is greater than the threshold energy of their hydride-ion production, especially in the case that the ions have branches to metastable states, as does Yb^+, and they are not depleted. If other gases which react with Yb^+ in the excited states are present in vacuum, the production of other molecular ions is also a problem. However, except for H_2 gas, the pressure of the reactive gases seems to decrease to a level where reaction occurs at a negligibly slow rate.

Finally, we describe a positive application of our results. Determing the wavelengths of photodissociation lines of molecular ions enables the use of laser-cooled ions in the field of molecular physics and chemistry, because molecular ions can be kept cool by photodissociating them and laser cooling the dissociated ions again. It should also be possible to demonstrate cooled single molecular ion photodissociation spectroscopy by frequency sweeping of photodissociating radiation, as is the case with single atomic ion spectroscopy [32]. In the case of single molecular ion photodissociation spectroscopy, fluorescence on and off states correspond to atomic and molecular ion states, respectively. Fluorescence intensity switching of single ions associated with molecular formation and dissociation has been reported by Sankey and Madej [24].

Chapter 5

Laser Cooling of Yb⁺ Stored in a rf Trap

5.1. Introduction

Laser cooling is a solution to reducing the second-order Doppler shift, one of the major sources of uncertainty. The fractional second-order Doppler shift can be reduced to the order of 10^{-18} at the Doppler cooling limit. Laser cooling is also essential to confine the trapped ions within the Lamb-Dicke region of the optical wavelength. Laser cooling of Yb⁺ stored in a rf trap has already been realized [1-7], but seems to require the use of isotope-enriched Yb. Difficulty in laser cooling a natural isotope mixture of Yb⁺ may reflect the following facts. Yb has three major even isotopes and two odd isotopes. The natural abundances of these isotopes are similar, i.e., 14 %, 22 %, 16 %, 32 % and 13% for ^{171}Yb⁺, ^{172}Yb⁺, ^{173}Yb⁺, ^{174}Yb⁺ and ^{176}Yb⁺, respectively. The isotope shifts of the $^2S_{1/2}$ - $^2P_{1/2}$ cooling transition of the three even isotopes are over 1.2 GHz [8], and laser cooling of odd isotopes requires avoidance of optical pumping between hyperfine structures. Therefore, it is possible to efficiently laser cool only one isotope. Moreover, there is a possibility that the frequency of the cooling laser may be in a region where other isotopes not intended to be cooled are laser-heated. All isotopes are simultaneously trapped at the usual trapping parameters and coupled to each other by Coulomb interaction. The isotopes not directly laser cooled are sympathetically cooled by Coulomb interaction with the directly laser-cooled isotopes [9]. However, rf heating, which may limit the achievable minimum kinetic

energy, depends on the total number of trapped ions, while cooling power decreases to the value of the natural abundance of the directly laser-cooled isotope. To avoid this difficulty, enriched isotopes of Yb are used as a source of Yb^+ at other laboratories. Unlike other laboratories, we demonstrate that it is possible to laser cool Yb^+ ions stored in a rf trap even when a natural isotope mixture of Yb is used [10]. The results are described in Sec. 5.2.

When we decreased the number of trapped Yb^+ to be laser-cooled, we encountered a problem of micromotion caused by an unexpected dc field, as has been the case in other laboratories [11,12]. In 5.2.3, we describe how we eliminated this problem. As a result, we successfully laser cooled single $^{174}Yb^+$ ions [13]. We describe the fluorescence signals of single $^{174}Yb^+$ ions and the determined temperature in Sec. 5.3.

It is necessary to measure the number of trapped Yb^+ ions to evaluate their effect on laser cooling. For this purpose, we detected sudden drops of fluorescence intensity by shelving the electron of each ion to the $^2F_{7/2}$ metastable state [10]. These are quantum jump signals. We describe them in Sec. 5.4. We later found four transitions to deexcite the $^2F_{7/2}$ state. By using two radiation beams for pumping to and deexciting the $^2F_{7/2}$ state, we observed quantum jump signals repeatedly [14].

5.2. Laser Cooling of a Natural Isotope Mixture of Yb^+

5.2.1. Theory of Laser Cooling

In this subsection, we introduce a principal of laser cooling of trapped atoms or ions. At the end of this subsection, we consider laser cooling in the simple case of a natural isotope mixture of Yb^+.

(1) Summary of general theory of laser cooling [15-18]

Laser cooling and heating of atoms are caused by scattering forces generated by interaction between the atoms and radiation. This force arises, by averaging over the cycles of the momentum transfers occurring upon the absorption of a photon of radiation and subsequent spontaneous emission. We assume that the atom, which has a two-level term scheme, is irradiated with resonant radiation. In the case that the atom moves against the propagation direction of the radiation, as shown in Fig. 5.1, the atom receives the momentum of the photon $\hbar \mathbf{k}$ when the atom absorbs a photon of radiation, where $\mathbf{k}$ is the photon wave vector of the radiation. Therefore, the atom is decelerated by this momentum. Subsequently, the atom emits a photon by spontaneous emission. At this time, the atom also receives momentum due to the reaction of the emitted photon. In the spontaneous emission, the photons are emitted isotopically. Therefore, the momentum change per spontaneous emission is averaged to zero after several spontaneous emissions. Consequently, the atom is decelerated only by the momentums of the absorbed photons of radiation. The averaged velocity change per cycle of absorption and spontaneous emission process is given by $\Delta \mathbf{v} \simeq \hbar \mathbf{k}/m$, where m is the atomic mass. When the atom moves with the propagation direction of the radiation, the atom is accelerated by the same principle.

For example, in the case of ^{171}Yb$^+$, Δv is estimated to be 6×10^{-3} m/s when the $^2S_{1/2}$ - $^2P_{1/2}$ transition at 369.52 nm is used for laser cooling. The speed of a ^{171}Yb$^+$ ion is 120 m/s at a kinetic energy corresponding to room temperature. Therefore, to stop the ^{171}Yb$^+$ ion from this condition, twenty-thousands cycles of absorption and spontaneous emission process are required.

150

(a) Deceleration

at absorption

at spontaneous emission

$$m \Delta v = -\hbar k$$

$$m \overline{\Delta v} = 0$$

(b) Acceleration

$$m \Delta v = +\hbar k$$
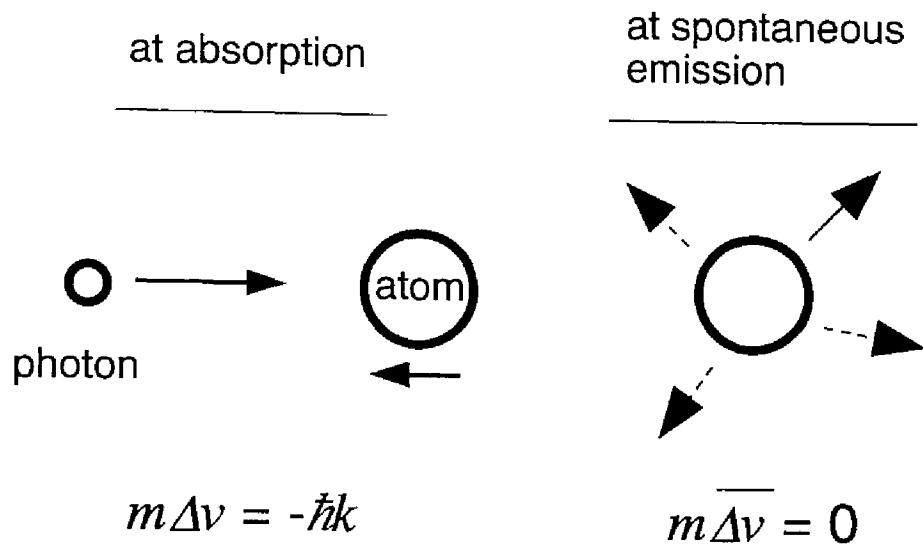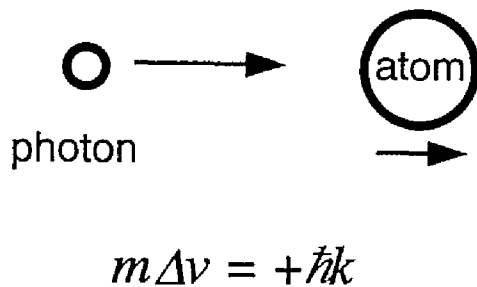
Fig. 5.1. Qualitative description of laser cooling and heating. In the case of (a) where the atom moves against the propagation direction of the radiation, in the absorption process, the atom is decelerated by an amount of $\Delta v = \hbar k/m$. In the spontaneous emission process, the average change in velocity is zero. Therefore, the atomic velocity can be reduced in the cycles of absorption and spontaneous emission processes. In the case of (b) where the atom moves along with the propagation direction of the radiation, the atom is accelerated in the same principle.

Although the average momentum change of the atom at spontaneous emission is zero, the atom makes a random walk owing to the reaction of each spontaneous emission event, in other words, $|v|^2 \neq 0$. The minimum temperature attainable by laser cooling is determined by the balance between this heating due to recoil and cooling by scattering force.

We express laser cooling more quantitatively, as discussed by Wineland and Itano [15]. We first consider the resonance (angular) frequencies at absorption and spontaneous emission, ω_{abs} and ω_{em}, respectively:

$$\omega_{abs} = \omega_0 + \mathbf{k}_{abs} \cdot \mathbf{v} - \frac{1}{2}\omega_0\beta^2 + \frac{R}{\hbar},$$ (5.1a)

$$\omega_{em} = \omega_0 + \mathbf{k}_{em} \cdot \mathbf{v}' - \frac{1}{2}\omega_0\beta^2 - \frac{R}{\hbar},$$ (5.1b)

where R is the recoil energy given by

$$R = \frac{(\hbar k)^2}{2m},$$ (5.2)

$\beta = |\mathbf{v}|/\hbar$, $\omega_0/2\pi$ is the frequency of the transition, $|\mathbf{k}_{abs}| = \omega_{abs}/c$, $|\mathbf{k}_{em}| = \omega_{em}/c$, $\mathbf{v}$ is the atom velocity in the ground state, and $\mathbf{v}'$ is the atom velocity in the excited state. The second term on the right-hand side of Eqs.(5.1) is the first-order Doppler shift, the third term is the second-order Doppler shift, and the last term is the recoil shift. We neglect the relativistic term, i.e., the third term in Eqs. (5.1). On a averaging many spontaneous emission events, as discussed above, the second term in Eq. (5.1b) becomes equivalent to zero. Finally, we obtain the change in atom kinetic energy per cycle of absorption and spontaneous emission process as

$$\Delta E = \hbar\left(\omega_{abs} - \omega_{cm}\right) = \hbar\mathbf{k} \cdot \mathbf{v} + 2R.$$ (5.3)

Here we replace k_{abs} with k for a general case.

We assume that the radiation is incident along the x direction and neglect saturation. The rate of kinetic energy change is obtained from Eq. (5.3) as,

$$\frac{dE}{dt} = \frac{I}{\hbar\omega}\sigma(\omega)\left(\hbar k v_x + 2R\right),$$ (5.4)

where I is the energy flux of the radiation and $\sigma(\omega)$ is the atomic cross section for absorption. In the case that the atom has a velocity with a Maxwell-Boltzmann distribution, the $\sigma(\omega)$ shows a Voigt profile. When the natural linewidth at FWHM, γ, and $R/\hbar$ are much less than the Doppler width, we can approximate the cooling rate by

$$\frac{dE}{dt} = \frac{I\sigma_0}{\hbar\omega}\left[\hbar\left(\omega - \omega_0\right) + R\right]\frac{\gamma\sqrt{\pi}}{2\omega_D}\exp\left[-\left(\frac{\omega - \omega_0'}{\omega_D}\right)^2\right],$$ (5.5)

where $\omega_D = \omega_0\left(\sqrt{(2k_B T/m)}/c\right)$, and $\omega_0' = \omega_0 + R/\hbar$.

Deceleration by scattering force works only in the propagation direction of the radiation. Therefore, to cool all degrees of freedom of free atoms, we need six components of deceleration force directed along the $\pm x$, $\pm y$, and $\pm z$ directions of a Cartesian coordinate system. To realize this condition, at least four narrow-band laser beams are required [19].

To estimate the temperature limit on cooling, we assume that the unpolarized atoms are irradiated with six laser beams along the $\pm x$, $\pm y$, and $\pm z$ directions and that the kinetic energy of the atom has already

153

decreased to a region where the Doppler width is much less than the natural linewidth. The maximum cooling rate is obtained when $\omega_0 = \omega_0{}'$ - $(1/2)\gamma$, and is given by

$$\frac{dE_x}{dt} = \frac{I}{\hbar\omega}\left[\sigma_+\left(\hbar k v_x + 2R\right) + \sigma_-\left(-\hbar k v_x + 2R\right)\right]$$

$$= \frac{2I\sigma_0}{\hbar\omega}\left(-\frac{\hbar k^2 \langle v_x^2 \rangle}{\gamma} + R\right). \qquad (5.6)$$

The minimum kinetic energy derived when $dE_x/dt = 0$ is given by

$$\langle E_x \rangle_{\min} = \frac{1}{4}\hbar\gamma. \qquad (5.7)$$

This is called the Doppler cooling limit.

Next, we consider a case in which an atom is confined in a trap. We first present discussions on only one dimension, as shown in Fig. 5.2. If we irradiate a trapped atom with one beam of radiation, the atom moves against and with the radiation in turn. According to the direction of the movement, the atom is decelerated or accelerated by scattering forces. To make only the deceleration force work effectively, we tune the frequency of the radiation to lower than the resonance center. In this case, when the atom moves against the radiation, the atom recognizes the frequency of the radiation to be higher one and be closer to the resonance center due to the Doppler shift. This results in increase of the absorption rate and cooling power. However, when the atom moves in the direction of the radiation, due to the Doppler shift, the atom recognizes the frequency of the radiation to be lower and be further from the resonance center. This results in decrease of the absorption rate and heating power. Consequently, the cooling process is only effective.
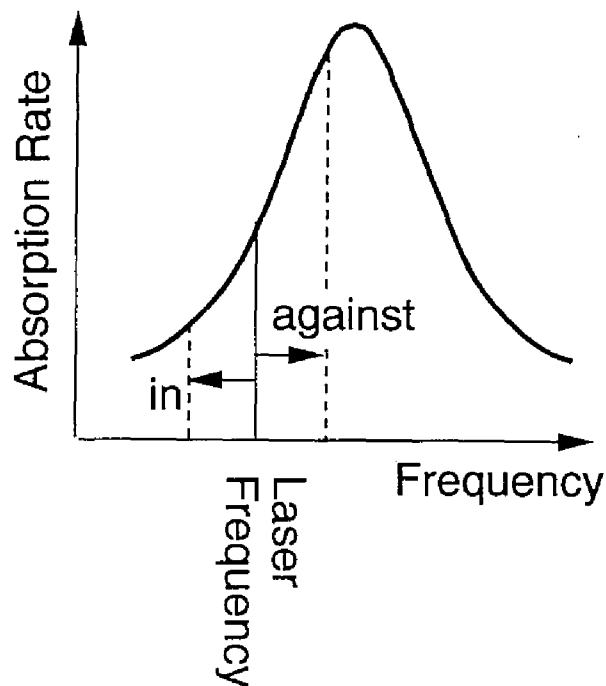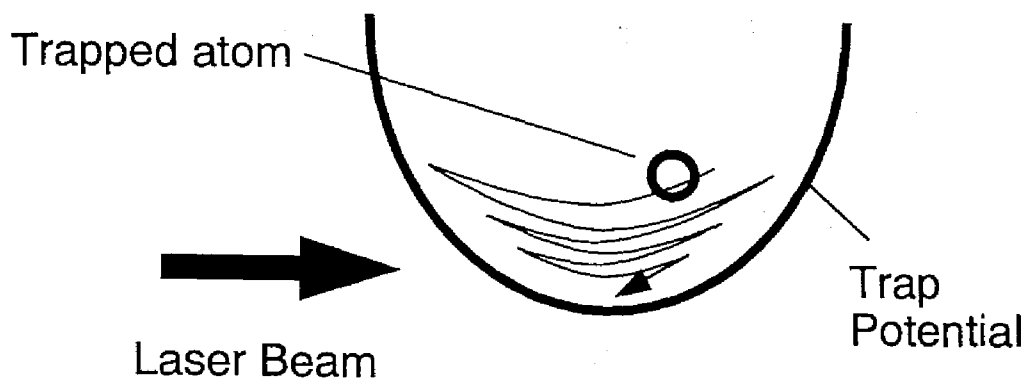
Fig. 5.2. Qualitative explanation of laser cooling of a trapped atom (in the case of one dimension). If we irradiate the trapped atom with a beam as shown in (a), the atom moves against and along with the radiation in tern. To increase the absorption rate only when the atom moves against the radiation, we detune the frequency of the radiation lower than the resonance center. Owing to the Doppler shift, the absorption rate increases when the atom moves against the radiation, and decreases when the atom along with the radiation, as shown in (b). This fact makes the cooling process essential. This explanation is valid in the case of weak bounding, i.e., $\gamma \gg \omega_x$.

We express the laser cooling of trapped atoms more quantitatively. When the radiation is directed along the x axis, the trapped atom recognizes the optical electric field to be

$$E_{\text{atom}} = E_0 \sin(kx - \omega t). \tag{5.8}$$

We assume that the trapped atom undergoes a harmonic oscillation of frequency ω_x. The position of the trapped atom is expressed by

$$x = x_0 \sin(\omega_x t + \phi_x). \tag{5.9}$$

Choosing $\phi_x = 0$, we have

$$E_{\text{atom}} = E_0 \sin(kx_0 \sin \omega_x t - \omega t). \tag{5.10}$$

This expression is that of a frequency-modulated electrical wave. Therefore, Eq. (5.10) can be expanded in terms of a series of Bessel functions.

$$E_{\text{atom}} \cong E_0 \sum_{n=-\infty}^{\infty} J_n(kx_0) \sin(-\omega + n\omega_x)t \tag{5.11}$$

Therefore, the trapped atom recognizes the optical electric field to be a composition of a carrier at ω_0 and sidebands at $\omega_0 + n\omega_x$, where n is an integer. In the case of the spontaneous emission, the trapped atom also has a spectrum of a carrier and sidebands, and each component has a natural linewidth. For strong bounding, i.e., $\gamma \ll \omega_x$, each component of the spectrum is resolved, as shown in Fig. 5.3. At the spontaneous emission, the average energy of the emitted photon is $\hbar\omega_0$. Therefore, if we irradiate the trapped atom with radiation whose frequency is in

Trapped atoms (ions)

Laser Beam

ω_x

Absorption

γ

$\omega_0 - 2\omega_x \quad \omega_0 - \omega_x \quad \omega_0 \quad \omega_0 + \omega_x \quad \omega_0 + 2\omega_x$
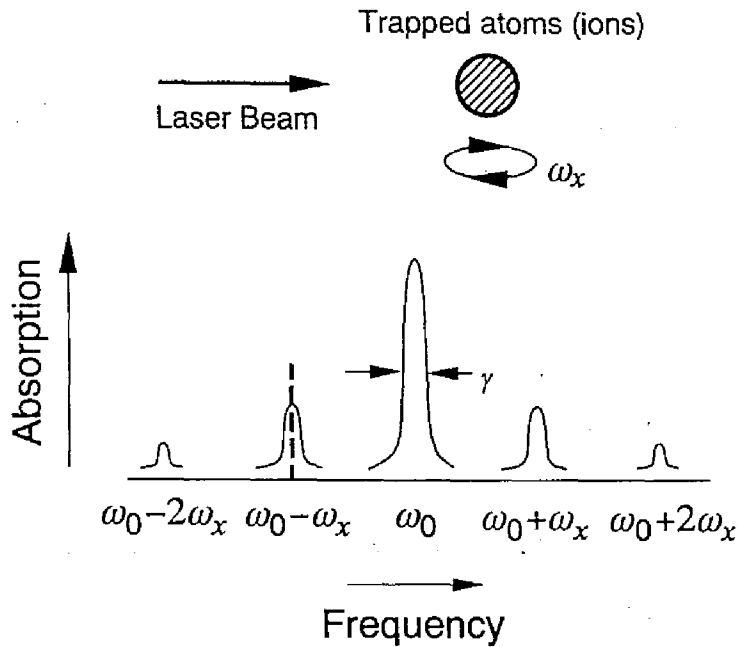
Frequency

Fig. 5.3.   Absorption spectrum of a trapped atom. It is assumed that γ $\ll \omega_x$. When the atom confined in the Lamb-Dicke region, or, $k\langle x^2\rangle^{1/2} \ll$ 1, the maximum cooling rate occurs when the frequency of the laser is tuned to the first lower sideband (dashed line).

accordance with that of the lower sideband, e.g., $\omega_0 - m\omega_x$, the kinetic energy of the trapped atom can be reduced by $m\hbar\omega_x$ per cycle of absorption and spontaneous emission.

If substantial cooling has already been realized and the amplitude of the ion motion satisfies with $k\langle x^2\rangle^{1/2} \ll$ 1, the components of the spectrum are the carrier and the first upper and lower sidebands. The maximum cooling rate occurs when the frequency of the radiation is tuned to the lower first sideband. In this region, the kinetic energy is given in terms of the mean occupation number $\langle n_x \rangle$ of the harmonic oscillator state for the atoms in the well. The minimum kinetic energy is given by [18]

$$\langle n_x \rangle_s = C_s \left(\frac{\gamma}{\omega_x} \right)^2 . \tag{5.12}$$

The minimum temperature, determined from a thermal distribution of occupation number, is given by

$$T_{\min} = \frac{\hbar \omega_x}{k_B \ln\left(\dfrac{\omega^2}{C_s \gamma^2} \right)} . \tag{5.13}$$

This is called the sideband cooling limit. C_s is a constant on the order of 1. In the ideal case, the value of C_s is 5/16 [18].

In the case of trapped ions, if we confine the more than one ion, the kinetic energies in all degree of freedom can be laser cooled by one laser beam due to thermalization by Coulomb coupling. Even in the case of single ion and $\gamma \gg \omega_x$, if one laser beam is directed at some oblique angle with respect to the x, y, and z direction, the kinetic energies in all degree of freedom can be laser cooled. However, this requires that the trap potential has no axial symmetry. In the case of sideband cooling, i.e., $\gamma \ll \omega_x$, a detailed discussion on the conditions of single-ion laser cooling is given in Ref. [18].

(b) Laser cooling of a natural isotope mixture of Yb⁺ [10]

We discuss laser cooling of a natural isotope mixture of Yb⁺. Laser cooling was performed by driving the $^2S_{1/2}$ - $^2P_{1/2}$ transition at the UV wavelength of 369.52 nm. The $^2D_{3/2}$ metastable state, pumped by spontaneous decay from the $^2P_{1/2}$ state, was depleted by driving the $^2D_{3/2}$ - $^3[3/2]^\circ_{1/2}$ transition at IR 935 nm [2].

At the usual trapping parameters, all isotopes of Yb^+ ions are simultaneously trapped. We assume that all trapped ions are strongly coupled with each other by the Coulomb interaction. Under this condition, we can assume that the net cooling or heating of the trapped ions is determined by the sum of the cooling or heating rate for each isotope of Yb^+ ions. In our trapping parameters, $\omega_x << \gamma$, i.e., our laser cooling approximates that in the case of free atoms. We can use Eq. (5.5) for estimating of cooling/heating rate. Taking into account the isotope shifts in the $^2S_{1/2}$ - $^2P_{1/2}$ transition and the natural abundance of the isotopes, and neglecting the odd isotopes because of optical pumping in hyperfine structures of the $^2S_{1/2}$ ground state, we sum Eq. (5.5) for each even isotope, and then obtain the net cooling/heating rate. In Fig. 5.4, we show it as a function of the temperature of the trapped ions. According to the result shown in Fig. 5.4, we cannot laser cool all of the whole trapped Yb^+ ions when we set the frequency of UV radiation in the lower-frequency side of
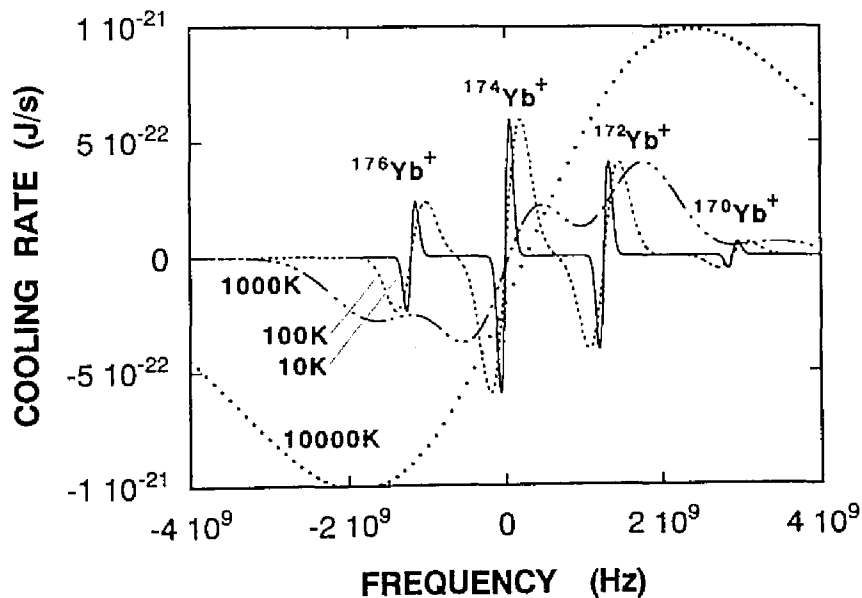
Fig. 5.4. Calculated cooling rate of a natural isotope mixture of Yb^+ ions at the various temperatures. Temperatures are given in the figure. We assume that all isotopes of Yb^+ ions are simultaneously trapped and rapidly thermalized. Cooling occurs when the sign of the cooling rate is negative. We only take into account the isotope shift of the $^2S_{1/2}$ - $^2P_{1/2}$ transition.

159

the resonance of ^{172}Yb$^+$, if the temperature of the ions is over 770 K. Under this condition, the sum of the heating rate of ^{174}Yb$^+$ and ^{176}Yb$^+$ ions exceeds the cooling rate of ^{172}Yb$^+$ ions.

In the above discussion above, we do not take into account the isotope shifts of the $^2D_{3/2}$ - $^3[3/2]_{1/2}$ transition at 935 nm. Therefore, this discussion is valid in the case that the linewidth of the radiation at 935 nm is wider than the isotope shifts of the transition. Fortunately, we found that the isotope shifts of the $^2D_{3/2}$ - $^3[1/2]_{1/2}$ transition were over 2.6 GHz, as described in Sec. 3.4, and wider than those of the $^2S_{1/2}$ - $^2P_{1/2}$ transition. We used a single-frequency Ti:Al$_2$O$_3$ laser for driving of the transition. Therefore, we were able to cool the all of the trapped Yb$^+$ ions even when we set the frequency of UV radiation in the lower-frequency side of the resonance of ^{172}Yb$^+$, by carefully setting the IR frequency to the isotope to be cooled, as will be shown in the results in the next subsection. In this case, ^{174}Yb$^+$ and ^{176}Yb$^+$ ions stay in the $^2D_{3/2}$ state because the radiation at 935 nm is off-resonant for these isotopes. Therefore, these isotopes do not sympathetically heat all of the ions.

5.2.2.　　Result for a Large Number of Ions

When we cooled a large number of Yb$^+$ ions, we turned on the electron and neutral Yb sources for two minutes, and then we carried out irradiation with the UV and IR beams. The frequencies of the two beams are important owing to the isotope shifts. We carefully set them using the signals of Yb$^+$ in a lamp as a reference. The frequency of UV radiation was fixed at a few hundred MHz below the resonance center of the isotope to be cooled. For IR radiation, we set the wavelength at that of the isotope cooled by UV radiation, using a wavemeter. The experimental set up is shown in Fig. 5.5.
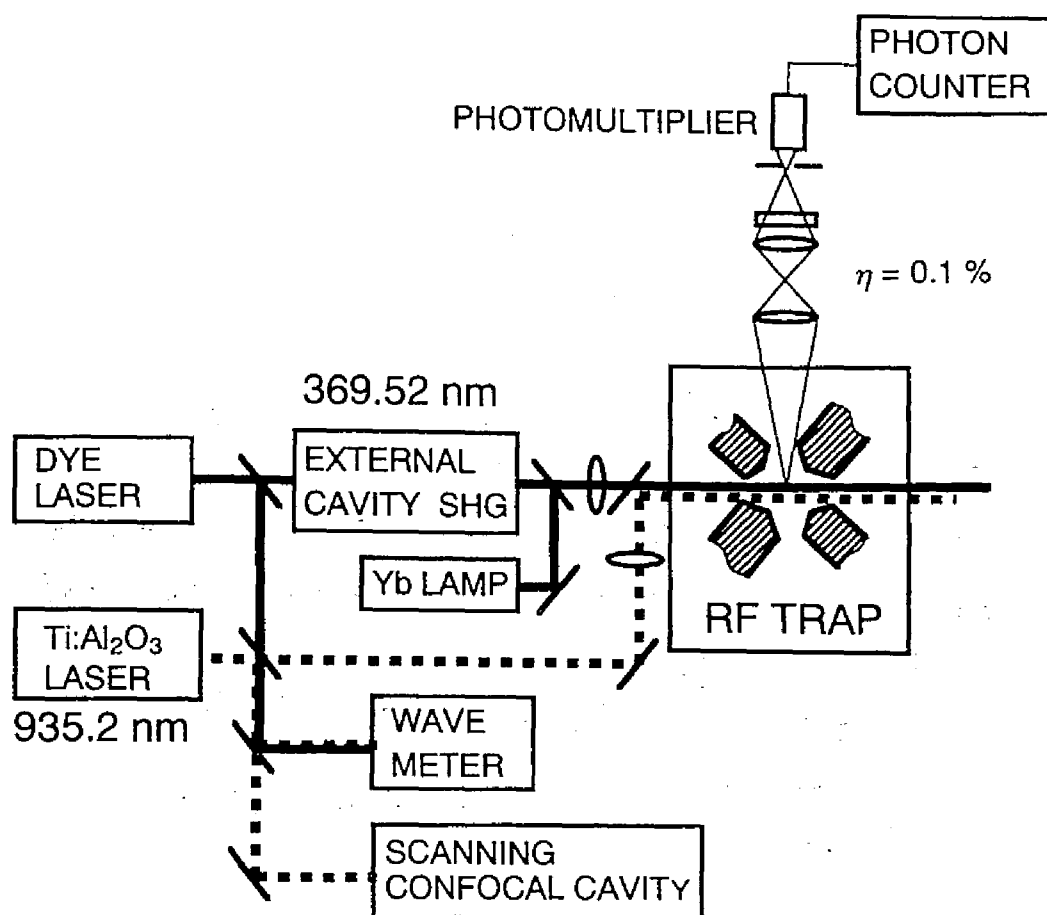
Fig. 5.5.   Experimental setup for laser cooling of Yb^+

We observed that the fluorescence signals increased within 10 s for the three major even isotopes. After the signals were observed, we selected the longitudinal mode of the IR laser by rotating the thin etalon until the maximum fluorescence signals were obtained. It is sufficient to select one or two adjacent modes. We observed the spectra by frequency scanning of UV radiation from low to high. The results are shown in Fig. 5.6. We observed spectra of only the directly laser-cooled isotope. However, when we switched the longitudinal mode of the IR laser to that of the optimum for each isotope as UV radiation was frequency scanned,
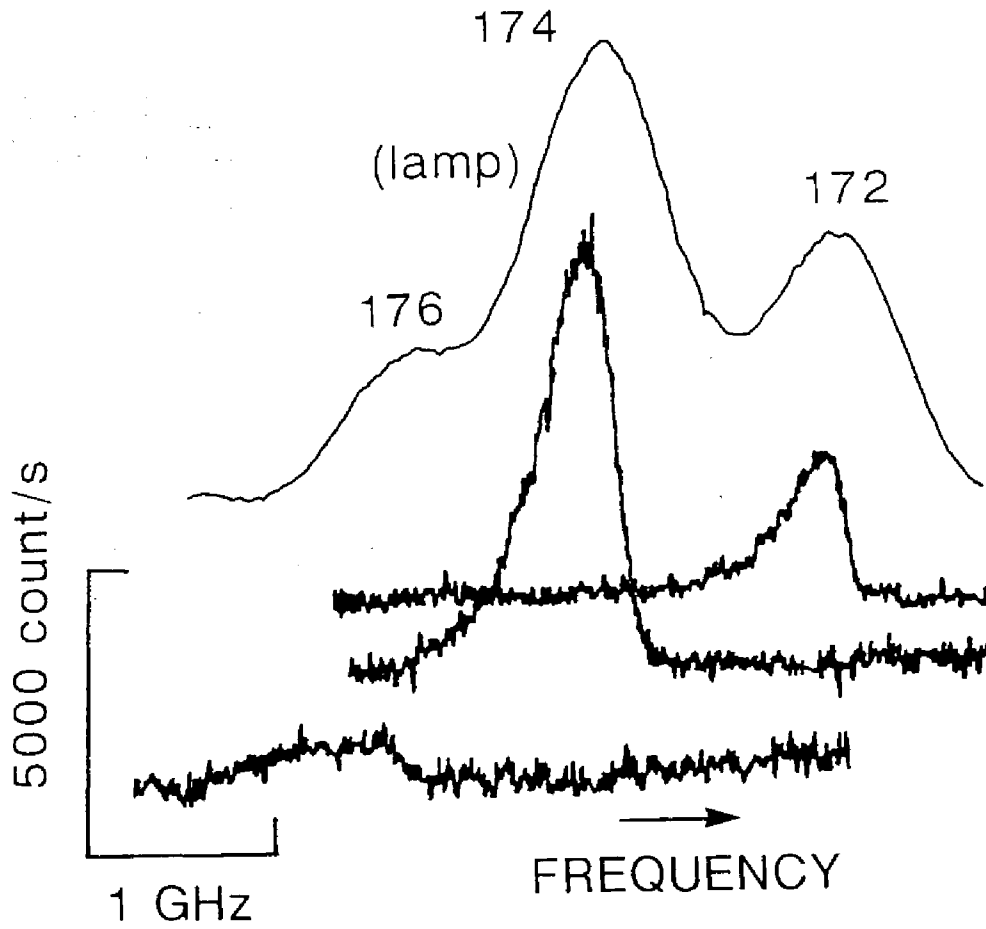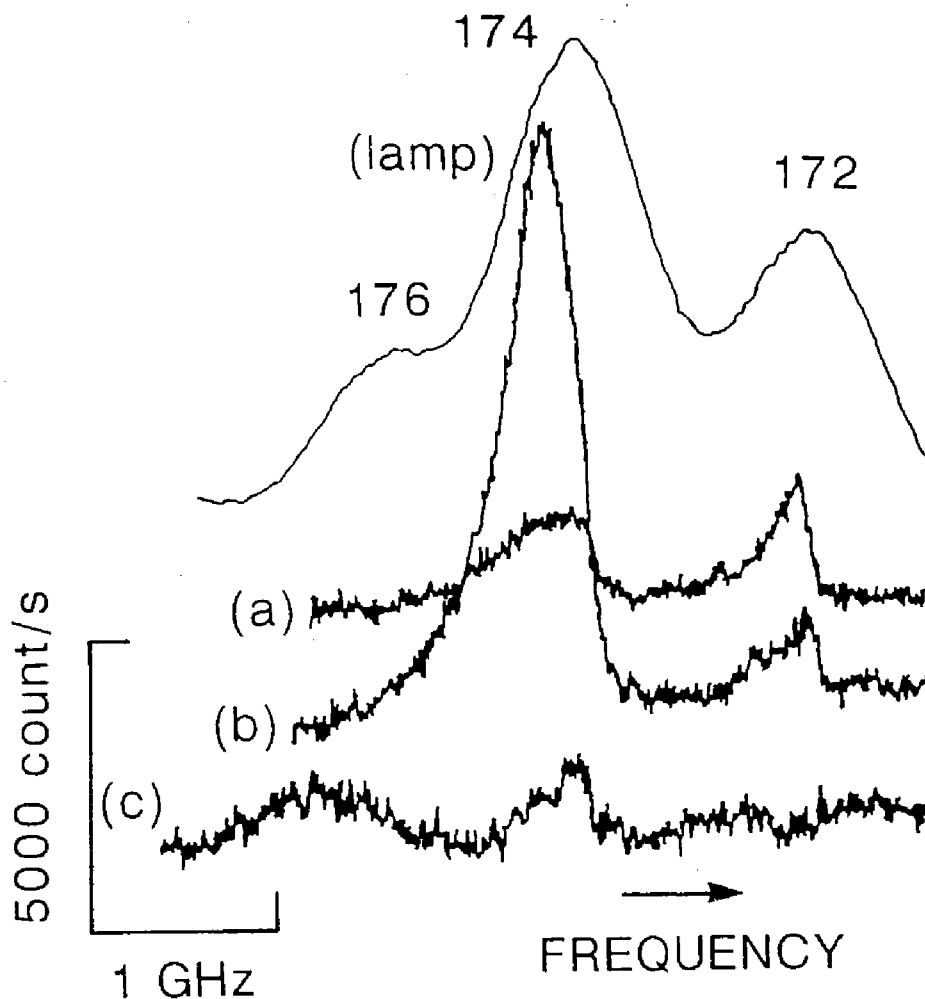
Fig. 5.6. Spectra of a large number of laser-cooled trapped Yb$^+$ ions by frequency scanning of UV radiation. Before scanning, we laser cooled (a) ^{172}Yb$^+$, (b) ^{174}Yb$^+$, and (c) ^{176}Yb$^+$. The frequency of IR radiation was fixed to the resonance frequency of the laser-cooled isotope. The upper trace is an absorption signal of Yb$^+$ in a lamp simultaneously detected. q_z = 0.53 and a_z = -0.03. Scanning speed was 7 MHz/s. UV power was (a) 70, (b) 100, and (c) 120 mW. IR power was 30 mW.

we observed the spectra of isotopes not directly laser-cooled, as shown in Fig. 5.7. We memorized the optimum longitudinal mode of the IR laser for each isotope, using the scanning confocal cavity, before frequency scanning. We estimated the temperature of Yb$^+$ from the half-width at half-maximum on the lower-frequency side. For ^{172}Yb$^+$ and ^{174}Yb$^+$, we obtained about 100 K.

To achieve a lower temperature, it is necessary to reduce rf heating. Two methods are used for this purpose: reducing the rf driving amplitude

[11,20] and decreasing the number of trapped ions [21]. First, we examined the effect of reducing the rf driving amplitude V_{ac}. We trapped and laser cooled $^{174}Yb^+$ ions with the same parameters as those in the case of Figs. 5.6 and 5.7, and then, we reduced V_{ac} (we also made the dc voltage of the ring electrode zero, i.e., $a_z = 0$) and frequency scanned the UV radiation. The temperature of Yb^+ decreased as V_{ac} became smaller, as shown in Fig. 5.8. We obtained a temperature of 34 K at $q_z = 0.19$.

Fig. 5.7. Spectra of a large number of laser-cooled trapped Yb^+ ions by frequency scanning of UV radiation. Before scanning, we laser cooled (a) $^{172}Yb^+$, (b) $^{174}Yb^+$, and (c) $^{176}Yb^+$. The frequency of IR radiation was switched during frequency scanning to make it resonant on (a) $^{174}Yb^+$ to $^{172}Yb^+$, (b) $^{174}Yb^+$ to $^{172}Yb^+$, and (c) $^{176}Yb^+$, $^{174}Yb^+$ to $^{172}Yb^+$ (missing). The upper trace is an absorption signal of Yb^+ in a lamp simultaneously detected. $q_z = 0.53$ and $a_z = -0.03$. Scanning speed was 7 MHz/s. UV power was (a) 70, (b) 150, and (c) 130 mW. IR power was 30 mW.
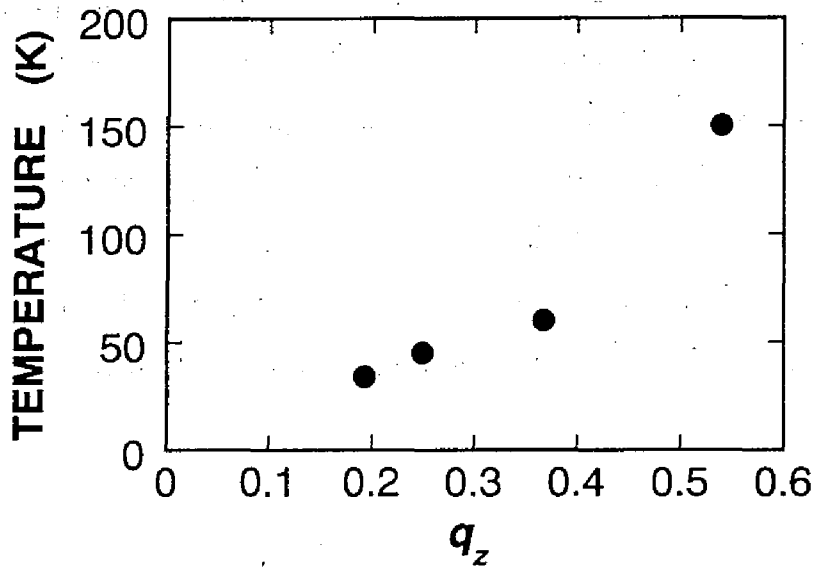
Fig. 5.8. Dependence of the temperature of large number of laser-cooled trapped $^{174}Yb^+$ on a trap parameter of q_z.

We next decreased the number of trapped Yb^+ ions by shortening the period during which the filament emitted electrons to $1 \sim 4$ s. We obtained a temperature of 45 K even at $q_z = 0.54$ and $a_z = 0$. At q_z less than 0.3, however, we observed the spectra shown in Fig. 5.9 and could not narrow the spectral width. The reason for and our solution of this effect are described in 5.2.3.

5.2.3.   DC Field Compensation

(1)   Effect of micromotion on spectra

When a single ion is located at the center of rf traps, the micromotion of the trapped ion is minimized because there is no rf driving electric field at the center of the trap. Although we decreased the number of trapped Yb^+ ions, we always observed the spectra shown in
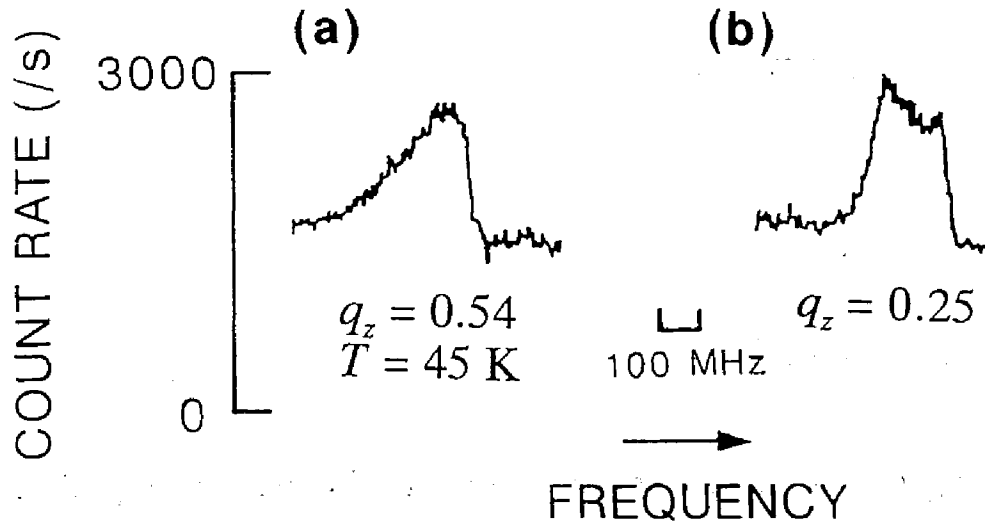
Fig. 5.9.   Spectra of a small number of laser-cooled trapped Yb⁺ ions
by frequency scanning of UV radiation. (a) q_z = 0.54, (b) q_z = 0.25. No
dc field compensation was performed.

Fig. 5.9(b), rather than narrow spectra. This is considered to be caused by the fact that unexpected stray dc field existed and pushed the trapped ions away from the center of the trap [11]. If the ions move from the center of the trap, their micromotions are forced by the rf driving field because the rf driving field is not zero there. Consequently, spectra are frequency modulated due to the Doppler shift caused by the micromotions, while one can laser cool the secular motion around the shifted position of the trapped ions. The origin of the stray dc field may be the contact potential caused by Yb deposited on the electrodes, or the charges on the surface of insulators. We estimate the effect of micromotion on the spectra in one dimension, as we refer to Ref. [18].

If one of the endcap electrodes has a stray dc potential ΔV_{stray}, a single ion is displaced by $\Delta \bar{z}$ from the center of the trap, where the force of the trap, F_{trap}, and that caused by the stray dc field, F_{stray}, are balanced, where the position $\bar{z}$ shows the averaged position over one cycle of micromotion, i.e., over time $2\pi/\Omega$. F_{trap} and F_{stray} are given by

$$F_{stray} = \frac{e\Delta V_{stray}}{2(z_0 / \alpha_{ed})} \qquad (5.14)$$

and

$$F_{trap} = -m\omega_z^2 \Delta\bar{z}, \qquad (5.15)$$

where α_{ed} is a factor used to compensate the fact that the trap electrodes are not parallel plates. From Eqs. (5.14) and (5.15), $\Delta\bar{z}$ is given by

$$\Delta\bar{z} = -\frac{4e\Delta V_{stray}}{mq_z^2\Omega^2(z_0 / \alpha_{ed})} = -\frac{mr^3\Omega^2\alpha_{ed}\Delta V_{stray}}{2\sqrt{2}eV_{ac}^2}. \qquad (5.16)$$

If we assume that the kinetic energy in the micromotion of trapped ions, E_{micro}, is equal to that of their secular motion, E_{micro}, at $\Delta\bar{z}$, it is given by

$$E_{micro}(\Delta\bar{z}) = \frac{1}{m}\left(\frac{e\Delta V_{stray}}{q_z\Omega(z_0 / \alpha_{ed})}\right)^2 = \frac{1}{m}\left(\frac{mr_0^2\Omega\Delta V_{stray}}{4V_{ac}(z_0 / \alpha_{ed})}\right)^2. \qquad (5.17)$$

The modulation index β due to the micromotion is given by

$$\beta = k\bar{z}_0 = \frac{2\sqrt{2}\pi}{\lambda}\left(\frac{e\Delta V_{stray}}{mq_z\Omega^2(z_0 / \alpha_{ed})}\right) = \frac{\pi}{\sqrt{2}\lambda}\left(\frac{r_0^2\Delta V_{stray}}{V_{ac}(z_0 / \alpha_{ed})}\right), \qquad (5.18)$$

where $\bar{z}_0$ is the amplitude of the micromotion. The frequency between the resonance center and the peak of the sideband spectrum is approximately equal to $\beta\Omega/2\pi$.

166

For example, if we assume that $\Delta V = 1$ V, $q_z = 0.263$, and $\alpha_{ed} = 0.85$ for the case of hyperboloid electrodes [22], we estimate that $\Delta z = 80$ μm, $E_{micro} = 220$ K, $\beta \cong 130$, and $\beta\Omega/2\pi \cong 280$ MHz for ^{174}Yb$^+$. These values are close to those of the spectrum of Fig. 5.9(b).

(2) Result

To compensate the stray dc field, we first applied dc voltage to one of the endcap electrodes (the other was at the ground potential), as commonly performed for compensation [12], and sometimes also to the filament of the electron source, as reported in Ref. [6]. We show the observed spectra after dc field compensation in Fig. 5.10. Before frequency scanning of UV radiation, we needed fine frequency tuning of the IR laser owing to the narrow Doppler width. This procedure was carried out by applying dc voltage to the PZT on which one of the cavity mirrors of the Ti:Al$_2$O$_3$ laser was mounted. In the case of ^{174}Yb$^+$, we often observed a sharp drop in the fluorescence signal, indicating the cloud-to-crystal phase transition [23], during frequency scanning.

We found that the problem of unexpected dc field was more severe when we observed single Yb$^+$. This demonstrates the need for more precise tree-dimensional compensation. Unfortunately, we found that the filament of the electron source had little effect in compensating dc field, probably owing to the long distance between the filament and the trap center. Therefore, we added two compensation electrodes, as shown in Fig. 5.11 and applied appropriate dc voltages to them and to one of the endcap electrodes.

We obtained the spectra of a small number of (but not single) laser-cooled Yb$^+$ ions by frequency sweeping of UV radiation as we changed the compensation dc voltage. We show the frequency between the sideband

COUNT RATE (s^{-1})

5000 ⌐ (a)174

1 MHz/s
120 μW

1000 ⌐

100 MHz

6000 ⌐ (b)172

3 MHz/s
·230 μW

(c)176

3 MHz/s
170 μW

3000 ⌐

2000 ⌐

1000 ⌐

100 MHz

100 MHz

(d)176(wide scannig) 8 MHz/s
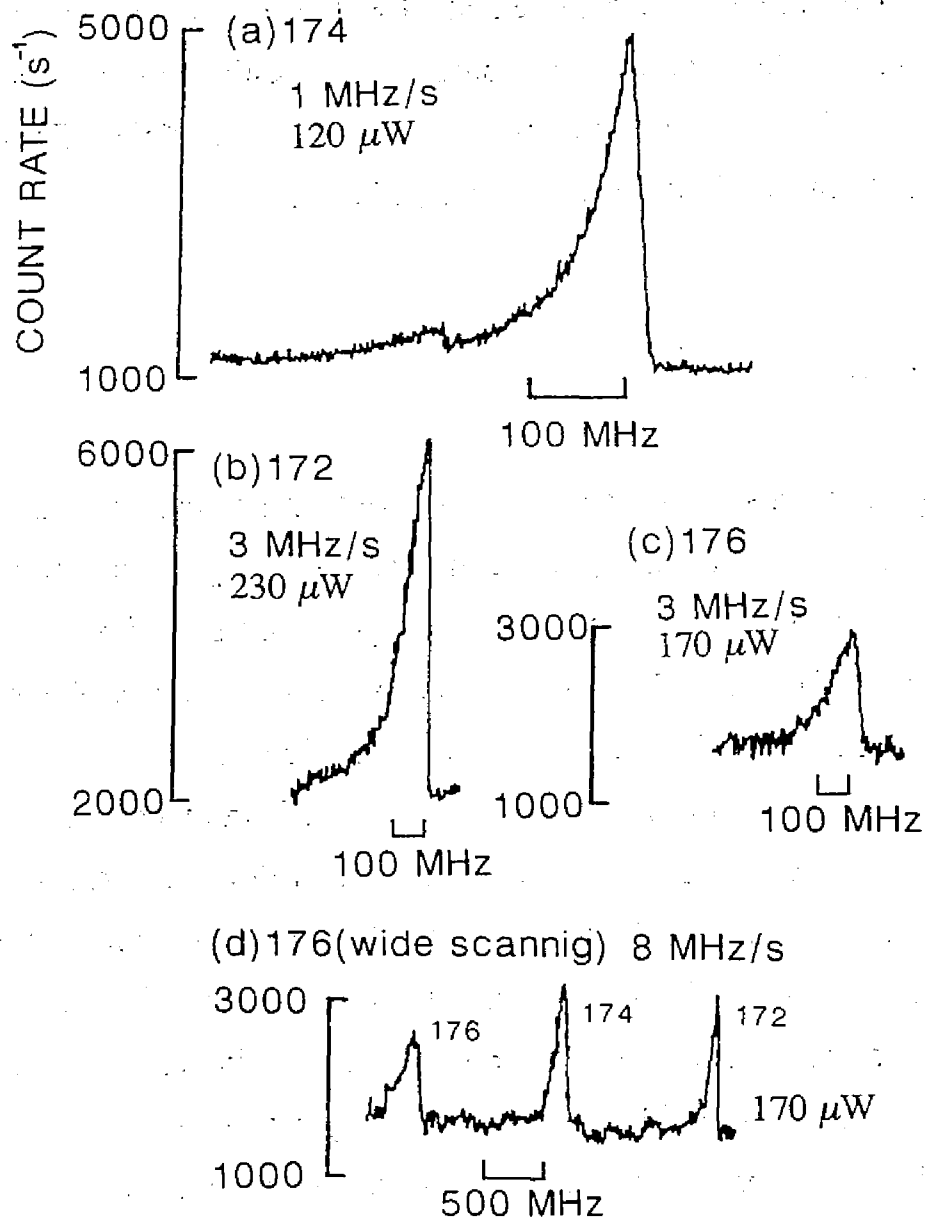
3000 ⌐

176   174   172

170 μW

1000 ⌐

500 MHz

Fig. 5.10 Spectra of a small number of laser-cooled trapped Yb$^+$ ions by frequency scanning of UV radiation when we applied compensation dc voltage to one of the endcap electrode and the filament of electron source. Laser-cooled isotope was (a) ^{174}Yb$^+$, (b) ^{172}Yb$^+$, and (c) and (d) ^{176}Yb$^+$. In the case of (d), we switched the frequency of IR radiation during frequency scanning to make it resonant on each isotope. We estimated the temperature of the laser-cooled isotopes from the half-width at half-maximum in the lower- frequency side of the spectra to be (a) 2 K, (b) 11 K, and (c) 15 K. Applied dc compensation voltages were (a) -0.95 V, and (b,c,d) -0.6 V to one of the endcap electrodes. In the case of (a), compensation voltage of -80 V was applied to the filament of electron source. The values of q_z were (a) 0.19, (b) 0.21, and (c, d) 0.25, and a$_z$ = 0 for all cases. Scanning speed and the power of UV radiation are shown in the figure.
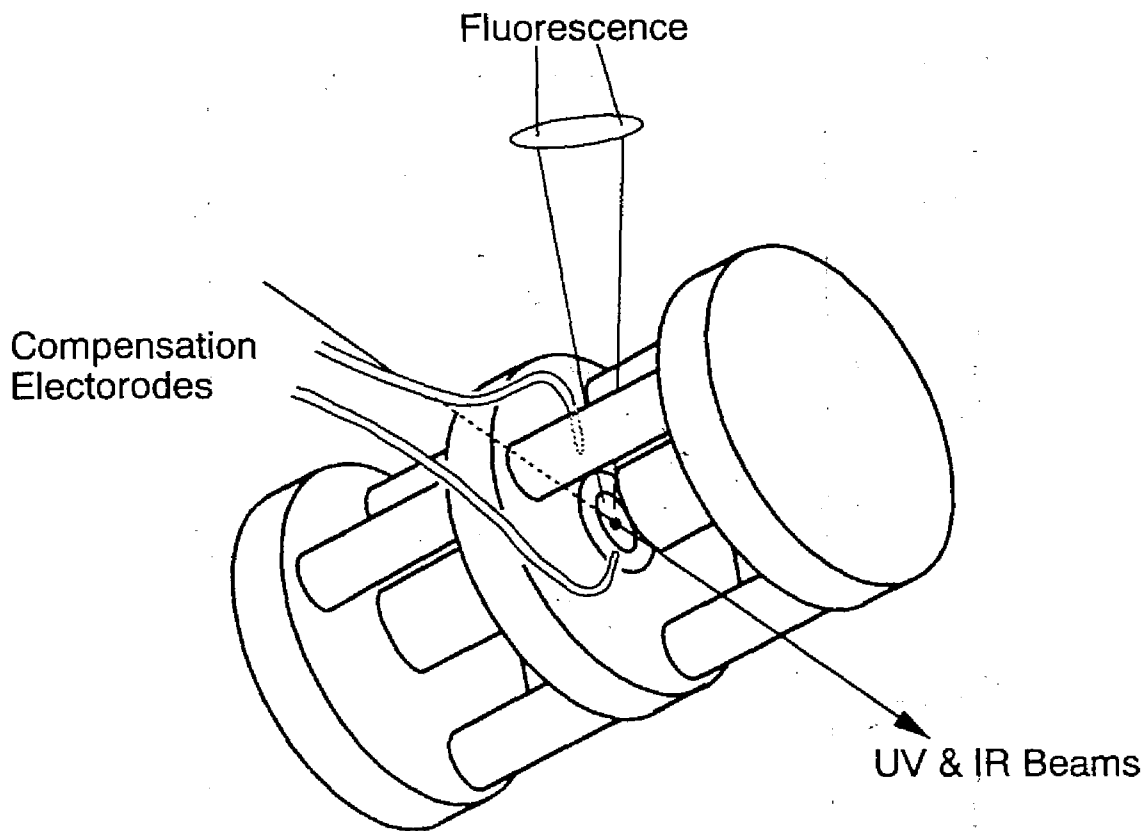
Fig. 5.11. A view of our small rf trap with compensation electrodes. Compensation electrodes are copper wires of the diameter of 0.5 mm.

peak and the center of the spectra as a function of compensation dc voltage in Fig. 5.12. For Fig. 5.12(a), we changed the dc voltage applied to one of the endcap electrodes V_{ed}, while the voltages to the compensation electrodes were fixed to 0 V. For Fig. 5.12(b), we changed the voltage applied to one of the compensation electrodes, while $V_{ed} = -1.0$ V and the voltage to the other compensation electrode $V_{comp2} = 0$ V. In Fig. 5.12(b), we plot the HWHM of the spectra, where the peak of the sideband was unclear as a result of the compensation. According to Fig. 5.12(a), it seems to be sufficient to apply the dc compensation voltage only to one of the endcap electrodes. Unfortunately, that was a very rare case and we

169
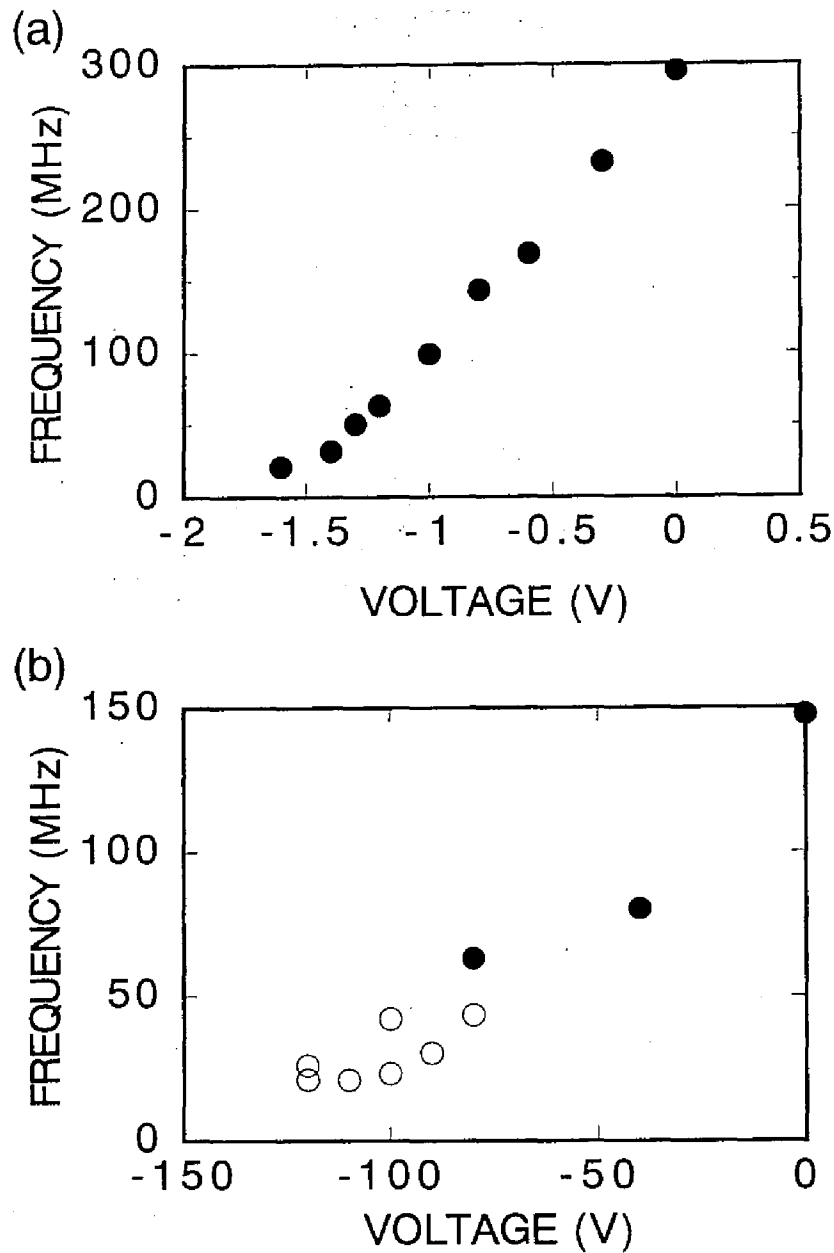
Fig. 5.12. Frequency between sideband peak and center of the laser-cooled ^{174}Yb$^+$ spectra as a function of the compensation dc voltages. (a) vs. compensation voltage applied to one of the endcap electrodes, while compensation voltages to the two compensation electrode were 0 V. (b) vs. compensation voltage applied to one of the compensation electrodes, while the compensation voltages to the other compensation electrode and one of the endcap electrode were 0 V and -1 V, respectively. When the sideband peak was not clearly resolved, we plotted the HWHM of the spectra in place of it (open circles).

usually needed to apply compensation voltages to all three of the electrodes. According to Fig. 5.12(a), the best compensation voltage applied to the endcap electrode, i.e., -1.5 V, is approximately in agreement with our estimated relation, as described above, between the stray dc field on one of the endcap electrodes ΔV_{stray} and the frequency between the sideband peak and the resonance center.

According to Eq.(5.16), $\Delta \bar{z}$ becomes large when the potential is shallow. We confirmed this with the results using a small number of (but not single) laser-cooled Yb^+ ions shown in Fig. 5.13, where we measured the relative center of the ion cloud by scanning the position of the UV beam as a function of the amplitude of rf driving voltage. Applying the compensation voltage reduced the change in position of the center of the ion cloud.
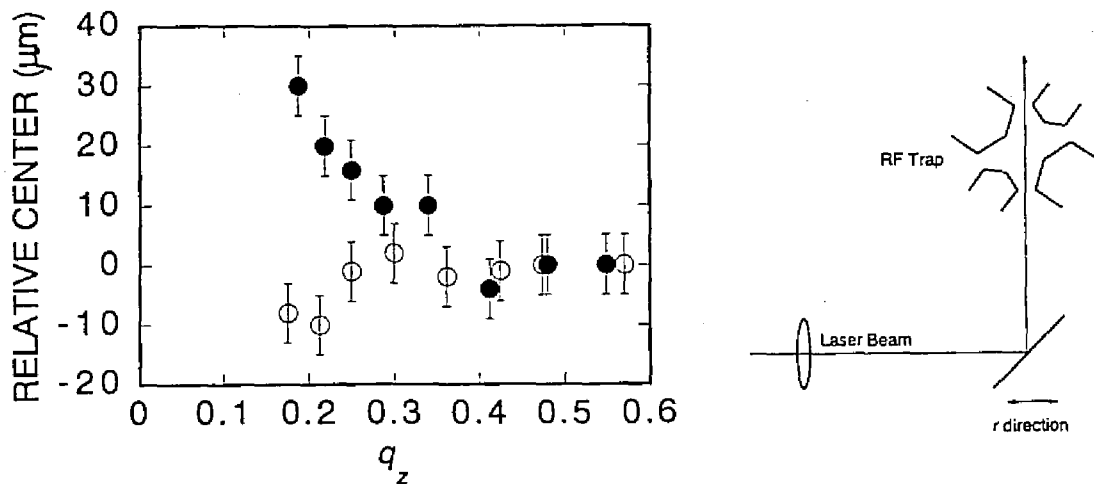
Fig. 5.13. Movement of the center of the ion cloud as a function q_z. We changed the voltage applied to one of the compensation electrodes. ●: 0 V; ○: 150 V. We scanned the beam position by moving the position of the mirror mounted on a precision stage, as shown in the right figure.

5.2.4.   Discussion

Figures 5.7 and 5.10(d) show that one of the three major even isotopes of Yb^+ can be directly laser cooled under the condition that the other isotopes are simultaneously trapped. We could not determine the temperature of the not directly laser-cooled isotopes, because we frequency scanned the cooling radiation itself to obtain the spectra, and the isotopes were directly laser-cooled when UV radiation was resonant on them during frequency scanning. Judging from the fact that the storage time of uncooled Yb^+ was 1 minute, however, we conclude that the not directly laser-cooled isotopes were trapped as a result of sympathetic cooling by Coulomb interaction with the laser-cooled isotope.

The experimental results in Figs. 5.10 (c) and (d) indicate that direct laser cooling of 13 % of the trapped ions sufficiently cools them, and sympathetically cools the not directly laser-cooled ions at least to some degree in the case where the total number of trapped ions was small. However, this seems to become more difficult, as shown in Fig. 5.7(c), as the number of trapped ions increases, owing to the increase in rf heating.
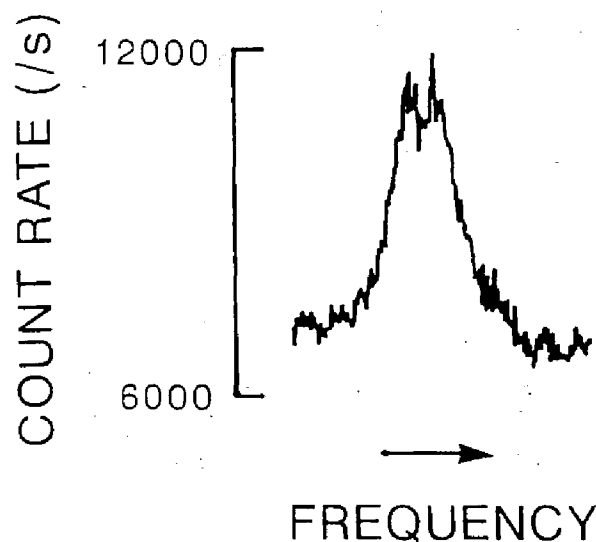
Fig. 5.14   A spectrum of a large number of laser-cooled Yb^+ ions obtained by frequency sweep of IR radiation.

A closer investigation is needed; we must observe the spectra of the ions not directly laser-cooled with a second radiation while one of the isotopes is simultaneously directly laser-cooled. Also, it is of interest to observe the spatial distribution of isotopes. In sympathetic cooling in the Penning trap, the ion of the higher mass-to-charge ratio is located in the outer part of the trap [9].

The spectra shown in Fig. 5.10(d) show the possibility that laser-cooled trapped ions may be useful for the measurement of isotope shifts. We obtained symmetric spectra by frequency scanning of IR radiation, as shown in Fig. 5.14, as predicted in Ref. [2] (we performed this test only for a large number of laser cooled Yb^+). This makes it possible to measure the isotope shifts of the $^2D_{3/2}$ - $^3[3/2]^o_{1/2}$ transition precisely, as well as to perform more precise measurement of the ion temperature, because it is easy to determine the resonance center. Also, frequency scanning of IR radiation is useful for performing more precise measurement of the ion temperature and to observing micromotion-induced sidebands due not only to the symmetry of the spectra but also to the narrower natural linewidth than that of the $^2S_{1/2}$ - $^2P_{1/2}$ transition at 369.52 nm. Clearer spectra obtained by frequency sweeping of IR radiation have recently been demonstrated by Tailar et al. at NPL [24], and researchers at Universitat Hamburg where the $^2D_{3/2}$ - $^3D[1/2]_{1/2}$ transition at 609 nm was used [25].

5. 3. Laser Cooling of Single Yb^+

After dc field compensation, we observed strong fluorescence of single Yb^+ ions with an intensity of over 1,500 counts/s. We determined the number of trapped ions by observing sudden drops of fluorescence

intensity by electron shelving in the $^2F_{7/2}$ state ('quantum jumps' signal), as described in Sec. 5.4. Even though strong fluorescence of single Yb^+ ions was observed after dc field compensation, we could not obtain narrow spectra by frequency scanning of UV radiation. We found that this was caused by saturation broadening in the $^2S_{1/2}$ - $^2P_{1/2}$ transition. We measured the fluorescence intensity and HWHM of the spectra as a function of UV power, as shown in Figs. 5.15 and 5.16, respectively. The narrowest spectra obtained so far are presented in Fig. 5.17. The saturation count rate of the fluorescence intensity was 1,800 /s and the saturation power of UV radiation was about 10 μW.

To substitute the saturation broadening and to estimate the residual linewidth, we replot Fig. 5.16 with the square of FWHM to UV power as shown in Fig. 5.18. The saturation-broadened spectra show a Lorentzian profile, as do ordinary saturated-broadened spectra. Therefore, we obtained the non-saturated-broadened width by fitting the points in
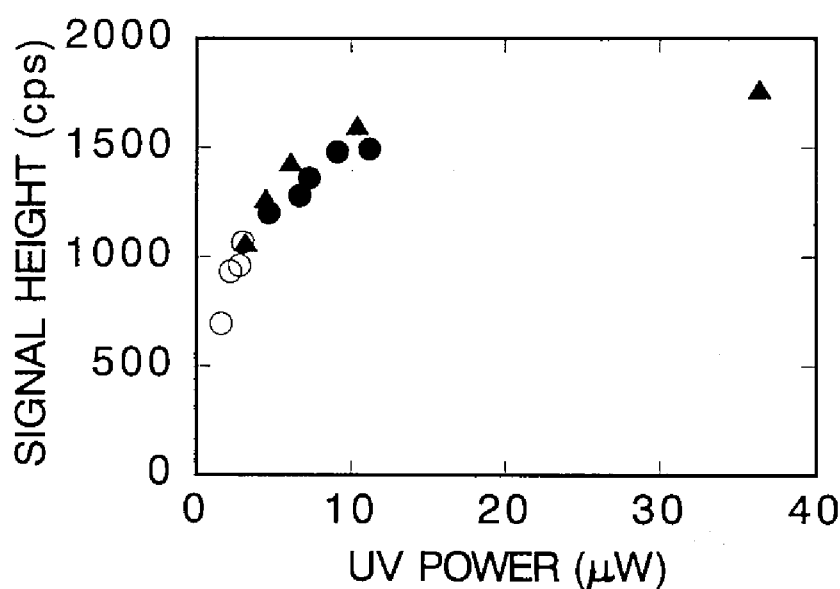
Fig. 5.15. Fluorescence intensity of a single laser-cooled trapped $^{174}Yb^+$ as a function of UV power. Different marks indicate different single $^{174}Yb^+$ ions (i.e., reloading of it).
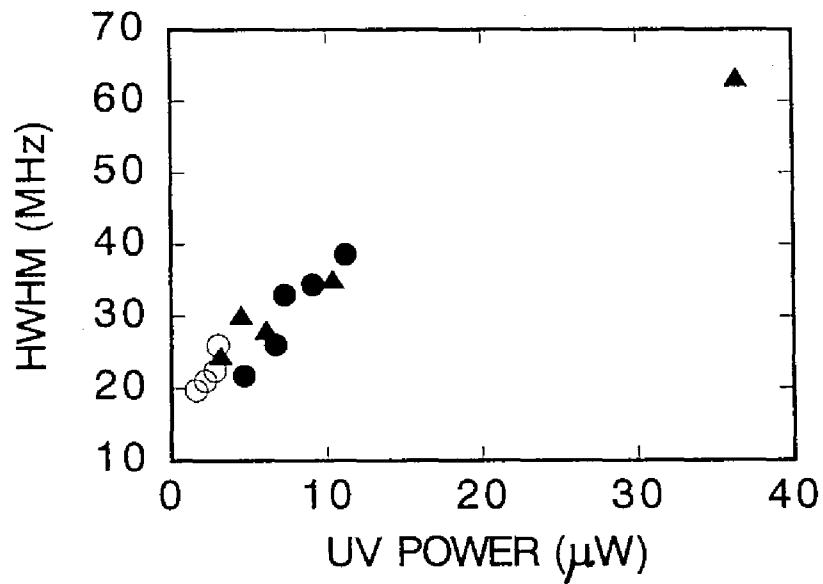
Fig. 5.16. Low-frequency-side HWHM of the spectra of a single laser-cooled trapped ^{174}Yb$^+$ as a function of UV power. Different marks indicate different singles ^{174}Yb$^+$ ion (i.e., reloading of it).
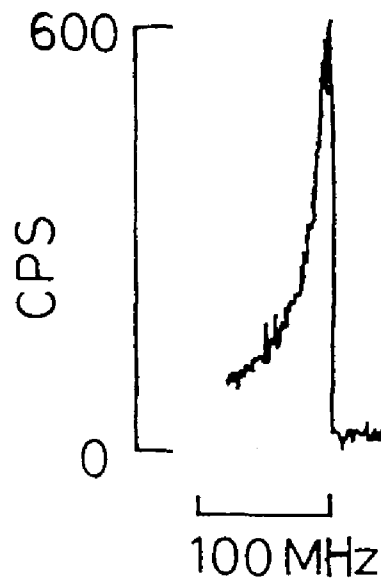

Fig. 5.17. Narrowest spectrum of a single laser-cooled trapped ^{174}Yb$^+$ obtained so far.

Fig. 5.18 with a line and by extrapolating the fitting line to zero UV power [26]. The value of the non-saturated-broadened width was estimated to be 30.2 (± 3.5) MHz at FWHM. This value was in excess of the natural linewidth of 19.8 MHz [27]. If we assume that the excess width is caused by the Doppler width, we estimate the temperature from the Doppler width to be 150 (+70, -60) mK from decomolution of a Voigt profile composed of the natural width and the Doppler width. However, it is more appropriate to conclude that the width in excess of the natural width was caused by sidebands due to the residual micromotion, and dc field compensation was still not completely perfect. Actually, we obtained all of the data points in Fig. 5.16 by re-loading single $^{174}Yb^+$ ions three times. The degree of perfection of the compensation was slightly different between each loading.
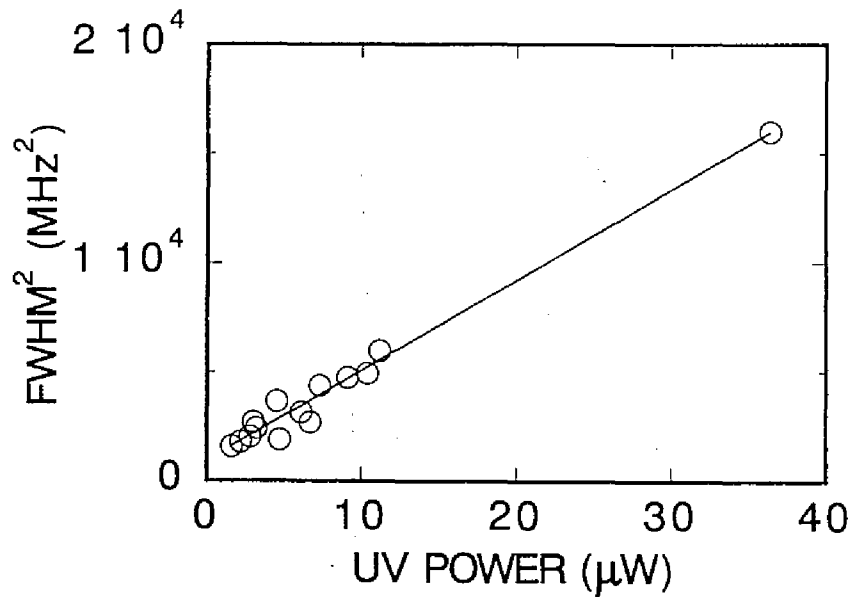
Fig. 5.18. Replot of Fig. 5.16 as square of HWHM to the UV power.

Because we use a natural isotope mixture of Yb^+, the question of whether other isotopes would be simultaneously trapped even though the observed ion is certainly single arise. To check for the existence of other isotopes, we observed the excitation of a stretch mode of ion crystals [11,28] from a decrease in fluorescence intensity with rf voltage applied between endcap electrodes. When the frequency of the applied rf voltage is in agreement with that of one of the ion oscillation modes, the ions absorb the rf electric power and their kinetic energies increase. This results in broadening of the Doppler width or an increase in the amplitude of ion oscillation outside the laser beam. Consequently, a decrease in the fluorescence intensity can be observed. This method was demonstrated by Wineland, Bollinger, and Itano as a method of mass spectroscopy [29].

By scanning of the frequency of the rf voltage, we observed number of resonances, which were assigned to be ω_x, ω_y, ω_z, $\omega_z - \omega_y$, $\omega_z - \omega_x$(or $\omega_z/2$), $\omega_z + \omega_x$(or $2\omega_z - \omega_y$), $\omega_z + \omega_y$(or $2\omega_z - \omega_x$), $2\omega_z$. The measured frequencies are summarized in. Although we applied the rf voltage only between the endcap electrodes, the anharmonicity of the trapping pseudopotential, e.g., C_4' terms as shown in Eq. (2.16), makes it possible to excite ω_x, ω_y, and other nonlinear terms. The anharmonicity is caused by the imperfection of the trap itself and/or the space charge potential of the ion cloud, as described in 2.3.2 . We found that ω_x and ω_y did not degenerate in our trap, i.e., our trap did not have perfect axial symmetry about the line $r = 0$. The difference between ω_x and ω_y was approximately 20 %. This allows us to laser cool trapped Yb^+ in all three dimensions using a single laser beam even in the case that only a single ion is trapped.

Figure 5.19 proves that the proposed method is effective for determing the existence of not-directly laser-cooled trapped ions which do not emit fluorescence. In Fig. 5.19, two $^{174}Yb^+$ ions were first trapped and a stretch mode of ion crystals at $\sqrt{3}\,\omega_x$ [11,28] was then observed. In the second frequency sweep of the rf voltage, excitation of the stretch mode
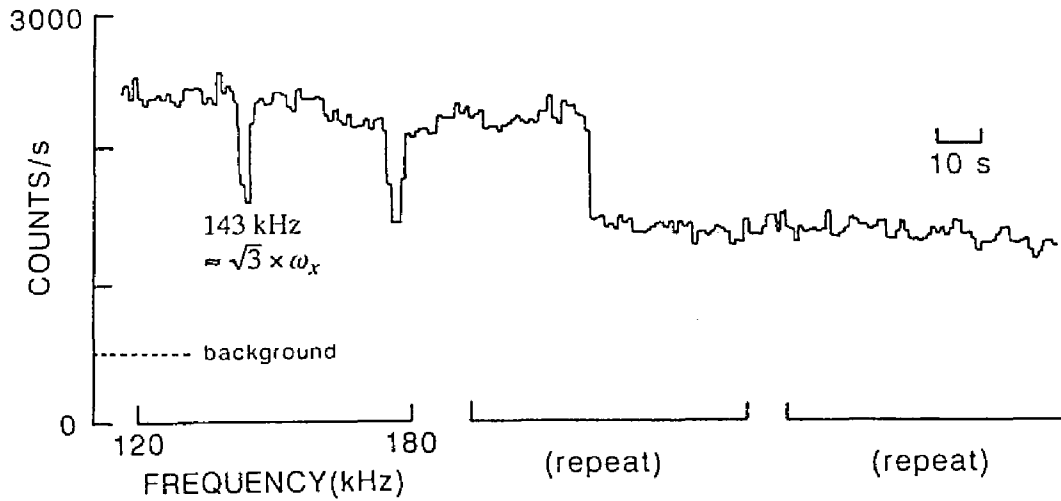
3000

COUNTS/s

143 kHz
$\approx \sqrt{3} \times \omega_x$

-------- background

0

120   180

FREQUENCY(kHz)

10 s

(repeat)   (repeat)

Fig. 5. 19   Excitation of a stretch-mode of two trapped ^{174}Yb$^+$ ions. In the second sweep, excitation resulted in loss of one ion. Then, no signals was detected at the third sweep because the residual ion was single. A resonance at the highest frequency in the sweep range observed at the first sweep may be the edge of the strong resonance of ω_z.

caused loss of one of the two ^{174}Yb$^+$ ions. Then, in the third sweep, we could not detect excitation of the stretch mode which indicates that no other isotopes were trapped. Therefore, if other not-directly-cooled isotopes which do not emit fluorescence exist in the trap, the stretch mode of ion crystals can be excited even when the observed ion is single. More detailed investigations would be useful for evaluating laser cooling of a natural isotope mixture of Yb$^+$, using this method to confirm the existence of the ions which do not emit fluorescence and a high-sensitivity imaging system to observe the spatial distribution of trapped ions.

178

5. 4. Quantum Jumps [10,14]

A method of measuring the number   (the number here means the number of isotopes directly laser cooled and emitting fluorescence) is to observe sudden drops (quantum jumps) of the fluorescence signals due to electron shelving of each ion [30]. Quantum jumps are easily observed when Yb^+ is pumped to the $^2F_{7/2}$ state because of the very long lifetime of the state. We found a scheme to optically pump Yb^+ to the $^2F_{7/2}$ state. Because the lifetime of the $^2F_{7/2}$ state is extremely long, we must pump out of the state in order to observe quantum jumps repeatedly. We investigated several transitions for this purpose.

To pump Yb^+ to the $^2F_{7/2}$ state, we drove the $^2D_{3/2}$ - $4f^{13}5d6s(^1D)^1[3/2]^o_{3/2}$ transition at 861 nm using radiation from an extended-cavity diode laser. The $^1D[3/2]^o_{3/2}$ state has strong connections to the $^2S_{1/2}$, $^2D_{3/2}$, and $^2D_{5/2}$ states [31]. Therefore, driving this transition can transfer Yb^+ to the $^2F_{7/2}$ state via the decay to the $^2D_{5/2}$ state, which has a spontaneous decay path to the $^2F_{7/2}$ state. The scheme of the related term of Yb^+ is shown in Fig. 5.20. This scheme was effective as shown in Fig. 5.21, where we trapped and laser-cooled three $^{174}Yb^+$ ions. Comparing the count rate of the spectra with one step in Fig. 5.21, which corresponds to the fluorescence intensity of a single Yb^+ ion, we estimate the number of trapped Yb^+ ions in Fig. 5.10 to be less than 10 for each isotope. The drops of fluorescence owing to pumping to the $^2F_{7/2}$ state were observed by Tamm et al. at PTB in a different pumping scheme [32], and more recently, by Gill et. al. at NPL in a scheme of driving the $^2S_{1/2}$ - $^2D_{5/2}$ transition at 411 nm [33].

Gill et al. at NPL recently found an optical scheme to deexcite the $^2F_{7/2}$ state, where by the $^2F_{7/2}$ - $4f^{13}(^2F_{7/2})5d6s^1D[5/2]^o_{5/2}$ transition is driven at 639 nm [34], and observed quantum jump signals repeatedly [33]. Referring to their results, we inferred that there is a possibility of
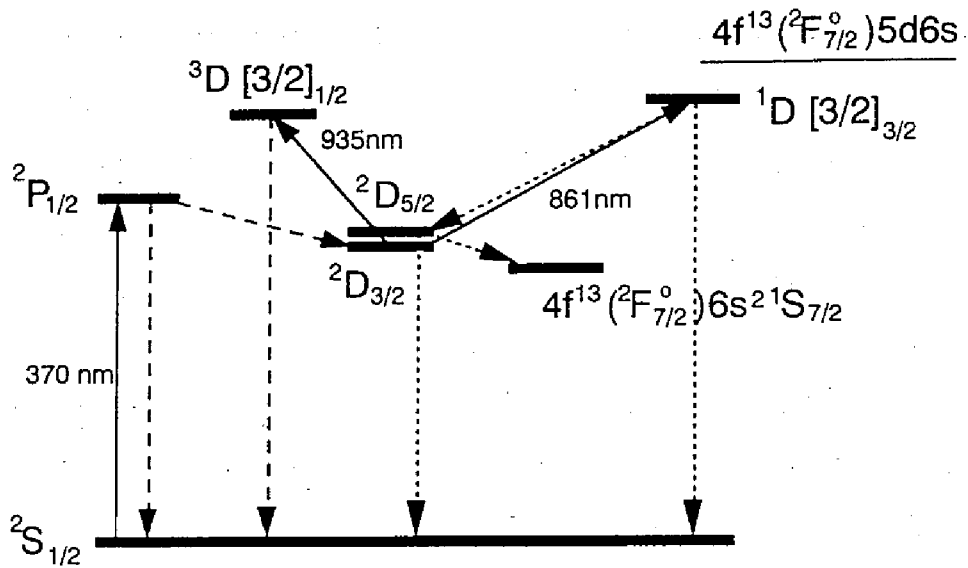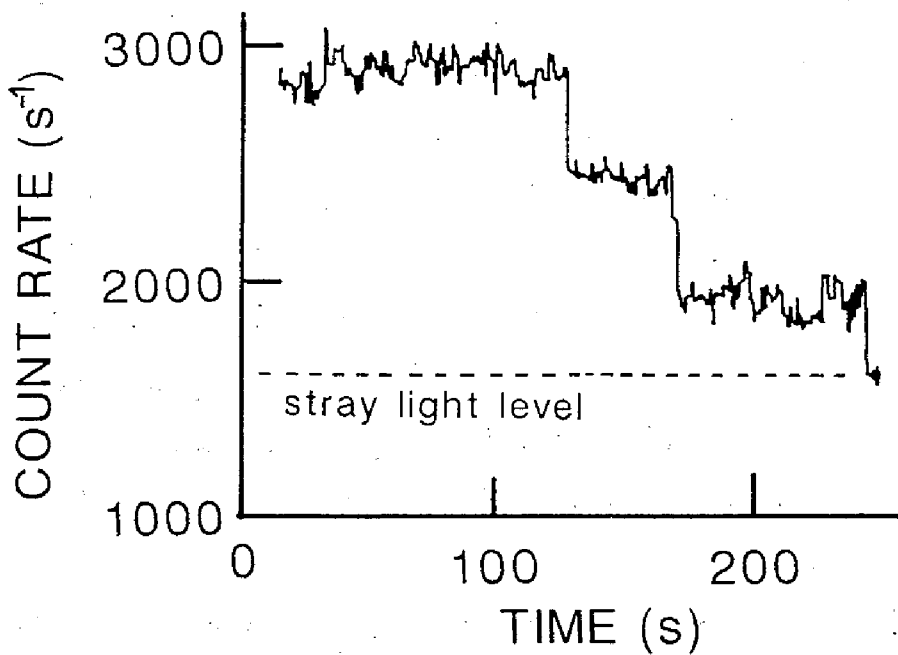
179

Fig. 5.19. Pumping scheme to the $^2F_{7/2}$ state

Fig. 5.20. Sudden drops of the fluorescence signal of $^{174}Yb^+$ ions by electron shelving to the $^2F_{7/2}$ state by driving the $^2D_{3/2}$ - $^1D[3/2]_{3/2}$ transition. The number of steps, i.e., three, shows the number of trapped $^{174}Yb^+$ ions.

deexcitation of the $^2F_{7/2}$ state by driving the transitions from the $^2F_{7/2}$ state to states in the $4f^{13}(^2F_{7/2})5d6s(^1D^\circ)$ or $4f^{13}(^2F_{7/2})5d6s(^3D^\circ)$ configurations. The parity of the $^2F_{7/2}$ states and those of the $^1D^\circ$ or $^3D^\circ$ terms are the same, i.e., odd. Therefore, the transitions between $^2F_{7/2}$ and states in the $^1D^\circ$ or $^3D^\circ$ terms are primarily quadrupole transitions. This means that transitions with $\Delta J = 0$, ±1, ±2 should be allowed. The possible transitions has the upper states of $J = 3/2$, $5/2$, $7/2$, $9/2$, $11/2$. In the possible transitions, the states of $J = 3/2$ have a short lifetime and their primary decay path is to the $^2S_{1/2}$ ground state. These would be better candidates for the deexcitation of the $^2F_{7/2}$ state if high-power radiation can be prepared at these wavelengths. The $^1D^\circ$ or $^3D^\circ$ states of $J = 5/2$ or $7/2$ are also useful because these states seem to have decay paths to the $^2D_{3/2}$ and $^2D_{5/2}$ states, or $^2D_{5/2}$ states, respectively. The $^1D^\circ$ or $^3D^\circ$ states of $J = 9/2$ or $11/2$ may not be effective for deexcitation of the $^2F_{7/2}$ state because these states have no dipole transitions to the $^2S_{1/2}$, $^2P_{1/2,3/2}$, and $^2D_{3/2,5/2}$ states. On the other hand, if the transition has an upper state with a long lifetime, e.g., to $^3D[3/2]_{5/2}$ at 1873 nm, to $^3D[5/2]_{5/2}$ at 913 nm, or to $^3D[5/2]_{7/2}$ at 947 nm states [31], it may have a potential for a clock transition because of the extremely long lifetime of the $^2F_{7/2}$ state (however, use of $^{171}Yb^+$ may be difficult because of the many hyperfine structures and Zeeman splittings of the $^2F_{7/2}$ state)

We examined the possibility of deexcitation of the $^2F_{7/2}$ state by several transitions using a large number of laser-cooled Yb^+ ions. The scheme of the related term of Yb^+ is shown in Fig. 5.22. In addition to the states in the $^1D^\circ$ or $^3D^\circ$ terms, we also examined a straightforward method, i.e., driving the $^2F_{7/2}$ - $^2D_{5/2}$ transition at 3.43 μm. It should be possible to generate radiation at 3.43 μm by difference-frequency mixing of a diode-laser-pumped Nd:YAG laser at 1064 nm and diode-laser radiation at 812 nm or 1543 nm. AgGaS$_2$ and KTA (or KTP) crystals should be phase-matched in the case of 812 nm and 1543 nm, respectively. We generated about 100 nW of 3.43 μm radiation from 65 mW of a 812 nm diode-laser
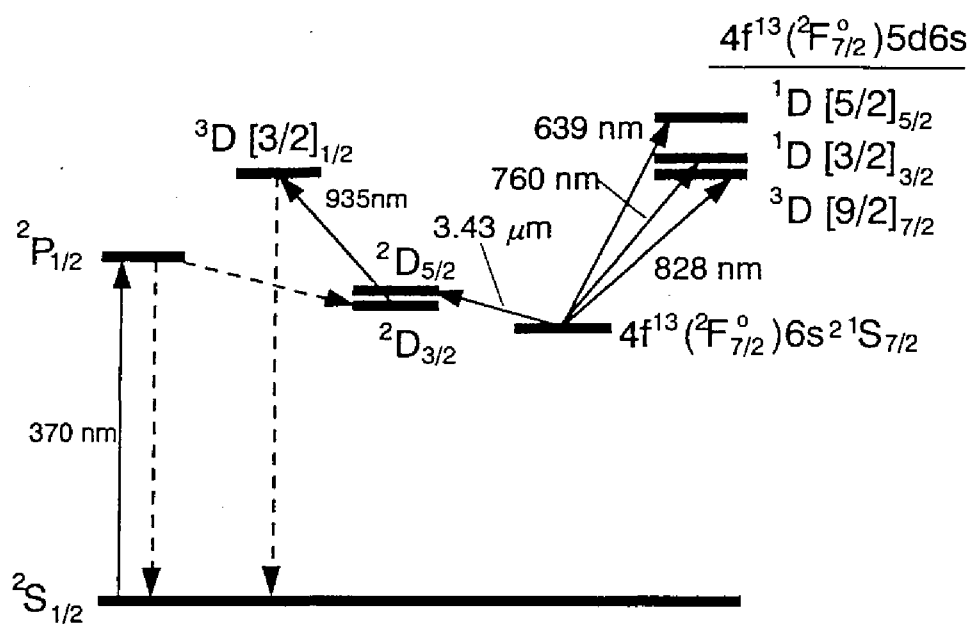
Fig. 5.22. Transitions for deexcitation of the $^2F_{7/2}$ state

Table 5.1. Summary of the transitions examined for deexcitation of the $^2F_{7/2}$ state.

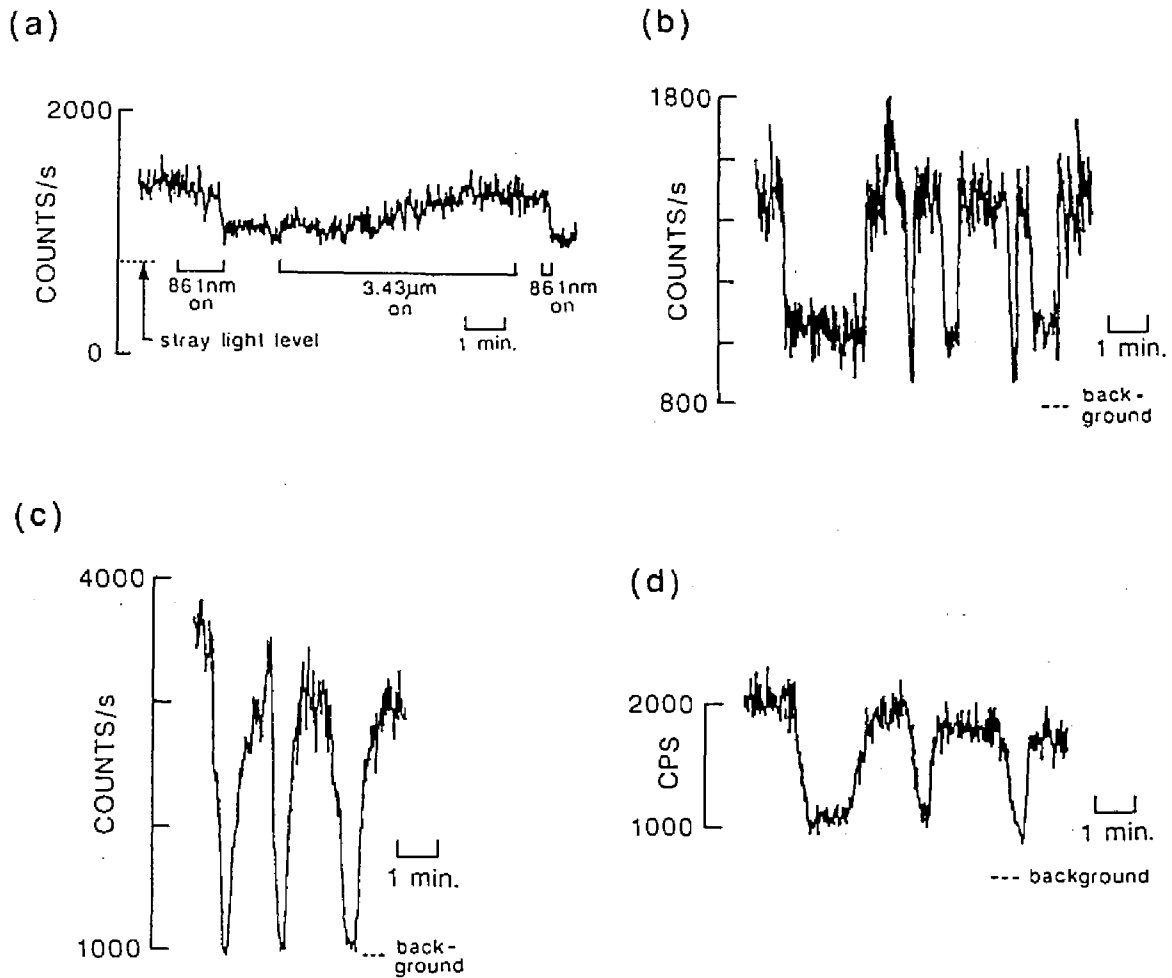| Transition	Wavelength (Isotope) (nm)		Laser Power(mW)	Fluorescence Recovery	
$^2F_{7/2}$ - $^2D_{5/2}$	3431.7	(172)	10^{-4}	○	
$^1[5/2]_{5/2}$	638.619	(174)	0.36	○	(○NPL [34])
$^1[3/2]_{3/2}$	760.076	(174)	0.58	○	
$^3[9/2]_{7/2}$	828.098	(174)	13	○	
$^3[5/2]_{3/2}$	~864.84	(174)	7	×	(○NPL [24])

(a)

(b)

(c)

(d)

Fig. 5.22. Fluorescence recovery by optically deexcitation of the $^2F_{7/2}$ state by driving (a) the $^2F_{7/2}$ - $^2D_{5/2}$ transition at 3.43 μm, (b) the $^2F_{7/2}$ - $^1D[5/2]_{5/2}$ transition at 639 nm, (c) the $^2F_{7/2}$ - $^1D[3/2]_{3/2}$ transition at 760 nm, and (d) the $^2F_{7/2}$ - $^3D[9/2]_{7/2}$ transition at 828 nm.

and 150 mW of Nd:YAG-laser radiation with a $AgGaS_2$ crystal of length 5 mm. All of the diode lasers used here were extended-cavity laser diodes composed of commercial diode lasers and gratings as the extended-cavity mirror [35], except in the case of radiation at 812 nm for which we used the prism configuration [36].

The results are summarized in Table 5.1, and the observed fluorescence recovery is shown in Fig. 5. 23. For pumping to the $^2F_{7/2}$ state, we irradiated trapped Yb^+ ions with radiation at 861 nm, as described above. The $^2F_{7/2}$ - $^1D[3/2]_{3/2}$ transition has the potential for fast deexcitation of the $^2F_{7/2}$ state due to the short lifetime of the $^1D[3/2]_{3/2}$ state of 19 ns, if much higher radiation at 760 nm is available. We conducted the experiment of deexcitation of the $^2F_{7/2}$ state under an UHV condition. However, there was still the possibility that the observed fluorescence recovery could be caused by the photodissociation of YbH^+, as was done previously by researchers including us in the case of 369.48 nm, as described in Sec. 4.4. We checked whether or not photodissociation of YbH^+ occurred with irradiation at 639 nm in the presence of buffer gas, as was done the experiment in Fig. 4.16. We confirmed that YbH^+ ions were not photodissociated by irradiation at 639 nm. Therefore, this wavelength should be the deexcitation line of the $^2F_{7/2}$ state. Although we performed this test only for radiation at 639 nm, it is highly possible that other wavelengths are deexcitation lines of the $^2F_{7/2}$ state because the condition of the deexcitation experiment for each wavelength was the same as that for radiation at 639 nm.

Although we did not succeed in deexciting the $^2F_{7/2}$ state by driving the $^2F_{7/2}$ - $^3D[5/2]_{3/2}$ transition at 865 nm, researchers at NPL observed fluorescence recovery by driving this transition with radiation of a higher intensity than ours [24]. Researchers at Universitat Hamburg observed deexcitation of the $^2F_{7/2}$ state by driving the $^2F_{7/2}$ - $^3D[7/2]_{5/2}$ transition at 771 nm [25].

With a combination of radiation at 861 nm and 639 nm, we succeeded in observing quantum jump signals by repeated pumping to and deexcitation of the $^2F_{7/2}$ state, as shown in Fig. 5. 24.
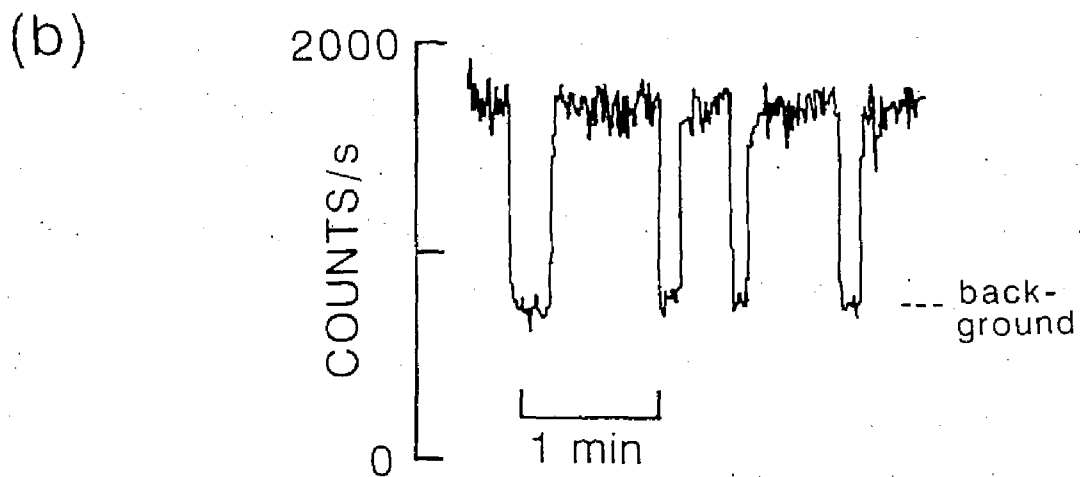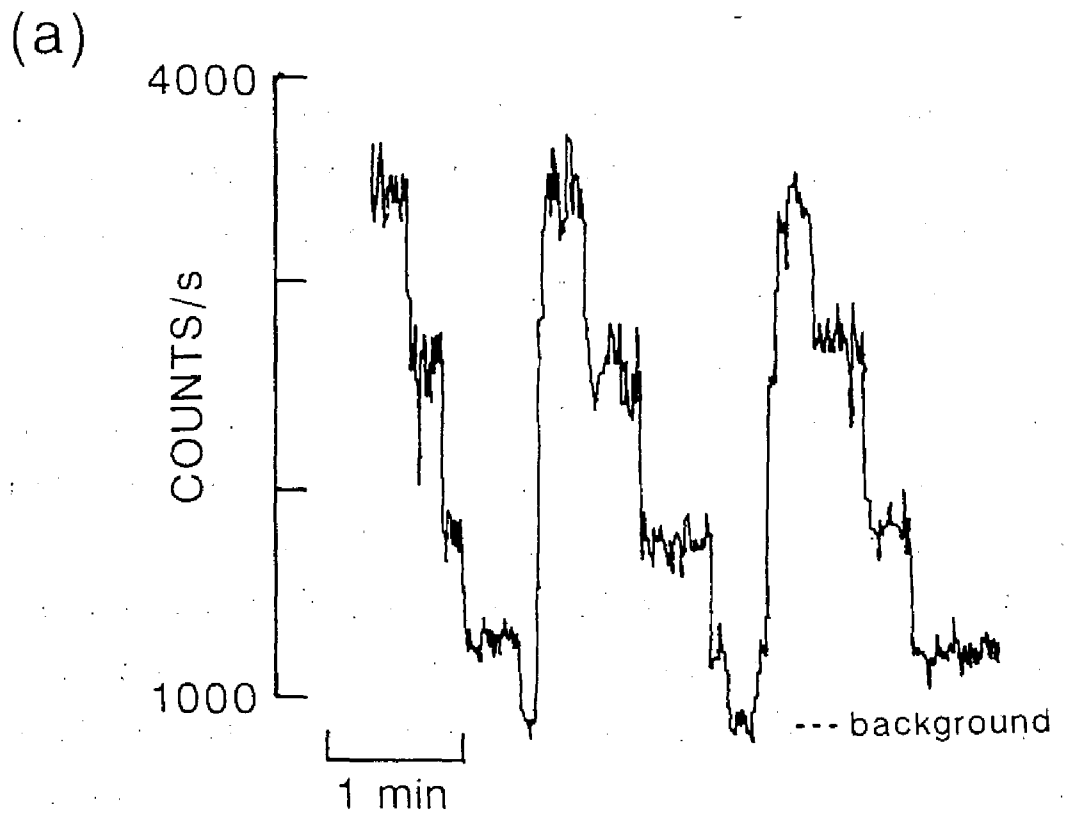
Fig. 5.24. Continuous observation of quantum jump signals of laser cooled ^{174}Yb$^+$ by pumping to and deexcitation of the $^2F_{7/2}$ state using radiation at 861 nm and at 639 nm, respectively. (a) Four ^{174}Yb$^+$ ions, (b) single ^{174}Yb$^+$ ion.

5. 6. Conclusions

We demonstrated that Yb^+ can be laser-cooled from a natural isotope mixture of Yb as a source. It was possible to directly laser cool one of the three major even isotopes without serious laser heating of the other isotopes, owing to relatively large isotope shifts of the $^2D_{3/2}$ - $^3[3/2]_{1/2}$ transition at 935 nm. According to the results for $^{176}Yb^+$, direct laser cooling of 13 % of the trapped ions is sufficient to cool them and to sympathetically cool the not directly laser-cooled ions simultaneously trapped, when the total number of trapped ions is small.

It was possible to trap and laser cool single $^{174}Yb^+$ ions also from a natural isotope mixture. We had a problem of an unexpected dc field which induced micromotion of trapped ions, as is often the case with other laboratories. We introduced two compensation electrodes to resolve this problem. Applying condensation voltages to the compensation electrodes and one of the endcap electrode, we observed narrow spectra of single $^{174}Yb^+$ ions. We evaluated saturation broadening of the $^2S_{1/2}$ - $^2P_{1/2}$ cooling transition, then, determined the temperature of a laser-cooled single $^{174}Yb^+$ ion to be 150 mK. However, we suppose that residual linewidth of the spectra was still caused by imperfection of the dc field compensation. It may be possible that not-directly laser-cooled isotopes of Yb^+ are simultaneously trapped even in the case that a single Yb^+ ion is observed, because we use a natural isotope mixture of Yb as a source. We proposed that excitation of a stretch mode of trapped ions can be used for judging the existence of other isotopes.

We observed quantum jump signals by pumping to the $^2F_{7/2}$ state. This signal was useful to determine the number of (directly laser-cooled) trapped Yb^+ ions. To observed quantum jump signals repeatedly, some methods for deexciting the $^2F_{7/2}$ state are necessary. We observed the fluorescence recovery by deexcitation of the $^2F_{7/2}$ state with driving the

following four transitions: the $^2F_{7/2}$ - $^2D_{5/2}$ transition at 3.43 μm, the $^2F_{7/2}$ - $^1D[5/2]_{5/2}$ transition at 639 nm, the $^2F_{7/2}$ - $^1D[3/2]_{3/2}$ transition at 760 nm, and the $^2F_{7/2}$ - $^3D[9/2]_{7/2}$ transition at 828 nm. Using radiation for pumping to and deexcitation of the $^2F_{7/2}$ state simultaneously, we observed quantum jump signals repeatedly. Deexcitation of the $^2F_{7/2}$ state is essential when we conduct high-resolution spectroscopy of the $^2S_{1/2}$ - $^2D_{5/2}$ transition at 411 nm, because Yb$^+$ in the $^2D_{5/2}$ state spontaneously decays to the $^2F_{7/2}$ state.

Chapter 6

Conclusions

In this thesis, we described mainly our investigation of Yb^+ stored in rf traps. Since we began our investigation by constructing light sources for Yb^+, and thereafter studied the characteristics of buffer-gas-cooled and laser-cooled Yb^+. Yb^+ is a candidate for providing a reference transition for use in future microwave or optical frequency standards. For this reason, trapped Yb^+ ions have been extensively investigated at several laboratories throughout the world including ours. On the other hand, unlike other ion species considered as candidates for frequency standards, Yb^+ shows several unique characteristics originating from the fact that Yb is one of the lanthanoids. Therefore, it is important, or essential in some cases, to understand them in order to establish a new frequency standard using Yb^+. This work makes some contributions to the goal of complete understanding of the characteristics of Yb^+ stored in rf traps.

In Chapter 2, we described our experimental setup of rf traps used for the investigation of Yb^+, and detection of trapped ions by an electric method, i.e., the rf resonance absorption method. We made two sizes of rf traps: The larger one of $2r_0 = 22.6$ mm was used for the investigation of buffer-gas-cooled Yb^+, and the smaller one of $2r_0 = 5$ mm for laser-cooled Yb^+.

In the case of the larger trap, we were able to detect rf signals of trapped ions. We investigated the anharmonic oscillation of trapped ions.

We found that rf signals changed considerably as a function of the pressure of buffer gases even when the same number of ions was trapped. In the case that Ba^+ was trapped, rf signals obtained by sweeping dc voltage of the trap in a certain direction (sweep direction f in this thesis) disappeared at a high buffer gas pressure in the case of Ba^+. Also, anharmonicity in rf signals depended on the number of trapped ions when the pressure of the buffer gas was fixed. These observations indicate that the space charge potential caused by the trapped ions had anharmonicity which changed as a function of the spatial distribution of trapped ions. We pointed out that anharmonicity in rf signals limits the accuracy in estimating of the total number of trapped ions by the rf resonance absorption method.

In Chapter 3, we described our light sources for Yb^+. For the radiation at 369.52 nm to drive the $^2S_{1/2} - {}^2P_{1/2}$ transition, we established a simple method of UV generation, i.e., SFM of diode-laser and argon-ion-laser radiation. We obtained more than 1 μW of tunable cw radiation at 370 nm from 21 mW of radiation at 1310 nm from a diode laser, and 1.3 W at 515 nm from an argon-ion laser. We successfully detected the fluorescence of trapped Yb^+ ions using this radiation. We used β-BaB_2O_4 as a crystal of SFM, and found that phase-mismatching tolerance was several times larger with a strong focusing of input beams than with no focusing. In the case of strong focusing, the aperture length was shorter than the crystal length. We suggested that phase-mismatching tolerance should be calculated using the aperture length in place of the crystal length.

We propose that radiation generated by sum- or difference-frequency mixing can be frequency stabilized by controlling only one of the two fundamental lasers. We demonstrated this simple frequency stabilization method by the sum-frequency mixing of diode-laser and argon-ion-laser radiation, where we controlled only a diode laser to lock

the sum frequency to the frequency reference, while an argon-ion laser was free-running. We propose that this frequency-stabilization method could be applied to other combinations of fundamental lasers. In particular, diode lasers are suitable for this method owing to their wide tunability.

For laser cooling, we needed more power than the radiation generated by SFM. We obtained over 100 μW of radiation by SHG of dye-laser radiation using an external cavity technique. We successfully laser cooled trapped Yb^+ ions using this UV radiation. To laser cool Yb^+, the $^2D_{3/2}$ metastable state must be depleted. For this purpose, we generated radiation at 935 nm using a $Ti:Al_2O_3$ laser to drive the $^2D_{3/2}$ - $^3[3/2]^o_{1/2}$ transition. We installed a homemade rough frequency scanning mechanism in the $Ti:Al_2O_3$ laser and determined isotope shifts of the $^2D_{3/2}$ - $^3[3/2]^o_{1/2}$ transition. This was important in our laser cooling of Yb^+, because we used a natural isotope mixture of Yb^+.

In Chapter 4, we presented the characteristics of Yb^+ stored in a rf trap in the presence of buffer gases. First, we frequency scanned radiation at 369.52 nm to drive the $^2S_{1/2}$ - $^2P_{1/2}$ transition of Yb^+ and observed the spectra of the transition. We revealed that fluorescence of odd isotopes was not observed by frequency sweeping of only one UV beam due to optical pumping in the hyperfine structures. We confirmed the cooling effect by collision with light buffer gas.

Our investigation focused on the characteristics of buffer-gas-cooled Yb^+ observed when we continuously drove the $^2S_{1/2}$ - $^2P_{1/2}$ transition using radiation at 369.52 nm. It is known that the fluorescence of Yb^+ ions fades with continuous driving of the $^2S_{1/2}$ - $^2P_{1/2}$ transition in the presence of buffer gases. In addition, we found that rf signals disappeared while fluorescence faded. We found rf signals disappear occurs when some background gases exist in vacuum. For example, O_2 and H_2O gases enhance

190

the disappearance of rf signals. We observed that the resonance point of rf signals shifted to that of a heavier mass while rf signals disappeared. Therefore, we proposed that, with rf-signal disappearance, molecular ions were produced by chemical reaction of Yb^+ in the excited states with background gases. We confirmed this proposal by mass-selective ionic detection of trapped ions.

The mass-selective ionic detection system was constructed by combining a quadrupole mass analyzer with the rf trap in order to clarify the reason for the disappearance of rf signals and to confirm the production of molecular ions. By mass-selective detection, we found that YbH^+ is produced by the chemical reaction of Yb^+ in excited states with H_2 gas. The YbH^+ production is one of the causes of fluorescence decay, but is not directly related to the disappearance of rf signals. The time scale of the reaction is the same as that of the fluorescence decay. YbH^+ is photodissociated by irradiation at 369.482 nm, 369.202 nm, and 368.947 nm, which were formerly assigned as wavelengths for deexcitation of Yb^+ in the $^2F_{7/2}$ state to the $^2S_{1/2}$ ground state. The resonance point of rf signals shifted in accordance with the mass change from Yb^+ to YbH^+ (rf signals did not disappear in the case of YbH^+ productions.) and returned to the initial point by photodissociation of YbH^+.

To clarify the reason for the disappearance of rf signals, we measured the time variance in signal height of the mass-selective signals for several ion species with continuous irradiation at 369.52 nm in the presence of O_2 gas. We found that YbO^+ is produced by the chemical reaction of Yb^+ in excited states with O_2 gas, as previously predicted. However, no significant decrease in the number of YbO^+ ions from that of the initially trapped Yb^+ ions was observed, even after the disappearance of rf signals. In addition, UV radiation was terminated after the rf signals disappeared,

and then rf signals recovered, although the rate of recovery was very slow. Therefore, the disappearance of rf signals was not caused by the decrease in the total number of trapped ions.

In the final part of the chapter, we summarized our present interpretation of the causes of fluorescence decay and rf signal disappearance.

In Chapter 5, we demonstrated that it is possible to laser cool a natural isotope mixture of Yb^+ ions by setting the frequencies of the two cooling lasers properly. We found that one of the three major even isotopes, i.e., $^{172}Yb^+$, $^{174}Yb^+$, or $^{176}Yb^+$, can be directly laser cooled without serious laser heating of the other isotopes owing to the relatively large isotope shifts of the $^2D_{3/2} - {}^3[3/2]^\circ_{1/2}$ transition at 935 nm. Other isotopes not directly laser cooled were simultaneously trapped as a result of sympathetic cooling. According to the results for $^{176}Yb^+$, direct laser cooling of 13 % of the trapped ions is sufficient to cool them and to sympathetically cool the not directly laser-cooled ions, in the case where the number of trapped ions is small and consequently, the effect of rf heating is small.

We found that it is possible to trap and laser cool single $^{174}Yb^+$ ions from a natural Yb isotope mixture source. To laser cool single Yb^+ ions, we found that it was necessary to compensate the undesired dc field, as was found at many laboratories. We added two compensation electrodes and applied appropriate dc voltages to them and one of the endcap electrodes. After the dc field compensation, the temperature of a single $^{174}Yb^+$ was 150 mK. The temperature was estimated from the linewidth of the spectrum obtained by a frequency sweep of the cooling laser at 369.52 nm. We removed saturation broadening from the observed spectrum to determine the temperature.

To evaluate the number of trapped ions, we induced sudden drops of

fluorescence intensity, quantum jumps signals, by pumping to the $^2F_{7/2}$ state by driving the $^2D_{3/2}$ - $^1[3/2]^o_{3/2}$ transition at 861 nm. We found that Yb^+ is deexcited from the $^2F_{7/2}$ state by driving the $^2F_{7/2}$ - $^2D_{5/2}$ transition at 3.43 mm, the $^2F_{7/2}$ - $^1[3/2]^o_{3/2}$ transition at 760 nm, and the $^2F_{7/2}$ - $^3[3/2]^o_{7/2}$ transition at 829 nm, in addition to the $^2F_{7/2}$ - $^1[5/2]^o_{5/2}$ transition at 638 nm found at NPL. By using of radiation for both pumping to and from the $^2F_{7/2}$ state, we observed quantum jump signals repeatedly.

Through our investigations of Yb^+, our understanding of the characteristics of Yb^+ ions in the presence of buffer gases has progressed significantly. The remaining problems are (i) to clarify whether or not population trapping in the $^2F_{7/2}$ state actually occurs in the presence of buffer gases, and (ii) to elucidate the cause of the disappearance of rf signals. For problem (i), it is helpful to apply the results concerning the $^2F_{7/2}$ state obtained by laser-cooled Yb^+ under an ultrahigh-vacuum condition to investigations of buffer-gas-cooled Yb^+. The production of YbH^+ is important in the field of frequency standards, because the production of YbH^+ may be a problem in establishing a frequency standard using buffer-gas-cooled Yb^+, owing to the difficulty in removing H_2 gas from vacuum systems.

We have succeeded in preparing laser-cooled single Yb^+ even from a natural isotope mixture source. It was necessary for us to establish techniques for laser cooling of a single $^{174}Yb^+$ ions, because we plan to proceed to high-resolution spectroscopy of a single Yb^+ ions in the optical wavelength region. Determining the transition which deexcites the $^2F_{7/2}$ state, and observation of quantum jumps are regarded as the first steps toward this aim. In particular, driving the $^2S_{1/2}$ - $^2D_{5/2}$ clock transition at 411 nm causes subsequent spontaneous decay to the $^2F_{7/2}$ state. Therefore, it is essential to

establish some methods for efficient deexcitation of the $^2F_{7/2}$ state to achieve high-resolution spectroscopy of the $^2S_{1/2}$ - $^2D_{5/2}$ transition.

Finally, by combining the results concerning the chemical reaction of Yb$^+$ in excited states, obtained in investigations of buffer-gas-cooled Yb$^+$, with techniques of laser cooling of a single Yb$^+$, we propose the possibility of applying a single laser-cooled Yb$^+$ ion to chemical investigation, e.g., cooled single-molecular-ion photodissociation spectroscopy.

References

Chapter 1

[1] H. G. Dehmelt, Adv. At. Mol. Phys. **3**, 53 (1967).

[2] H. G. Dehmelt, Adv. At. Mol. Phys. **5**, 53 (1969).

[3] D. J. Wineland, W. M. Itano, and R. S. Van Dyck, Jr., Adv. At. Mol. Phys. **3**, 53 (1967).

[4] P. E. Toschek, in *New Trends in Atomic Physics, Les Houches, Session 1982*, edited by G. Grynberg and R. Stora (North-Holland, Amsterdam, 1984) p.383.

[5] D. J. Wineland, Science, **226**, 395 (1984).

[6] H. G. Dehmelt, IEEE Trans. Instrum. Meas. **31**, 83 (1982).

[7] D. J. Wineland, W. M. Itano, J. C. Bergquist, and R. G. Hulet, Phys. Rev. A **36**, 2220 (1987).

[8] See articles, in *Proceedings of fourth symposium on Frequency Standards and Metrology, Ancona, 1988*, edited A. DeMarchi (Springer, Berlin, 1988).

[9] See articles, in *Proceedings of the fifth Symposium on Frequency Standards and Metrology, Woods Hole, 1995* , edited by J. C. Bergquist (World Scientific, Singapore, 1996).

[10] D. J. Wineland, J. C. Bergquist, J. J. Bollinger, W. M. Itano, D. J. Heinzen, S. L. Gilbert, C. H. Manney, and M. G. Raizen, IEEE Trans. Ultrason. Ferroelec. Freq. Contr. **37**, 515 (1990).

[11] R. H. Dicke, Phys. Rev. **89**, 472 (1953).

[12] T. W. Hansch and A. L. Schawlow, Opt. Commun. **13**, 68 (1975).

[13] D. J. Wineland and H. G. Dehmelt, Bull. Am. Phys. Soc. **20**, 637 (1975).

[14]   D. J. Wineland, R. E. Drullinger, F. L. Walls, Phys. Rev. Lett. **40**, 1639 (1978).

[15]   W. Neuhauser, M. Hohenstatt, P. E. Toschek, and H. G. Dehmelt, Phys. Rev. Lett. **41**, 233 (1978).

[16]   W. Neuhauser, M. Hohenstatt, P. E. Toschek, and H. G. Dehmelt, Phys. Rev. A **22**, 1137 (1980).

[17]   J. C. Bergquist, W. M. Itano, and D. J. Wineland, Phys. Rev. A **36**, 428 (1987).

[18]   W, M. Itano and D. J. Wineland, Phys. Rev. A **25**, 35 (1982).

[19]   L. S. Cutler, C. A. Flory, R. P. Giffard, and M. D. McGuire, Appl. Phys. B **39**, 251 (1986).

[20]   L. S. Cutler, R. P. Giffard, and M. D. McGuire, Appl. Phys. B **36**, 137 (1985).

[21]   Y. Moriwaki, M. Tachikawa, Y. Maeno, and T. Shimizu, Jpn. J. Appl. Phys. **31**, L1640 (1992).

[22]   L. D. Prestage, G. J. Dick, and L. Maleki, J. Appl. Phys. **66**, 1013 (1989).

[23]   D. J. Wineland, W. M. Itano, J. C. Bergquist, J. J. Bollinger, and J. D. Prestage, Ann. Phys. Fr. **10**, 737 (1985).

[24]   D. J. Wineland, W. M. Itano, J. C. Bergquist, and J. J. Bollinger, F. Diedrich, and S. L. Gilbert, in *Proceedings of fourth symposium on Frequency Standards and Metrology, Ancona, 1988,* edited A. DeMarchi (Springer, Berlin, 1988) p.71.

[25]   N. Yu, X. Zhao, H. Dehmelt, and W. Nagourney, Phys. Rev. **50**, 2738 (1984).

[26]   See, *Proceedings of the fifth Symposium on Frequency Standards and Metrology, Woods Hole, 1995* , edited by J. C. Bergquist (World Scientific, Singapore, 1996), and references therein.

[27]   J. C. Berquist, W. M. Itano, F. Elsner, M. G. Raizen and D. J. Wineland, in *Proceedings of LIKE Workshop* (1990).

[28]   R. W. P. Drever, J. H. Hall, F. V. Kowalski, J. Hough, G. M. Ford, A. J. Munley, and H. Ward, Appl. Phys. B 31. 97 (1983).

[29]   D. Hils and J. Hall, in *Proceedings of fourth symposium on Frequency Standards and Metrology*, *Ancona*, *1988*, edited A. DeMarchi (Springer, Berlin, 1988) p. 162.

[30]   K. Sugiyama and A. Morinaga, Jpn. J. Appl. Phys., 30, L1811 (1991).

[31]   K. Nakagawa, T. Katsuda, and M. Ohtsu, Appl. Phys., B 60, 489 (1995).

[32]   R. L. Tjoelker, J. D. Prestage, and L. Maleki, in *Proceedings of the fifth Symposium on Frequency Standards and Metrology*, *Woods Hole*, *1995* , edited by J. C. Bergquist (World Scientific, Singapore, 1996) p. 33.

[33]   P. T. H. Fisk, M. J. Sellars, M. A. Lawn, and C. Coles, in *Proceedings of the fifth Symposium on Frequency Standards and Metrology*, *Woods Hole, 1995* , edited by J. C. Bergquist (World Scientific, Singapore, 1996) p. 27.

[34]   J.J. Bollinger, J. D. Prestage, W. M. Itano, and D. J. Wineland, Phys. Rev. Lett. 54, 1000 (1985).

[35]   J. J. Bollinger, D. J. Heinzen, W. M. Itano, S. L. Gilbert, and D. J. Wineland, IEEE Trans. Instrum. Meas. IM 40, 126 (1991).

[36]   M. G. Raizen, J. M. Gilligan, J. C. Bergquist, W. M. Itano, and D. J. Wineland, Phys. Rev. A 45, 6493 (1992).

[37]   M. E. Poitzsch, J. C. Bergquist, W. M. Itano, and J. D. Wineland, Rev. Sci. Instrum. 67, 129 (1996).

[38]   W. Nagourney, J. Sandberg, and H. Dehmelt, Phys. Rev. Lett. 56, 2797 (1986).

[39] Th. Sauter, W. Neuhauser, R. Blatt, and P. E. Toschek, Phys. Rev. Lett. **57**, 1696 (1986).

[40] J. C. Bergquist, R. G. Hulet, W. M. Itano, and D. J. Wineland, Phys. Rev. Lett. **57**, 1699 (1986).

[41] F. Diedrich, E. Peik, J. M. Chen, W. Quint, and H. Walther, Phys. Rev. Lett. **59**, 2931 (1987).

[42] F. Diedrich and H. Walther, Phys. Rev. Lett. **58**, 203 (1987).

[43] F. Diedrich, J. C. Bergquist, W. M. Itano, and D. J. Wineland, Phys. Rev. Lett. **62**, 403 (1989).

[44] W, M. Itano, D. J. Heinzen, J. J. Bollinger, and D. J. Wineland, Phys. Rev. A **41**, 2295 (1990).

[45] C. Monroe, D. M. Meekhof, B. E. King, W. M. Itano, and D. J. Wineland, Phys. Rev. Lett. **75**, 4714 (1995).

[46] H. Lehmitz, J. Hattendorf-Ledwoch, R. Blatt and H. Harde, Phys. Rev. Lett. **62**, 2108 (1989).

[47] Chr. Tamm and D. Engelke, in *Proceedings of eighth European Frequency and Time Forum, 1994*, p.40.

[48] B. C. Fawcett and M. Wilson, At. Data Nucl. Data Tables **47**, 241 (1991).

[49] K. Sugiyama and J. Yoda, in *Proceedings of the fifth Symposium on Frequency Standards and Metrology, Woods Hole, 1995* , edited by J. C. Bergquist (World Scientific, Singapore, 1996) p. 432.

[50] Chr. Tamm, Appl. Phys. B **56**, 295 (1993).

[51] Chr. Tamm and D. Schnier, Opt. Commun. **87**, 240 (1992).

[52] R. Blatt, H. Schnatz, and G. Werth, Phys. Rev. Lett. **48**, 1601 (1982).

[53] A. Munch, M. Berkler, Ch. Gerz, D. Wilsdorf, and G. Werth, Phys. Rev. A **35**, 4147 (1987).

[54]   Ch. Gerz, J. Roths, F. Vedel, and G. Werth, Z. Phys. D **8**, 235 (1988).

[55]   H. A. Klein, A. S. Bell, G. P. Barwood, and P. Gill, Appl. Phys. B **50**, 13, (1990).

[56]   A. Bauch, D. Schnier and Chr. Tamm, J. Mod. Opt. **39**, 389 (1992)

[57]   K. Sugiyama and J. Yoda, Hyperfine Interact. **74**, 251 (1992).

[58]   J. Yoda and K. Sugiyama, J. Mod. Opt. **39**, 403 (1992).

[59]   A. S. Bell, P. Gill, H. A. Klein, A. P. Levick, Chr. Tamm, and D. Schnier, Phys. Rev. A **44**, R20 (1991).

[60]   V. Enders, Ph. Courteille, R. Huesmann, L. S. Ma, W. Neuhauser, R. Blatt, and P. E. Toschek, Europhys. Lett. **24**, 325 (1993).

[61]   P. T. H. Fisk, M. A. Lawn, and C. Cole, Appl. Phys. B **57**, 287 (1993).

[62]   K. Sugiyama and J. Yoda, IEEE Trans. Instrum. Meas. IM **44**, 140 (1995).

[63]   Chr. Tamm, D. Schnier, and A. Bauch, Appl. Phys. B **60**, 19 (1995).

[64]   P .T. H. Fisk, M. J. Sellars, M. A. Lawn, and C. Coles, Appl. Phys. B **60**, 519 (1995).

[65]   A. S. Bell, P. Gill, H. A. Klein, A. P. Levick, and W. R. C. Rowley, J. Mod. Opt. **39**, 381 (1992).

[66]   P. Gill, H. A. Klein, A. P. Levick, M. Roberts, W. R. C. Rowley, and P. Taylor, Phys. Rev. A **52**, R909 (1995).

[67]   P. Taylor, M. Roberts, S. V. Gateva-Kostava, P. Gill, H. A. Klein, and W. R. C. Rowley, presented at ICAP'96, and to be published in Phys. Rev. A.

[68]   D. Engelke and Chr. Tamm, Europhys. Lett. **33**, 347 (1996).

[69]   M. Roberts, P. Taylor, G. P. Barwood, P. Gill, H. A. Klein, and W.

R. C. Rowley, presented at ICAP'96, and to be published in Phys. Rev. Lett.

[70]   K. Sugiyama and J. Yoda, Phys. Rev. A **55**, R10 (1997).

[71]   K. Sugiyama and J. Yoda, in *Conference Digest of 1996 Conference on Precision Electromagnetic Measurement, Braunschweig, 1996* (IEEE, Piscataway, NJ, 1996), p. 308.

[72]   K. Sugiyama and J. Yoda, IEEE Trans. Instrum. Meas. IM **42**, 467 (1993).

[73]   K. Sugiyama and J. Yoda, Jpn. J. Appl. Phys. **34**, L584 (1995).

[74]   D. J. Seidel and L. Maleki, Phys. Rev. A **51**, R2699 (1995).

[75]   J. Yoda, , Jpn. J. Appl. Phys. **26**, 1390 (1987).

[76]   K. Sugiyama and J. Yoda, Appl. Phys. B **51**, 146 (1990).

[77]   L. S. Brown, G. Gabrielse, Rev. Mod. Phys. **58**, 233(1986)

[78]   M. N. Gaboriaud, M. Desaintfuscien, F. G. Major, Int. J. Mass Spectr. Ion Phys. **41**, 109 (1981).

[79]   K. Sugiyama, J. Yoda, and T. Sakurai, Opt. Lett. **16**, 449 (1991).

[80]   K. Sugiyama and J. Yoda, Opt. Commun. **95**, 77 (1993).

[81]   Y. Chaiko, Opt. Spectrosc. **20**, 424 (1966).

[82]   A-M. Martensson-Pendrill, D. S. Gough, and P. Hannaford, Phys. Rev. A **49**, 3351 (1994).

[83]   T. Andersen, O. Poulsen, P. S. Ramanujam, A. Petrakiev Perkov, Solar Phys. **44**, 257 (1975).

[84]   M. L. Burshtein, Ya. F. Verolainen, V. A. Komarovskii, A. L. Osherovich, and N. P. Penkin, Opt. Spectrosc. **37**, 351 (1974).

[85]   K. B. Blagoev, V. A. Komarovskii, and N. P. Penkin, Opt. Spectrosc. **45**, 832 (1978).

[86]   R. W. Berends, E. H. Pinnington, B. Guo and Q. Ji, J. Phys. B **26**, L701 (1993).

[87]   R. M. Lowe, P. Hannaford, and A.-M. Martensson Pendrill, Z. Phys.

D **28**, 283 (1993).

[88]   F. H. K. Rambow and L. D. Schearer, Phys. Rev. A **14**, 738 (1978).

Chapter 2

[1]   J. Yoda, Jpn. J. Appl. Phys., **26**, 1390 (1987).

[2]   J. Yoda and K. Sugiyama, IEEE Trans. Instrum. Meas. IM **38**, 521 (1989).

[3]   K. Sugiyama and J. Yoda, Appl. Phys. B **51**, 146 (1990).

[4]   K. Sugiyama and J. Yoda, Hyperfine Interact. **74**, 251 (1992).

[5]   J. Yoda and K. Sugiyama, J. Mod. Opt. **39**, 403 (1992).

[6]   K. Sugiyama and J. Yoda, IEEE Trans. Instrum. Meas. IM **42**, 467 (1993).

[7]   K. Sugiyama and J. Yoda, Jpn. J. Appl. Phys., **34**, L584 (1995).

[8]   K. Sugiyama and J. Yoda, IEEE Trans. Instrum. Meas., IM **44**, 140 (1995).

[9]   L. S. Brown, G. Gabrielse, Rev. Mod. Phys., **58**, 233 (1986), and references therein.

[10]   M. N. Gaboriaud, M. Desaintfuscian, F. G. Major, Int. J. Mass Spectrom. Ion Phys., **41**, 109 (1981).

[11]   H. G. Dehmelt, Adv. At. Mol. Phys., **3**, 53 (1967).

[12]   R. F. Wuerker, H. Shelton, and R. V. Langmuir, J. Appl. Phys., **30**, 342 (1959).

[13]   R. Ifflander and G. Werth, Metrologia, **13**, 167 (1977).

[14]   K. Sugiyama and J. Yoda, Phys. Rev. A **55**, R10 (1997).

[15]   J. D. Sankey and A. A. Madej, Appl. Phys. B **49**, 69 (1989).

[16]   E. C. Beaty, J. Appl. Phys. **61**, 211 (1987).

[17]   J. Yoda and K. Sugiyama, Jpn. J. Appl. Phys. **26**, L1780 (1987).

[18]   D. J. Wineland and H. G. Dehmelt, J. Appl. Phys. **46**, 919 (1975).

[19]   G. Gabrielse, Phys. Rev. A **27**, 2277 (1983).

[20]   H. Schaaf, U. Schmeling, and G. Werth, Appl. Phys. **25**, 249 (1981).

[21]   R. D. Knight and M. H. Prior, J. Appl. Phys. **50**, 3044 (1979).

[22]   I. Siemers, R. Blatt, Th. Sauter, and W. Neuhauser, Phys. Rev. A **38**, 5121(1988).

[23]   C. Meis, M. Desaintfuscien, and M. Jardino, Appl. Phys. B **45**, 59 (1988).

[24]   S. Urabe, J. Umezu, and M. Ishizu, Oyo Buturi, **54**, 964 (1985) in Japanese.

[25]   R. Schneider and G. Werth, Z. Phys. A **293**, 103 (1979).

[26]   H. Knob, H-D. Niebling, and G. Werth, IEEE Trans. Instrum. Meas. IM **34**, 242 (1985).

[27]   K. Sugiyama and J. Yoda, in *Proceedings of the fifth Symposium on Frequency Standards and Metrology, Woods Hole, 1995* , edited by J. C. Bergquist (World Scientific, Singapore, 1996) p. 432.

[28]   R. S. Van Dyck, Jr., D. J. Wineland, P.A. Ekstrom, and H. G. Dehmelt, Appl. Phys. Lett., **28**, 446 (1976)

[29]   E. C. Beaty, Phys. Rev. A **33**, 3645 (1986)

Chapter 3

[1]   J. C. Bergquist, W. M. Itano, and D. J. Wineland, Phys. Rev. A **36**,

428 (1987).

[2]   K. Sugiyama, J. Yoda, and T. Sakurai, Opt. Lett. **16**, 449 (1991).

[3]   P. Gunter, Appl. Phys. Lett. **34**, 650 (1979).

[4]   T. Taniuchi and K. Yamamoto, Technical Digest of Conference on Lasers and Electro-Optics, paper WR3 (1986).

[5]   D. Feng, N. B. Ming, J. F. Hong, Y. S. Yang, J. S. Zhu, Z. Yang, and Y. N. Wang, Appl. Phys. Lett. **37**, 607 (1980).

[6]   G. J. Dixson, C. E. Tanner, and C. E. Wieman, Opt. Lett. **14**, 731 (1989).

[7]   Chr. Tamm, Appl. Phys. B **56**, 295 (1993).

[8]   M. K. Chun, L. Goldberg, and J. F. Weller, Appl. Phys. Lett. **53**, 1170 (1988).

[9]   D. Mehuys, D. F. Welch, and L. Goldberg, Electron. Lett. **28**, 1944 (1992).

[10]   K. Sugiyama and J. Yoda, Opt. Commun. **95**, 77 (1993).

[11]   K. Sugiyama and J. Yoda, IEEE Trans. Instrum. Meas. IM **44**, 140 (1995).

[12]   B. C. Fawcett and M. Wilson, At. Data Nucl. Data Tables, **47**, 242 (1991).

[13]   H. A. Klein, A. S. Bell, G. P. Barwood, and P. Gill, Appl. Phys. B **50**, 13 (1995).

[14]   A. S. Bell, P. Gill, H. A. Klein, A. P. Levick, Chr. Tamm, and D. Schnier, Phys. Rev. A **44**, R20 (1991).

[15]   Chen, B. Wu, A. Jiang, and G. You, Scientia Sinica, B **28**, 235 (1985).

[16]   D. Eimerl, L. Davis, S. Velsko, E. K. Graham, and A. Zalkin, J. Appl. Phys. **62**, 1968 (1987).

[17]   K.Kato, IEEE J. Quantum. Electron. QE **22**, 1013 (1986).

[18]   G. D. Boyd and D. A. Kleinman, J. Appl. Phys. **39**, 3597 (1968).

[19]   .S. Guha and J. Falk, J. Appl. Phys. **51**, 50 (1980).

[20]   H. Schmidt and R. Wallenstein, Laser and Optoelektronik, **19**, 302 (1987).

[21]   P. Qiu and A. Penzkofer, Appl. Phys. B **45**, 225 (1988).

[22]   H. Hemmati, J. C. Bergquist, and W. M. Itano, Opt. Lett. **8**, 73 (1983).

[23]   L. J. Bromley, A. Guy, and D. C. Hanna, Opt. Commn. **67**, 316 (1988).

[24]   H. W. Kogelnik, E. P. Ippen, A. Dienes, and C. V. Shank, IEEE J. Quantum. Electron. QE **8**, 373(1972).

[25]   Y. Chaiko, Opt. Spectroscopy, **20**, 424 (1966).

[26]   M. Ohtsu, M. Murata, and M. Kourogi, IEEE J. Quant. Electron. QE **26**, 231 (1990).

[27]   Ch. Salmon, D. Hils, and J. L. Hall, J. Opt. Soc. Am. B **5**, 1576 (1988).

[28]   K. Sugiyama and A. Morinaga, Jpn. J. Appl. Phys. **30**, L1811 (1991).

[29]   A. Ashkin, G. C. Boyd, and J. M. Dziedzic, IEEE J. Quant. Electron. QE **2**, 109 (1966).

[30]   M. Brieger, H. Busener, A. Hese, F. v. Moers, and A. Renn, Opt. Commun. **38**, 423 (1981).

[31]   A. Morinaga, Laser Kenkyu **15**, 805 (1987) in Japanese.

[32]   M. H. Dunn and A. I. Ferguson, Opt. Commun. **20**, 214 (1977).

[33]   T. W. Hansch and B. Couillaud, Opt. Commun. **20**, 214 (1980).

[34]   Chr. Tamm and D. Schnier, Opt. Commun. **87**, 240 (1992).

[35]   P. Gill, H. A. Klein, A. P. Levick, M. Roberts, W. R. C. Rowley, and P. Taylor, Phys. Rev A **52**, R909 (1995).

[36]   H. A. Klein, A. S. Bell, G. P. Barwood, and P. Gill, Appl. Phys. B **50**, 13, (1990).

[37]   A. Bauch, D. Schnier, and Chr. Tamm, in *Proceedings of seventh European Frequency and Time Forum*, *1993*, p.583.

[38]   Chr. Tamm, D. Schnier, and A. Bauch, Appl. Phys, B **60**, 19 (1995).

Chapter 4

[1]   Ch. Gerz, J. Roths, F. Vedel, and G. Werth, Z. Phys D **8**, 235 (1988).

[2]   H. Lehmitz, J. Hattendorf-Ledwoch, R. Blatt, and H. Harde, Phys. Rev. Lett. **62**, 2108 (1989).

[3]   H. A. Klein, A. S. Bell, G. P. Barwood, and P. Gill, Appl. Phys. B **50**, 13 (1990).

[4]   A. Bauch, D. Schnier, and Chr. Tamm, J. Mod. Opt. **39**, 389 (1992).

[5]   K. Sugiyama and J. Yoda, Hyperfine Interact. **74**, 251 (1992).

[6]   J. Yoda and K. Sugiyama, J. Mod. Opt. **39**, 403 (1992).

[7]   K. Sugiyama and J. Yoda, IEEE Trans. Instrum. Meas. IM **42**, 467 (1993).

[8]   K. Sugiyama and J. Yoda, Jpn. J. Appl. Phys. **34**, L584 (1995).

[9]   D. J. Seidel and L. Maleki, Phys. Rev. A **51**, R2699 (1995).

[10]   K. Sugiyama and J. Yoda, Phys. Rev. A **55**, R10 (1997).

[11]   K. Sugiyama and J. Yoda, in *Proceedings of the fifth Symposium on Frequency Standards and Metrology*, *Woods Hole, 1995* , edited by J. C. Bergquist (World Scientific, Singapore, 1996) p. 432.

[12]   L. S. Cutler, R. P. Giffard, M. D. McGuire, Appl. Phys. B 36, 137 (1985).

[13]   Y. Moriwaki, M. Tachikawa, Y. Maeno, and T. Shimizu, Jpn. J. Appl. Phys. 31, L1640 (1992).

[14]   A. S. Bell, P. Gill, H. A. Klein, A. P. Levick, Chr. Tamm, and D. Schnier, Phys. Rev. A 44, R20 (1991).

[15]   Chr. Tamm and D. Schnier, Opt. Commn. 87, 240, (1992).

[16]   M. N. Gaboriaud, M. Desaintfuscien, and F. G. Major, Int. J. Mass Spectom. Ion Phys. 41, 109 (1981).

[17]   J. Yoda, Jpn. J. Appl. Phys. 26, 1390 (1987).

[18]   Yu. Chaiko, Opt. Spectrosc. 20, 424 (1966).

[19]   B. C. Fawcett and M. Wilson, At. Data Nucl. Data Tables, 47, 247 (1991).

[20]   L. S. Cutler, R. P. Giffard, and M. D. McGuire, Appl. Phys. B 36, 137 (1985).

[21]   K. B. Blagoev, V. A. Komarovski, and N. P. Penkin, Opt. Spectrosc. 45, 832 (1978).

[22]   K. Jungmamm, J. Hoffnagle, R. G . DeVoe, and R. G. Brewer, Phys. Rev. A 36, 3451 (1987).

[23]   W. Kalber, G. Meisel, J. Rink and R. C. Thonpson, J. Mod. Opt. 39, 335 (1992).

[24]   J. D. Sankey and A. A. Madej, Appl. Phys. B 50, 433 (1990).

[25]   R. J. Ackermann, E. G. Rash, and R. J. Thorn, J. Chem. Phys. 65, 1027 (1976).

[26]   A. A. Radzig and B. M. Smirnov: *Reference Data on Atoms, Molecules, and Ions*, (Springer-Verlag, Berlin, Heidelberg, 1985)

[27]   Y. Matsuo, H. Maeda, and M. Takami, Chem. Phys. Lett. 201, 341 (1993)

[28]   A. S. Bell, P. Gill, H. A. Klein, A. P. Levick, and W. R. C. Rowley, J. Mod. Opt. **39**, 381 (1992).

[29]   J. L, Elkind and P. B. Armentrout, J. Phys. Chem. **91**, 2037 (1987). R. Georgiadis and P. B. Armentrout, ibid. **92**, 7060 (1988). K. K. Irikura and J. L. Beauchamp, ibid. **95**, 8344 (1991).

[30]   R. Georgiadis and P. B. Armentrout, J. Phys. Chem. **92**, 7060 (1988).

[31]   P. Gill, H. A. Klein, A. P. Levick, M. Roberts, W. R. C. Rowley, and P. Taylor, Phys. Rev. A **52**, R909 (1995).

[32]   J. C. Bergquist, W. M. Itano, and D. J. Wineland, Phys. Rev. A **36** 428 (1987).

Chapter 5

[1]   H. A. Klein, A. S. Bell, G. P. Barwood, and P. Gill, Appl. Phys. B **50**, 13 (1990).

[2]   A. S. Bell, P. Gill, H. A. Klein, A. P. Levick, Chr. Tamm, and D. Schnier, Phys. Rev. A **44**, R20, (1991).

[3]   V. Enders, Ph. Courteille, F. Elsner, R. Blatt, W. Neuhauser, and P. E. Toschek, IQEC '92, MoM2, June 1992.

[4]   V. Enders, Ph. Courteille, R. Huesmann, L. S. Ma, W. Neuhauser, R. Blatt, and P. E. Toschek, Europhys. Lett. **24**, 325 (1993).

[5]   P. T. H. Fisk, M. A. Lawn, and C. Coles, Appl. Phys. B **57**, 287 (1993).

[6]   Chr. Tamm and D. Engelke, in *Proceedings of eighth European Frequency and Time Forum, 1994*, p.40.

[7]   D. Engelke and Chr. Tamm, Europhys. Lett. **33**, 347 (1996).

[8] Y. Chaiko, Opt. Spectrosc. **20**, 424 (1966).

[9] D. J. Larson, J. C. Bergquist, J. J. Bollinger, W. M. Itano, and D. J. Wineland, Phys. Rev. Lett. **57**, 70 (1986).

[10] K. Sugiyama and J. Yoda, IEEE Trans. Instrum. Meas. IM **44**, 140 (1995).

[11] R. Blumel, C. Kappler, W. Quint, and H. Walther, Phys. Rev. A **40**, 808 (1989).

[12] A. A. Madej and J. D. Sankey, Opt. Lett. **15**, 634 (1990).

[13] K. Sugiyama and J. Yoda, in *Proceedings of the fifth Symposium on Frequency Standards and Metrology, Woods Hole, 1995* , edited by J. C. Bergquist (World Scientific, Singapore, 1996), p. 432.

[14] K. Sugiyama and J. Yoda, in *Conference Digest of 1996 Conference on Precision Electromagnetic Measurement, Braunschweig, 1996* (IEEE, Piscataway, NJ, 1996), p. 308.

[15] T. W. Hansch and A. L. Schawlow, Opt. Commun. **13**, 68 (1975).

[16] D. J. Wineland and H. G. Dehmelt, Bull. Am. Phys. Soc. **20**, 637 (1975).

[17] D. J. Wineland and W. M. Itano, Phys. Rev. A **20**, 1521 (1979).

[18] D. J. Wineland, W, M. Itano, J. C. Bergquist, and R. G. Hulet, Phys. Rev. A **36**, 2220 (1987).

[19] F. Shimizu, K. Shimizu, and H. Takuma, Opt. Lett. **16**, 339 (1991).

[20] Y. Maeno, M. Tachikawa, Y. Moriwaki, and T. Shimizu, Jpn. J. Appl. Phys. **34**, L174 (1995).

[21] W. Neuhauser, M. Hohenstatt, P. E. Toschek, and H. Dehmelt, Phys. Rev. A **22**, 1137 (1980).

[22] M. N. Gaboriaud, M. Desaintfuscian, and F. G. Major, Int. J. Mass Spectr. Ion Phys. **41**, 109 (1981).

[23] F. Diedrich, E. Peik, J. M. Chen, W. Quint, and H. Walther, Phys. Rev. Lett. **59**, 2931 (1987).

[24] private communication.

[25] private communication.

[26] W. Nagourney, G. Janik, and H. G. Dehmelt, Proc. Natl. Acad. Sci. USA **80**, 643 (1983).

[27] R. M. Lowe, P. Hannaford, and A.-M. Martensson Pendrill, Z. Phys. D **28**, 283 (1993).

[28] D. J. Wineland, J. C. Bergquist, W. M. Itano, J. J. Bollinger, and C. H. Manney, Phys. Rev. Lett. **59**, 2935 (1987).

[29] D. J. Wineland, J. J. Bollinger, and W. M. Itano, Phys. Rev. Lett. **50**, 628 (1983).

[30] For example, W. M. Itano, J. C. Bergquist, and D. J. Wineland, Science, **237**, 612 (1987).

[31] W. F. Meggers (ed. C. E. Moore), J. Res. Nat. Bur. Stand. **71A**, 396 (1967).

[32] Chr. Tamm, private communication.

[33] P. Gill, H. A. Klein, M. Roberts, W. R. C. Rowley, and P. Taylor, in *Proceedings of the fifth Symposium on Frequency Standards and Metrology, Woods Hole, 1995*, edited by J. C. Bergquist (World Scientific, Singapore, 1996), p. 159.

[34] P. Gill, H. A. Klein, A. P. Levick, M. Roberts, W. R. C. Rowley, and P. Taylor, Phys. Rev. A **52**, R909 (1995).

[35] K. B. MacAdam, A. Steinbach, and C. Wieman, Am. J. Phys. **60**, 1098 (1992).

[36] Chr. Tamm, Appl. Phys, B **56**, 295 (1993).

Appendix

Signal Strength of |Fluorescence from Yb^+ in the Steady State

We simplify the process of the fluorescence decay by introducing "dark" state, which includes "YbH^+" state and, probably, the $^2F_{7/2}$ state (see Chapter 4). We can analyze some time constants in the observed fluorescence signals of trapped Yb^+. However, the validity of this simplification should be clarified when the actual <u>micro</u> processes of the fluorescence decay is elucidated in future.

If N_i are the populations of the state indicated by subscripts (where [3/2] means the $4f^{13}5d6s(^3D)^3[3/2]^o_{1/2}$ state, and *dark* represents the dark state which includes "YbH^+" state and, probably, the $^2F_{7/2}$ state (see Chapter 4)), A_j the spontaneous decay rate where subscripts 1 - 5 for j mean the $^2S_{1/2}$ - $^2P_{1/2}$, $^2P_{1/2}$ - $^2D_{3/2}$, $^2D_{3/2}$ - $^2S_{1/2}$, $^2D_{3/2}$ - [3/2], and [3/2] - $^2S_{1/2}$ transitions, respectively, S_j the excitation rate by resonant radiation, R_6 the pumping rate from the $^2D_{3/2}$ to the dark state including "YbH^+" state and, probably, the $^2F_{7/2}$ state (see Chapter 4), R_3 and R_7 the deexcitation rate to the $^2S_{1/2}$ from $^2D_{3/2}$ and dark states, respectively, and r_j the fraction of the ion cloud irradiated, the rate equations for N_i are given by

$$\frac{dN_S}{dt} = -r_1 S_1 N_s + S_1 N_P + A_1 N_P + A_3 N_D + A_5 N_{[3/2]}$$

$$+ R_7 N_{dark}$$

$$\frac{dN_P}{dt} = r_1 S_1 N_s - S_1 N_P - A_1 N_P - A_2 N_P$$

$$\frac{dN_D}{dt} = A_2 N_P - A_3 N_D - R_6 N_D - r_4 S_4 N_D + S_4 N_{[3/2]} \qquad (A.1)$$

$$+ A_4 N_{[3/2]}$$

$$\frac{dN_{[3/2]}}{dt} = r_4 S_4 N_D - S_4 N_{[3/2]} - A_4 N_{[3/2]} - A_5 N_{[3/2]}$$

$$\frac{dN_{dark}}{dt} = R_6 N_D - R_7 N_{dark}$$

If $N_S + N_P + N_D + N_{[3/2]} + N_{dark} = N_0$, we can express the detected photon number N_f in the steady state in the same equation as that for the three-level system including only the S, P, and D states [1,2] by replacing A_s by R_3', as described later.

$$N_f = \frac{\eta x_1 r_1 A_1 N_0}{1 + \dfrac{A_2}{A_1} + \left[1 + r_1 + r_1 \dfrac{A_2}{R_3'} \right] x_1} \qquad (A.2)$$

$$\approx \frac{\eta x_1 r_1 A_1 N_0}{1 + \dfrac{A_2}{A_1} + r_1 x_1 \dfrac{A_2}{R_3'}} \qquad (x_1 \ll 1) \qquad (A.2')$$

where $x_j \equiv S_j/A_j$ is a saturation parameter for the transition indicated by subscript, and η the overall detection efficiency.

The equations expressing R_3' are presented as follows:

(1) three-level system (without irradiation at 935.2 nm at low buffer gas pressure, i.e., $S_4 = 0$, $R_6 \ll R_3$):

$$R_3{}' = R_3 \equiv A_3 + \text{(collisional deexcitation rate from}$$

$$\text{the } {}^2D_{3/2} \text{ to } {}^2S_{1/2} \text{ state)} \tag{A.3}$$

(2) five-level system

$$\frac{1}{R_3'} = \frac{1}{R_3} \left[\frac{1}{1 + \dfrac{R_6}{R_3} + \dfrac{r_4 S_4}{R_3}\left(\dfrac{A_5}{A_4 + S_4 + A_5}\right)} \right]\left(1 + \frac{R_6}{R_7}\right)$$

$$+ \frac{1}{A_5 + \dfrac{(R_3 + R_6)}{r_4 S_4}(A_4 + S_4 + A_5)} . \tag{A.4}$$

Bibliography

Papers related to this work

K. Sugiyama and J. Yoda, "Anharmonic oscillation of ions trapped in a rf trap with light buffer gas," Appl. Phys. B **51**, 146 (1990).

K. Sugiyama, J. Yoda, and T. Sakurai, "Generation of continuous-wave ultraviolet light by sum-frequency mixing of diode-laser and argon-ion-laser radiation in β-BaB$_2$O$_4$," Opt. Lett. **16**, 449 (1991).

K. Sugiyama and J. Yoda, "Optical detection of Yb$^+$ trapped in an rf trap," Hyperfine Interact. **74**, 251 (1992).

K. Sugiyama and J. Yoda, "Stabilization of sum or difference frequency by controlling one of the fundamental lasers of frequency mixing," Opt. Commun. **95**, 77 (1993).

K. Sugiyama and J. Yoda, "Study of Yb$^+$ trapped in a rf trap with light buffer gas by irradiation with resonant light," IEEE Trans. Instrum. Meas. IM **42**, 467 (1993).

K. Sugiyama and J. Yoda, "Laser cooling of a natural isotope mixture of Yb$^+$ stored in an rf trap," IEEE Trans. Instrum. Meas. IM **44**, 140 (1995).

K. Sugiyama and J. Yoda, "Disappearance of Yb$^+$ in excited states from rf trap by background gases," Jpn. J. Appl. Phys. **34**, L584 (1995).

K. Sugiyama and J. Yoda, "Production of YbH^+ by chemical reaction of Yb^+ in excited states with H_2 gas," Phys. Rev. A **55**, R10 (1997).

Proceedings related to this work

K. Sugiyama and J. Yoda, "Characteristics of buffer-gas-cooled and laser-cooled Yb^+ in rf traps," in *Proceedings of the fifth Symposium on Frequency Standards and Metrology, Woods Hole, 1995* , edited by J. C. Bergquist (World Scientific, Singapore, 1996), p. 432.

K. Sugiyama and J. Yoda, "Investigation for high-resolution spectroscopy of the $^2S_{1/2}$ - $^2D_{5/2}$ transition of laser-cooled trapped Yb^+," in *Conference Digest of 1996 Conference on Precision Electromagnetic Measurement, Braunschweig, 1996* (IEEE, Piscataway, NJ, 1996), p. 308.

Papers not related to this work

J. Yoda and K. Sugiyama, "Measurement of the storage time on N_2 ion trapped in an rf ion trap," Jpn. J. Appl. Phys. **26**, L1780 (1987).

K. Sugiyama, S. Iwasaki, and A. Morinaga, "Hyperfine structure of the P(48) line in the 11-3 band of iodine molecules by FM saturation spectroscopy," Opt. Lett. **13**, 556 (1988).

J. Yoda and K. Sugiyama, "Effect of buffer gas on the total number and the storage time of Ba ions trapped in an rf ion trap," IEEE Trans. Instrum.

Meas. IM **38**, 521 (1989).

A. Morinaga, K. Sugiyama, N. Ito, and J. Helmcke, "Hyperfine structure of low-lying vibrational levels in the B electric state of molecular iodine" J. Opt. Soc. Am., B **6**, 1656 (1989).

T. Tanaka, K. Mitsui, K. Sugiyama, M. Kitano, and T. Yabuzaki. "Shapes of laser-produced CsH particles," Phys. Rev. Lett. **63**, 1390 (1989).

A. Morinaga, N. Ito, and A. Morinaga, "A dye laser spectrometer with an external iodine cell designed for optical Ramsey-fringe spectroscopy in a Ca atomic beam," Jpn. J. Appl. Phys. **29**, L1727 (1990).

K. Sugiyama and A. Morinaga, "Frequency stabilization of a dye laser to a reference cavity with sub-Hertz relative linewidth," Jpn. J. Appl. Phys. **30**, L1811 (1991).

J. Yoda and K. Sugiyama, "Disappearance of trapped Yb^+ ions by irradiation of the resonance radiation", J. Mod. Opt. **39**, 403 (1992).

J. Yoda and K. Sugiyama, "Resonance of the macromotion of ions trapped in a rf trap by the subharmonic oscillation," Jpn. J. Appl. Phys. **31**, 3744 (1992).

J. Yoda and K. Sugiyama, "Determination of characteristics of Yb^+ ion cloud trapped in a rf trap with He buffer gas," Jpn. J. Appl. Phys. **31**, 3750 (1992).

A .Morinaga, N. Ito, J. Ishikawa, K. Sugiyama, and T. Kurosu, "Accuracy and stability if a calcium stabilized dye laser by means of the optical Ramsey fringes," IEEE Trans. Instrum. Meas. IM **42**, 338 (1993).

M. Mitsunaga, N. Uesugi, and K. Sugiyama, "Kilohertz-resolution pump-probe spectroscopy in Pr^{3+}:$YAlO_3$, Opt. Lett. **18**, 1256 (1995).

Acknowledgments

We would like to thank Dr. R. Lang and Dr. I. Mito of NEC Corporation for technical discussions of the diode laser used in sum-frequency mixing.

Finally, the author would like to give his special thanks to his father, mother, and sister. They always accept that the author does as he like to do.